DOT/FAA/AR-10/6

Air Traffic Organization
NextGen & Operations Planning
Office of Research and
Technology Development
Washington, DC 20591

Determining the Fatigue Life of Composite Aircraft Structures Using Life and Load-Enhancement Factors

June 2011

Final Report

This document is available to the U.S. public through the National Technical Information Services (NTIS), Springfield, Virginia 22161.

This document is also available from the Federal Aviation Administration William J. Hughes Technical Center at actlibrary.tc.faa.gov.

U.S. Department of Transportation
Federal Aviation Administration

NOTICE

Technical Report Documentation Page

1. Report No.	2. Government Accession No.	3. Recipient's Catalog No.
DOT/FAA/AR-10/6		

4. Title and Subtitle	5. Report Date
DETERMINING THE FATIGUE LIFE OF COMPOSITE AIRCRAFT STRUCTURES USING LIFE AND LOAD-ENHANCEMENT FACTORS	June 2011
	6. Performing Organization Code

7. Author(s)	8. Performing Organization Report No.
John Tomblin and Waruna Seneviratne	

9. Performing Organization Name and Address	10. Work Unit No. (TRAIS)
Department of Aerospace Engineering National Institute for Aviation Research Wichita State University Wichita, KS 67260-0093	11. Contract or Grant No.

12. Sponsoring Agency Name and Address	13. Type of Report and Period Covered
U.S. Department of Transportation Federal Aviation Administration Air Traffic Organization NextGen & Operations Planning Office of Research and Technology Development Washington, DC 20591	Final Report
	14. Sponsoring Agency Code ACE-110

15. Supplementary Notes

The Federal Aviation Administration William J. Hughes Technical Center COTRs were Curtis Davies and Peter Shyprykevich.

16. Abstract

Current regulations require airframes to demonstrate fatigue service life by testing and/or analysis. This requirement is identical for both metals and composites. As composites exhibit higher scatter than metals, extensive scatter analysis was conducted by Northrup/Grumman using several material databases. These data represented several structural details and variables such as laminate lay-up, loading mode, load transfer, specimen geometry, and environment. The U.S. Navy program included only autoclaved 350°F-cure graphite-epoxy materials, and the analysis was conducted primarily on fiber-dominated failures of laminated construction and did not include sandwich construction or bonded joints. The data analysis of this program developed a load-enhancement factor (LEF) that shortened the fatigue testing time while maintaining equivalent reliability to that of metals. The research performed in this study extended the developed methodology to new material systems and construction techniques. This study included data for materials commonly used in aircraft applications, including adhesives and sandwich construction. Testing consisted of various element-type tests and concentrated on tests that were generic in nature and were representative of various loading modes and construction techniques. In addition, the database available at the National Institute of Aviation Research (NIAR) was included to expand the data for the scatter analysis. Three different techniques are discussed for scatter analysis of fatigue data: individual Weibull, joint Weibull, and the Sendeckyj wearout model. It is recommended that the analysis include specimens or elements representative of features of a particular structure, i.e., materials, design details, failure modes, loading conditions, environments, rather than pool various material databases. Also, it is noted that the primary goal in scatter analysis is not to select shape parameters from the critical lay-up, R-ratio, environment, etc. (which may result in skewed data that will produce unconservative LEF), but rather to select the design details representing the critical areas of the structure. When designing test matrices for generating fatigue shape parameters, it is essential to investigate the design details and conditions that produce the most data scatter, which consequently affects the reliability of test data in higher levels of building blocks of testing. The examples in this report show that the LEF are lower for modern composite structures. However, care must be taken to ensure the integrity of test matrices to produce safe and reliable certification requirements. This report provides guidance on generating shape parameters for calculating life factor and LEFs as well as application of these factors to a fatigue load spectrum without compromising or significantly altering the fatigue life of the structure, especially in the case of hybrid (composite and metal) structures.

17. Key Words	18. Distribution Statement
Scatter analysis, Life factor, Load-enhancement factor, Test data, Composite fatigue, Weibull statistics	This document is available to the U.S. public through the National Technical Information Service (NTIS), Springfield, Virginia 22161. This document is also available from the Federal Aviation Administration William J. Hughes Technical Center at actlibrary.tc.faa.gov.

19. Security Classif. (of this report)	20. Security Classif. (of this page)	21. No. of Pages	22. Price
Unclassified	Unclassified	155	

ACKNOWLEDGEMENT

The authors would like to acknowledge the technical guidance and support of Mr. Curtis Davis, Dr. Larry Ilcewicz, and Mr. Peter Shyprykevich (retired) of the Federal Aviation Administration. The support of the Composites and Structures Laboratories of the National Institute for Aviation Research, especially test support from Govind Ramakrishna Pillai and Jason Yeoh and program support from Upul Palliyaguru, is greatly appreciated. The authors would also like to thank Cessna Aircraft of Wichita, Kansas, and Toray Composites (America), Inc., Tacoma, Washington, for providing material support during specimen fabrication, and Liberty Aerospace of Melbourne, Florida, for sharing their test data.

TABLE OF CONTENTS

LIST OF FIGURES

LIST OF TABLES

LIST OF ACRONYMS

4PB	Four-point bend
ACG	Advanced Composites Group
BVID	Barely visible impact damage
CAI	Compression after impact
CFPW	Carbon fabric plain weave
CTD	Cold temperature dry
CTU	Carbon tape unidirectional
CV	Coefficient of variation
DaDT	Durability and damage tolerance
DLL	Design limit load
DLT	Design lifetime
DNC	Double-notched compression
EOD	Effects of defects
ETD	Elevated temperature dry
ETW	Elevated temperature wet
FAA	Federal Aviation Administration
FGSW	E-glass satin weave
FH	Filled hole
LEF	Load-enhancement factor
LID	Large impact damage
LLD	Load-life damage
LVM	Lamina variability method
MIA	Mechanical impedance analysis
MLE	Maximum likelihood estimation
MLSP	Modal fatigue-life shape parameter
MSSP	Modal static-strength shape parameter
MTS	Material Test Systems
NASA	National Aeronautics and Space Administration
NDI	Nondestructive inspection
NIAR	National Institute for Aviation Research
OH	Open hole
OHC	Open-hole compression
OHT	Open-hole tension
PFS	Picture-frame shear
RRX	Rank regression in X
RRY	Rank regression in Y
RTA	Room temperature ambient
RTW	Room temperature wet
SACC	Scatter Analysis Computer Code
SLS	Single-lap shear
SLS-C	Single-lap shear compression
SLS-T	Single-lap shear tension
SMT	Shear-moment torque
S/N	Stress to number of cycles

TAI	Tension after impact
TTU	Through-transmission ultrasonic
UNI	Unidirectional lay-up
VID	Visible impact damage
VNRS	V-notch rail shear

EXECUTIVE SUMMARY

Over the past 25 years, the use of advanced composite materials in aircraft primary structures has increased significantly. In 1994, with the Advanced General Aviation Transport Experiments program, the National Aeronautics and Space Administration and the Federal Aviation Administration revitalized the use of composites in general and commercial aviation. Driven by the demand for fuel-efficient, light-weight, and high-stiffness structures that have fatigue durability and corrosion resistance, modern large commercial aircraft are designed with more than 50 percent composite materials. Although there are key differences between metal and composite damage mechanics and durability concerns, the certification philosophy for composites must meet the same structural integrity, safety, and durability requirements as that of metals. Despite the many advantages, composite structural certification becomes challenging due to the lack of experience in large-scale structures, complex interactive failure mechanisms, sensitivity to temperature and moisture, and scatter in the data, especially in fatigue. The overall objective of this research was to provide guidance into structural substantiation of composite airframe structures under repeated loads through an efficient approach that weighs both the economic aspects of certification and the timeframe required for testing, while ensuring safety. The research methodology reported here consisted of combining existing certification approaches used by various aircraft manufacturers with protocols for applying these methodologies. This will permit extension of the methodologies to new material systems and construction techniques.

This study included data for materials commonly used in aircraft applications, including adhesives and sandwich construction. Testing consisted of various element-type tests and concentrated on tests that were generic in nature and were representative of various loading modes and construction techniques. In addition, the database available at the National Institute of Aviation Research was included to expand the data for the scatter analysis. Three different techniques were used for scatter analysis of fatigue data: individual Weibull, joint Weibull, and the Sendeckyj wearout model. Procedures to generate reliable and economical scatter and load-enhancement factors necessary for a particular structural test by selecting the design details representing the critical areas of the structure is outlined with several examples and case studies. The effects of laminate stacking sequence, test environment, stress ratios, and several design features, such as sandwich and bonded joints on the static-strength and fatigue-life shape parameters, are discussed with detailed examples. Furthermore, several analytical techniques for obtaining these shape parameters are discussed with examples. Finally, the application of load-enhancement factors and life factors for a full-scale test spectrum without adversely affecting the fatigue life and the damage mechanism of the composite structure is discussed.

1. INTRODUCTION.

In the early 1970s, composite materials were introduced to airframe structures to increase the performance and life of the airframe. In 1977, the National Aeronautics and Space Administration (NASA) Advanced Composite Structures Program introduced the use of composites in primary structures in commercial aircraft, i.e., the Boeing 737 horizontal stabilizer [1]. In 1994, the Advanced General Aviation Transport Experiments consortium, led by NASA and supported by the Federal Aviation Administration (FAA), industry, and academia, revitalized composite material product development in general aviation by developing cost-effective composite airframe structures. Modern improved composite materials and matured processes have encouraged commercial aircraft companies to increase the use of composites in primary and secondary structures. Driven by the demand for fuel-efficient, light-weight, and high-stiffness structures that have fatigue durability and corrosion resistance, the Boeing 787 Dreamliner is designed with more than 50 percent composite structure, marking a striking milestone in composite usage in commercial aviation. Meanwhile, the Airbus A350 commercial airplane is being designed with a similar percentage of composite materials in its structure. Figure 1 shows the use of composites in several commercial aircraft applications.

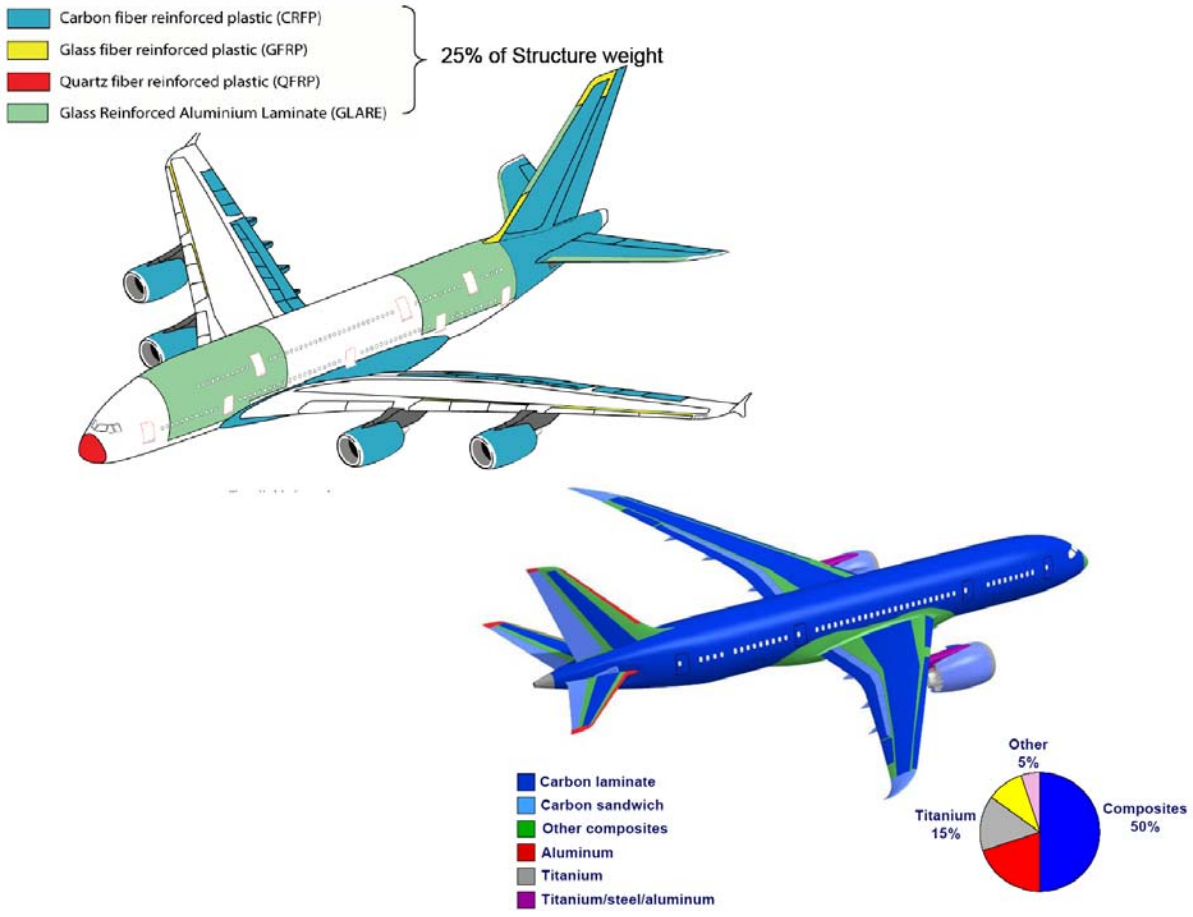

Figure 1. Composite Materials Applications in Commercial Aircraft

Although there are key differences between metal and composite damage mechanics and durability concerns, the certification philosophy for composites must meet the same structural integrity, safety, and durability requirements as for metal aircraft. Over the years, composite and hybrid structural certification programs have adopted methodologies used for metal structures that are based on several decades of experience in full-scale structural certification and service. Despite the advantages, such as high specific weight, tailorability, and fatigue resistance, composite structural certification becomes challenging due to the lack of experience with large-scale structures, complex interactive failure mechanisms, sensitivity to temperature and moisture, and scatter in the data, especially relative to fatigue.

Most current fatigue life assessment methodologies for advanced composite structures rely on empirical stress to number of cycles (S/N) data in the lower levels of the building block. Variation of material characteristics for different fiber-resin systems, lay-up configurations, environments, loading conditions, etc., often make the analysis and testing of composites challenging. Anisotropic heterogeneous characteristics and a change in failure modes over the fatigue life, as well as multiple failure mechanisms that interact with each other, make it challenging to predict damage growth in composite structures. Consequently, most of the damage mechanisms and wearout approaches (discussed later in this section) also depend on empirical data for refinement or calibration. Some approaches only discuss failure progression under certain loading configurations and often specific to a material system. Fatigue life assessment methodologies that are based on empirical data can be separated into two categories:

- Reliability or scatter analysis
- Curve-fit based on flaw growth

Both approaches require a considerable amount of empirical data. However, the first approach was extended to several programs through the concept of shared databases and in terms of general scatter of composite data in contrast to metal data. The cumulative effects of data scatter in different design details of a particular structure are analyzed in the lower levels of the building block in terms of reliability to determine a safe design service goal or life representative of the weakest member of the population after a specified life in service. The major limitation in the second approach is that it is often specific to a certain material system, a loading configuration, and failure mechanism. As part of the U.S. Navy F/A-18 certification, a probabilistic methodology was developed to certify composite structures with the same level of confidence as metallic structures [2]. This methodology was formulated to account for the uncertainties of applied loads as well as the scatter in static strength and fatigue life related to composite structures. Over the years, several composite structural certification programs employed this certification methodology, which was developed for materials and test methods that were considered current at the time. Since then, materials and process techniques as well as test methods for evaluating composites have evolved. Consequently, test data often display significantly less scatter and therefore higher reliability. Thus, the probabilistic approach employed by Whitehead, et al. [2], can be re-evaluated for newer material forms and to represent structural details of current aircraft structures to obtain improved life and load-enhancement factors [3 and 4].

Current regulations require airframes to demonstrate adequate static strength, fatigue life, and damage tolerance capability by testing and/or analysis with a high degree of confidence. These requirements are intended to account for uncertainties in usage and scatter exhibited by materials. Analysis is the primary means of structural substantiation for most aircraft certification programs. It is expected that the analysis is supported by appropriate test evidence.

To develop a certification methodology for composite structures that has the same level of reliability as observed in metal certification approaches, accounting for the inherent difference between metal and composites, the FAA and U.S. Navy developed a certification approach for bolted composite structures [2 and 5] as part of the U.S. Navy F/A-18 certification (figure 2). This methodology is referred to as NAVY, or the load-life combined approach, throughout this report.

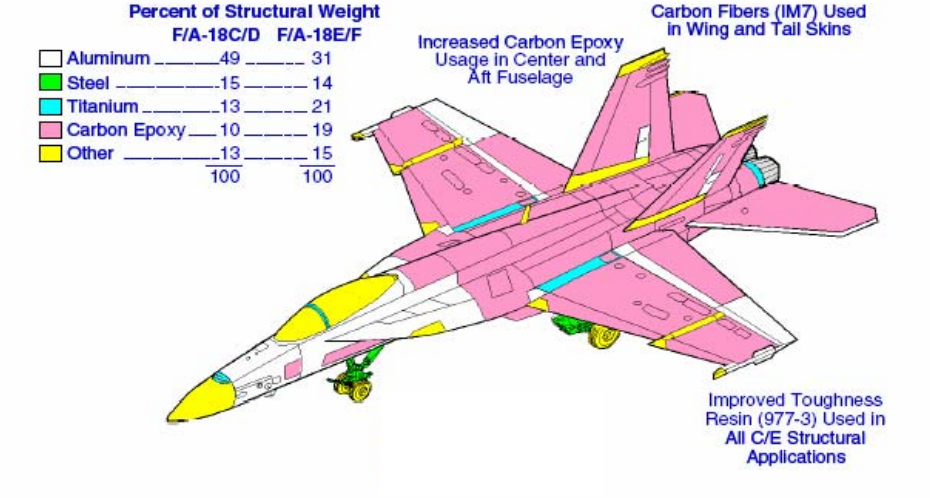

Figure 2. Material Distribution for U.S. Navy F-18 Aircraft [6]

This approach adopted two key requirements in metallic aircraft certification: (1) the full-scale static test article must demonstrate a strength that is equal to or exceeds 150 percent of the design limit load (DLL), and (2) the full-scale fatigue test article must demonstrate a life that is equal to or exceeds twice the design service life. This approach analyzes the data scatter in the static strength and fatigue life of composites to establish a certification methodology that has the same level of reliability as for metal structures. Furthermore, this approach attempts to address the issues related to hybrid (composite and metallic) structures through a combined approach referred to as the load-life approach, which will be further discussed in this report. The load-life approach was developed for what, at that time, was current composite usage and did not explicitly account for the damage in composite structures or adhesively bonded structural details. Kan and Whitehead [7] proposed a damage tolerance certification methodology to determine the reliability of impact damage on a composite structure and to calculate the allowable impact threat at a given applied load and specified reliability. Subsequent application of this methodology on

a U.S. Navy F/A-18 inner-wing structure demonstrated successful damage tolerance capabilities during certification.

The NAVY load-life methodology was adopted by Shah, et al. [8], for certification of a stiffener run-out detail. They found that the static-strength and life shape parameters are similar to that developed for the NAVY approach. This research successfully demonstrated the combined load-life approach for large-component tests. The applicability of the U.S. Navy damage tolerance approach of Kan and Whitehead [7] to certification of general and commercial aircraft was investigated by Kan and Dyer [9]. The Kan and Dyer study showed that the U.S. Navy damage-tolerance approach based on military requirements is too severe for the all-composite LearFan 2100 structure.

Early developments of the B-737 graphite/epoxy horizontal stabilizer [10] and the Airbus A310 [11] and A320 [12] all-composite vertical tail used the combined load-life approach for full-scale demonstrations. The no-growth, damage-tolerant design concept was also adopted whereby a composite structure must demonstrate the ability to contain intrinsic manufacturing defects and the maximum allowable service damage(s) in adverse operational conditions and throughout the design life of the structure. Following the early approach developed for the NASA/B-737 horizontal stabilizer, B-777 empennage certification was primarily based on analysis supported by coupon and component test evidence [13]. The certification process included general requirements for environmental effects in design allowables, static strength, and fatigue and damage tolerance with a no-growth approach. By making predictions prior to testing, such demonstrations contribute to a solid basis for acceptance of "certification by analysis" by the FAA and the aviation industry. This is consistent with current certification practices that allow the use of analysis for certification when supported by tests.

Several all-composite business aircraft, including the Beechcraft 2000 Starship, evolved in the early 1980s and completed FAA damage tolerance certification requirements [14]. The all-composite Beechcraft Starship was certified in 1989 using the damage tolerance approach, identifying environmental effects and concerns related to bonded joints. To meet FAA damage tolerance requirements, major structural modifications had to be made to the wing. For full-scale durability and damage tolerance tests, a combined load-life approach based on flaw-growth threshold stress was employed [15]. The environmental effects were addressed by an analytical approach validated by testing.

Under the Composite Affordability Initiative, Kan and Kane [16] explored the feasibility of extending probabilistic methodology for adhesive-bonded composite structures. Three areas were thoroughly reviewed to determine maturity level: (1) probability theories and probabilistic methods, (2) probabilistic structural analysis tools, and (3) probabilistic structural criteria and requirements. The Composite Affordability Initiative identified that the same level of structural reliability with equivalent level of confidence can be achieved by the probabilistic method compared to the deterministic method.

Sumich and Kedward [17] investigated the use of the wearout model, on the basis of its applicability to matrix-dominant failure modes to examine the fatigue performance of the Rotor Systems Research Aircraft X-wing vehicle. Wearout models assume that structural degradation

occurs with use and can be monitored by measuring parameters such as residual strength and stiffness. Halpin, et al. [18], discussed this methodology in the early 1970s, and several certification programs, such as the A-7 outer wing and F-16 empennage, have adopted this methodology for composite structures. This method, which was applied to metal crack growth, determines fatigue failure when pre-existing damage grows until the specimen can no longer support the applied cyclic load. In addition, the residual strength of runout is related to crack length through fracture mechanics. This approach was improved by Sendeckyj [19] using a deterministic equation that converts static, fatigue, and residual strength data into a pool of equivalent static-strength data. Sendeckyj's basic model assumes that the failure in a constant-amplitude fatigue test occurs when the residual strength is equal to the maximum cyclic-fatigue load. This pooling technique for fatigue data is useful for cases where there are not enough fatigue data in individual stress levels for Weibull analysis, which requires a minimum of six specimens in each stress level. This model was further improved for pooling fatigue tests with multiple stress ratios [20], but was not validated since it requires a significant amount of test data. Stress ratio, or R ratio, is the ratio of minimum-to-maximum cyclic stress in a fatigue test.

O'Brien and Reifsnider [21] studied fatigue life analytically using the fatigue modulus concept. This approach assumed that fatigue failure occurs when the fatigue secant modulus (residual stiffness) degrades to the secant modulus at the moment of failure in a static test. In this study, stiffness reductions resulting from fatigue damage were measured for unnotched $[\pm 45]_s$, $[0/90]_s$, and $[0/90/\pm 45]_s$ boron/epoxy laminates. Degradation in the various in-plane stiffnesses (axial, shear, and bending) was measured using a combination of uniaxial tension, rail shear, and flexure tests. Damage growth and stiffness loss were identified to be load-history dependent. Hence, the secant modulus criterion was not a valid criterion for general applications. A similar study was conducted on the fatigue behavior of $[0/\pm 45/90]_s$ glass/epoxy laminate by Hahn and Kim [22] in which the secant modulus was used as a measure of damage extent.

Following an extensive review of different damage models, Hwang and Han [23] identified various cumulative damage models using several physical variables, such as fatigue modulus and resultant strain. They introduced a new concept called "fatigue modulus," which is defined as the slope of applied stress and resultant strain at a specific cycle [24]. Fatigue modulus degradation assumes that the fatigue modulus degradation rate follows a power function of the fatigue cycle. The theoretical equation for predicting fatigue life is formulated using the fatigue modulus and its degradation rate. This relation is simplified by the strain failure criterion for practical applications. Mahfuz, et al. [25], analytically studied the fatigue life of an S2-glass/vinyl-ester composite using the fatigue modulus concept. This study revealed that the fatigue modulus is not only a function of loading cycle but also a function of applied stress level and thickness of the test specimen. This life-prediction methodology requires two parameters that are obtained empirically either at two different stress levels or two different fatigue lifetimes.

Halpin, et al. [26], suggested that the fatigue behavior of composites should be based empirically under particular design spectra. The main disadvantage of such an approach is that test results are specific to a loading spectrum. Also, a large number of test data is required for a complete analysis, like the extensive fatigue sensitivity study conducted by Jeans, et al. [27], on bolted and bonded composite joints under various loading spectra. For metals, Miner's rule is often used to

study the cumulative damage under a loading spectrum. However, Rosenfeld and Huang [28] conducted a fatigue study with different stress ratios to determine the failure mechanisms under compression of graphite/epoxy laminates and showed that Miner's rule fails to predict composite fatigue under spectrum loading. This is confirmed by several authors in the composite community. A study conducted by Agarwal and James [29] on the effects of stress levels on fatigue of composites confirmed that the stress ratio had a strong influence on the fatigue life of composites. Further, they showed that microscopic matrix cracks are observed prior to gross failure of composites under both static and cyclic loading.

For practical consideration, Yang and Du [30] investigated the possibility of statistically predicting the fatigue behavior of composites under service-loading spectra, based on some baseline constant-amplitude fatigue data. Although such a phenomenological statistical model does not account for the intrinsic failure mechanisms that are quite complex in composite materials, it can be very simple for practical applications and requires significantly less empirical effort.

Kassapoglou [31] presented a probabilistic approach for determining fatigue life for composite structures under constant-amplitude loading. This approach assumes that the probability of failure during any cycle is constant and equal to the probability of failure obtained from static test results and associated statistically quantified scatter. This methodology does not require any fatigue data for calibration or for the expression of the cycles to failure as a function of stress ratio. Comparison of fatigue life predictions for several stress ratios with a number of experimental data shows good correlation. However, the assumptions used in this model neglect the complex progressive damage mechanism that takes place during repeated loading.

1.1 BACKGROUND FOR CURRENT APPROACH.

The current practice is to test composite structures with loads that are enhanced to reduce long test duration requirements. This accounts for the data scatter observed in composites relative to metals. The load-life approach proposed for U.S. Navy F/A-18 certification [2] is used such that the same level of reliability as for metal structures can be achieved. Compared to the metal static and fatigue data, composite materials exhibit high data scatter due to their anisotropic heterogeneous characteristics, such as lay-up, manufacturing defects and imperfections, test complications, and environment. To interpret the information in a meaningful manner and to incorporate any of their effects into the certification of composite structures, the life-factor approach and the load-enhancement factor (LEF) approach are commonly used and require composite scatter analysis, which is described in this report. The life-factor approach, which has been successfully used for metallic structures to assure structural durability, accounts for the scatter in life (S/N) data in terms of the shape parameter of the population. The life shape parameter (often referred to as the modal life shape parameter) is obtained by analyzing the distribution of the shape parameters corresponding to S/N curves representing different design details of the structure. The life factor corresponds to the relation between the central tendency (mean) of the population and the extreme statistics (allowable). The underlying objective of the life-factor approach is to ensure that the design service goal or life is representative of the weakest member of the population after a specified life in service. Thus, a successful repeated load test to mean fatigue life would demonstrate the B-basis reliability on the design lifetime. The NAVY approach showed that the life shape parameters of metal and composite are 4.00 and

1.25, respectively, and they correspond to life factors of 2.093 and 13.558, respectively, for B-basis reliability [2]. Therefore, due to the large scatter in composite test data, a composite structure is required to test additional fatigue life to achieve the desired level of reliability, i.e., a test duration of more than 13 design lifetimes is required for composite in contrast to two design lifetimes for metal to achieve B-basis reliability.

An alternative approach to the life factor, which requires an excessive test duration, is to increase the applied loads in the fatigue spectrum so that the same level of reliability can be achieved with a shorter test duration [2]. This approach is referred to as the LEF approach and was derived from combining the life factor and the static factor (ratio of mean-to-allowable fatigue strength) at one lifetime to form a relationship between the LEF and the test duration. The static factor is defined in terms of a static-strength shape parameter that is obtained by analyzing the distribution of the shape parameters corresponding to static-strength data sets representing different design details of the structure as described in section 4. The formal relationship between the LEF and the test duration provides the flexibility of conducting the durability test of a composite structure with different LEFs and corresponding test durations to achieve the desired reliability. Although the materials, processes, lay-up, loading modes, failure modes, etc., are significantly different, most current certification programs use the load-life factors generated for the U.S. Navy F/A-18 certification program. Lameris [3] showed that both LEFs and life factors can be significantly reduced by using strength and life shape parameters generated for materials, processes, loading modes, failure modes, etc., applicable to a specific structure. However, guidance for developing these shape parameters is greatly needed.

Although fatigue life is adversely affected by damage (notch), the scatter in damaged composites, both in static and fatigue, tends to decrease due to localized stress concentration. This will result in lower life and load-enhancement factors. Therefore, scatter analysis of coupons/elements in lower levels of building blocks can be used to develop a synergy among the life factor, LEF, and damage in composites. This approach is beneficial for the damage tolerance phase of full-scale substantiation and minimizes the risks associated with the introduction of large damage to durability test articles.

Development of scatter analysis applicable to current composite materials and processes using improved test methodologies demonstrate lower requirements for the life factor and LEFs. Introduction of damage philosophy into the scatter analysis further reduces these factors. The probabilistic approach employed in the NAVY load-life combined approach shows the potential use of improved shape parameters for estimating the effects of design changes, i.e., gross weight changes, on design life. This requires a probabilistic approach to redefine basis (A- or B-basis) fatigue life requirements set forth in the load-life combined approach to any deviation from the life (i.e., reduction in life factor due to damage introduction) or load factor (i.e., high spectrum fatigue loads due to gross weight change). For a full-scale test that is conducted using a higher LEF or is completed more than the required test duration, this technique can be used to redefine original design service goals (number of hours equivalent to one life) associated with the fatigue spectrum.

1.2 RESEARCH OBJECTIVES AND OVERVIEW.

The research methodology discussed here consists of combining existing certification approaches utilized by various aircraft manufacturers with protocols for applying these methodologies. This will extend the methodologies to new material systems and construction techniques. This report includes data for materials commonly used in aircraft applications, including adhesives and sandwich construction. The testing consisted of various element-type tests and concentrated on tests that were generic in nature and representative of various loading modes and construction techniques. Three different techniques are discussed for scatter analysis of fatigue data: individual Weibull, joint Weibull, and the Sendeckyj wearout model. Procedures to generate reliable and economical scatter and LEFs necessary for a particular structural test by selecting the design details representing the critical areas of the structure are outlined with several examples and case studies. The effects of laminate stacking sequence, test environment, stress ratios, and several design features, such as sandwich and bonded joints, on the static-strength and fatigue shape parameters are discussed with detailed examples. Furthermore, several analytical techniques for obtaining these shape parameters are discussed with examples. Finally, the application of LEFs and life factors on a full-scale test spectrum without adversely affecting the fatigue life and the damage mechanism of the composite structure is discussed.

The data from this report describes the first phase of a research program outlined in figure 3. The key objective of this research was to develop a probabilistic approach to synthesizing the life factor, LEF, and damage in composite structures to determine the fatigue life of a damage-tolerant aircraft. This methodology was extended to the current certification approach to explore extremely improbable high-energy impact threats, i.e., damages that reduce the residual strength of aircraft to limit-load capability and allow incorporating certain design changes into full-scale substantiation without the burden of additional time-consuming and costly tests. Research was conducted in three phases (figure 3):

- Load-life combined approach
- Damage tolerance and flaw-growth tests
- Load-life damage (LLD) hybrid approach

The first subtask of this research phase was intended to generate a database of fatigue life data for several composite material systems that are commonly used in general aviation. The second subtask in this phase was to add static-strength shape parameters to the database and generate improved LEFs for several example materials. These data were then used to generate necessary load-life combined data, for example, full-scale demonstrations included in the final stage of the research. The improvements in materials and processes and test methods produced life factors and LEFs lower than the values commonly used in most certification programs based on the NAVY approach. Data gathered in this phase were used to provide guidance for generating safe and reliable LEFs and life factors pertaining to a specific structure. In addition, a user-friendly computer code that can be used for scatter analysis of composites was developed. This code alleviates misinterpretation of any statistical or mathematical processes during the analysis and provides guidance for selecting different techniques appropriate for a particular application. This report only contains the data generated during the first phase of the research.

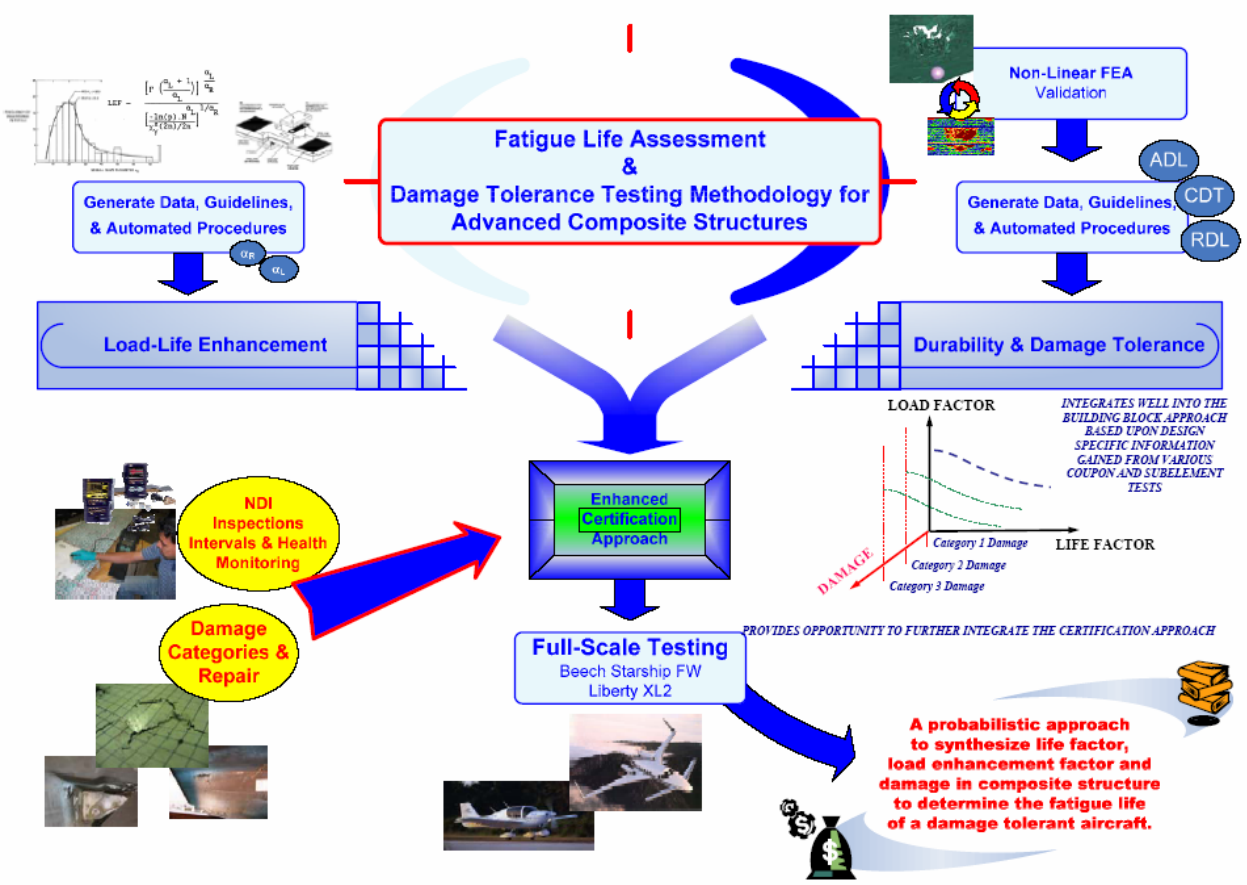

FEA = Finite element analysis
ADL = Allowable damage limit
CDT = Critical damage threshold
RDL = Repairable damage limit

Figure 3. Overview of Research

2. EXPERIMENTAL PROCEDURE.

The primary goal in the first phase of the research was to interrogate the methodology for the development of Weibull parameters to be used in the load-life combined approach. Two key parameters were needed: static-strength and the fatigue-life shape parameters. The first subtask in this phase was to investigate the life factor for several composite material systems using the fatigue shape parameter. Then, using fatigue-life and static-strength shape parameters, the LEF for several material systems was calculated. Finally, a comparison of the load-life approach for several material systems and design scenarios was shown with two benchmark case studies: the Beechcraft Starship forward wing and Liberty XL2 fuselage. The second phase incorporated different damage categories into a full-scale test article and investigated the effects of damages on life factors and LEFs. The final phase was intended to develop a hybrid approach using the life factor, LEF, and damage in the composite. Once the load-life factors were generated for the Beechcraft Starship material, full-scale fatigue tests of the last phase were performed to verify the LLD approach.

2.1 MATERIAL SYSTEMS.

The three main material systems studied for the purpose of generating static and fatigue shape parameters were Cytec AS4/E7K8 plain-weave fabric (AS4-PW), Toray T700SC-12K-50C/#2510 plain-weave fabric (T700-PW), and 7781/#2510 8-Harness glass-fiber fabric (7781-8HS) [32]. The test data for these three materials are referred to as FAA-LEF data throughout this report. In addition to the FAA-LEF data, a detailed static scatter analysis was conducted on the following materials available through an extensive laminate database [33]: Toray T700G-12K-31E/#2510 unidirectional tape and T700SC-12K-50C/#2510 plain-weave fabric, Advanced Composites Group (ACG) MTM45/AS4C 12K unidirectional tape and MTM45/AS4C 6K 5-harness graphite fabric, and Nelcote® (formally FiberCote) T700-24K/E765 unidirectional tape and T300-3K/E765 plain-weave fabric. This data set is referred to as the FAA lamina variability method (FAA-LVM) data throughout this report and was generated to analyze the LVM [34] on generating laminate allowables.

In addition to the above two data sets, fatigue scatter analysis for Loctite, Hysol EA9696, and PTM&W ES6292 adhesive systems were included from the data obtained from FAA research to investigate the durability of adhesive joints [35]. These test specimens were fabricated according to an ASTM standard test method for thick-adhered metal lap-shear joints to determine the shear stress-strain behavior of adhesives in shear by tension (ASTM D 5656). This data set is referred to as FAA-D5656 data throughout this report. Finally, element test data of adhesively bonded composite joints that were loaded in picture-frame shear (PFS) and single-lap shear (SLS) [36] test configurations were included in the analysis. Data from this database are referred to as the FAA effects of defects (FAA-EOD) data throughout this report. Once the scatter analysis was completed, LEFs were generated, combining scatter analysis of the above data sets for available fatigue cases.

The Beechcraft Starship was primarily fabricated using an AS4/E7K8 epoxy material system (original manufacturer: U.S. Polymeric). Hercules AS4 fibers are continuous carbon filaments made from a PAN precursor, and their surface is treated to improve handling characteristics and structural properties. Typical fiber tensile modulus and strength are 34 Msi and 550 ksi [37]. The E7K8 medium-flow epoxy resin system has good tack characteristics for handling and a 20-day out-time at ambient temperature. The AS4/E7K8 3K plain weave material system (AS4-PW) has an aerial weight of 195 g/m^2, a typical cured-ply thickness of 0.0087 inch, and a low-exotherm profile for processing thick parts. This material is currently being used by Hawker Beechcraft and Cessna Aircraft in Wichita, Kansas, for several aircraft applications.

2.2 TEST MATRICES.

Testing included various element-type tests and concentrated on generic tests that would be representative of various loading modes and construction techniques. In general, this program primarily focused on stress ratios within the wing and fuselage envelopes for the development of the Weibull fatigue shape parameter. Using the data gathered in the lamina, laminate, and element tests, the methodology used to develop the Weibull static-strength parameters was compared for various scenarios.

Commonly used laminate stacking sequences—hard (50/40/10 for unidirectional tape and 40/20/40 for fabric), quasi-isotropic (25/50/25), and soft (10/80/10) laminate constructions—were used for the FAA-LEF database (table 1).

Table 1. Laminate Configurations for FAA-LEF Database

Laminate	Lay-Up % 0°/45°/90°	Ply Stacking Sequence	Total Plies
Hard	40/20/40 (weave)	$[0/90/0/90/45/-45/90/0/90/0]_S$	20
Quasi-isotropic	25/50/25	$[(45/0/-45/90)_2]_S$	16
		$[(45/0/-45/90)_4]_S$	32
Soft	10/80/10	$[45/-45/90/45/-45/45/-45/0/45/-45]_S$	20
		$[45/-45/90/45/-45/45/-45/0/45/-45]_{2S}$	40
All ±45	0/100/0	$[(45/-45)_5]_S$	20

In addition, sandwich specimens were fabricated with three-ply facesheets (plies in the 0° direction) with a 0.25-inch-thick HRH-10 Nomex core. Test methods and fixture requirements for FAA-LEF tests are shown in table 2. Although these test methods are recommended for static testing, a similar test setup was used for fatigue tests. Double-notched compression (DNC) specimens were modified to have similar geometry to open-hole compression (OHC) (12 x 1.5 inches), and the OHC fixture was used for both static and fatigue testing. Similarly, ASTM D 3165 specimens were modified to have the same overall specimen dimensions with a 1.5-inch overlap so the OHC fixture could be used for compression loading.

Table 2. The FAA-LEF Test Methods and Fixture Requirements

Test Description	Abbreviation	Test Method	Test Fixture
Tension, open hole	OHT	ASTM D 5766	No
Compression, open hole	OHC	ASTM D 6484	Yes
Double-notched compression	DNC	Modified ASTM D 3846	Yes
Single-lap shear, tension	SLS-T	Modified ASTM D 3165	No
Single-lap shear, compression	SLS-C	Modified ASTM D 3165	Yes
Sandwich four-point bend	4PB	ASTM C 393	Yes
Compression after impact	CAI	ASTM D 7137	Yes
Tension after impact	TAI	Modified ASTM D 3518	No

The basic FAA-LEF test matrix is shown in table 3. All 10/80/10 laminates in this table were fabricated with a 20-ply stacking sequence, as shown in table 1. To support the full-scale demonstration and the damage tolerance efforts shown in figure 3, a supplemental test matrix was added for AS4-PW (table 4). These test matrices represent different lay-ups, test environments, loading modes, bonded joints, and sandwich structures. Sandwich specimens were fabricated with HexWeb® HRH-10 manufactured from Nomex® aramid fiber sheets. This core was selected because of its application in the Beechcraft Starship.

Table 3. The Basic FAA-LEF Test Matrix

Laminate	Test Method	Loading Condition	Standard	Static Test Environment		RTA—Cyclic Test R-Ratio (Three Stress Levels)			
				RTA	ETW	-0.2	0	-1	5
10/80/10 Laminate	OH	Tension	ASTM D 5766	6	6	18	18		18
		Compression	ASTM D 6484	6	6			18	
	SLS (t = 0.01″)	Adhesive In-Plane Shear	Modified ASTM D 3165	6	6				
	SLS (t = 0.06″)			6	6				
	DNC	Interlaminar Shear	Modified ASTM D 3846	6	6	18		18	
Sandwich	4PB	Flexure	Modified ASTM C 393	6	6		18		

RTA = Room temperature ambient
ETW = Elevated temperature 180°F, wet
OH = Open hole

The 10/80/10 CAI specimens in table 4 were fabricated with the 40-ply stacking sequence, while the 25/50/25 CAI specimens were fabricated using the 32-ply stacking sequence, as shown in table 1. The 25/50/25 CAI specimens were machined to 6 inches by 9 inches to minimize the edge effects for larger damages and to leave room for damage propagation during cyclic loading. Extensive testing of coupons [38] and components [39] of adhesive joints has shown a significant decrease in static strength for thick bondlines. Thus, the adhesive joints with different bondline thicknesses were included in the test matrix. ASTM D 3518 was modified to have a 4-inch width for the TAI specimen, with impact at the center.

Table 4. Supplemental FAA-LEF Test Matrix

Laminate	Test Method	Loading Condition	Standard	Static Test Environment		Cyclic Test R-Ratio (Three Stress Levels)			
				RTA	ETW	-0.2	0	-1	5
10/80/10 Laminate	CAI	Compression BVID	ASTM D 7137	6					18
		Compression VID		6					18
25/50/25 Laminate	OH	Compression RTA	ASTM D 6484	6				18	
		Compression ETW			6				
	CAI	Unimpacted RTA	ASTM D 7137	6					
		Compression BVID/RTA		6					18
		Compression VID/RTA		6					18
		Compression LID/RTA		6					18
40/20/40 Laminate	CAI	Compression VID	ASTM D 7137	6					18
0/100/0 Laminate	OH	Compression RTA	ASTM D 6484	6				18	
	TAI	Shear BVID/RTA	Modified ASTM D 3518	6					18
		Shear VID/RTA		6					18

RTA = Room temperature ambient
ETW = Elevated temperature 180°F, wet
LID = Large impact damage

2.3 EXPERIMENTAL SETUP.

This section contains information regarding the experimental setup and equipment used for impact, nondestructive inspection (NDI), and residual strength tests of the FAA-LEF test specimens.

2.3.1 Impact Tests.

CAI and TAI test specimens were impacted using an Instron Dynatup 8250 drop-weight impact tester (figure 4). The impact force was measured using a piezoelectric load cell attached to the impact mass assembly. This impact tester was equipped with a pneumatic rebound catch

mechanism, which prevents secondary impacts on the test specimens, and a photo-detector/flag system, which provides impact velocity information. Data acquisition software, which runs on a computer connected to the drop-weight impact tester, collected and reduced the impact test data. A sensor (flag), which was placed close to the impact location, triggered the data acquisition system a few milliseconds prior to the impact event. This sensor and another flag placed a known distance away were used for calculating impact velocity (velocity = distance/time).

Prior to impacting, specimens were placed in the support fixtures, as shown in figure 5, and held rigidly. These fixtures use dowel pins for aligning the specimens. The total impact event duration was at most 10 milliseconds. Therefore, a very high-frequency triggering mechanism, an Instron Dynatup impulse data acquisition system, was used to collect data during the impact event.

Figure 4. Instron Dynatup Drop-Weight Tester

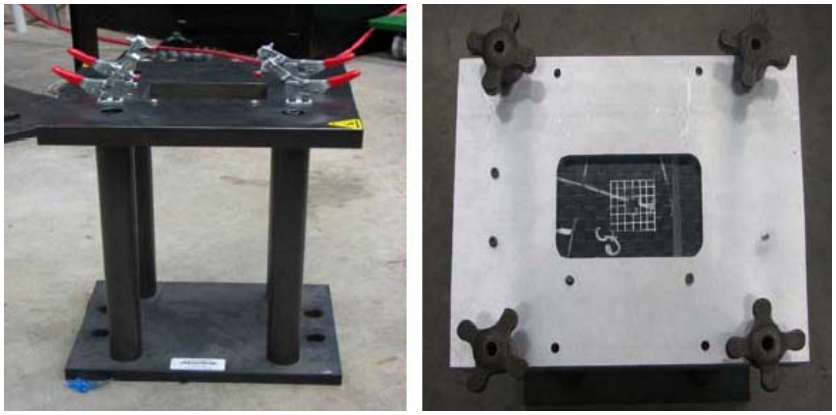

Figure 5. Support Fixture for CAI and TAI Impact Specimens

2.3.2 Nondestructive Inspections.

Impacted specimens were subjected to through-transmission ultrasonic (TTU) NDI that generated C-scans to quantify the planar-damaged areas using image analysis software (figure 6). Additional inspections techniques, e.g., microscopy and thermal imaging, were also used for the damage tolerance investigation. For those cases involving glass fiber composite, damage can be seen clearly with the naked eye due to the translucent nature of these fibers.

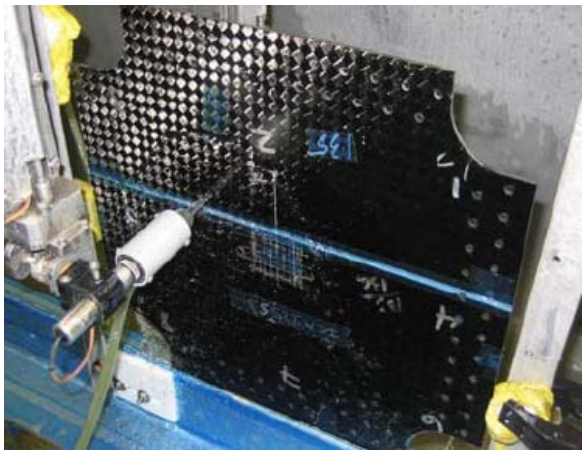

Figure 6. The TTU Scanning of PFS Test Specimen

In addition to TTU C-scans, test specimens were inspected with the Sonic 1200 ultrasonic flaw detector and BondMaster™ 1000 hand-held NDI inspection units while the specimens were in the test setup. The BondMaster™ 1000 is capable of resonance, mechanical impedance analysis (MIA), and pitch/catch mode, and the user has the ability to select the method best suited for inspecting a particular composite structure. The MIA technique, which was used for inspecting test specimens in this program, measures the stiffness and mass of the material under test and requires no coupling agents. The output was measured in both amplitude and phase. Both of these hand-held units are equipped with color displays and provide real-time data.

2.3.3 Full-Field Strain Evolution.

The ARAMIS photogrammetry full-field strain measurement system (figure 7) was used to measure localized buckling in the region of disbonds/defects. ARAMIS [40] is a noncontact, optical, three-dimensional deformation measuring system. It uses two high-definition cameras to track translation and rotation of the surface details (object characteristics) with subpixel accuracy. Surface details are obtained by applying a stochastic color pattern that follows surface displacement during loading. ARAMIS uses this pattern to recognize the surface structure and then uses digitized images from both cameras for triangulation of surface details (micro-pattern) to determine the precise location of each point. Therefore, this system has the capability of digitizing the precise shape (surface) of the structure during loading. The first set of coordinates for object characteristics is obtained in the undeformed stage. After load application, a new set of coordinates (digital images) is recorded. Then, ARAMIS compares the digital images and calculates the displacement and deformation of the object characteristics.

Figure 7. Portable Version of ARAMIS Photogrammetry System [40]

ARAMIS is capable of three-dimensional deformation measurements under static and dynamic load conditions to analyze deformations and the strain of real components. In addition, this system is able to eliminate the rigid-body motion component from the displacement results. Therefore, it can be used for specimens that exhibit large displacements. Strain sensitivity of the system is approximately 100-200 microstrains, and the scan area can be as large as 47 inches by 47 inches. Full-field displacement/strain data are then used to examine any propagation of the defects according to the procedures outlined by Tomblin, et al. [41], which assess the localized skin buckling (out-of-plane displacement) around the disbonded or delaminated region. The full-field strain evaluation of CAI specimens during static (figure 8) and fatigue loading was measured using the ARAMIS photogrammetry system.

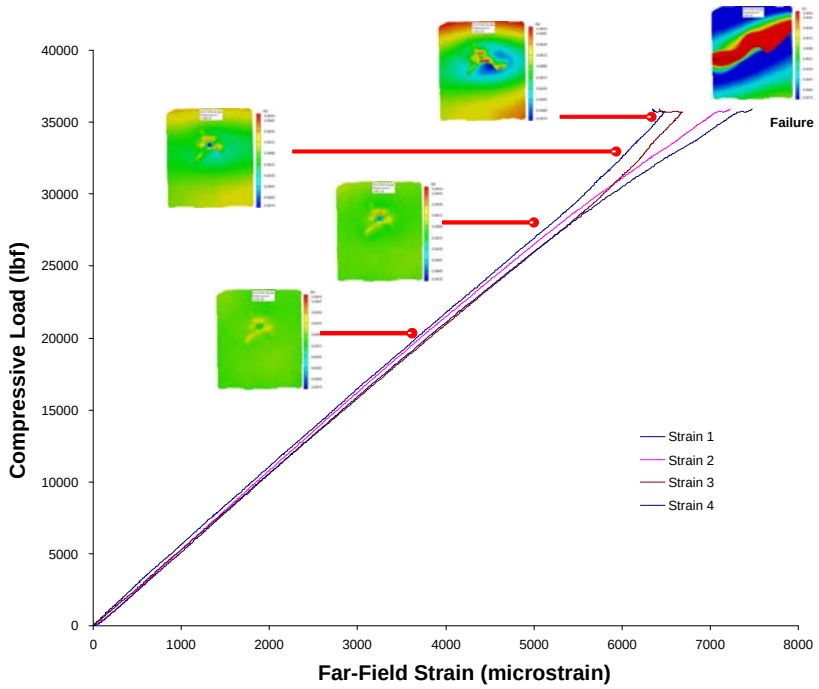

Figure 8. Damage Evolution of a CAI Specimen Under Static Loading

2.3.4 Static and Residual Strength Tests.

All static and residual strength tests were conducted using Material Test Systems (MTS) servohydraulic test frames. Test specimens that did not require fixtures were mounted to the test frame using a hydraulic grip assembly, as shown in figure 9. While gripping the specimens, the actuator was programmed in load-control mode to prevent unnecessary preloading due to grip pressure. Static tests were conducted in displacement-control mode at a rate of 0.05 in/min while acquiring data at a rate of 10 Hz.

Figure 9. The MTS Servohydraulic Test Frame

2.3.5 Fatigue Life Evaluation.

Fatigue tests were conducted in load-control mode at a frequency of 5 Hz. Fatigue specimens included several R-ratios that represented loading levels in different parts of the aircraft (section 2.2). Fatigue tests were conducted at three different stress levels with a minimum of six specimens per stress level to support the minimum requirements of individual Weibull analysis. Specimen compliance degradation was monitored throughout fatigue duration to examine damage evolution.

To investigate the damage progression, full-field strain data were interpreted according to the NDI method outlined by Tomblin, et al. [41]. Both ARAMIS and C-scan data were used to establish guidelines for determining the fatigue failure of specimens that was not obvious, e.g., a four-point bend sandwich specimen did not indicate any sign of complete delamination across the width and continued to hold applied cyclic loading (figure 10).

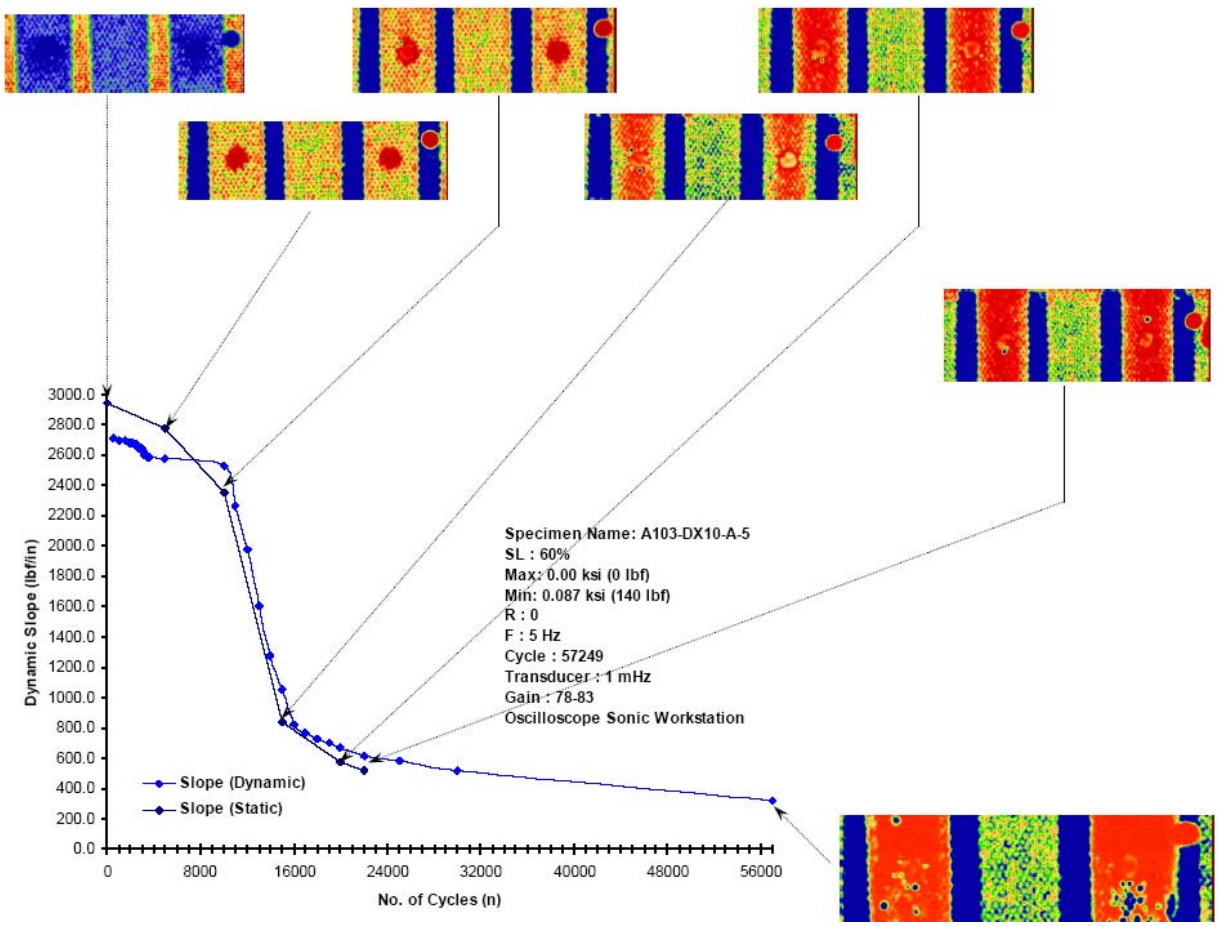

Figure 10. Compliance Change and Damage Area During Fatigue Tests of 4PB Sandwich Specimen

Antibuckling fixtures were used for compression fatigue specimens, such as open hole (OH), DNC, and CAI, to prevent premature failure. The OHC fixture, which is designed for static tests, indicated wear as the specimen compliance changed during the fatigue tests and required modifications to prevent further damage to the fixture and load misalignment during the fatigue tests. The change in temperature was monitored for several specimens with defects and was found to be insignificant, i.e., less than 10°F.

Several trial specimens were used at the beginning of each loading mode and lay-up to determine appropriate stress levels so that at least two provided fatigue failures. Fatigue loads for each specimen were calculated with respect to static strength using the actual specimen dimensions.

3. ANALYSIS OF COMPOSITE TEST DATA.

Compared to metal static and fatigue data, composite materials exhibited higher data scatter due to their anisotropic heterogeneous characteristics, such as lay-up, manufacturing defects and imperfections, test complications, and environment (figure 11). To interpret this information in a meaningful manner and to incorporate any effects of this into the certification of composite

structures, several approaches were used. Life factor, LEF, and the load-life combined approach are three of the commonly used approaches that require composite scatter analysis.

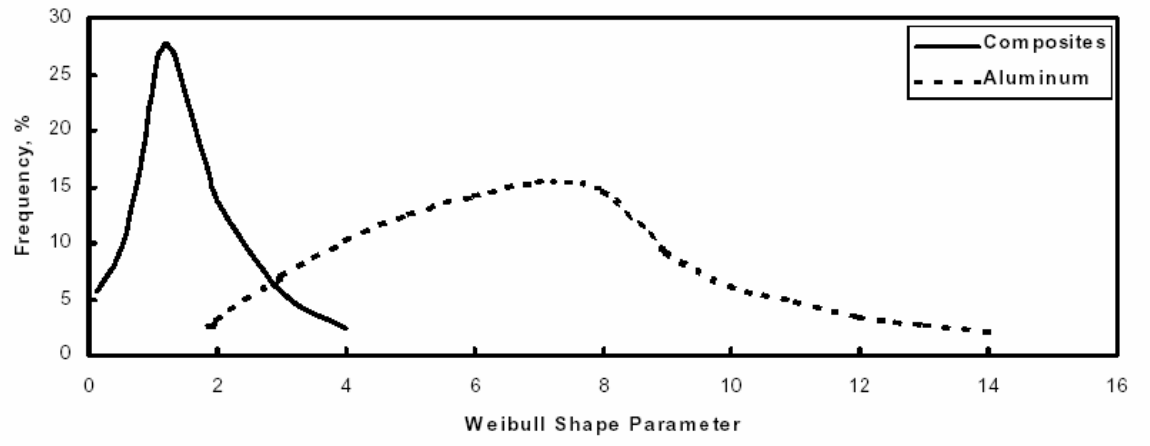

Figure 11. Life Scatter in Composites and Metal [2]

3.1 SCATTER ANALYSIS.

The primary goal in scatter analysis of composites is to interpret the variability in data in lower levels of the building blocks of testing and translate the statistical significance of such phenomenon into full-scale test substantiation. To determine the shape parameters for static strength and fatigue life for the purpose of full-scale test substantiation, test matrices must be designed so that at least the design details and loading modes of critical locations of the structure are represented by coupon and/or element tests. The influence of material, lay-up sequence, loading mode, sandwich construction, joints, environmental effects, etc., is typically considered during static-strength scatter analysis. Fatigue analysis includes the influence of the stress ratio in addition to the above-mentioned design details.

Scatter in composites can be analyzed as Weibull distribution or normal distribution. Since the shape parameter provides information with respect to the data scatter, the two-parameter Weibull distribution is commonly used in composite static and fatigue scatter analyses. Fatigue scatter in composite test data can be analyzed using several different techniques. These techniques are mainly subdivided into two categories: individual analysis and pooling. Joint Weibull and Sendeckyj are the two pooling techniques discussed in this report.

First, the shape parameters corresponding to the different data sets representing different design detail (denoted by $\hat{\alpha}$) are obtained using Weibull analysis; then, the shape and scale parameters, α and β, corresponding to the Weibull distribution of $\hat{\alpha}$'s are used to calculate the modal or mean $\hat{\alpha}$, which is referred to as the static-strength or fatigue-life shape parameter. To be conservative, the modal value of the distribution of shape parameters is selected as the strength or life shape parameter, rather than the mean value (figure 12), and this is referred to as the modal static-strength shape parameter (MSSP) or modal fatigue-life shape parameter (MLSP), respectively.

Determination of fatigue life scatter requires a large number of test replications at different stress levels. To reduce cost and test duration while maintaining the reliability of data analysis, it is recommended that the fatigue scatter analysis be conducted using pooling methods such as the joint Weibull or Sendeckyj wearout analysis.

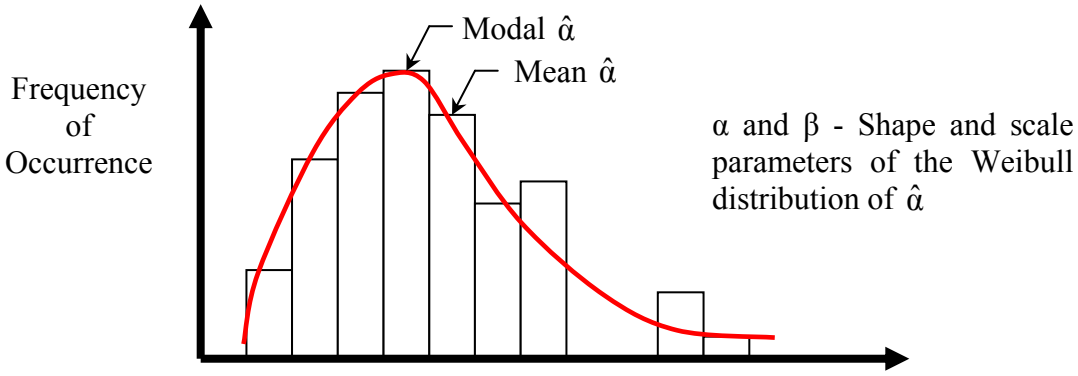

Figure 12. Scatter Analysis Using Weibull Distribution of Shape Parameters

3.1.1 Individual Weibull Method.

Weibull distribution is used in statistical analysis of composites, especially for small samples, due to its simple functionality and ease of interpretation. The commonly used two-parameter Weibull distribution expressed by the cumulative survival probability function is shown as

$$P(X \le x = e)^{-(x/\hat{\beta})^{\hat{\alpha}}} \tag{1}$$

where, x is the random variable, $\hat{\alpha}$ is the shape parameter, and $\hat{\beta}$ is the scale parameter.

The population mean, μ, and standard deviation, σ, are calculated with the Gamma (Γ) distribution function in equations 2 and 3, respectively.

$$\mu = \beta \cdot \Gamma\left(\frac{\hat{\alpha}+1}{\hat{\alpha}}\right) \tag{2}$$

$$\sigma = \hat{\beta}\sqrt{\Gamma\left(\frac{\hat{\alpha}+2}{\hat{\alpha}}\right) - \Gamma^2\left(\frac{\hat{\alpha}+1}{\hat{\alpha}}\right)} \tag{3}$$

The shape and scale parameters are estimated in an iterative process using either the maximum likelihood estimation (MLE) or rank regression [42]. Rank regression in X (RRX) tends to produce reliable results for small samples, while MLE works well for samples containing more than 20 or 30 data points.

During the individual Weibull analysis of fatigue data, each stress level is analyzed, and then the shape parameters are arithmetically averaged to define life scatter. Since Weibull analysis

considers only the data at a certain stress level at a time, five or more data points must be included in each stress level. For S/N data that has less than five data points per stress level, either joint Weibull analysis or Sendeckyj analysis must be used.

3.1.2 Joint Weibull Method.

In the joint Weibull analysis, M groups of data having a common shape parameter, but different scale parameters, are pooled [43]. The common shape parameter is obtained using the joint maximum likelihood estimate method, as shown in equation 4a. For the special case, where there is equal number of failures across all stress levels (i.e., $n_{f1}, n_{f2,..,} n_{fi} = n_f$), equation 4a reduces to the form shown in equation 4b.

$$\sum_{I=1}^{M}\left\{ n_{fi}\cdot\left[\frac{\sum_{j=1}^{M} x_{ij}^{\hat{\alpha}}\cdot 1n\left(x_{ij}\right)}{\sum_{j=1}^{n_i} x_{ij}^{\hat{\alpha}}}-\frac{1}{\hat{\alpha}}-\frac{\sum_{j=1}^{n_{fi}} 1n(x_{ij})}{n_{fi}}\right]\right\}=0 \tag{4a}$$

$$\sum_{i-1}^{M}\left[\frac{\sum_{j=1}^{n_i} x_{ij}^{\hat{\alpha}}\cdot 1n(x_{ij})}{\sum_{j=1}^{n_i} x_{ij}^{\hat{\alpha}}}\right]-\frac{M}{\hat{\alpha}}-\sum_{i=1}^{M}\left[\frac{\sum_{j=1}^{n_{fi}} 1n(x_{ij})}{n_{fi}}\right]=0 \tag{4(b)}$$

where n_i = number of data points in the i^{th} group of data (i = 1,2,…., M)
n_{fi} = number of failures in the i^{th} group of data (i = 1,2,…., M)

The common scale parameter for the S/N data is obtained using equation 5.

$$\beta_i=\left(\frac{1}{n_{fi}}\cdot\sum_{j=1}^{n_i} x_{ij}^{\hat{\alpha}}\right)^{1/\hat{\alpha}} \tag{5}$$

3.1.3 Sendeckyj Equivalent Static-Strength Model.

The Sendeckyj equivalent static-strength (wearout) model [19] uniquely relates the static strength and residual strength to fatigue life. Thus, the analysis pools static strength, fatigue life, and residual static-strength data and converts it into equivalent static-strength data. To characterize the S/N behavior of composite materials, the Sendeckyj model assumes:

- The S/N behavior can be determined by a deterministic equation. The equation can be based on theoretical considerations or experimental observations of the fatigue damage accumulation process.

- The static strengths are uniquely related to the fatigue lives and residual strengths at runouts. This specific relationship assumes that the strongest specimen has the longest fatigue life or the highest residual strength at runout; fatigue failure is assumed when the residual strength is equal to the maximum amplitude cyclic stress. This assumption may not hold for cases where competing failure modes are observed during fatigue testing.

- The statistical variability of static-strength data can be described by a two-parameter Weibull distribution.

The basic Sendeckyj model is presented in the deterministic equation given by

$$\sigma_e = \sigma_\alpha \left[\left(\frac{\sigma_r}{\sigma_\alpha} \right)^{1/S} + (n_f - 1 \cdot C \right]^S \tag{6}$$

where σ_e is the equivalent static strength, σ_a is the maximum applied cyclic stress, σ_r is the residual strength, n_f is the number of fatigue cycles, and S and C are Sendeckyj fitting parameters. During scatter analysis of fatigue data, these parameters are recalculated for each fatigue data set (S/N curve) and are used for developing fitting curve for each S/N curve. Setting the maximum amplitude cyclic stress equal to residual strength for fatigue failures, the power law is obtained as

$$\sigma_\alpha \cdot (1 - C + C \cdot n_f)^S = \sigma_u \tag{7}$$

where σ_u is the static strength.

Using the Sendeckyj analysis, fatigue life and residual strength data for each S/N curve are converted into a pool of equivalent static-strength data points. Then, this data set is fitted into a Weibull distribution to obtain the life shape parameter as described by Sendeckyj [19].

3.2 LIFE-FACTOR APPROACH.

The life-factor approach has been successfully used for metal to assure structural durability. In this approach, the structure is tested for additional fatigue cycles to achieve the desired level of reliability. This is graphically illustrated in figure 13 in terms of B-basis statistics, i.e., successful repeated load test to mean fatigue life demonstrates B-basis reliability on design lifetime. Since the true population distribution of life is not readily available, a shape parameter obtained from fatigue life data used for design from different levels in the building-blocks of testing is used for representing this probability density function, i.e., fatigue-life shape parameter in section 5.

The ratio of the mean repeated load life to A- or B-basis repeated life is defined as life factor, N_F, and given by equation 8. The derivation of the general form of this equation is included in Whitehead, et al. [2].

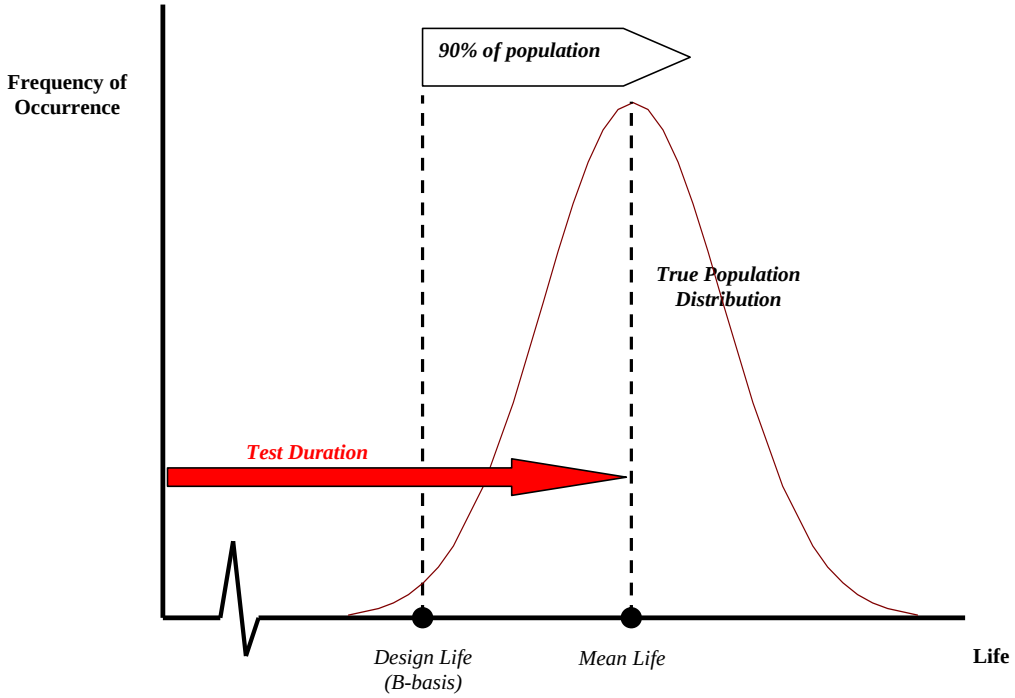

Figure 13. Life-Factor Approach for Substantiating B-Basis Design Life

$$N_F = \frac{\Gamma\left(\frac{\alpha_L + 1}{\alpha_L}\right)}{\left\{\frac{-\ln(R)}{\left[\chi^2_\gamma(2n)/2n\right]}\right\}^{1/\alpha_L}} \tag{8}$$

where α_L is the modal fatigue-life shape parameter (MLSP), n is the number of articles, and R is the reliability. For $\gamma = 0.95$, A- and B-basis reliabilities are 0.99 and 0.90, respectively. $\chi^2_\gamma(2n)$ is the Chi-square distribution with $2n$ degrees of freedom at γ-level confidence.

Figure 14 shows the influence of the shape parameter on the life factor, which is the ratio between mean repeated life to B-basis life [2]. For small α, life factor reduces with the increasing number of test articles. This figure shows that the life factor rapidly increases for fatigue shape parameters that are less than 2. Due to large scatter in the composite test data, the life shape parameter of composite was found to be 1.25 for the data analyzed for the NAVY approach, while it was found to be 4.00 for metal. Therefore, a composite structure is required to test additional fatigue life to achieve the desired level of reliability, i.e., a test duration of more than 13 design lifetimes (DLT) is required for composite in contrast to 2 DLT for metal. As shown in equation 8, life factor is a function of MLSP. Thus, improvements in MLSP for newer forms of materials that exhibit less scatter can significantly reduce the life factor.

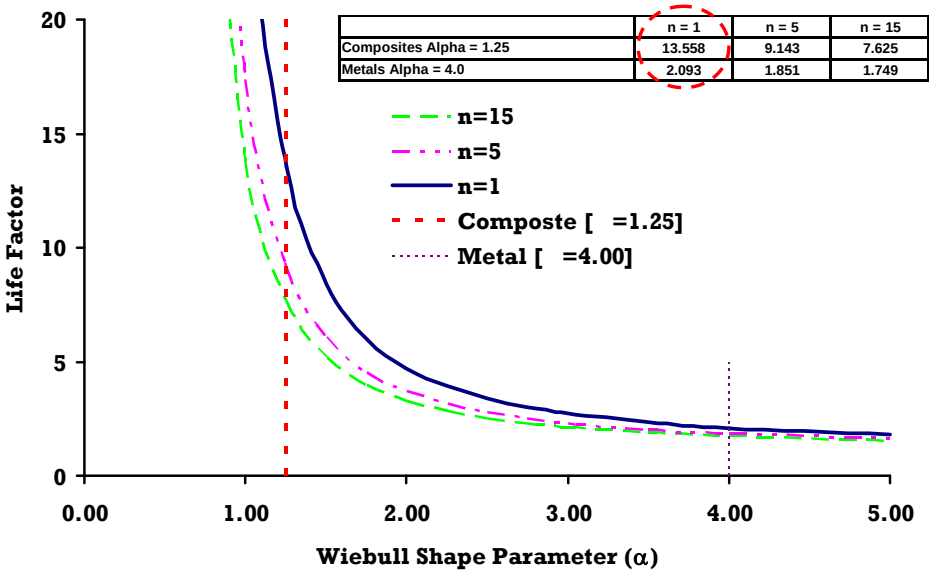

Figure 14. Influence of Fatigue Shape Parameter on B-Basis Life Factor

Furthermore, the analysis in reference 4 shows that the data scatter of notched or damaged composite elements can be significantly less than that of the unnotched composite specimens. Such improvements in fatigue-life shape parameter can significantly reduce the life factor. However, the life factor becomes insensitive to small changes in the life shape parameter beyond a value of 4, which is considered to be the life shape parameter for metal. The composite MLSP of 1.25, which was used for the NAVY approach, lies within the highly sensitive region of life factor versus shape parameter curve (figure 14); thus, even a small improvement resulted in a dramatic reduction of life factor, which reflects the required number of test durations to achieve a certain level of reliability in the design life. The MLSP is obtained from a distribution of shape parameters representing numerous S/N curves of different critical structural details. Thus, it is common to have large scatter in S/N data of design details that have competing failure modes and less scatter in notched test data due to stress concentration. For example, a V-notched, rail shear (VNRS) test specimen that has a soft (10/80/10) laminate stacking sequence has a majority of its fibers aligned with the tensile and compressive load resultant axes during in-plane shear loading. Although the applied (external) load is an in-plane shear load, the tensile and compressive (internal) loads along the fiber directions often cause fiber breakage and buckling, respectively, and significantly contribute to the final failure. In some cases, the competing (tensile and compressive) loading configurations result in unacceptable failure modes of these in-plane shear specimens. Often, the complex state of stress and these competing failure modes, coupled with other variabilities associated with composites such as batch variability, porosity, and fiber misalignments, tend to cause large scatter in both static strength and fatigue life. On the other hand, the stress concentrations in notched composites cause the final failure of the specimen, negating or minimizing the collective effects of the above-mentioned secondary variables.

3.3 LOAD-FACTOR APPROACH.

LEF is an alternative approach to the life-factor approach, which requires an excessive test duration and increases the applied loads in the fatigue spectrum so that the same level of reliability can be achieved with a shorter test duration [2]. A formal relationship between LEF and the test duration, *N*, as shown in equation 9, is defined for composite structural certification [2].

$$LEF(N) = \frac{\Gamma\left(\frac{\alpha_L + 1}{\alpha_L}\right)^{\alpha_L/\alpha_R}}{\left\{\frac{-1n(R)\cdot N^{\alpha_L}}{\left[\chi^2_\gamma(2n)/2n\right]}\right\}^{1/\alpha_R}} \tag{9}$$

Tables 5 and 6 include A- and B-basis LEFs, respectively, using equation 9 for α_R =17.5 to 32.5 and α_L=1.25 to 2.50. In these tables, the LEFs are calculated for combinations of test duration, *N*, ranging from 1 through 5 design lifetimes, and for 1, 2, and 3 test articles.

LEF for a test duration of 1 DLT, referred to as load factor (*LF*), is calculated as

$$LF = \lambda \cdot \frac{\Gamma\left(\frac{\alpha_R + 1}{\alpha_R}\right)}{\left\{\frac{-1n(R)}{\left[\chi^2_\gamma(2n)/2n\right]}\right\}^{1/\alpha_R}} \tag{10}$$

where, α_R is the MSSP, and λ is a function of both MSSP and MLSP, as defined in equation 11. Equation 10 has the same form as equation 8, except α_L is replaced by α_R, and the new parameter λ is included so that both life factor and LEF have the same level of reliability.

$$\lambda = \frac{\Gamma\left(\frac{\alpha_L + 1}{\alpha_L}\right)^{\alpha_L/\alpha_R}}{\Gamma\left(\frac{\alpha_R + 1}{\alpha_R}\right)} \tag{11}$$

Table 5. A-Basis LEFs

	n	1							2							3						
N	α_L / α_R	1.00	1.25	1.50	1.75	2.00	2.25	2.50	1.00	1.25	1.50	1.75	2.00	2.25	2.50	1.00	1.25	1.50	1.75	2.00	2.25	2.50
1	17.5	1.385	1.378	1.373	1.369	1.366	1.363	1.361	1.366	1.360	1.355	1.351	1.348	1.345	1.343	1.357	1.350	1.345	1.341	1.338	1.336	1.334
	20.0	1.330	1.324	1.319	1.316	1.314	1.312	1.310	1.314	1.308	1.304	1.301	1.298	1.296	1.295	1.306	1.300	1.296	1.293	1.290	1.288	1.287
	22.5	1.288	1.283	1.279	1.277	1.274	1.273	1.271	1.275	1.270	1.266	1.263	1.261	1.259	1.258	1.268	1.263	1.259	1.257	1.254	1.253	1.251
	25.0	1.256	1.251	1.248	1.246	1.244	1.242	1.241	1.244	1.240	1.237	1.234	1.232	1.231	1.229	1.238	1.234	1.231	1.228	1.226	1.225	1.223
	27.5	1.230	1.226	1.223	1.221	1.219	1.218	1.217	1.220	1.216	1.213	1.211	1.209	1.208	1.207	1.214	1.210	1.208	1.205	1.204	1.202	1.201
	30.0	1.209	1.206	1.203	1.201	1.199	1.198	1.197	1.200	1.196	1.194	1.192	1.190	1.189	1.188	1.195	1.191	1.189	1.187	1.185	1.184	1.183
	32.5	1.192	1.188	1.186	1.184	1.183	1.182	1.181	1.183	1.180	1.178	1.176	1.174	1.173	1.172	1.179	1.175	1.173	1.171	1.170	1.169	1.168
	35.0	1.177	1.174	1.172	1.170	1.169	1.168	1.167	1.169	1.166	1.164	1.162	1.161	1.160	1.159	1.165	1.162	1.160	1.158	1.157	1.156	1.155
1.5	17.5	1.353	1.338	1.326	1.314	1.304	1.294	1.285	1.335	1.321	1.308	1.297	1.287	1.277	1.268	1.326	1.312	1.299	1.288	1.278	1.268	1.259
	20.0	1.303	1.291	1.280	1.270	1.261	1.253	1.245	1.288	1.276	1.265	1.256	1.247	1.239	1.231	1.280	1.268	1.257	1.248	1.239	1.231	1.223
	22.5	1.265	1.255	1.245	1.237	1.229	1.222	1.215	1.252	1.242	1.232	1.224	1.217	1.209	1.203	1.245	1.235	1.226	1.218	1.210	1.203	1.196
	25.0	1.236	1.226	1.218	1.211	1.204	1.198	1.192	1.224	1.215	1.207	1.200	1.193	1.187	1.181	1.218	1.209	1.201	1.194	1.187	1.181	1.175
	27.5	1.212	1.204	1.197	1.190	1.184	1.178	1.173	1.202	1.194	1.186	1.180	1.174	1.168	1.163	1.197	1.188	1.181	1.175	1.169	1.163	1.158
	30.0	1.193	1.185	1.179	1.173	1.167	1.162	1.157	1.184	1.176	1.170	1.164	1.158	1.153	1.148	1.179	1.171	1.165	1.159	1.154	1.149	1.144
	32.5	1.177	1.170	1.164	1.159	1.154	1.149	1.144	1.168	1.162	1.156	1.150	1.145	1.141	1.136	1.164	1.157	1.151	1.146	1.141	1.136	1.132
	35.0	1.163	1.157	1.151	1.147	1.142	1.138	1.133	1.155	1.149	1.144	1.139	1.134	1.130	1.126	1.151	1.145	1.140	1.135	1.130	1.126	1.122
2	17.5	1.331	1.311	1.294	1.277	1.262	1.247	1.233	1.313	1.294	1.276	1.260	1.245	1.231	1.217	1.304	1.285	1.267	1.251	1.236	1.222	1.208
	20.0	1.284	1.268	1.253	1.239	1.226	1.213	1.201	1.269	1.253	1.238	1.224	1.211	1.199	1.187	1.262	1.245	1.230	1.217	1.204	1.192	1.180
	22.5	1.249	1.235	1.222	1.210	1.198	1.187	1.177	1.236	1.222	1.209	1.197	1.186	1.175	1.165	1.229	1.215	1.202	1.191	1.179	1.169	1.158
	25.0	1.222	1.209	1.197	1.187	1.177	1.167	1.158	1.210	1.198	1.186	1.176	1.166	1.156	1.147	1.204	1.192	1.180	1.170	1.160	1.151	1.142
	27.5	1.200	1.188	1.178	1.168	1.159	1.151	1.143	1.189	1.178	1.168	1.159	1.150	1.141	1.133	1.184	1.173	1.163	1.153	1.145	1.136	1.128
	30.0	1.182	1.171	1.162	1.153	1.145	1.137	1.130	1.172	1.162	1.153	1.144	1.136	1.129	1.121	1.168	1.157	1.148	1.140	1.132	1.124	1.117
	32.5	1.166	1.157	1.149	1.141	1.133	1.126	1.119	1.158	1.149	1.140	1.133	1.125	1.118	1.111	1.154	1.144	1.136	1.128	1.121	1.114	1.107
	35.0	1.154	1.145	1.137	1.130	1.123	1.117	1.110	1.146	1.137	1.130	1.123	1.116	1.109	1.103	1.142	1.134	1.126	1.119	1.112	1.105	1.099
3	17.5	1.301	1.274	1.249	1.226	1.205	1.184	1.164	1.283	1.257	1.233	1.210	1.189	1.168	1.148	1.274	1.248	1.224	1.202	1.180	1.160	1.140
	20.0	1.259	1.236	1.215	1.196	1.177	1.159	1.142	1.244	1.222	1.201	1.182	1.163	1.146	1.129	1.236	1.214	1.194	1.174	1.156	1.139	1.122
	22.5	1.227	1.207	1.189	1.172	1.156	1.140	1.125	1.214	1.195	1.177	1.160	1.144	1.128	1.113	1.208	1.188	1.170	1.154	1.138	1.122	1.107
	25.0	1.202	1.185	1.169	1.154	1.139	1.125	1.112	1.191	1.174	1.158	1.143	1.129	1.115	1.102	1.185	1.168	1.152	1.137	1.123	1.109	1.096
	27.5	1.182	1.167	1.152	1.139	1.126	1.113	1.101	1.172	1.157	1.142	1.129	1.116	1.104	1.092	1.167	1.151	1.137	1.124	1.111	1.099	1.087
	30.0	1.166	1.152	1.139	1.126	1.115	1.103	1.092	1.157	1.143	1.130	1.118	1.106	1.095	1.084	1.152	1.138	1.125	1.113	1.102	1.090	1.080
	32.5	1.152	1.139	1.127	1.116	1.105	1.095	1.085	1.144	1.131	1.119	1.108	1.098	1.087	1.077	1.139	1.127	1.115	1.104	1.093	1.083	1.073
	35.0	1.140	1.129	1.118	1.107	1.098	1.088	1.079	1.133	1.121	1.110	1.100	1.090	1.081	1.072	1.129	1.117	1.106	1.096	1.086	1.077	1.068
4	17.5	1.279	1.248	1.219	1.192	1.166	1.141	1.117	1.262	1.231	1.203	1.176	1.150	1.126	1.102	1.254	1.223	1.194	1.168	1.142	1.118	1.094
	20.0	1.241	1.214	1.189	1.166	1.144	1.122	1.101	1.226	1.200	1.175	1.152	1.130	1.109	1.089	1.219	1.192	1.168	1.145	1.123	1.102	1.082
	22.5	1.211	1.188	1.166	1.146	1.127	1.108	1.090	1.199	1.176	1.154	1.134	1.115	1.096	1.078	1.192	1.169	1.148	1.128	1.109	1.090	1.073
	25.0	1.188	1.168	1.149	1.131	1.113	1.097	1.080	1.177	1.157	1.138	1.120	1.103	1.086	1.070	1.171	1.151	1.132	1.115	1.098	1.081	1.065
	27.5	1.170	1.151	1.134	1.118	1.102	1.087	1.073	1.160	1.142	1.125	1.109	1.093	1.078	1.064	1.155	1.137	1.120	1.104	1.088	1.073	1.059
	30.0	1.155	1.138	1.122	1.108	1.094	1.080	1.067	1.146	1.129	1.114	1.099	1.085	1.071	1.058	1.141	1.124	1.109	1.095	1.081	1.067	1.054
	32.5	1.142	1.127	1.112	1.099	1.086	1.074	1.061	1.134	1.119	1.105	1.091	1.078	1.066	1.054	1.129	1.114	1.100	1.087	1.074	1.062	1.050
	35.0	1.131	1.117	1.104	1.092	1.080	1.068	1.057	1.124	1.110	1.097	1.084	1.072	1.061	1.050	1.120	1.106	1.093	1.081	1.069	1.057	1.046
5	17.5	1.263	1.228	1.196	1.165	1.136	1.109	1.082	1.246	1.212	1.180	1.150	1.121	1.094	1.067	1.238	1.203	1.172	1.142	1.113	1.086	1.060
	20.0	1.227	1.197	1.169	1.143	1.118	1.094	1.071	1.213	1.183	1.156	1.130	1.105	1.082	1.059	1.205	1.176	1.149	1.123	1.099	1.075	1.052
	22.5	1.199	1.173	1.149	1.126	1.105	1.083	1.063	1.187	1.161	1.137	1.115	1.093	1.072	1.052	1.180	1.155	1.131	1.109	1.087	1.066	1.046
	25.0	1.178	1.155	1.133	1.113	1.094	1.075	1.057	1.167	1.144	1.123	1.103	1.083	1.065	1.047	1.161	1.138	1.117	1.097	1.078	1.060	1.042
	27.5	1.160	1.140	1.121	1.102	1.085	1.068	1.051	1.150	1.130	1.111	1.093	1.076	1.059	1.042	1.145	1.125	1.106	1.088	1.071	1.054	1.038
	30.0	1.146	1.127	1.110	1.093	1.077	1.062	1.047	1.137	1.119	1.101	1.085	1.069	1.054	1.039	1.132	1.114	1.097	1.080	1.065	1.049	1.035
	32.5	1.134	1.117	1.101	1.086	1.071	1.057	1.043	1.126	1.109	1.093	1.078	1.064	1.049	1.036	1.122	1.105	1.089	1.074	1.060	1.046	1.032
	35.0	1.124	1.108	1.094	1.080	1.066	1.053	1.040	1.116	1.101	1.086	1.072	1.059	1.046	1.033	1.113	1.097	1.082	1.069	1.055	1.042	1.030

Table 6. B-Basis LEFs

	n	1							2							3						
N	α_L / α_R	1.00	1.25	1.50	1.75	2.00	2.25	2.50	1.00	1.25	1.50	1.75	2.00	2.25	2.50	1.00	1.25	1.50	1.75	2.00	2.25	2.50
1	17.5	1.211	1.205	1.200	1.197	1.194	1.192	1.190	1.195	1.189	1.184	1.181	1.178	1.176	1.175	1.186	1.180	1.176	1.173	1.170	1.168	1.166
	20.0	1.182	1.177	1.173	1.170	1.168	1.166	1.165	1.168	1.163	1.160	1.157	1.154	1.153	1.151	1.161	1.156	1.152	1.150	1.147	1.146	1.144
	22.5	1.160	1.156	1.153	1.150	1.148	1.146	1.145	1.148	1.144	1.141	1.138	1.136	1.135	1.133	1.142	1.138	1.134	1.132	1.130	1.128	1.127
	25.0	1.143	1.139	1.136	1.134	1.132	1.131	1.130	1.133	1.129	1.126	1.124	1.122	1.120	1.119	1.127	1.123	1.120	1.118	1.116	1.115	1.114
	27.5	1.129	1.126	1.123	1.121	1.120	1.118	1.117	1.120	1.116	1.114	1.112	1.110	1.109	1.108	1.115	1.111	1.109	1.107	1.105	1.104	1.103
	30.0	1.118	1.115	1.112	1.111	1.109	1.108	1.107	1.109	1.106	1.104	1.102	1.100	1.099	1.098	1.105	1.102	1.099	1.097	1.096	1.095	1.094
	32.5	1.108	1.105	1.103	1.102	1.100	1.099	1.098	1.101	1.098	1.095	1.094	1.092	1.091	1.090	1.096	1.093	1.091	1.090	1.088	1.087	1.086
	35.0	1.100	1.098	1.096	1.094	1.093	1.092	1.091	1.093	1.090	1.088	1.087	1.086	1.085	1.084	1.089	1.086	1.084	1.083	1.082	1.081	1.080
1.5	17.5	1.183	1.170	1.159	1.149	1.140	1.132	1.123	1.167	1.155	1.144	1.134	1.125	1.117	1.108	1.159	1.147	1.136	1.126	1.117	1.109	1.101
	20.0	1.158	**1.148**	1.138	1.129	1.122	1.114	1.107	1.145	1.134	1.125	1.116	1.109	1.101	1.094	1.138	1.127	1.118	1.110	1.102	1.095	1.088
	22.5	1.140	1.130	1.122	1.114	1.107	1.101	1.095	1.128	1.118	1.110	1.103	1.096	1.090	1.083	1.122	1.112	1.104	1.097	1.090	1.084	1.077
	25.0	1.125	1.116	1.109	1.102	1.096	1.090	1.085	1.114	1.106	1.099	1.092	1.086	1.080	1.075	1.109	1.101	1.093	1.087	1.081	1.075	1.069
	27.5	1.113	1.105	1.099	1.093	1.087	1.082	1.077	1.104	1.096	1.089	1.083	1.078	1.073	1.068	1.099	1.091	1.084	1.079	1.073	1.068	1.063
	30.0	1.103	1.096	1.090	1.085	1.080	1.075	1.070	1.094	1.088	1.082	1.076	1.071	1.066	1.062	1.090	1.083	1.077	1.072	1.067	1.062	1.058
	32.5	1.095	1.088	1.083	1.078	1.073	1.069	1.065	1.087	1.081	1.075	1.070	1.065	1.061	1.057	1.083	1.077	1.071	1.066	1.061	1.057	1.053
	35.0	1.088	1.082	1.077	1.072	1.068	1.064	1.060	1.080	1.075	1.070	1.065	1.061	1.057	1.053	1.077	1.071	1.066	1.061	1.057	1.053	1.049
2	17.5	1.164	1.146	1.131	1.117	1.103	1.090	1.078	1.148	1.131	1.116	1.102	1.089	1.076	1.064	1.140	1.123	1.108	1.094	1.081	1.068	1.056
	20.0	1.142	1.127	1.114	1.101	1.090	1.079	1.068	1.129	1.114	1.101	1.089	1.077	1.066	1.056	1.122	1.107	1.094	1.082	1.071	1.060	1.049
	22.5	1.125	1.112	1.100	1.090	1.079	1.070	1.060	1.114	1.101	1.089	1.078	1.068	1.059	1.049	1.108	1.095	1.083	1.073	1.062	1.053	1.044
	25.0	1.112	1.100	1.090	1.080	1.071	1.062	1.054	1.102	1.090	1.080	1.070	1.061	1.053	1.044	1.096	1.085	1.075	1.065	1.056	1.047	1.039
	27.5	1.101	1.091	1.081	1.073	1.065	1.057	1.049	1.092	1.082	1.072	1.064	1.056	1.048	1.040	1.087	1.077	1.068	1.059	1.051	1.043	1.036
	30.0	1.093	1.083	1.074	1.067	1.059	1.052	1.045	1.084	1.075	1.066	1.058	1.051	1.044	1.037	1.080	1.070	1.062	1.054	1.047	1.039	1.033
	32.5	1.085	1.076	1.069	1.061	1.054	1.048	1.041	1.077	1.069	1.061	1.054	1.047	1.040	1.034	1.073	1.065	1.057	1.050	1.043	1.036	1.030
	35.0	1.079	1.071	1.063	1.057	1.050	1.044	1.038	1.072	1.064	1.056	1.050	1.043	1.037	1.031	1.068	1.060	1.053	1.046	1.040	1.034	1.028
3	17.5	1.137	1.114	1.092	1.072	1.053	1.035	1.017	1.122	1.099	1.078	1.058	1.039	1.021	1.004	1.114	1.091	1.070	1.051	1.032	1.014	
	20.0	1.119	1.099	1.080	1.063	1.046	1.031	1.015	1.106	1.086	1.068	1.051	1.034	1.019	1.003	1.099	1.079	1.061	1.044	1.028	1.012	
	22.5	1.105	1.087	1.071	1.056	1.041	1.027	1.014	1.094	1.076	1.060	1.045	1.030	1.017	1.003	1.088	1.070	1.054	1.039	1.025	1.011	
	25.0	1.094	1.078	1.064	1.050	1.037	1.024	1.012	1.084	1.068	1.054	1.040	1.027	1.015	1.003	1.079	1.063	1.049	1.035	1.022	1.010	
	27.5	1.085	1.071	1.058	1.045	1.034	1.022	1.011	1.076	1.062	1.049	1.037	1.025	1.014	1.002	1.071	1.057	1.044	1.032	1.020	1.009	
	30.0	1.078	1.065	1.053	1.042	1.031	1.020	1.010	1.069	1.057	1.045	1.034	1.023	1.012	1.002	1.065	1.052	1.040	1.029	1.019	1.008	
	32.5	1.072	1.060	1.049	1.038	1.028	1.019	1.009	1.064	1.052	1.041	1.031	1.021	1.011	1.002	1.060	1.048	1.037	1.027	1.017	1.008	
	35.0	1.066	1.055	1.045	1.036	1.026	1.017	1.009	1.059	1.048	1.038	1.029	1.019	1.011	1.002	1.056	1.045	1.035	1.025	1.016	1.007	
4	17.5	1.119	1.091	1.066	1.042	1.019			1.104	1.077	1.052	1.028	1.006			1.096	1.069	1.044	1.021			
	20.0	1.103	1.079	1.057	1.037	1.017			1.090	1.067	1.045	1.025	1.005			1.084	1.060	1.039	1.018			
	22.5	1.091	1.070	1.051	1.032	1.015			1.080	1.059	1.040	1.022	1.004			1.074	1.053	1.034	1.016			
	25.0	1.082	1.063	1.046	1.029	1.013			1.072	1.053	1.036	1.020	1.004			1.066	1.048	1.031	1.015			
	27.5	1.074	1.057	1.041	1.026	1.012			1.065	1.048	1.033	1.018	1.004			1.060	1.043	1.028	1.013			
	30.0	1.068	1.052	1.038	1.024	1.011			1.059	1.044	1.030	1.016	1.003			1.055	1.040	1.026	1.012			
	32.5	1.062	1.048	1.035	1.022	1.010			1.055	1.041	1.027	1.015	1.003			1.051	1.037	1.024	1.011			
	35.0	1.058	1.045	1.032	1.021	1.010			1.051	1.038	1.025	1.014	1.003			1.047	1.034	1.022	1.010			
5	17.5	1.104	1.074	1.046	1.019				1.090	1.060	1.032	1.005				1.082	1.052	1.025				
	20.0	1.091	1.064	1.040	1.017				1.078	1.052	1.028	1.005				1.072	1.046	1.021				
	22.5	1.080	1.057	1.035	1.015				1.069	1.046	1.025	1.004				1.063	1.040	1.019				
	25.0	1.072	1.051	1.032	1.013				1.062	1.041	1.022	1.004				1.057	1.036	1.017				
	27.5	1.065	1.046	1.029	1.012				1.056	1.038	1.020	1.003				1.052	1.033	1.016				
	30.0	1.060	1.042	1.026	1.011				1.051	1.034	1.018	1.003				1.047	1.030	1.014				
	32.5	1.055	1.039	1.024	1.010				1.047	1.032	1.017	1.003				1.043	1.028	1.013				
	35.0	1.051	1.036	1.023	1.009				1.044	1.029	1.016	1.003				1.040	1.026	1.012				

3.4 COMBINED LOAD-LIFE APPROACH.

The life-factor approach requires an excessive test duration and, by itself, may not be practical for full-scale test demonstration. In contrast, the LEF approach requires increasing the fatigue loads so that the same level of reliability can be achieved with one test duration. However, for hybrid structures, overloads may cause crack growth retardation, buckling, and premature failure of some of the metal components. Another approach, which has been applied in the past, is a combined approach using load and life factors, which is the general form of LEF given in equation 9. The procedure in this approach would be to apply a combined life factor with the load factor to achieve a compromise in the full-scale test requirements as well as the load spectrum. This approach allows using a lower LEF as a trade-off for more life cycles, which reduces the severity of the overload on metallic parts.

By combining equations 8 and 9, the LEF is defined in terms of test duration, as shown in equation 12. This is a condensed form of equation 9.

$$LEF = \left(\frac{N_F}{N} \right)^{\frac{\alpha_L}{\alpha_R}} \tag{12}$$

As shown in figure 15, LEF is significantly influenced by MSSP and MLSP. Thus, improvements in these shape parameters for newer forms of materials that exhibit less scatter can significantly reduce LEF.

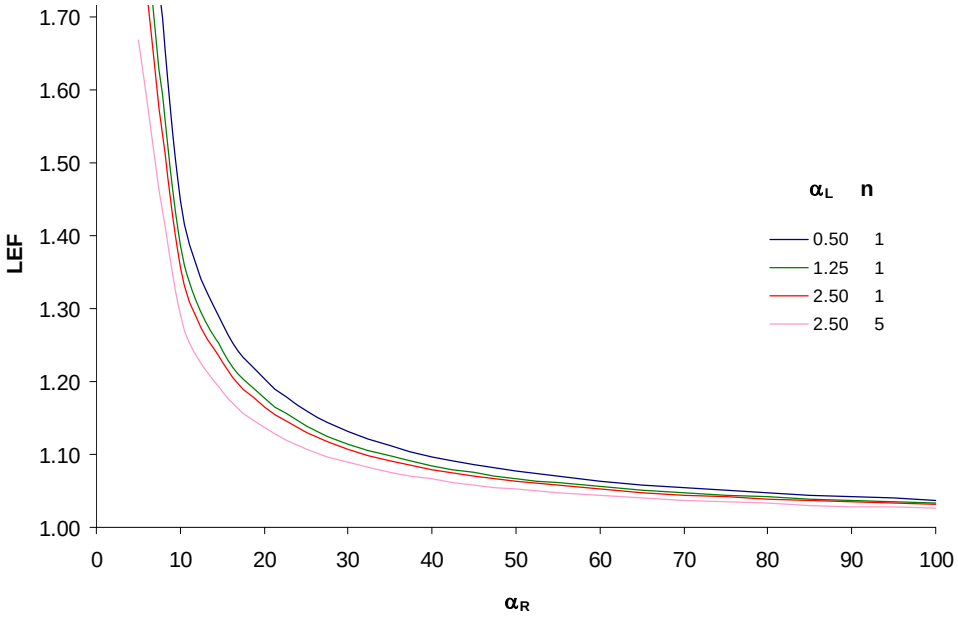

Figure 15. Influence of Strength and Life Parameter on LEF

As shown in figure 16, a significant reduction in LEF is achieved simply by increasing the test duration to 1.5 DLT. Furthermore, the influence of strength and life shape parameter on LEF changes as the test duration is increased. For example, as the test duration is increased, the

influence of the fatigue-life shape parameter on LEF increases. This is understood, as N_F is only influenced by MLSP. Also, note for small test durations, the influence of MSSP on LEF is significant due to the increased influence of load factor.

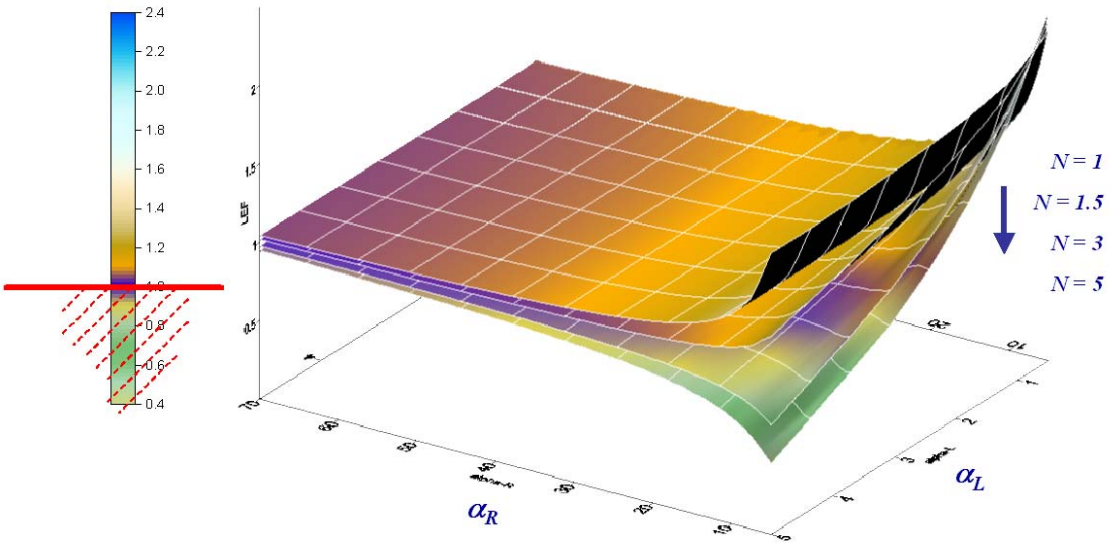

Figure 16. Influence of MSSP and MLSP on LEF (Combined Load-Life Approach)

Application of the combined load-life approach is illustrated in figure 17. The LEF is calculated as the ratio of the maximum applied load to the design maximum fatigue stress. This curve is generated by calculating LEF for several different test durations. Note that the LEF required for the test duration (which is equal to the life factor, N_F) is one, and N_F is obtained from figure 14 for the corresponding fatigue-life shape parameter. If the design maximum load in the repeated load test (P_F) is increased to the mean residual strength at one lifetime (P_T), then the A- or B-basis residual strength of the structure would be equivalent to the design maximum fatigue stress. Thus, a successful repeated load test to one lifetime at applied stress, P_T, or a repeated test to N_F at applied stress, P_F, (no LEF) would both demonstrate the corresponding reliability. Furthermore, a successful repeated load test to a test duration (less than N_F) with the corresponding LEF would demonstrate the same level or reliability on the design lifetime.

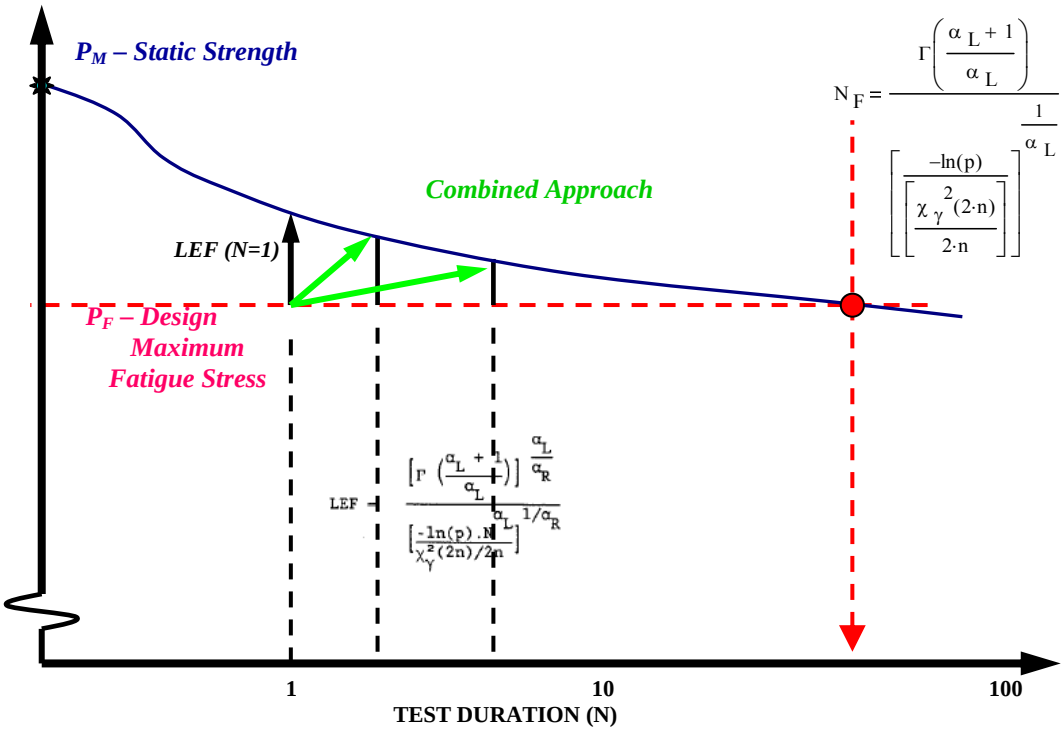

Figure 17. Combined Load-Life Approach for Composite Structures

Figure 18 shows the A- and B-basis LEF requirements based on the number of test specimens using equation 9 for the shape parameters reported in reference 2, $\alpha_R = 20$ and $\alpha_L = 1.25$. It shows that the increased number of test specimens reduces the LEF requirements. However, in large-scale testing, only a single fatigue test is conducted due to high cost and long test duration. This figure also shows that the A-basis requirements on LEF are significantly higher than for B-basis.

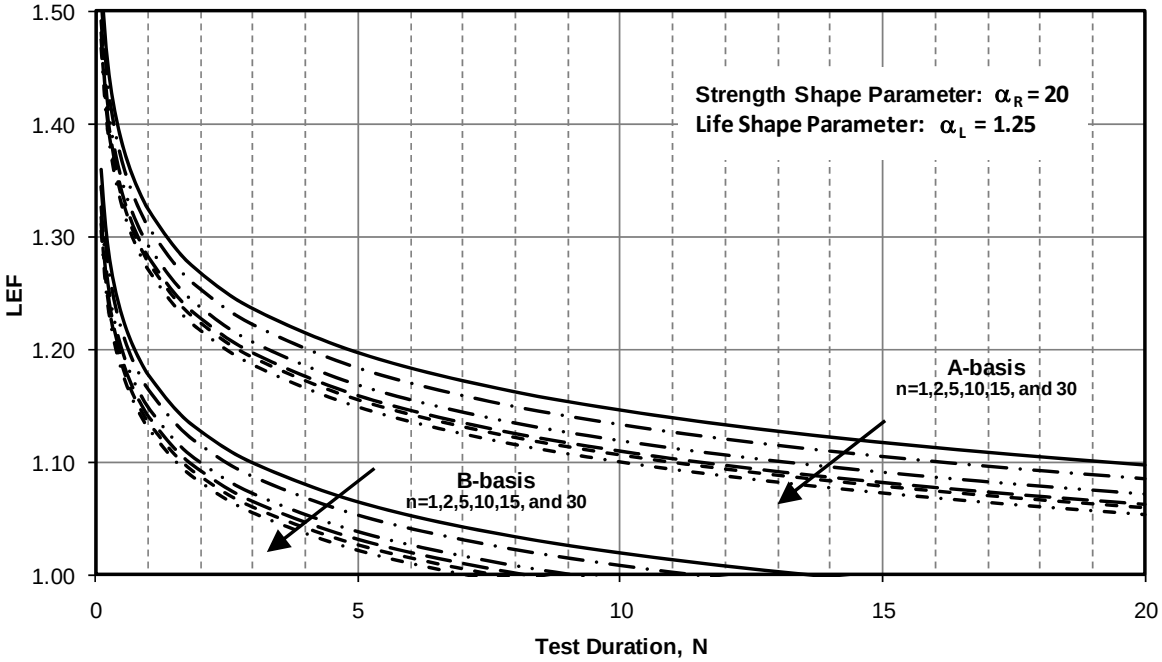

Sample Size	1 DLT		1.5 DLT		2 DLT	
	A-Basis	B-Basis	A-Basis	B-Basis	A-Basis	B-Basis
1	1.324	1.177	1.291	1.148	1.268	1.127
2	1.308	1.163	1.276	1.134	1.253	1.114
5	1.291	1.148	1.259	1.120	1.237	1.100
10	1.282	1.140	1.250	1.111	1.227	1.091
15	1.277	1.135	1.245	1.107	1.223	1.087
30	1.270	1.130	1.239	1.101	1.217	1.082

Figure 18. A- and B-Basis LEF Requirements With Respect to the Number of Test Specimens

3.4.1 Application of LEF to a Load Spectrum.

The combined load-life approach can be used in two different ways: (1) to apply the same LEF, which is calculated for a certain test duration, to the entire spectrum or (2) to apply a different LEF for different load blocks in the spectra based on the severity of enhanced load, i.e., cycles that have high loads are repeated for a longer test duration (with lower LEF) than the rest of the spectrum. This approach is particularly useful for hybrid structures that exhibit metallic component failure due to high LEF (overloads) and to avoid premature failure due to buckling. Both of these applications are illustrated in figure 19.

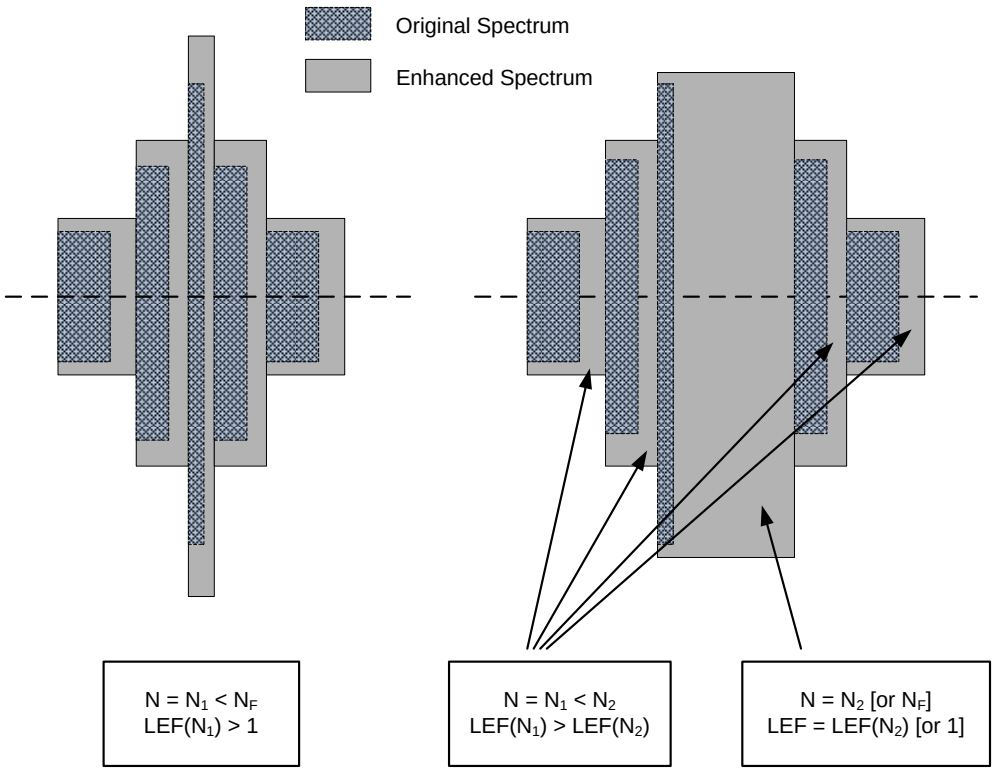

(a) Combined Load-Life Test (b) Combined Load-Life Spectrum

Figure 19. Application of Combined Load-Life Approach

One common practice for composite full-scale test substantiation is a 2 DLT, which is adopted from metallic structural certification (figure 14) using the design spectrum with the corresponding LEF under room temperature ambient (RTA) test conditions. Often, the test duration of 1.5 DLT is used with the corresponding LEF. The LEF approach accounts for the variability in design details and loading modes. To account for the service environmental effects on composites, additional factors are calculated from the design allowable tests. These additional factors for composite structures account for the difference between composite and metallic structure during design and analysis and are beyond what is normally done for metallic certifications. Such factors, accounting for both moisture and temperature effects on composites, depend significantly on the material system and the lay-up configuration and can be as high as 1.4.

In metallic structures, severe flight loads result in crack growth retardation. Therefore, it is common practice to clip the peak loads (i.e., reduce the peak loads to the clipping level, without omitting loads) after careful consideration of the appropriate clipping levels. In contrast, such severe flight loads significantly contribute to flaw growth in composite structures and reduce the fatigue life. Therefore, fatigue spectrum clipping must not be done during structural testing of composite structures. When additional LEFs and environmental factors are applied to composite load spectrum, the cumulative effects on test loads can be significantly higher than the clipping levels for metallic components. For hybrid structures, this can be addressed through the combined load-life spectrum approach shown in figure 19(b). Alternatively, fatigue tests with

LEFs (not combined with environmental compensation factors) can be performed by including periodic static tests with the environmental factors applied to relieve the severity of high loads.

To reduce the test duration, the fatigue test spectrum is truncated by eliminating the segments with stress levels below an endurance limit (stress level corresponds to an infinite life). The endurance limit of a particular composite material varies, based on parameters such as the lay-up configuration, test environment, and stress ratio. The S/N curves that are generated to obtain the life shape parameters can be used to determine the endurance limit for different design details of a composite structure. The life factor and the LEF are to be applied after truncation of the load spectrum as shown in figure 20.

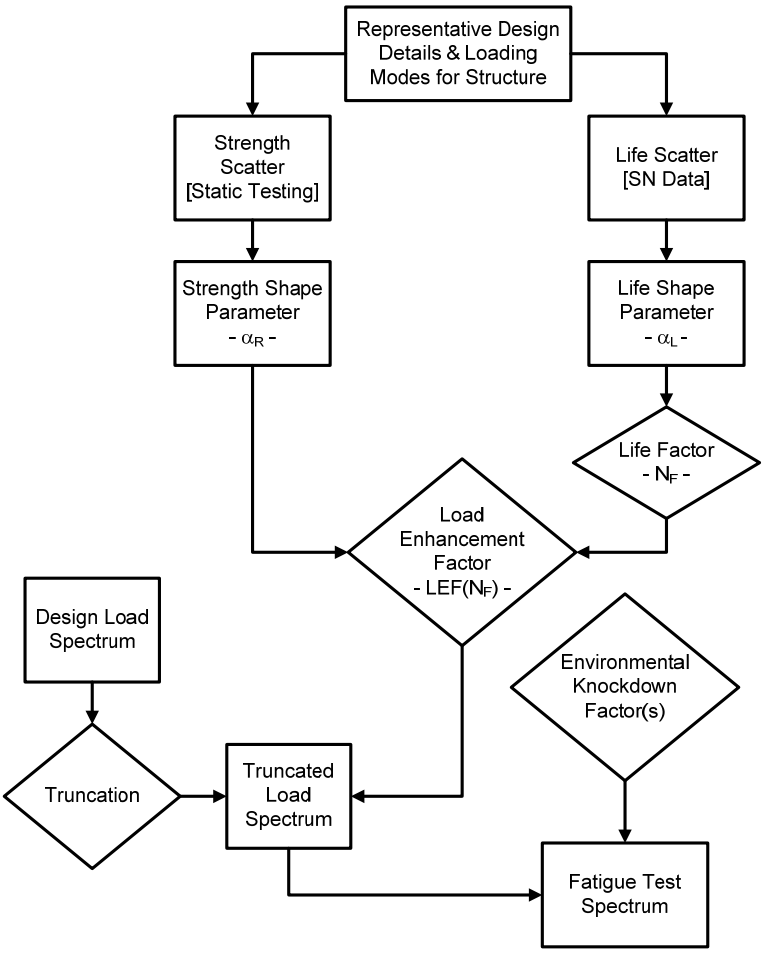

Figure 20. Fatigue Test Spectrum Development for Composite Structural Test

Composite material properties are susceptible to temperature and moisture. Therefore, when a full-sale test is conducted at RTA conditions, environmental compensation factors are applied to the load spectrum. The environmental factors are recommended to be applied to the truncated load spectrum. Although this approach provides an efficient way to ensure structural life reliability, the cumulative effects of the above-mentioned enhancement factors may result in an undesirably high cumulative LEF. For these cases, an approach similar to that shown in figure 19(b) is recommended to reduce the required LEFs for high-spectrum loads, i.e., test for

additional life. However, these additional high-stress cycles must be spread throughout the spectrum so that the damage growth mechanism is not adversely altered, and the practical limits of spectrum load sequence must be preserved. Although there are no significant load-sequencing effects on fatigue life, composites are extremely sensitive to variation in the number of high loads in the fatigue spectrum [2]. It is imperative that the effects of these parameters do not change the fatigue failure mode (and the failure mechanism) or reach the static strength of the structure. Furthermore, the application of load enhancements must preserve the stress ratio of each load cycle throughout the spectrum so that the fatigue damage mechanism and the life are not artificially influenced.

The LEF can be applied to the fatigue spectrum in several ways: (1) to 1-g mean fatigue load, (2) to amplitude, and (3) to minimum/maximum load. These three approaches are shown in equations 13 through 15 for a typical aircraft loads application.

$$P_{mean} = \left[\left(Load_{1-g} \right) \cdot LEF + \left(\frac{\Delta Load}{\Delta g} \right) \cdot \Delta g \right] \tag{13}$$

$$P_{amplitude} = \left[\left(Load_{1-g} \right) + \left(\frac{\Delta Load}{\Delta g} \right) \cdot \Delta g \cdot LEF \right] \tag{14}$$

$$P_{Min/Max} = \left[\left(Load_{1-g} \right) + \left(\frac{\Delta Load}{\Delta g} \right) \cdot \Delta g \right] \cdot LEF \tag{15}$$

where

$(Load_{1\text{-}g})$ = mean fatigue load (i.e., 1-g maneuver shear/moment/torque) of a load block

Δg = amplitude with respect to 1-g fatigue load

$\left(\frac{\Delta Load}{\Delta g} \right)$ = load (shear/moment/torque) per Δg

When applying the LEFs to mean fatigue loads, as shown in equation 13, the mean load is offset in either the positive (for positive mean loads) or negative (for negative mean loads) direction. For cycles with load reversal (stress ratio R <0), this causes a reduction in load magnitudes in the opposite loading direction, i.e., shifts the mean load, as shown in figure 21. Consequently, this alters the damage growth caused by reversible loads to the composite structure. Furthermore, for higher LEF values, this may convert a tension-compression cycle to a tension-tension cycle or compression-compression cycle for positive and negative enhancement of mean loads, respectively. Specimen-level data for composite materials show that reversible load cases (R <0) are critical and have a significantly lower fatigue life than that of tension-tension or compression-compression (R >0) cases. Similarly, application of LEF to stress amplitude about the mean load, as shown in equation 14, results in an alteration of the stress ratio and possibly load reversal for high LEFs. Therefore, equations 13 and 14 are not recommended for applying

the LEF to a spectrum loading with negative stress ratios (tension-compression loading) to avoid changes to stress ratios and unintentional reduction in fatigue damage to the test article.

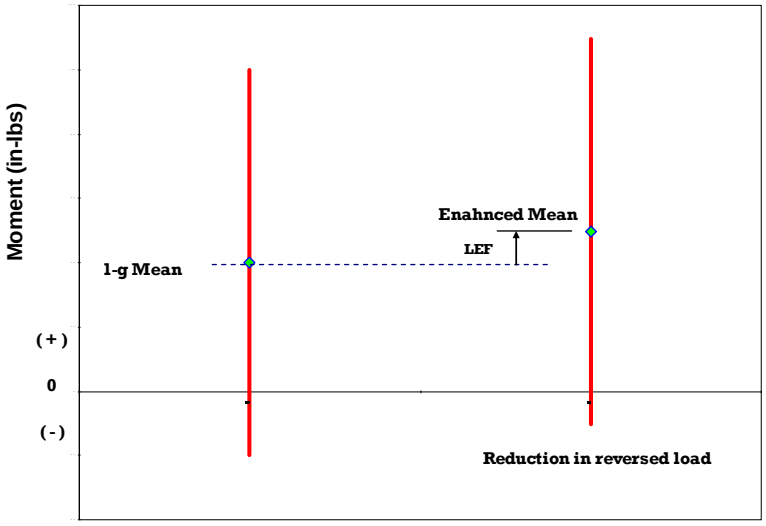

Figure 21. Application of LEF Only to Mean Load

Application of the LEF to both 1-g mean and amplitude, as in equation 15, results in considerably high loads but maintains the same stress ratios throughout the spectrum. Therefore, full-scale fatigue test spectrum loads are generated by applying the LEF to the minimum and maximum shear-moment torque (SMT) loads so that the reversible loads are not shifted but rather enhanced, depending on the sign of the maximum or minimum SMT load, and the stress ratio is maintained after load enhancement.

3.4.2 Generating Life Factor and LEFs.

To generate reliable LEFs with a statistical significance, a large number of test data is required. Figure 22 shows the minimum required test matrix for generating strength and life shape parameters so that life factors and LEFs for a particular structure can be developed. Such a test matrix must consider the following:

- Critical design details, loading modes, and stress ratios must be represented in coupon and element level.

- Specimens must be fabricated from a minimum of three distinctive material batches, unless otherwise proven that significant batch variability does not exist through lamina-level statistics (i.e., alpha = 0.01 significance level using the Anderson-Darling test [44]).

- Excluding the static stress level, a minimum of three fatigue stress levels must be included in the test matrix for each S/N curve. At least two stress levels must show fatigue failures for analysis techniques that utilize residual strength of runouts, or else all stress levels must have a minimum of six fatigue failures.

- Based on the fatigue analysis technique (i.e., analysis of individual stress levels or pooling fatigue data across stress levels using either joint Weibull or Sendeckyj analysis), the minimum recommended number of specimens, as shown in figure 22, must be included.

- A minimum of six data sets for static are included (at least six Weibull shape parameters) in the static-strength scatter analysis for generating the strength shape parameter.

- A minimum of six data sets for fatigue are included (at least six Weibull shape parameters) in the fatigue-life scatter analysis for generating the life shape parameter.

Design Detail	Test Method	Loading Condition	Environmental Condition	Static-Critical Design Details	Fatigue-Critical Design Details - Cyclic Test R ratio (3 Stress Levels)			
					R1	R2	R3	R4
1	Method 1	1	1	B x 6				
2	Method 2	2	1	B x 6				
3	Method 3	3	1	B x 6				
4	Method 4	4	1	B x 6				
5	Method 5	5	1	B x 6				
5	Method 5	5	2	B x 6				
1	Method 1	1	1					B x 3 x F
2	Method 2	2	1					B x 3 x F
3	Method 3	3	1		B x 3 x F			
4	Method 4	4	1				B x 3 x F	
5	Method 5	5	1			B x 3 x F		
5	Method 5	5	2			B x 3 x F		

NOTES: Static - B x (# of test specimens); B = { 1, if no significant batch variability exists in lamina level; 3, if significant batch variability exists in lamina level

Fatigue - B x (# of stress levels) x F; F = { 2 for pooled fatigue analysis techniques; 6 for individual fatigue analysis techniques

Figure 22. Minimum Test Requirements for Generating Life Factors and LEFs

The composite data analyzed in reference 4 suggest that the LEFs shown in figure 18 are conservative for modern composites as a result of the improvements in materials and process techniques and test methods (i.e., less scatter in test data). Therefore, in the absence of sufficient test data, the values in figure 18 can be used during large-scale test substantiation. However, some of the modern, complex composite material forms or any composite material that exhibits large data scatter may have to be examined to ensure that the strength and life shape parameters are at least equivalent or better than the values shown in figure 18. This can be achieved through a minimum of a fatigue-life scatter analysis of representative coupon/element level S/N data obtained for one fatigue-critical design detail and a representative stress ratio (i.e., open-hole test with R=0), as shown in figure 23.

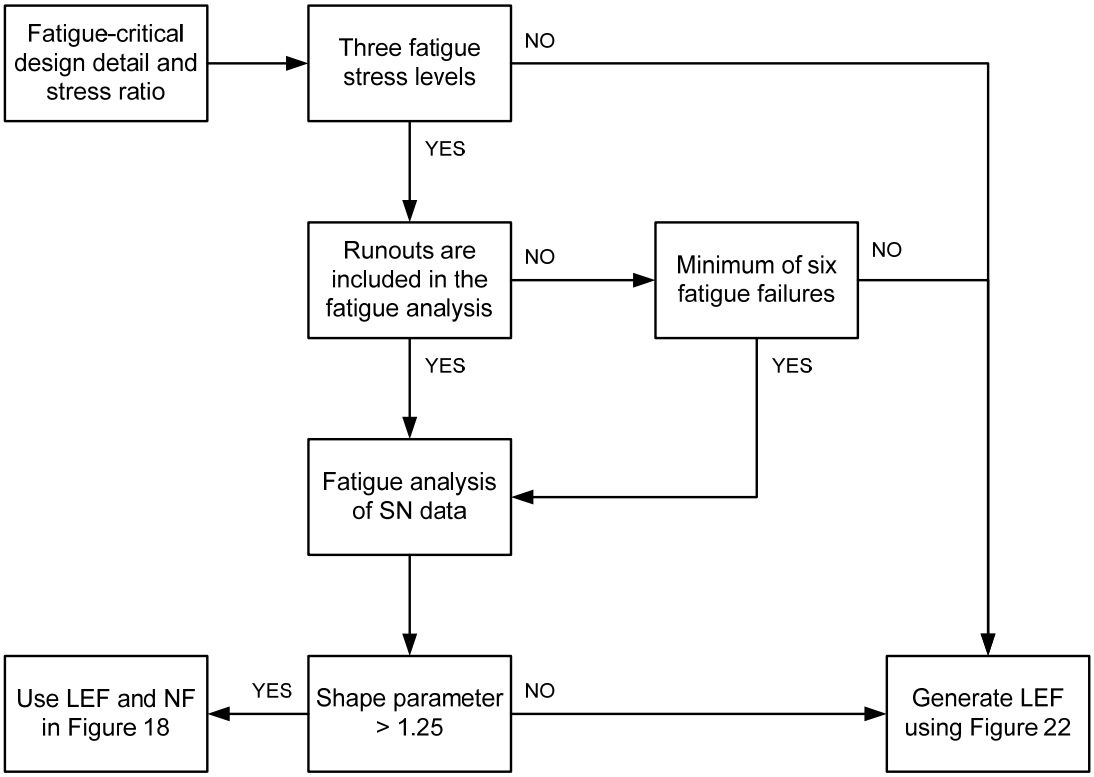

Figure 23. Minimum Requirements to be Fulfilled Prior to Using LEFs in Figure 18 for a Composite Structural Test

3.5 SCATTER ANALYSIS COMPUTER CODE.

The scatter analysis conducted for this report was carried out using a combination of Microsoft® Excel®, Visual Basic®, and ReliaSoft Weibull software [42]. Sendeckyj analysis was coded in Microsoft .NET Framework software. To alleviate the dependency on multiple software packages, the complete analysis with multiple analysis options was coded using a Microsoft Visual Basic macro that could be run in Microsoft Excel.

A user-friendly computer code, Scatter Analysis Computer Code (SACC) (figure 24), was developed so that the fatigue test data could be analyzed using the individual Weibull distribution, joint Weibull distribution, and Sendeckyj equivalent static-strength model. Appendix C contains the flow diagram for SACC. This program was designed to guide the analyst to select the most suitable approach for a given set of test data.

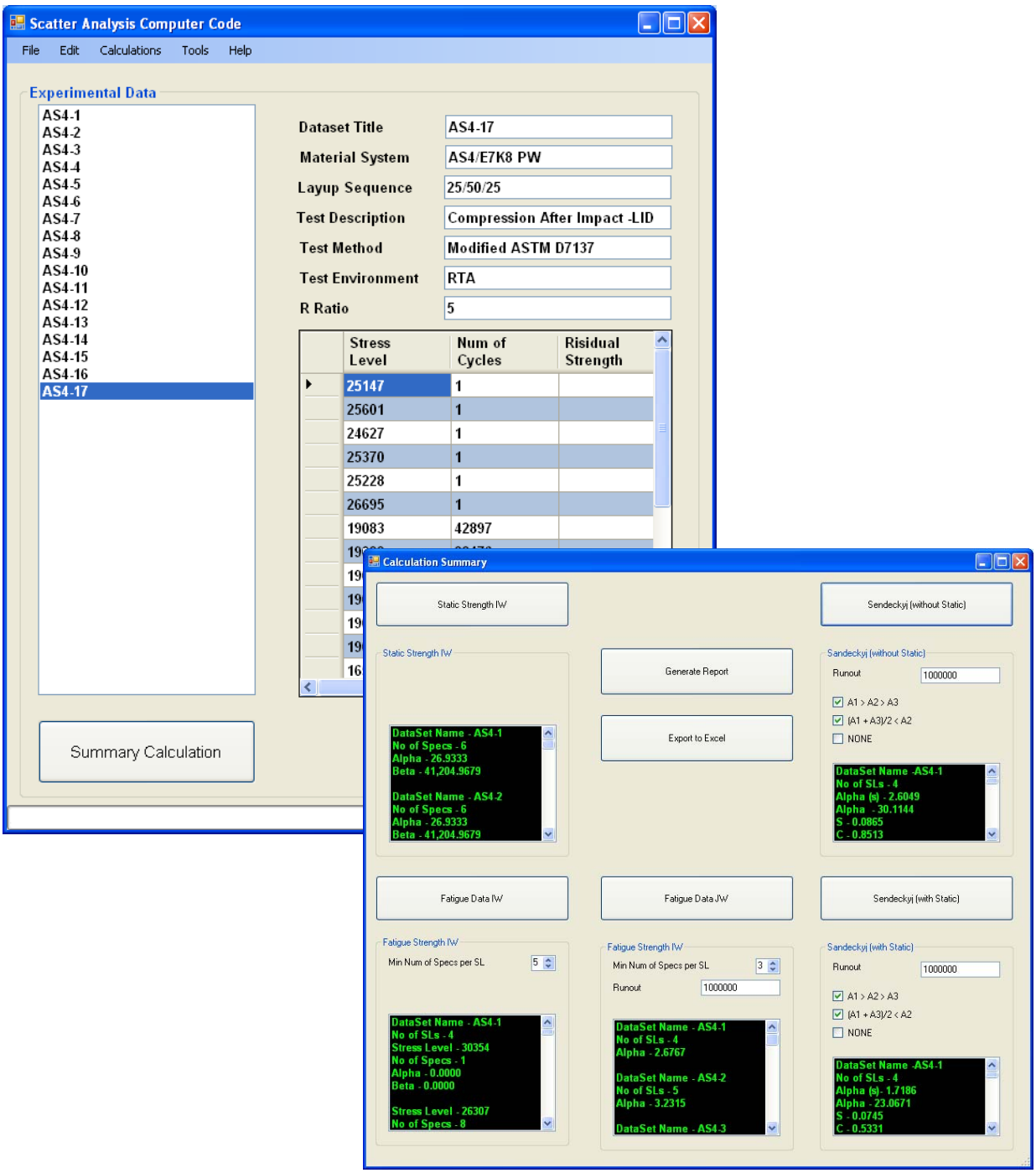

Figure 24. Scatter Analysis Using SACC

4. STATIC STRENGTH DATA SCATTER ANALYSIS.

An extensive material database is available in reference 2. Using this data, static scatter analysis was conducted to support U.S. Navy F/A-18 certification. These data represented several structural details and variables such as laminate lay-up, loading mode, load transfer, specimen geometry, and environment. To improve the accuracy of the Weibull analysis, only the data sets

containing six or more specimens were included. Also, the U.S. Navy F/A-18 certification program only included autoclaved 350°F-cure graphite-epoxy materials. This analysis was conducted primarily on fiber-dominated failures. In addition, these data were summarized primarily for laminated construction and did not include sandwich construction or bonded joints. The goal of the current research was to produce data for materials commonly used in aircraft applications and to promote the development of this type of data, not only for individual certification plans, but also for shared databases.

4.1 STRUCTURAL DETAILS FOR STATIC SCATTER ANALYSIS.

The current research obtained the static-strength data from several material databases, described in section 2.1. These data included details such as bonded joints, sandwich details, impact damage, disbonds, lightening strikes, process variability, in-plane shear and interlaminar shear specimens in addition to the variables studied in the U.S. Navy F/A-18 certification program. These structural details were included in the analysis to represent design variables or details in present aircraft applications. Data generated from coupons and elements were used to investigate the dependence of the static-strength shape parameter, which is a representation of static data scatter, on various coupon geometries, loading modes, environments, and lay-ups. The degree to which these parameters affect the overall LEF factors on a parametric basis is discussed in section 5.4. Several examples are shown for obtaining MSSP, or α_R, by pooling different data sets. When pooling data to estimate MSSP, the user is advised to select appropriate design details that are applicable to a certain application.

The material databases described in this section represent typical examples of commonly used composite materials. These materials are used in several ongoing certification programs and certified general aviation aircraft. The databases include coupon-level, static-strength data for the following primary variables:

- Different lay-ups—hard, quasi-isotropic, and soft (typically 50/40/10, 25/50/25, and 10/80/10, respectively, for unidirectional material and 40/20/40, 25/50/25, and 10/80/10, respectively, for fabric material) and all ±45° plies (0/100/0)
- Environments—cold temperature dry (CTD), RTA, room temperature wet (RTW), elevated temperature dry (ETD), elevated temperature wet (ETW)
- Tension—unnotched, OH, filled hole (FH)
- Compression—unnotched, OH, FH
- Bearing—single shear, double shear, bearing-bypass
- In-plane shear—VNRS
- Interlaminar shear—double-notched compression, short-beam shear

In addition to the coupon-level data, element-level static-strength data were included in the analysis, representing the following design details/requirements:

- Sandwich—core materials, facesheet
- Bonded joints—single-lap shear, picture frame
- Damage tolerance—CAI, TAI, sandwich
- Four-point bending—laminate, sandwich

The following sections include the generation of the shape parameter for several different material systems accounting for the effects of different geometries, environments, lay-ups, and loading modes.

4.1.1 Advanced Composites Group AS4/E7K8 3K Plain-Weave Fabric.

The static-strength test results of AS4/E7K8 plain-weave fabric (AS4-PW) for both RTA and ETW environmental conditions are shown in table 7.

Table 7. Static-Strength Test Results for AS4-PW

Specimen Configuration		RTA Strength (ksi)			ETW Strength (ksi)		
Lay-Up	Test Description	Average	STDEV	CV	Average	STDEV	CV
10/80/10	OHT	43.455	0.773	1.778	35.175	0.296	0.842
	OHC	40.472	1.571	3.882	28.579	1.156	4.045
	SLS–C (t=0.01″)	5.532	0.381	6.880			
	SLS–T (t=0.01″)	4.528	0.163	3.601			
	SLS–T (t=0.01″) No antibuckling	2.301	0.058	2.532			
	SLS–T (t=0.06″)	5.057	0.591	11.685	2.038	0.330	16.196
	DNC	3.988	0.160	4.022	3.004	0.154	5.130
	CAI – BVID (20 plies)	34.605	1.541	4.454			
	CAI – VID (40 plies)	30.263	0.814	2.690			
Sandwich	4PB – HRH 10	0.145	0.003	2.071	0.128	0.003	2.388
0/100/0	TAI – BVID	21.875	0.350	1.600	11.912	1.295	10.876
	TAI – VID	15.118	0.626	4.143			
	OHC	17.799	0.387	2.172			
25/50/25	OHC	45.375	1.624	3.579	32.019	1.347	4.208
	Unimpacted	55.736	0.839	1.505			
	CAI – BVID	36.025	0.851	2.361			
	CAI – VID	29.671	0.891	3.003			
	CAI – LID	25.445	0.692	2.721			
40/20/40	CAI – VID	31.845	1.026	3.223			

STDEV = Standard deviation
CV = Coefficient of variation
BVID = Barely visible impact damage
VID = Visible impact damage
LID = Large impact damage

Using ReliaSoft® Weibull software, the shape parameter ($\hat{\alpha}$) and the scale parameter ($\hat{\beta}$) of each data set were obtained and are shown in table 8.

Table 8. Weibull Parameters for Static-Strength Distributions of AS4-PW

Specimen Configuration		Test Environment	Weibull Statistics		
Lay-Up	Test Description		$\hat{\alpha}$	$\hat{\beta}$ (ksi)	n
10/80/10	OHT	RTA	58.036	43.826	6
		ETW	61.970	35.653	6
	OHC	RTA	26.930	41.205	6
		ETW	33.290	29.081	8
	SLS-C (t=0.01″)	RTA	22.665	5.683	6
	SLS-T (t=0.01″)	RTA	31.165	4.602	5
	SLS-T (t=0.01″) No antibuckling	RTA	40.072	2.239	6
	SLS-T (t=0.06″)	RTA	12.358	5.286	6
		ETW	6.919	2.174	8
	DNC	RTA	28.130	4.061	6
		ETW	23.845	3.072	6
	CAI-BVID (20 plies)	RTA	35.461	35.185	3*
	CAI-VID (40 plies)	RTA	49.383	30.608	6
7Sandwich	4PB-HRH 10	RTA	47.621	0.146	6
		ETW	43.177	0.129	6
0/100/0	TAI-BVID	RTA	44.694	17.992	5
	TAI-VID	RTA	34.344	15.379	6
	OHC	RTA	63.247	22.046	6
		ETW	11.766	12.431	5
25/50/25	OHC	RTA	33.424	46.101	6
		ETW	28.157	32.613	6
	CAI-BVID*	RTA	45.771	36.413	6
	CAI-VID*	RTA	32.222	30.103	6
	CAI-LID*	RTA	36.676	25.776	6
40/20/40	CAI-VID	RTA	32.984	32.324	6

* These shape parameters are not included in calculating MSSP. They were performed to investigate the data scatter with respect to the damage intensity.

BVID = Barely visible impact damage
VID = Visible impact damage
LID = Large impact damage

The Weibull distribution of the shape parameters ($\hat{\alpha}$) of RTA and ETW data shown in table 8 are compared against the pooled Weibull distribution of RTA and ETW data in table 9 (denoted by All). Weibull statistics obtained for these three distributions of shape parameters from MLE and both X and Y rank regression (RRX and RRY, respectively) are shown in table 9. Using the shape and scale parameters, α and β, respectively, the modal shape parameter corresponding to the distribution of $\hat{\alpha}$'s, which is denoted as α_{Modal}, was calculated for each case. Unlike the cases of test data distributions, the scale parameters here do not have units as they correspond to the distributions of shape parameters ($\hat{\alpha}$) obtained for different test data sets.

Table 9. Weibull Statistics for Combined Distribution of Scatter in Static-Strength Distributions of AS4-PW

Analysis Method	Weibull Parameter	Analysis Cases		
		All	RTA	ETW
MLE	α	2.514	3.1323	1.782
	β	39.387	41.777	33.629
	α_{Modal}	32.193	36.950	21.183
RRX	α	2.188	2.900	1.441
	β	39.882	41.980	34.452
	α_{Modal}	30.167	36.284	15.148
RRY	α	2.103	2.790	1.417
	β	40.285	42.288	34.665
	α_{Modal}	29.644	36.068	14.621

The probability density function of Weibull shape parameters and the reliability plot for both RTA and ETW static data (combined case denoted as All) are shown in figure 25. The shape and scale parameters for this distribution from MLE are 2.514 and 39.387, respectively. The corresponding modal value is 32.193. The difference between Weibull statistics obtained from different analysis methods (i.e., MEL, RRX, and RRY) is least significant for the RTA data set while it is most significant for the ETW data set. The scatter in ETW data sets is reflected in the combined case for all three analysis methods. Statistics from MLE portray the least scatter for all three cases while RRY portrays the most scatter. For large data sets, i.e., more than 20-30 samples, MLE produces reliable Weibull statistics, while for small data sets, RRX tends to produce relatively accurate data. A procedure to obtain reliable Weibull statistics and recommendations is documented in section 3.4.2. For example, if the structure does not contain adhesive joints, the shape parameters for adhesive static-strength distributions do not have to be pooled to determine MSSP.

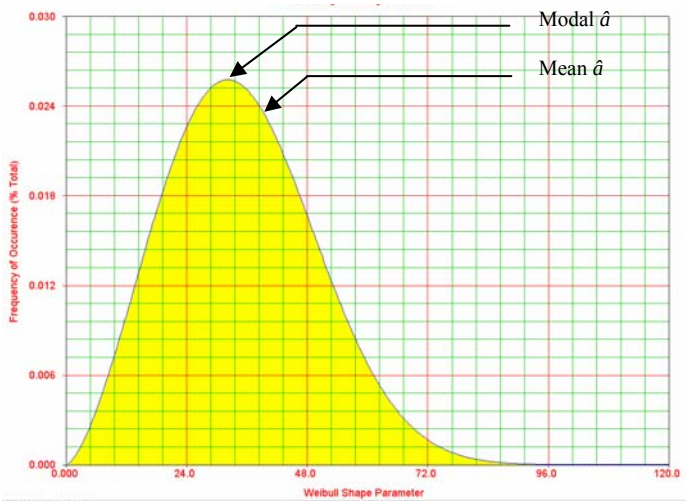

(a)

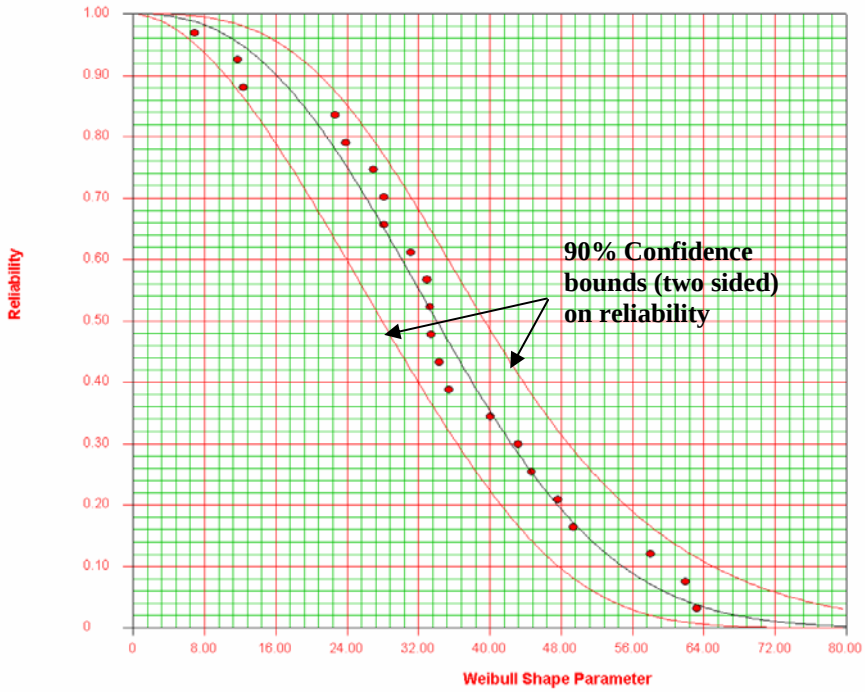

(b)

Figure 25. (a) Probability Density Function and (b) Reliability Plot of Shape Parameters for AS4-PW Static Strength Distributions

4.1.2 Toray T700/#2510 Plain-Weave Fabric.

Toray T700/#2510 plain-weave fabric (T700-PW) data from several material databases (section 2.1) are analyzed in this section. Static strength results obtained from FAA-LEF data are shown in table 10.

Table 10. Static-Strength Test Results for T700-PW

Specimen Configuration		RTA Strength (ksi)			ETW Strength (ksi)		
Lay-Up	Test Description	Average	Standard Deviation	CV	Average	Standard Deviation	CV
10/80/10	OHT	41.686	0.889	2.133	38.961	0.886	2.273
	OHC	34.986	0.923	2.639	28.626	0.788	2.752
	SLS-T (t = 0.06″)	5.064	0.197	3.900			
	DNC	3.007	0.197	6.568	3.242	0.179	5.530
40/20/40	CAI-BVID	43.408	0.610	1.405			
Sandwich	4PB-HRH 10	0.137	0.003	2.333	0.125	0.005	3.626

BVID = Barely visible impact damage
CV = Coefficient of variation

The corresponding Weibull statistics are shown in table 11 along with the number of specimens used for analysis. Although the Weibull analysis was conducted for 40/20/40 CAI specimens, the shape parameter was not included in the analysis for calculating MSSP of AS4-PW because this data set had less than the minimum recommended number of specimens for a reliable analysis.

Table 11. Weibull Parameters for Static-Strength Distributions of T700-PW

Specimen Configuration		Test Environment	Weibull Statistics		
Lay-Up	Test Description		$\hat{\alpha}$	$\hat{\beta}$ (ksi)	n
10/80/10	OHT	RTA	48.872	42.108	6
		ETW	45.242	39.387	6
	OHC	RTA	41.540	35.408	6
		ETW	40.170	28.989	7
	SLS-T (t = 0.06″)	RTA	36.927	5.144	6
	DNC	RTA	17.989	3.094	6
		ETW	25.000	3.317	6
40/20/40	CAI	RTA	67.713	43.700	3*
Sandwich	4PB-HRH 10	RTA	42.068	0.139	6
		ETW	42.190	0.127	6

*Not included in combined analysis due to insufficient data points.

Forty-eight additional FAA-LVM data sets [33] containing 863 specimens for T700-PW were added to the static-strength scatter analysis. These data sets represent hard (40/20/40, table 12), quasi-isotropic (25/50/25, table 13), and soft (10/80/10, table 14) lay-up sequences, as well as a wide range of loading modes and environmental conditions (CTD, RTA, and ETW). Furthermore, each data set contains specimens from three distinct material batches.

Distribution of shape parameters calculated for T700-PW using the static data in FAA-LEF and FAA-LVM is shown in figure 26. The scatter in shape parameters of 10/80/10 laminate is significantly higher than for the other two laminate stacking sequences.

Table 12. Weibull Parameters for Static-Strength Distributions of 40/20/40 T700-PW (FAA-LVM)

Test Description	Test Environment	Shape Parameter, $\hat{\alpha}$	Number of Specimens
Single-shear bearing tension	RTA	45.409	18
Double-shear bearing tension	RTA	49.696	30
Bearing-bypass 50% compression	RTA	42.102	15
Bearing-bypass 50% tension [t/D = 0.475]	RTA	40.040	18
Bearing-bypass 50% tension [t/D = 0.570]	RTA	42.594	18
Bearing-bypass 50% tension [t/D = 0.712]	RTA	43.426	15
Bearing-bypass 50% tension [t/D = 0.949]	RTA	38.198	18
Unnotched tension	RTA	29.820	18
Unnotched compression	RTA	20.584	18
Open-hole compression	RTA	30.453	19
Filled-hole tension	CTD	29.908	19
Filled-hole tension	RTA	20.296	19
Filled-hole tension	ETW	25.192	18
V-notched rail shear	RTA	59.208	18
Open-hole tension [w/D = 3]	RTA	20.594	18
Open-hole tension [w/D = 4]	RTA	27.054	18
Open-hole tension [w/D = 6]	RTA	27.202	20
Open-hole tension [w/D = 8]	RTA	25.441	18

Table 13. Weibull Parameters for Static-Strength Distributions of 25/50/25 T700-PW (FAA-LVM)

Test Description	Test Environment	Shape Parameter, $\hat{\alpha}$	Number of Specimens
Double-shear bearing tension	CTD	25.721	18
Double-shear bearing tension	RTA	43.827	18
Double-shear bearing tension	ETW	34.775	18
Single-shear bearing tension	CTD	28.956	18
Single-shear bearing tension	RTA	18.132	18
Single-shear bearing tension	ETW	33.850	18
Bearing-bypass 50% tension	RTA	44.264	15
Bearing-bypass 50% compression	RTA	48.028	15
Open-hole tension [w/D = 6]	CTD	35.816	18
Open-hole tension [w/D = 6]	RTA	34.049	18
Open-hole tension [w/D = 6]	ETW	25.223	21
Unnotched tension	CTD	51.153	18
Unnotched tension	RTA	40.186	18
Unnotched tension	ETW	38.383	18
Unnotched compression	CTD	31.498	18
Unnotched compression	RTA	27.074	18
Unnotched compression	ETW	23.676	19
Open-hole compression	CTD	34.475	19
Open-hole compression	RTA	46.999	18
Open-hole compression	ETW	33.319	21
V-notched rail shear	RTA	16.458	18

Shape parameters obtained from static-strength distributions were combined for several different analysis scenarios to investigate the degree to which these parameters affect the MSSP of T700-PW (table 15). Adhesively bonded T700-PW element data from FAA-EOD material database are included in section 4.1.9.

Table 14. Weibull Parameters for Static-Strength Distributions of 10/80/10 T700-PW (FAA-LVM)

Test Description	Test Environment	Shape Parameter, $\hat{\alpha}$	Number of Specimens
Bearing-bypass 50% tension	RTA	65.445	15
Bearing-bypass 50% compression	RTA	74.360	15
Open-hole tension [w/D = 6]	RTA	51.713	8
Unnotched tension	RTA	58.084	19
Unnotched compression	RTA	36.056	18
Open-hole compression	RTA	50.909	18
V-notched rail shear	CTD	9.963	18
V-notched rail shear	RTA	17.278	19
V-notched rail shear	ETW	13.103	18

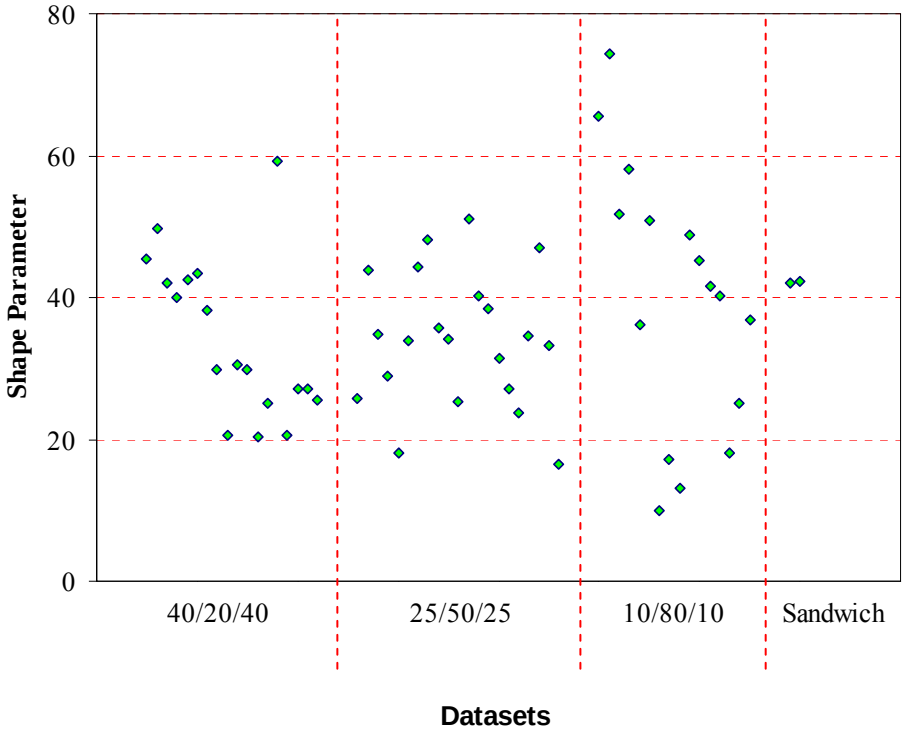

Figure 26. Shape Parameters for T700-PW Static-Strength Distributions

Table 15. Summary of Weibull Shape Parameter Analysis of T700-PW

Analysis Case	Analysis Variable	Weibull Statistics			Number of Data Sets
		α	β	α_{Modal}	
Database	FAA-LVM	2.801	40.038	34.196	48
	FAA-LEF	5.405	41.184	39.654	9
	Combined	2.961	40.307	35.071	57
Test environment	CTD	3.164	34.467	30.569	8
	RTA	2.912	43.359	37.524	32
	ETW	4.545	31.252	29.589	8
Lay-up	40/20/40	3.391	38.218	34.477	18
	25/50/25	4.139	37.585	35.155	21
	10/80/10	1.925	47.172	32.239	9
Loading mode	All bearing	3.412	46.947	42.409	17
	OH/FH	3.550	35.976	32.773	16
	VNRS	1.449	25.941	11.559	5
	Unnotched	3.379	39.728	35.809	10

4.1.3 Toray 7781/#2510 8-Harness Satin-Weave Fabric.

Toray 7781/#2510 8-harness satin-weave fabric (7781-8HS) data from the FAA-LEF material database are analyzed in this section. The static-strength test results for 7781-8HS are shown in table 16, and the corresponding Weibull statistics are shown in table 17.

Table 16. Static-Strength Test Results for 7781-8HS

Specimen Configuration		RTA Strength (ksi)			ETW Strength (ksi)		
Lay-Up	Test Description	Average	Standard Deviation	CV	Average	Standard Deviation	CV
10/80/10	OHT	26.808	0.366	1.364	21.120	0.186	0.882
	OHC	33.227	0.324	0.974	21.824	0.335	1.533
	DNC	3.494	0.170	4.861	2.364	0.264	11.167
Sandwich	4PB-HRH 10	0.139	0.002	1.795	0.128	0.002	1.206

CV = Coefficient of variation

Table 17. Weibull Parameters for Static-Strength Distributions of 7781-8HS

Specimen Configuration		Test Environment	Weibull Statistics		
Lay-Up	Test Description		$\hat{\alpha}$	$\hat{\beta}$ (ksi)	n
10/80/10	OHT	RTA	76.115	26.983	6
		ETW	116.288	21.211	6
	OHC	RTA	104.824	33.385	6
		ETW	62.351	21.998	6
	DNC	RTA	32.221	3.561	6
		ETW	10.116	2.476	6
Sandwich	4PB-HRH 10	RTA	80.260	0.142	6
		ETW	86.690	0.128	6

Table 18 shows the analysis results for the Weibull distribution of shape parameters shown in table 17. Compared to RRX and RRY analyses, MLE data indicate significant skewness, possibly due to an insufficient number of data sets. It is important to explore the other two regression techniques for such cases. For this case, the RRX method was selected to determine the static-strength shape parameter.

Table 18. Weibull Statistics for Combined Distribution of 7781-8HS

Analysis Method	Weibull Parameter	Analysis Cases	
		All	RTA
MLE	α	2.185	3.295
	β	79.512	82.038
	α_{Modal}	60.092	73.510
RRX	α	1.438	2.079
	β	83.239	84.814
	α_{Modal}	36.416	61.868
RRY	α	1.278	1.868
	β	87.043	87.042
	α_{Modal}	26.385	57.748

4.1.4 Toray T700/#2510 Unidirectional Tape.

Toray T700/#2510 unidirectional tape (T700-UT) data from the FAA-LVM material database [33] are analyzed in this section. This database contains 853 T700-UD specimens from 47 data sets. These data sets represent hard (50/40/10), quasi-isotropic (25/50/25), and soft (10/80/10) lay-up sequences, as well as a wide range of loading modes and environmental conditions (CTD, RTA, and ETW). Furthermore, each data set contains specimens from three distinct material batches. Shape parameters obtained from static-strength distributions were combined for several different analysis scenarios to investigate the degree to which these parameters affect the MSSP of T700-UT (table 19). The distribution of shape parameters calculated for T700-UT using the static data in FAA-LVM is shown in figure 27. As for T700-PW, scatter in the distribution of 10/80/10 static-strength shape parameters is significantly higher than for the other two laminate stacking sequences.

Table 19. Summary of Weibull Shape Parameter Analysis of T700-UT

Analysis Case	Analysis Variable	Weibull Statistics			Number of Data Sets
		α	β	α_{Modal}	
All	T700-UT	2.255	37.176	28.671	47
Test environment	CTD	3.465	35.279	31.977	8
	RTA	2.174	39.519	29.763	31
	ETW	3.139	29.188	25.830	8
Lay-up	50/40/10	3.006	37.479	32.760	17
	25/50/25	2.246	36.083	27.760	21
	10/80/10	1.648	38.205	21.678	9
Loading mode	All bearing	2.772	47.451	40.375	17
	OH/FH	4.197	30.659	28.734	16
	V-notch rail shear	2.471	15.719	12.743	5
	Unnotched	3.949	32.859	30.517	10

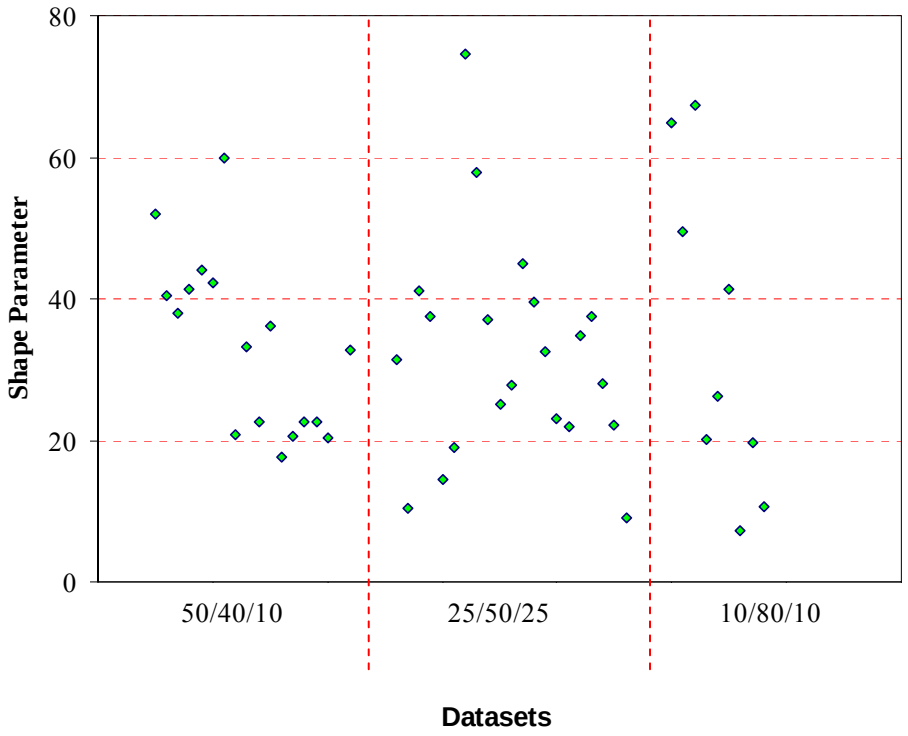

Figure 27. Shape Parameters for T700-UT Static-Strength Distributions

4.1.5 Advanced Composites Group AS4C/MTM45 Unidirectional Tape.

ACG AS4C/MTM45 12K unidirectional tape (AS4C-UT) data from the FAA-LVM material database [33] are analyzed in this section. This database contains 1151 AS4C-UT specimens from 86 data sets. These data sets represent hard (50/40/10), quasi-isotropic (25/50/25), and soft (10/80/10) lay-up sequences, as well as a wide range of loading modes and environmental conditions (CTD, RTA, ETD, and ETW). Most of these data sets contain specimens from multiple distinct material batches. Shape parameters obtained from static-strength distributions were combined for several different analysis scenarios to investigate the degree to which these parameters affect the MSSP of AS4C-UT (table 20). The distribution of shape parameters calculated for AS4C-UT using the static data in FAA-LVM is shown in figure 28.

Table 20. Summary of Weibull Shape Parameter Analysis of AS4C-UT

Analysis Case	Analysis Variable	Weibull Statistics			Number of Data Sets
		α	β	α_{Modal}	
All	AS4C-UT	2.151	34.779	26.004	86
Test environment	CTD	2.213	31.603	24.084	16
	RTA	3.094	35.541	31.329	30
	ETW	1.905	35.777	24.208	38

Table 20. Summary of Weibull Shape Parameter Analysis of AS4C-UT (Continued)

Analysis Case	Analysis Variable	Weibull Statistics			Number of Data Sets
		α	β	α_{Modal}	
Lay-up	50/40/10	2.040	36.953	26.560	14
	25/50/25	2.731	36.635	31.002	19
	10/80/10	2.378	46.883	37.267	19
	Lamina	3.0435	25.5518	22.4171	34
Loading mode	All bearing	2.729	33.131	28.028	6
	OH/FH	2.632	36.646	30.561	30
	Unnotched	2.252	51.868	39.964	12

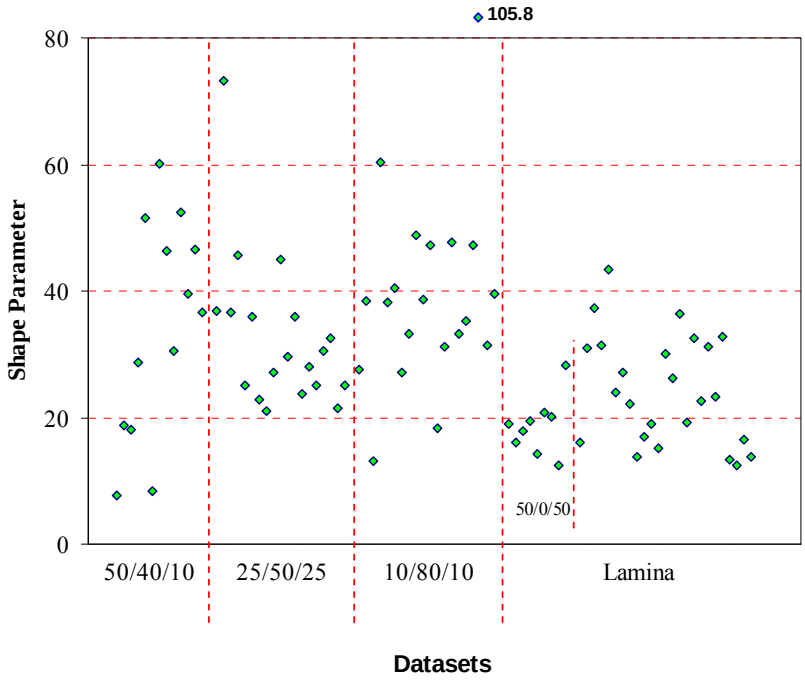

Figure 28. Shape Parameters for AS4C-UT Static-Strength Distributions

4.1.6 Advanced Composites Group AS4C/MTM45 5-Harness Satin-Weave Fabric.

ACG AS4C/MTM45 five-harness satin-weave fabric (AS4C-5HS) data from the FAA-LVM material database [33] are analyzed in this section. This database contains 1083 AS4C-5HS specimens from 78 data sets. These data sets represent hard (40/20/40), quasi-isotropic (25/50/25), and soft (10/80/10) lay-up sequences, as well as a wide range of loading modes and environmental conditions (CTD, RTA, ETD, and ETW). Most of these data sets contain specimens from multiple distinct material batches. Shape parameters obtained from static-strength distributions were combined for several different analysis scenarios to investigate the degree to which these parameters affect the MSSP of AS4C-5HS (table 21). The distribution of

shape parameters calculated for AS4C-5HS using the static data in FAA-LVM is shown in figure 29.

Table 21. Summary of Weibull Shape Parameter Analysis of AS4C-5HS

Analysis Case	Analysis Variable	Weibull Statistics			Number of Data Sets
		α	β	α_{Modal}	
All	AS4C-5HS	2.104	35.694	26.267	78
Test environment	CTD	2.263	37.711	29.144	14
	RTA	2.284	36.714	28.534	26
	ETW	1.976	34.586	24.207	34
Lay-up	40/20/40	2.926	29.475	25.549	13
	25/50/25	1.985	36.759	25.828	18
	10/80/10	2.834	46.860	40.190	16
	Lamina	2.062	26.579	19.266	20
Loading mode	All bearing	2.643	21.535	17.990	5
	OH/FH	2.454	41.192	33.279	29
	NH	2.293	42.576	33.163	16

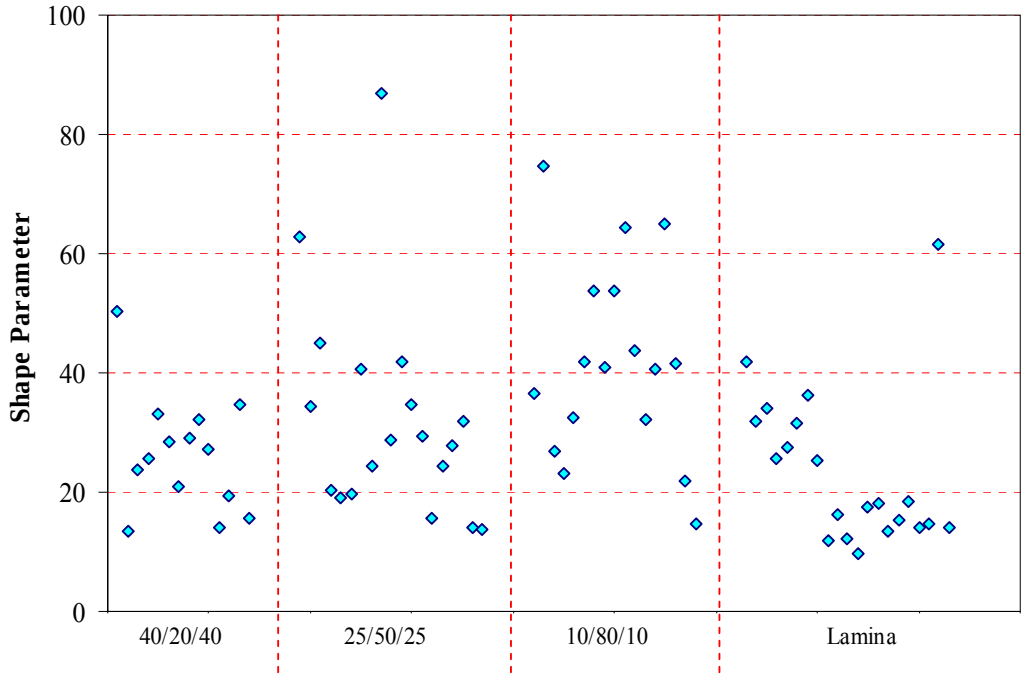

Figure 29. Shape Parameters for AS4C-5HS Static-Strength Distributions

4.1.7 Nelcote T700/E765 Graphite Unidirectional Tape.

Nelcote (formally FiberCote) T700/E765 24K graphite unidirectional tape (E765-UT) material from the FAA-LVM material database [33] are analyzed in this section. This database contains 834 E765-UT specimens from 47 data sets. These data sets represent hard (50/40/10), quasi-isotropic (25/50/25), and soft (10/80/10) lay-up sequences, as well as a wide range of loading modes and environmental conditions (CTD, RTA, and ETW). Most of these data sets contain specimens from multiple distinct material batches. Shape parameters obtained from static-strength distributions were combined for several different analysis scenarios to investigate the degree to which these parameters affect the MSSP of E765-UT (table 22). The distribution of shape parameters calculated for E765-UT using the static data in FAA-LVM is shown in figure 30.

Table 22. Summary of Weibull Shape Parameter Analysis of E765-UT

Analysis Case	Analysis Variable	Weibull Statistics			Number of Data Sets
		α	β	α_{Modal}	
All	E765-UT	2.0867	30.719	22.471	47
Test environment	CTD	2.241	22.254	17.095	7
	RTA	2.117	31.091	22.98	29
	ETW	1.779	23.739	14.920	7
Lay-up	40/20/40	1.976	32.334	22.627	16
	25/50/25	2.158	29.647	22.215	20
	10/80/10	2.445	30.220	24.372	8
Loading mode	All bearing	3.280	31.484	28.180	16
	OH/FH	2.343	39.705	31.312	14
	VNRS	3.229	14.368	12.810	4
	Unnotched	2.222	23.345	17.838	9

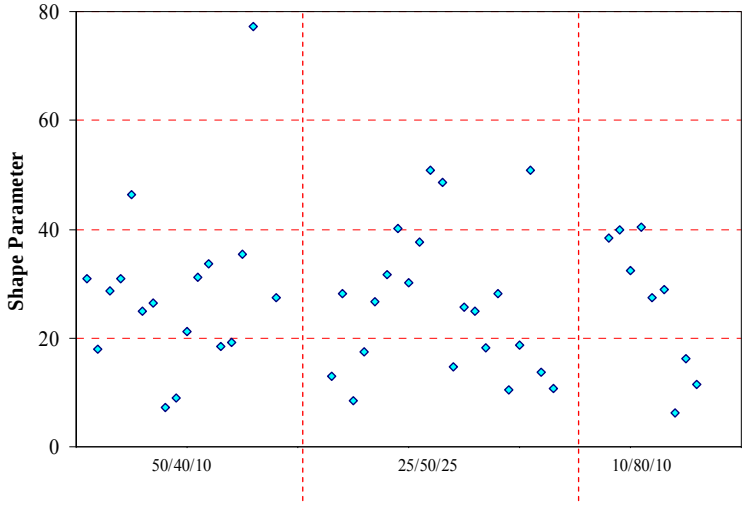

Figure 30. Shape Parameters for E765-UT Static-Strength Distributions

4.1.8 Nelcote T300/E765 3K Plain-Weave Fabric.

Nelcote (formally FiberCote) T700/E765 plain-weave fabric (E765-PW) material from the FAA-LVM material database [33] are analyzed in this section. This database contains 722 E765-PW specimens from 48 data sets. These data sets represent hard (40/20/40), quasi-isotropic (25/50/25), and soft (10/80/10) lay-up sequences, as well as a wide range of loading modes and environmental conditions (CTD, RTA, and ETW). Most of these data sets contain specimens from multiple distinct material batches. Shape parameters obtained from static-strength distributions were combined for several different analysis scenarios to investigate the degree to which these parameters affect the MSSP of E765-PW (table 23). The distribution of shape parameters calculated for E765-PW using the static data in FAA-LVM is shown in figure 31.

Table 23. Summary of Weibull Shape Parameter Analysis of E765-PW

Analysis Case	Analysis Variable	Weibull Statistics			Number of Data Sets
		α	β	α_{Modal}	
All	E765-PW	2.389	32.735	26.089	48
Test environment	CTD	2.434	24.535	19.740	7
	RTA	2.535	35.837	29.400	31
	ETW	2.751	27.714	23.516	7
Lay-up	40/20/40	2.484	37.800	30.723	17
	25/50/25	2.947	30.194	26.233	20
	10/80/10	1.907	27.820	18.843	8
Loading mode	All bearing	2.200	30.491	23.148	16
	OH/FH	3.098	32.641	28.782	15
	VNRS	1.288	26.488	8.269	4
	NH	4.619	38.055	36.097	9

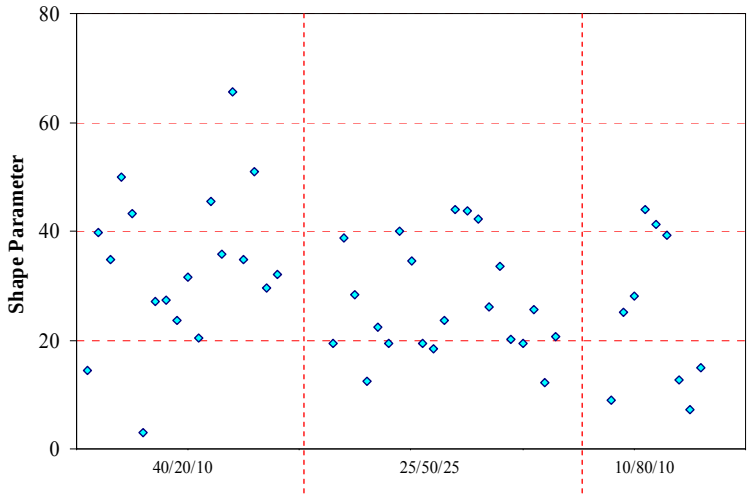

Figure 31. Shape Parameters for E765-PW Static-Strength Distributions

4.1.9 Adhesive Effects of Defects Data.

The FAA-EOD database [36] contains more than 70 bonded-joint PFS element tests that have disbonds, lightening strikes, and low-velocity impact damages. These specimens were fabricated using T700-PW and 7781-8HS and bonded with the EA9394 two-part paste adhesive system. Only data sets that contain more than five specimens were included in the Weibull analysis (table 24).

Table 24. Weibull Parameters for Bonded-Joint PFS Element Tests

Adherend Material	Defect Description	Shape Parameter, $\hat{\alpha}$	Number of Specimens
T700-PW	No disbonds	11.358	9
	Small disbonds (circle, diamond)	18.319	6
	Large rectangular disbonds	14.181	9
	Lightning strikes	22.390	6
	Low-velocity impact damages	20.255	20
7781-8HS	No disbonds	19.701	5

In addition to the above data, 60 bonded joints (elements), impacted at different energy levels [36] and tested in SLS, were analyzed. Specimens with a 4- by 4-inch gage section were fabricated using the following material systems (commonly used in aircraft applications) and bonded using EA9394 two-part paste adhesive system:

- Newport NB321/7781 E-glass satin weave (FGSW)
- Toray T700G-12K/3900-2 carbon fabric plain weave (CFPW)
- Toray T800S/3900-2B carbon tape unidirectional (CTU)

Although three different impactor diameters (0.50, 0.75, and 1.00 inch) and three different energy levels (88.5, 221, and 354 in-lbf) were used to inflict damage, the impact damages were contained mostly within the elastic trough and away from the side edges. Thus, although the damage states (i.e., residual indentation and damage area) were different, the residual strength was not significantly influenced by the impact parameters. Thus, the data for each material were pooled and analyzed for scatter (table 25).

Table 25. Weibull Parameters for Bonded SLS Element Tests

Adherend	Adhesive	Weibull Statistics		Number of Specimens
		$\hat{\alpha}$	$\hat{\beta}$ (lbf)	
FGSW	EA9394	14.134	847.347	20
CFPW		25.657	867.356	20
CTU		19.890	986.267	20

4.2 SUMMARY.

The databases used for the strength scatter analysis included coupon- and component-level static-strength data for different lay-up configurations, test environments, and loading modes, and included solid laminates, sandwich construction, and bonded joints. First, the shape parameters obtained for different strength data sets were pooled separately by material system and test environment, and compared to strength shape parameters obtained by pooling all the data (denoted by All) for each material system. Figure 32 shows that ETW data have the highest scatter while RTA data have the least scatter, for most cases analyzed in this section. The scatter in ETW data can be attributed to variations in total moisture absorption among test specimens and the time to reach the elevated test temperature prior to test. Furthermore, the shape parameter obtained by pooling test data from all environmental conditions is close to the shape parameter obtained by analyzing RTA test data of each material system. Also, the pooled values are higher than the MSSP of 20, which was the value used for U.S. Navy F/A-18 certification, for all the material systems analyzed in this report. This can be attributed to the improvements in materials, process techniques, and test methodologies of modern composite materials.

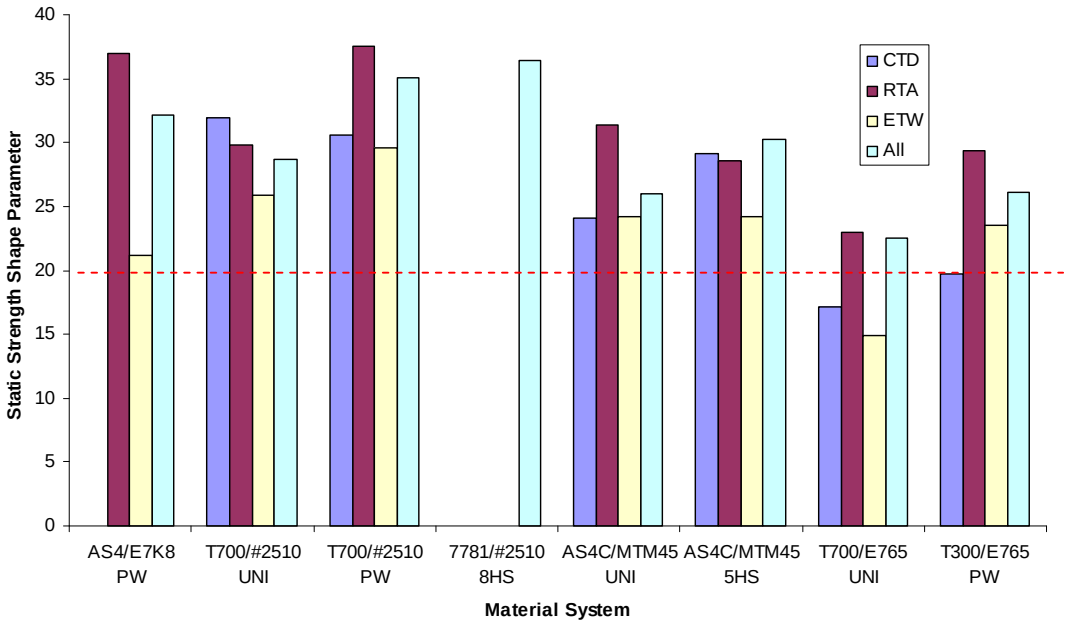

Figure 32. Comparison of Composite Strength Shape Parameters for Different Environments

Second, the previous exercise was repeated by pooling data by different lay-ups. Figure 33 indicates that the shape parameters of T700-PW and E765 unidirectional lay-up (UNI) are independent of lay-up sequence, while other material systems indicate large variations among lay-up sequences. Also, the shape parameter obtained by pooling test data from all laminate stacking sequences is close to the shape parameter obtained by analyzing the quasi-isotropic laminate (25/50/25) test data of most of the material systems. For both ACG material systems (AS4C-UT and AS4C-5HS), the soft laminate (10/80/10) test data indicate the least scatter while T700-UNI and E765-PW indicate the most scatter. The hard laminate (50/40/10) test data indicate the reverse trend for these four material systems.

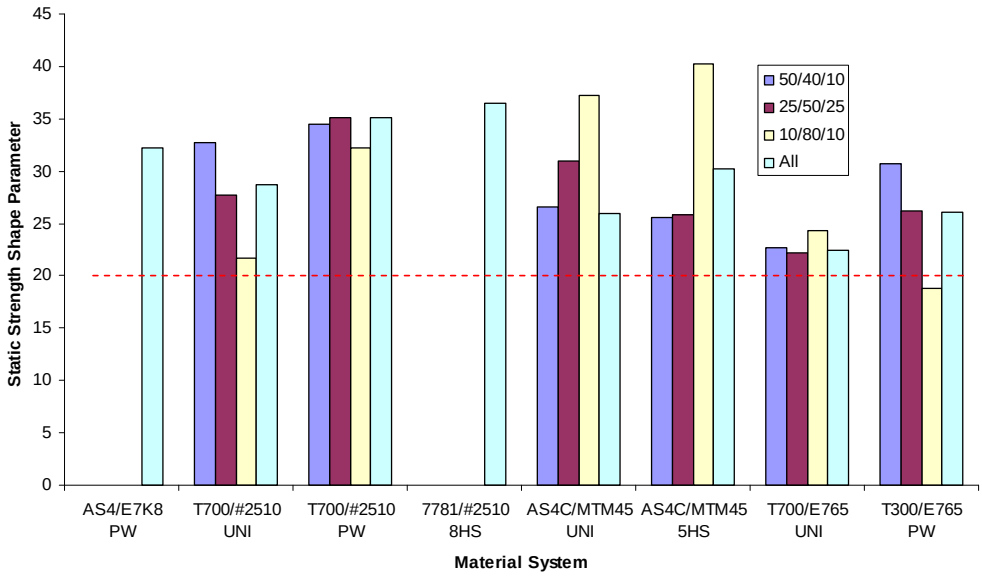

Figure 33. Comparison of Composite Strength Shape Parameters for Different Lay-Ups

Third, the data were pooled by specimen configuration. Figure 34 shows that the loading mode significantly influences the static scatter for all five material systems. For both Nelcote material systems (E765-UNI and E765-PW), unnotched (NH) test data indicate the most scatter, resulting in shape parameters significantly lower than 20, while OH and FH data indicate the least scatter. For both ACG material systems, bearing test data indicate the most scatter. For both Toray material systems (T700-UNI and T700-PW), OH and FH data indicate the most scatter, close to the scatter in unnotched test data, while bearing test data indicate the least scatter.

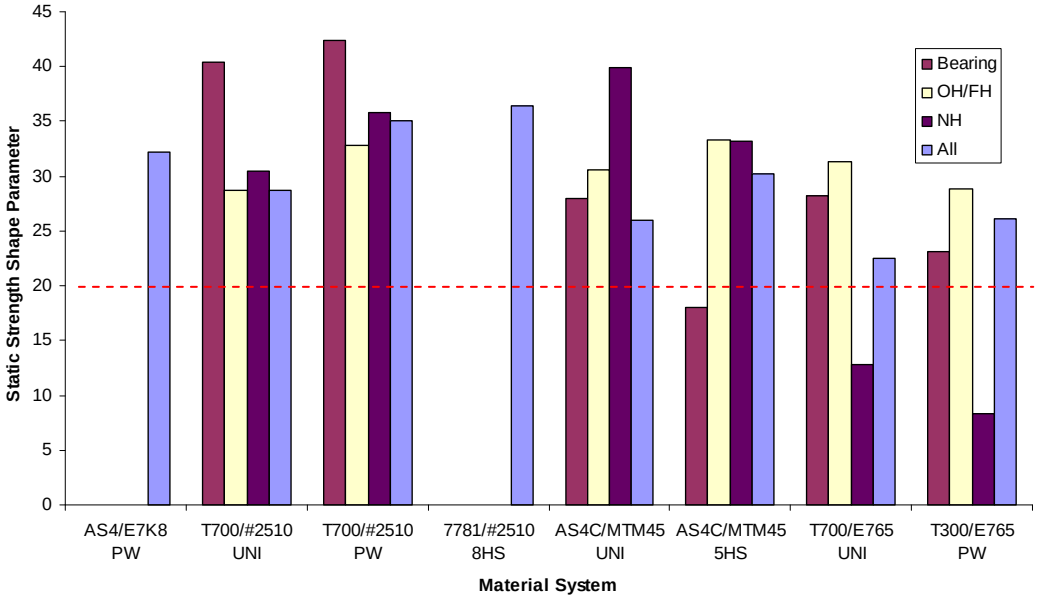

Figure 34. Comparison of Composite Strength Shape Parameters for Different Loading Modes

The scatter analysis results in this section provide guidance to design a cost-effective test matrix for generating reliable MSSP. The data are documented so they can be readily available for a particular case, and the user does not have to generate new data or analyze the scatter. To generate a life shape parameter that represents the general scatter of current typical aircraft composite materials, the shape parameters representing all composite and adhesive strength data sets included in this report are pooled. However, the authors recommend generating shape parameters based on the materials, processes, and design details related to the critical areas of a particular structure rather than using pooled data to ensure safety and reliability of fatigue life predictions based on scatter analysis. This exercise was done to establish a generic scatter distribution of modern composite strength data and to compare that against the values proposed by Whitehead, et al. [2]. The resulting (modal) strength shape parameter or α_R is 26.31.

5. FATIGUE LIFE DATA SCATTER ANALYSIS.

An extensive fatigue scatter analysis was conducted by Whitehead, et al. [2], on various material databases. These databases represented several structural details and variables such as R-ratio, laminate lay-up, loading mode, load transfer, specimen geometry, and test environment. The material database of Badaliance and Dill [43] included 204 graphite/epoxy data sets, whereas Whitehead and Schwarz [45] included 2925 data points from 120 data sets of graphite/epoxy, 450 data points from 26 data sets of E-glass/epoxy, and 419 step-lap bonded joints from 23 data sets. To increase the accuracy of the Weibull analysis, only the data sets containing five or more specimens were included in the individual Weibull analysis.

Typically, an S/N curve contains fatigue failures for multiple stress levels in addition to static-strength data points and any run-outs. In this report, the fatigue life scatter was analyzed using individual Weibull, joint Weibull, and Sendeckyj analyses. Only data sets containing more than five specimens within a stress level were included in the individual Weibull analysis. Residual strength data for all run-outs were included in the Sendeckyj analysis.

5.1 STRUCTURAL DETAILS FOR FATIGUE LIFE SCATTER ANALYSIS.

This section includes over one thousand data points from the following composite material systems commonly used in aircraft applications:

- AS4/E7K8 plain-weave fabric (AS4-PW)
- T700/#2510 plain-weave fabric (T700-PW)
- 7781/#2510 8-harness satin-weave fabric (7781-8HS)

In addition, adhesive fatigue data from the FAA-D5656 material database [35] in the following test environments for three adhesive systems are included:

- Hysol EA9696 film adhesive
- PTM&W ES6292 paste adhesive
- Cessna Aircraft proprietary paste adhesive (Loctite)

Data generated from coupons and elements were used to investigate the dependence of the fatigue shape parameter, which is a representation of fatigue-life scatter, on various coupon geometries, loading modes, environments, and lay-ups. The degree to which these parameters affect the overall LEF factors from a parametric basis is discussed in section 5.4. Since fatigue-life data inherently exhibit significantly more scatter than static-strength data, the MLSP, or α_L, is noticeably smaller than the MSSP, or α_R. Several examples are shown for obtaining MLSP by pooling different data sets. When pooling data to estimate MLSP, the user is advised to select appropriate design details that are applicable to a certain structure.

The material databases described in this section represent typical examples of commonly used composite material systems. These materials are used in several ongoing certification programs and certified general aviation aircraft. The databases include coupon-level static-strength data for the following primary variables:

- Lay-ups—hard, quasi-isotropic, and soft (typically 50/40/10, 25/50/25, and 10/80/10, respectively, for unidirectional material, and 40/20/40, 25/50/25, and 10/80/10, respectively, for fabric material) and all ±45° plies (0/100/0)
- Environments—CTD, RTA, RTW, ETW
- Tension—OH
- Compression—OH
- Interlaminar shear—DNC

In addition to coupon-level data, element-level static-strength data were included in the analysis to represent the following design details/requirements:

- Sandwich—core materials, facesheet
- Bonded joints—SLS
- Damage tolerance—CAI, sandwich

The following sections include the generation of shape parameters for several different material systems accounting for the effects of different geometries, environments, lay-ups, and loading modes.

5.2 FATIGUE SCATTER ANALYSIS.

ReliaSoft Weibull software and SACC were used for the Sendeckyj analysis of fatigue data in two steps: with and without static-strength data. Residual strength data of all runout specimens were included in the Sendeckyj analysis. Individual and joint Weibull analyses were conducted using only the fatigue data. Kassapoglou [31] life predictions based only on static-strength scatter were compared with Sendeckyj analysis of experimental data in appendix A. Sendeckyj fitting parameters were recalculated for each S/N data set using SACC to generate the Sendeckyj fitting curves. As shown in appendix A, currently Kassapoglou methodology either under- or

overpredicts the fatigue life significantly for some S/N curves. Note that Kassapoglou methodology predicts the fatigue life based only on static data distribution.

5.2.1 The AS4/E7K8 Plain-Weave Fabric.

Fatigue analysis of 385 AS4-PW specimens from 14 data sets is included in this section. Each data set contains a minimum of three fatigue stress levels and at least six static-strength data points (figure 35). Figure 35 includes the static data, fatigue data (failures and run-outs) and the residual strength data for run-outs. Once the Sendeckyj fitting parameters C and S are determined, the fitting curve for the S/N data is obtained as shown in figure 35. In addition, the equivalent static strength for each fatigue data point (failures and run-outs) is displayed. S/N curves for AS4-PW are included in appendix A. Fatigue-life scatter analysis data are shown in table 26. The shape parameters corresponding to each S/N curve using Sendeckyj, individual Weibull, and joint Weibull scatter analysis are denoted as $\hat{\alpha}_{Sendeckyj}$, $\hat{\alpha}_{IW}$, and $\hat{\alpha}_{JW}$, respectively.

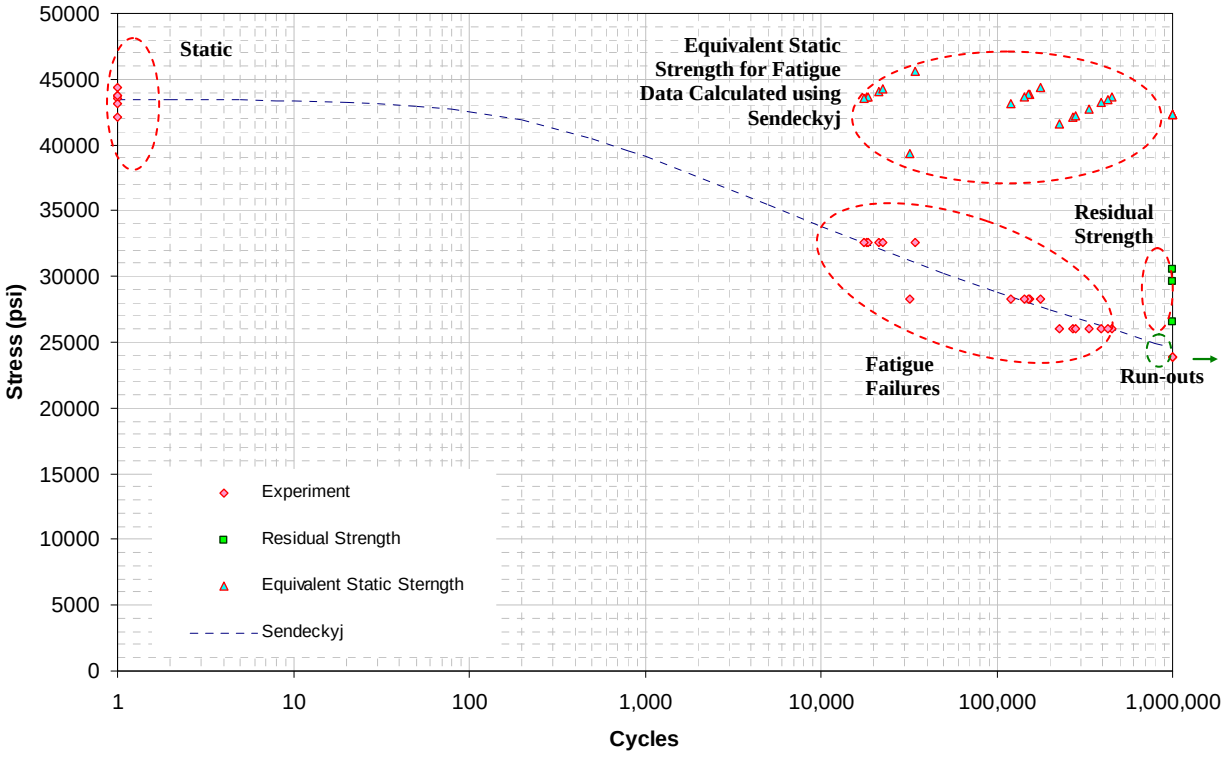

Figure 35. Sendeckyj Wearout Analysis Prediction of Fatigue Life of OHT (R = 0) – AS4-PW

Figure 36 shows a comparison of AS4-PW OHC fatigue data, where R = -1 for quasi-isotropic (25/50/25) and two resin-dominant lay-up configurations (10/80/10 and 0/100/0). The same data are normalized with respect to the ultimate static strength (average) and are shown in figure 37. Both figures show that the 0/100/0 lay-up with all ±45° plies exhibits the critical fatigue life but not the data set that has the highest scatter.

Table 26. Fatigue-Life Scatter Analysis for AS4-PW

Specimen Configuration			Sendeckyj		Weibull*	
Lay-Up	Test Description	R-Ratio	$\hat{\alpha}_{Sendeckyj}$ (with static)	$\hat{\alpha}_{Sendeckyj}$ (without static)	$\hat{\alpha}_{IW}$	$\hat{\alpha}_{JW}$
10/80/10	OH	-1	2.068	2.604	3.304	2.731
	OHC	5	1.792	2.328	3.223	3.329
	OHT	0	3.434	3.686	5.555	4.641
	OH	-0.2	3.319	4.090	4.003	3.962
	CAI-BVID (20 ply)	5	2.870	3.321	3.968	3.808
	CAI-VID (40 ply)	5	2.103	2.221	2.778	2.625
	DNC	-1	3.837	3.905	6.636	5.066
	DNC	-0.2	2.025	1.962	2.278	2.245
0/100/0	OH	-1	2.495	3.480	5.528	4.281
	TAI-BVID	0	1.640	1.515	2.477	2.144
	TAI-VID	0	1.111	1.065	1.974	1.931
Sandwich	4PB-HRH 10	0	1.924	2.020	5.131	2.795
25/50/25	OH	-1	3.224	3.661	5.713	4.745
	CAI-BVID[#]	5	1.774	2.234	2.446	2.355
	CAI-VID[#]	5	2.182	2.658	2.991	2.778
	CAI-LID[#]	5	2.466	2.799	3.272	2.948
40/20/40	CAI-VID	5	2.337	3.522	4.392	3.687

[*]Life scatter analysis using Weibull only includes fatigue data.
[#]Test data not included in the combined analysis for MLSP generation.

BVID = Barely visible impact damage
VID = Visible impact damage
LID = Large impact damage

Figure 38 shows a comparison of AS4-PW OH measured data for different R-ratios, and figure 39 shows a comparison of normalized data. Both figures indicate that R = -1 is the critical fatigue life and has the least scatter when pooled with static data points.

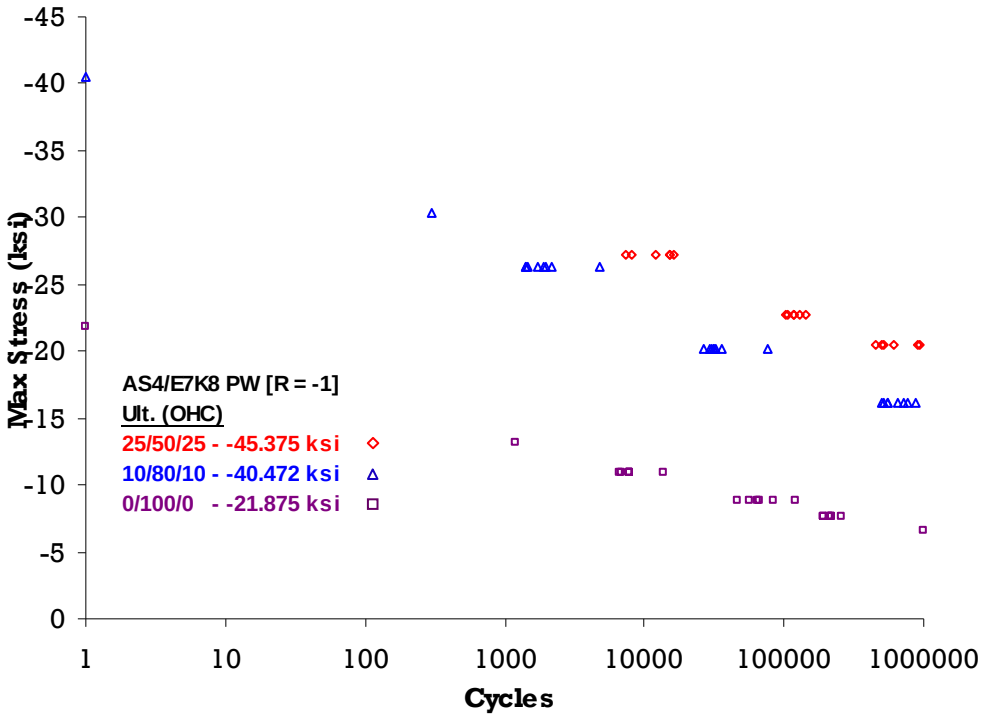

Figure 36. Effects of Lay-Up Sequence, AS4/E7K8, OH Measured Fatigue Data

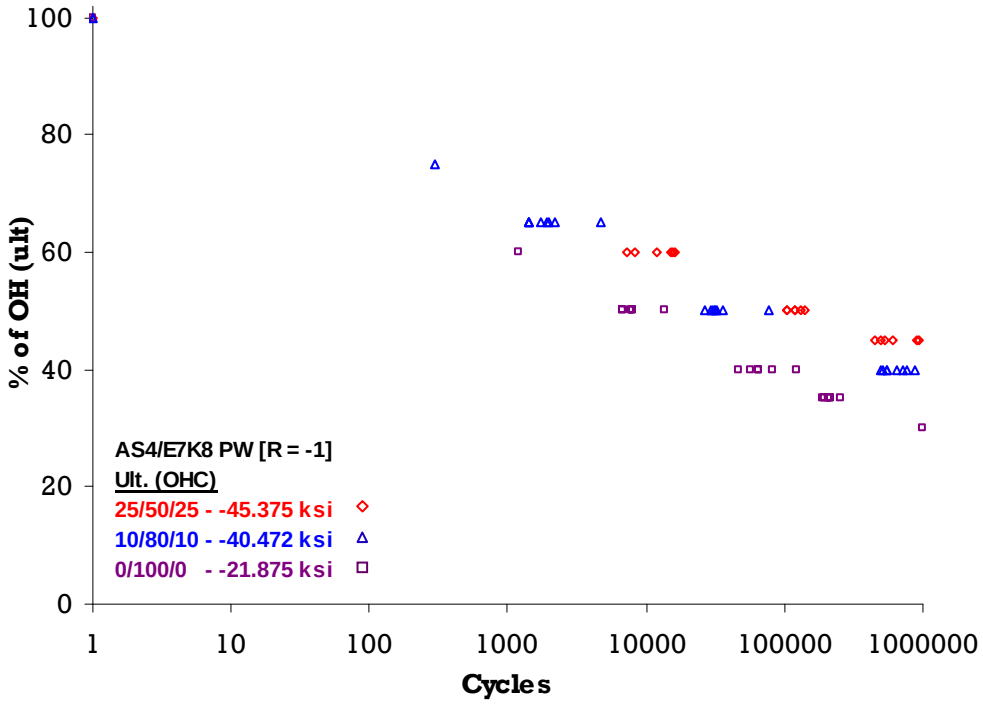

Figure 37. Effects of Lay-Up Sequence, AS4/E7K8, OH Normalized Fatigue Data

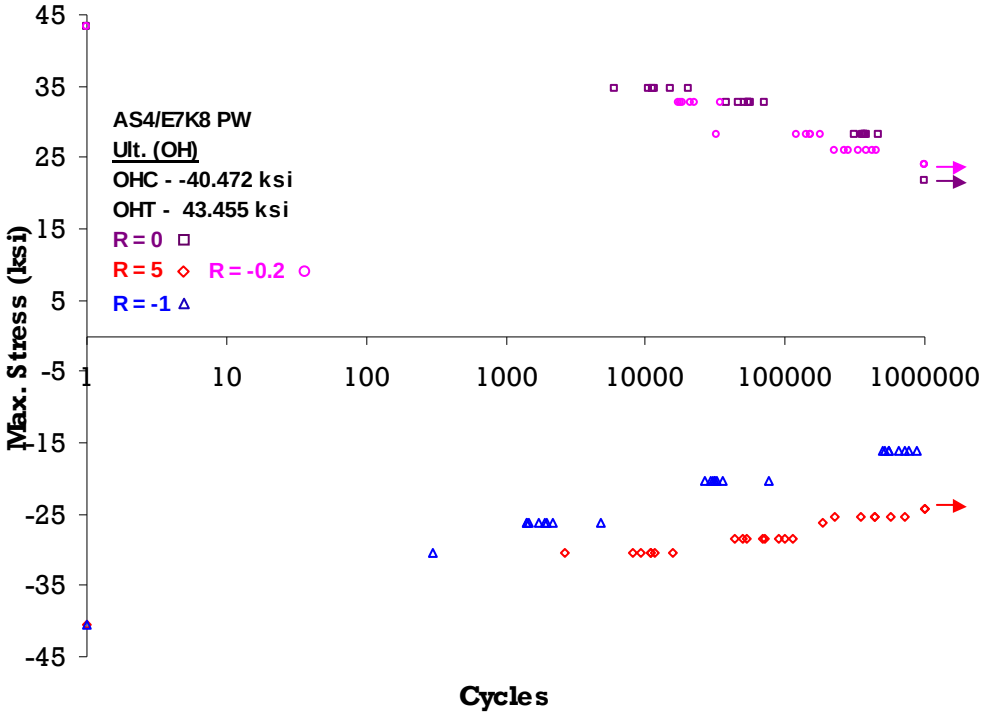

Figure 38. Effects of Stress Ratio for AS4-PW OH Measured Fatigue Data

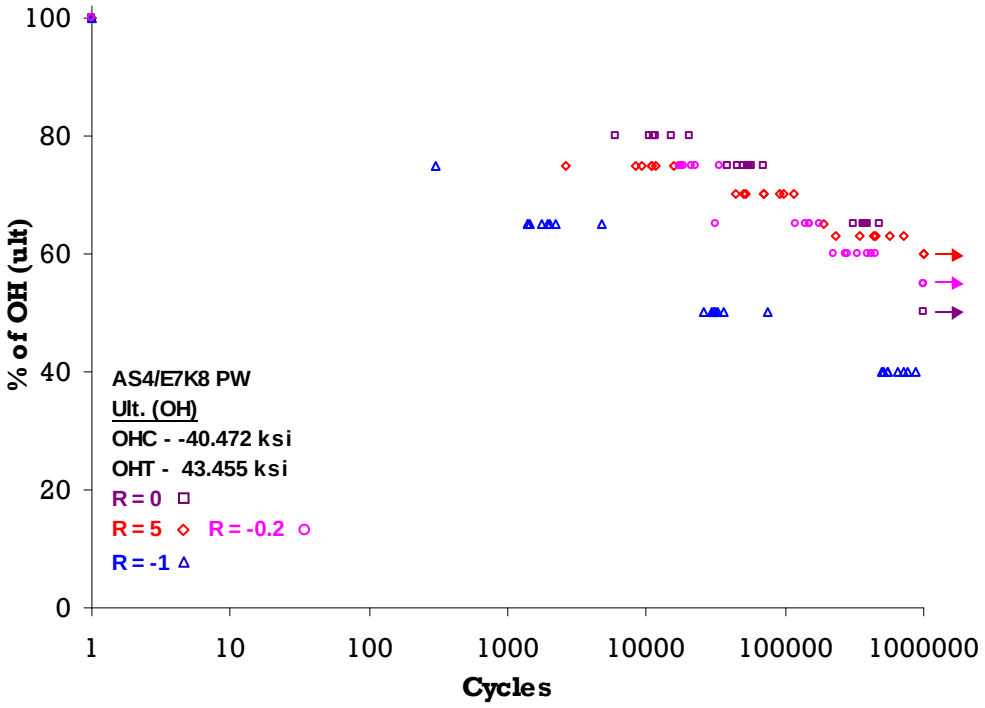

Figure 39. Effects of Stress Ratio for AS4-PW OH Normalized Fatigue Data

Figure 40 shows a comparison of AS4-PW CAI data for different lay-ups and impact energy levels. Normalized data indicate that the fatigue life is independent of lay-up, up to 1500 in-lbf/in impact energy. Figure 41 shows a comparison between CAI and TAI for different energy levels. Normalized data indicate that the fatigue life for TAI is independent of impact energy level up to 1500 in-lbf/in and is significantly lower than for CAI. The lower fatigue life for TAI can be attributed to the fact that these specimens are all ±45°, while the CAI specimens are 10/80/10 lay-up. TAI data also indicate significant scatter compared to CAI data.

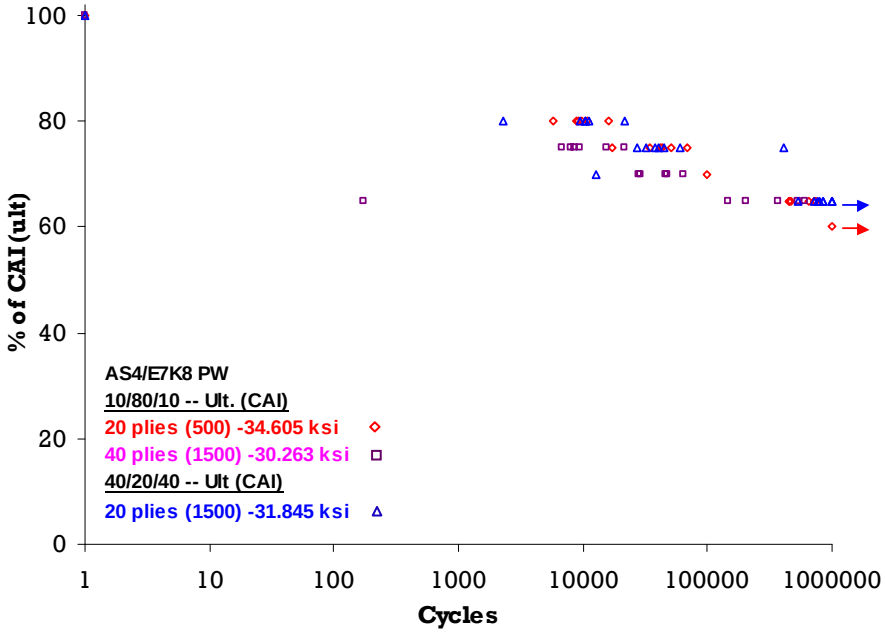

Figure 40. Effects of Lay-Up Sequence for AS4-PW CAI Normalized Fatigue Data

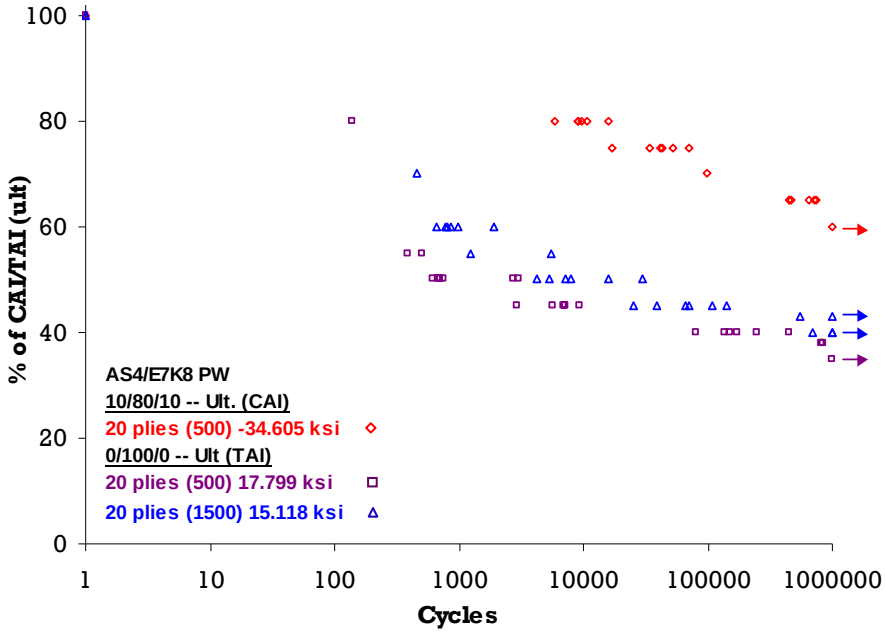

Figure 41. Comparison of CAI and TAI for AS4-PW

Figure 42 shows the summary of a detailed fatigue life scatter analysis conducted on AS4-PW using individual Weibull, joint Weibull, and Sendeckyj analyses (with and without static data in the S/N curves). These three techniques are also used in reference 2 for generating life and LEFs. However, the fatigue life scatter analysis for deriving life and LEFs is not limited to these three techniques. The Sendeckyj analysis includes runout and corresponding residual strength data points. Also, the Sendeckyj analysis produces a higher scatter as it is unbiased compared to the arithmetically averaged individual Weibull shape parameters (figure 42). Overall, the individual Weibull analysis provides the highest fatigue-life shape parameter, while the Sendeckyj analysis provides the lowest (conservative) fatigue-life shape parameter. For most cases, when the static data are included in the Sendeckyj analysis, the analysis resulted in significantly lower fatigue-life shape parameters than that without the static test data. For example, 7781-8HS OHT (R = 0) S/N data resulted in a fatigue-life shape parameter of 9.794 for Sendeckyj analysis without static data. When the static test data are included in the analysis, this value was reduced to 1.769. For most composite analysis cases, the Sendeckyj analysis without static test data and the joint Weibull analysis resulted in similar shape parameters.

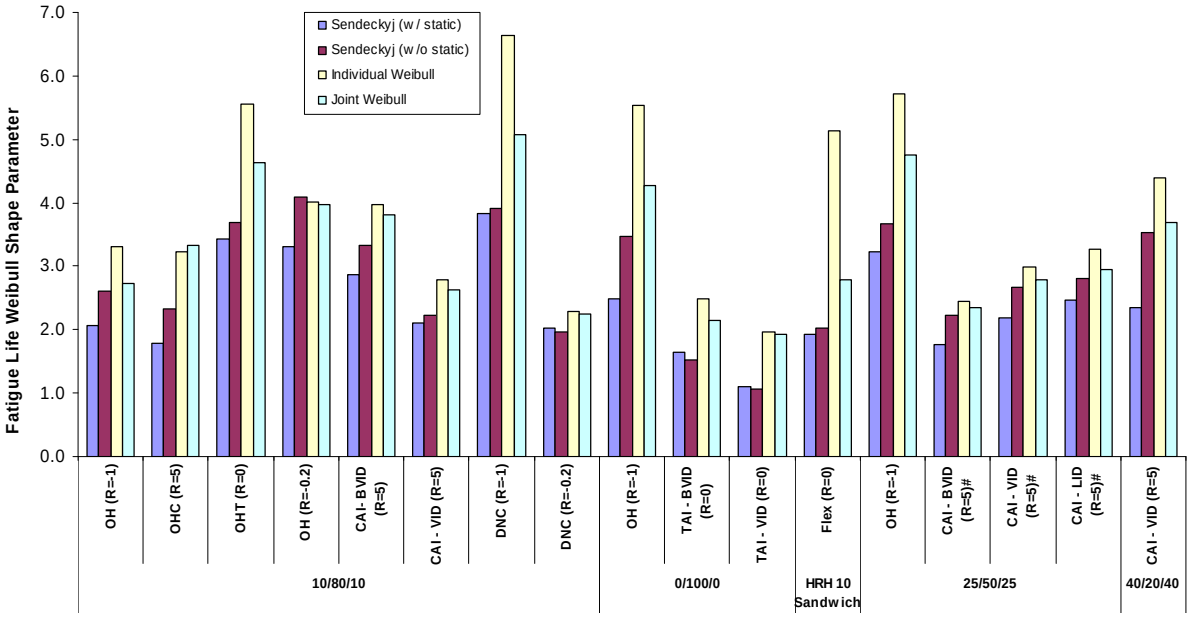

[OH (T/C): open-hole (tension/compression), CAI: compression after impact, TAI: Tension after impact, Flex: four-point bend flexure, DNC: double-notched compression, BVID: barely visible impact damage, VID: visible impact damage, LID: large impact damage]

Figure 42. Fatigue-Life Shape Parameters of AS4-PW From Different Analysis Methods

The Sendeckyj analysis is the most conservative of the above-mentioned methods because it includes static, fatigue failures, run-outs, and residual strength data. This analysis produces the equivalent static strength for each fatigue data point. These Sendeckyj equivalent strength values based on the fatigue data are pooled and compared against the tested static-strength data in table 27 and are shown in figure 43. Table 27 shows the coefficient of variation (CV) of each data set, i.e., static or pooled Sendeckyj equivalent static-strength data.

Table 27. Comparison of Static Strength of AS4-PW From Test and Sendeckyj Analysis

Specimen Configuration			Static Test		Pooled (Sendeckyj)	
Lay-Up	Test Description	R-Ratio	Strength (ksi)	CV	Strength (ksi)	CV
10/80/10	OH	-1	40.472	3.882	42.608	3.848
	OHC	5			41.360	2.783
	OHT	0	43.455	1.778	42.823	4.217
	OH	-0.2			42.942	5.055
	CAI-BVID (20 ply)	5	34.605	4.454	35.581	3.238
	CAI-VID (40 ply)	5	30.263	2.690	30.329	2.060
	DNC	-1	3.988	4.022	3.975	4.456
	DNC	-0.2	3.988	4.022	4.008	5.843
0/100/0	OH	-1	21.875	1.600	22.058	3.420
	TAI-BVID	0	17.799	2.172	16.709	9.695
	TAI-VID	0	15.118	4.143	14.807	5.112
Sandwich	4PB-HRH 10	0	0.145	2.071	0.141	8.411
25/50/25	OH	-1	45.375	3.579	45.882	2.499
	CAI-BVID	5	36.025	2.361	36.289	2.002
	CAI-VID	5	29.671	3.003	29.990	2.438
	CAI-LID	5	25.445	2.721	25.614	2.259
40/20/40	CAI-VID	5	31.845	3.223	31.586	3.945

BVID = Barely visible impact damage
VID = Visible impact damage
LID = Large impact damage

The fatigue-life shape parameters for AS4-PW shown in table 26 are then fitted into another Weibull distribution, and the shape parameters corresponding to the new distribution and the model shape parameter are obtained from three different techniques: MLE, RRX, and RRY. As shown in table 28, there were no significant differences between the results of the different techniques. The Sendeckyj-model shape parameter (with static data) for life scatter was 2.427, while it was 3.974 for individual Weibull.

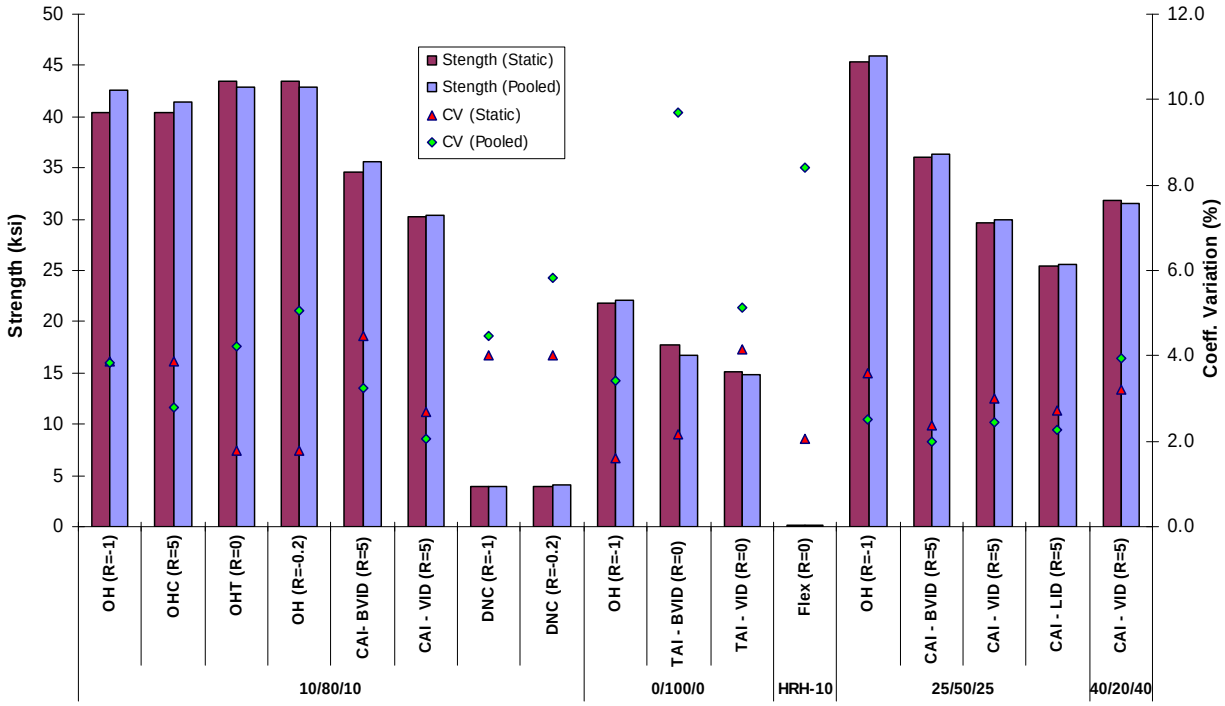

BVID = Barely visible impact damage
VID = Visible impact damage
LID = Large impact damage

Figure 43. Comparison of Static Strength and CV of AS4-PW From Test and Sendeckyj Analysis

Table 28. Weibull Statistics for Combined Distribution of AS4-PW

Analysis Method	Weibull Parameter	Fatigue Scatter Analysis Method			
		Sendeckyj (with static)	Sendeckyj (without static)	Individual Weibull	Joint Weibull
MLE	α	3.553	3.511	3.207	3.889
	β	2.716	3.138	4.558	3.800
	α_{Modal}	2.475	2.852	4.056	3.520
RRX	α	3.443	2.901	3.065	3.714
	β	2.710	3.163	4.541	3.786
	α_{Modal}	2.453	2.734	3.992	3.479
RRY	α	3.323	2.798	2.953	3.547
	β	2.725	3.184	4.572	3.811
	α_{Modal}	2.447	2.719	3.974	3.472

5.2.2 The T700/#2510 Plain-Weave Fabric.

Fatigue analysis of 240 T700-PW specimens from seven S/N curves is included in this section. Each data set contains a minimum of three fatigue stress levels and at least six static-strength data points. Similar to AS4-PW, T700-PW OH data show that R = -1 is the most critical stress ratio for both measured (figure 44) and normalized (figure 45) data comparisons. Fatigue-life scatter analysis data are shown in table 29. Figure 46 shows a comparison of fatigue-life scatter data obtained from different analysis techniques. Similar to AS4-PW, Sendeckyj analysis produces a higher scatter for T700-PW, as it is unbiased compared to the arithmetically averaged individual Weibull shape parameters. However, Sendeckyj data exhibit significantly less scatter compared to AS4-PW. As a result, the difference between Sendeckyj and individual Weibull fatigue-life shape parameters is not pronounced for T700-PW (table 30).

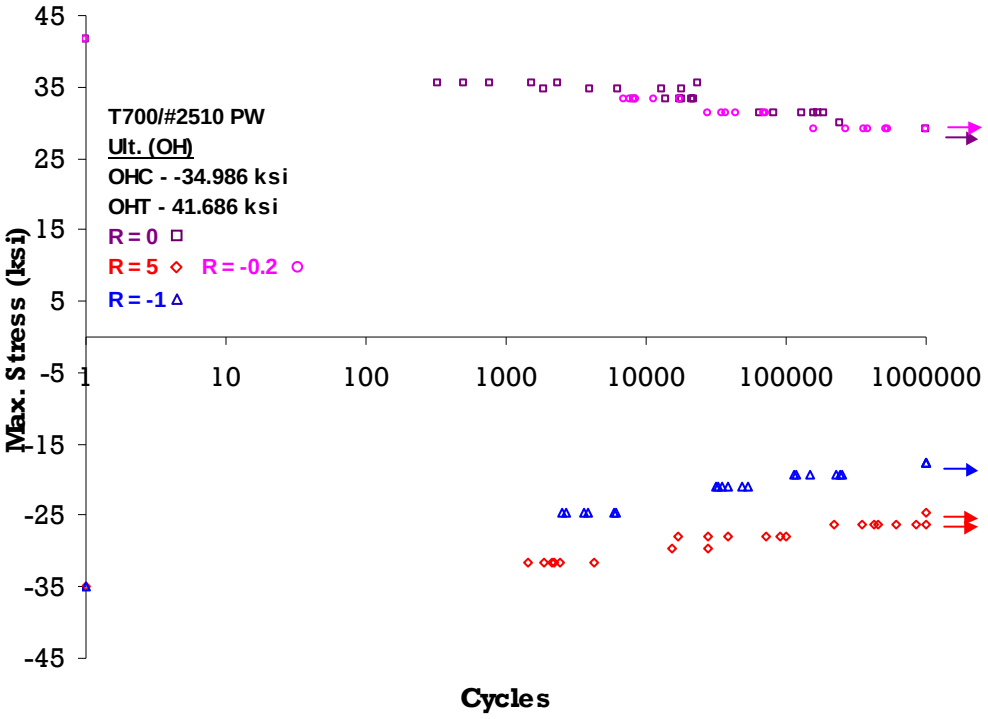

Figure 44. Effects of Stress Ratio for T700-PW OH Measured Fatigue Data

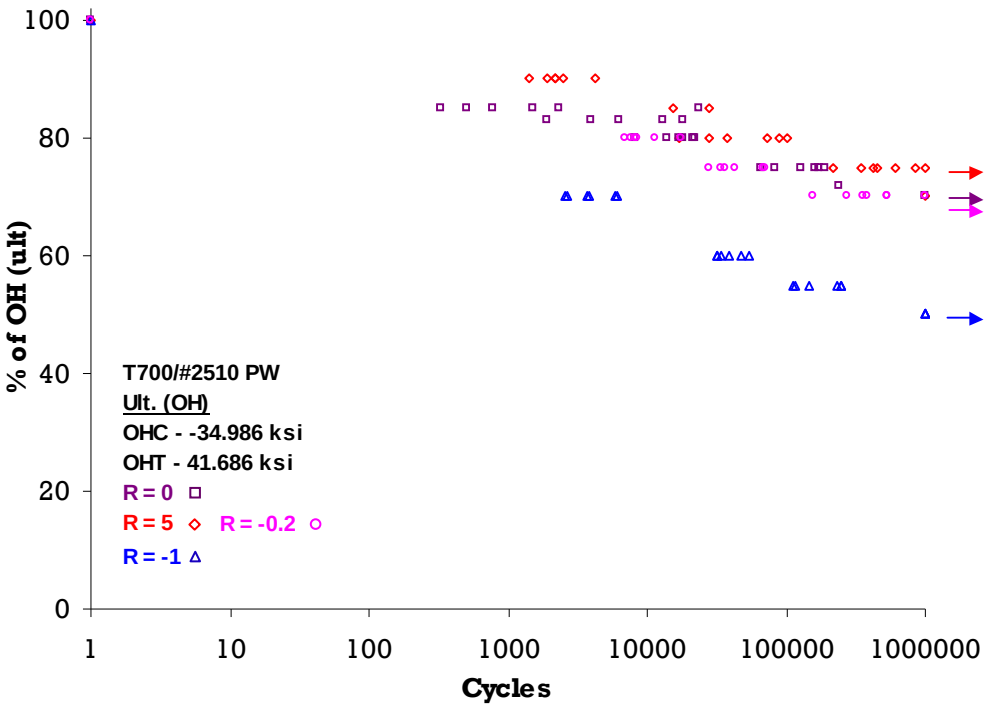

Figure 45. Effects of Stress Ratio for T700-PW OH Normalized Fatigue Data

Table 29. Fatigue-Life Scatter Analysis for T700-PW

Specimen Configuration			Sendeckyj		Weibull	
Lay-Up	Test Description	R-Ratio	$\hat{\alpha}_{Sendeckyj}$ (with static)	$\hat{\alpha}_{Sendeckyj}$ (without static)	$\hat{\alpha}_{IW}$	$\hat{\alpha}_{JW}$
10/80/10	OH	-1	2.796	3.389	3.932	3.793
	OHC	5	1.481	1.992	2.344	2.285
	OHT	0	1.367	2.086	2.721	2.207
	OH	-0.2	1.904	2.079	2.615	2.320
	DNC	-1	1.496	1.464	1.714	1.765
	DNC	-0.2	1.547	1.635	2.489	1.949
Sandwich	4PB-HRH 10	0	1.764	2.315	2.881	2.464

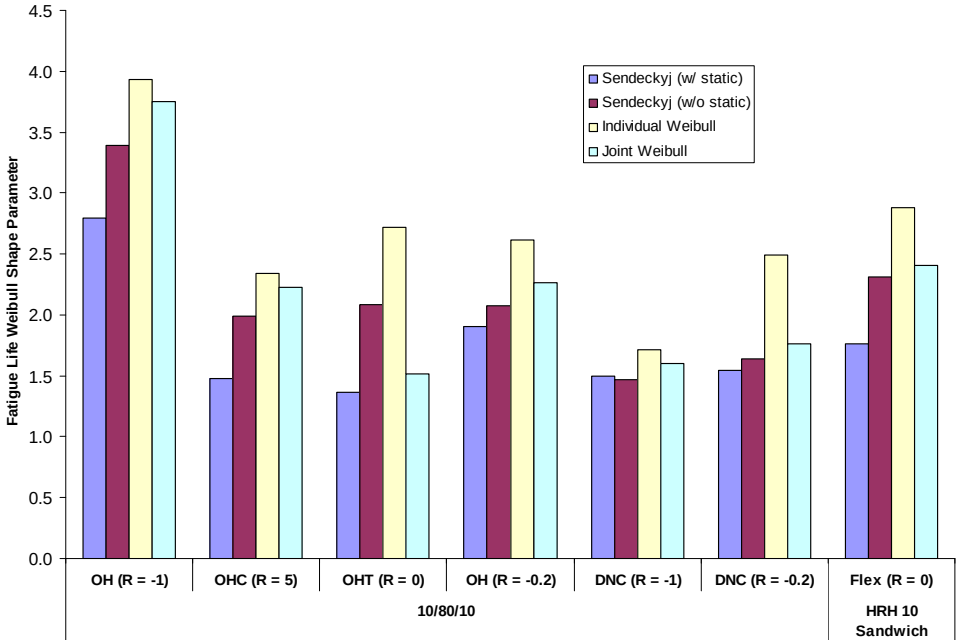

Figure 46. Fatigue-Life Shape Parameters of T700-PW From Different Analysis Methods

Table 30. Weibull Statistics for Combined Distribution of Life Distributions of T700-PW

Analysis Method	Weibull Parameter	Fatigue Scatter Analysis Method			
		Sendeckyj (with static)	Sendeckyj (without static)	Individual Weibull	Joint Weibull
MLE	α	3.795	3.728	4.433	3.825
	β	1.944	2.359	2.919	2.638
	α_{Modal}	1.793	2.170	2.756	2.437
RRX	α	5.255	4.344	4.570	5.085
	β	1.892	2.326	2.908	2.578
	α_{Modal}	1.817	2.190	2.755	2.470
RRY	α	3.780	3.729	4.145	3.905
	β	1.965	2.371	2.941	2.658
	α_{Modal}	1.811	2.181	2.752	2.464

5.2.3 The 7781/#2510 8-Harness Satin-Weave Fabric.

Fatigue analysis of 204, 7781-8HS specimens from seven S/N curves is included in this section. Each data set contains a minimum of three fatigue stress levels and at least six static-strength data points. As shown for the previous two material systems, OH with R = -1 data indicate the lowest fatigue life (figure 47). Normalized OH data for R = 5 indicate the lowest level of fatigue degradation for this material (figure 48). Fatigue-life scatter analysis data are shown in table 31.

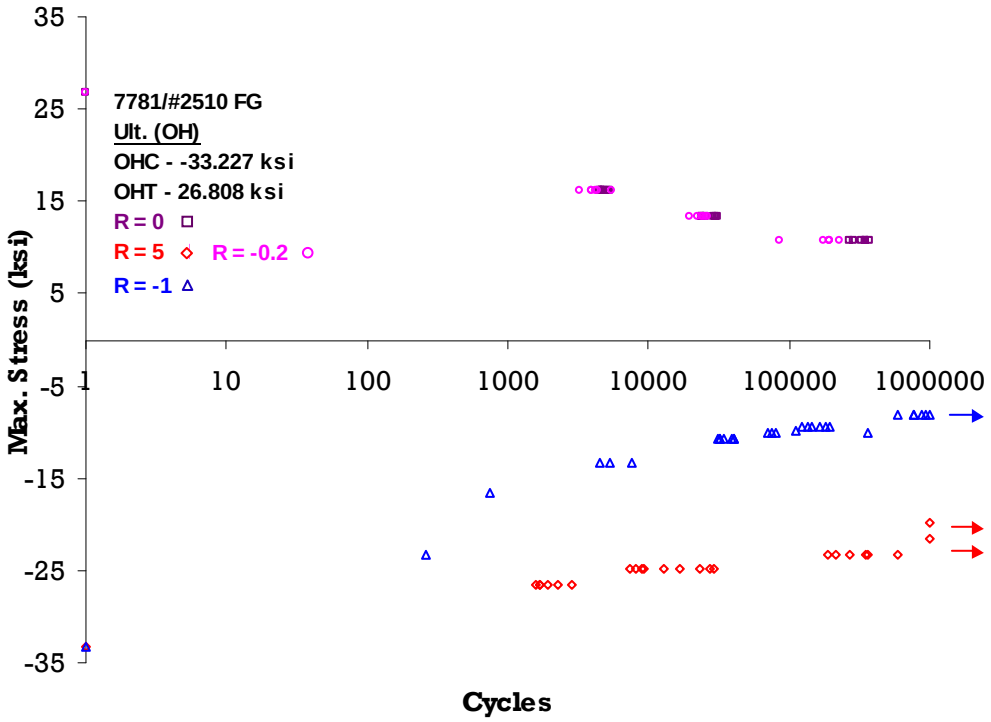

Figure 47. Effects of Stress Ratio for 7781-8HS OH Measured Fatigue Data

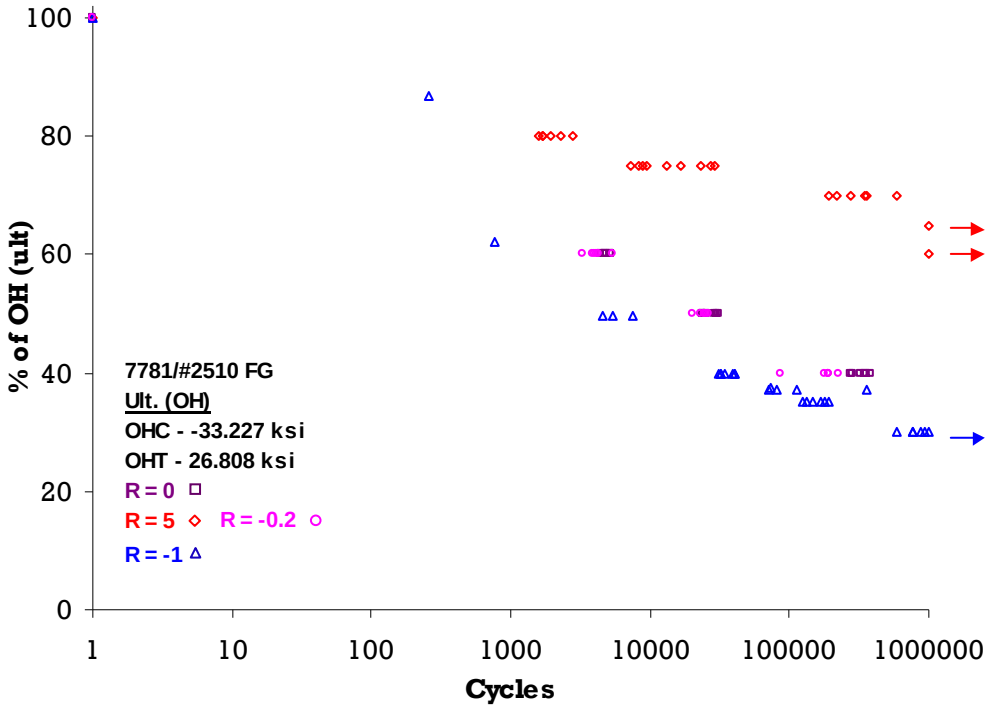

Figure 48. Effects of Stress Ratio for 7781-8HS OH Normalized Fatigue Data

Table 31. Fatigue-Life Scatter Analysis for 7781-8HS

Specimen Configuration			Sendeckyj		Weibull	
Lay-Up	Test Description	R-Ratio	$\hat{\alpha}_{Sendeckyj}$ (with static)	$\hat{\alpha}_{Sendeckyj}$ (without static)	$\hat{\alpha}_{IW}$	$\hat{\alpha}_{JW}$
10/80/10	OH	-1	1.876	1.730	6.258	5.139
	OHC	5	2.727	2.580	3.169	2.668
	OHT	0	1.769	9.794	13.866	12.667
	OH	-0.2	1.575	7.335	8.998	7.387
	DNC	-1	1.163	1.056	2.035	1.711
	DNC	-0.2	2.724	2.643	3.346	2.760
Sandwich	4PB-HRH 10	0	2.358	3.429	4.034	3.441

Figure 49 shows a comparison of fatigue-life scatter data obtained from different analysis techniques. Similar to AS4-PW and T700-PW, Sendeckyj analysis produces a higher scatter for 7781-8HS than individual Weibull shape parameters. Except for R = 5, OH data without static data show significantly high shape parameters, indicating an unrealistic skewness in OH fatigue data. Table 32 includes a summary of the fatigue-life parameter for 7781-8HS.

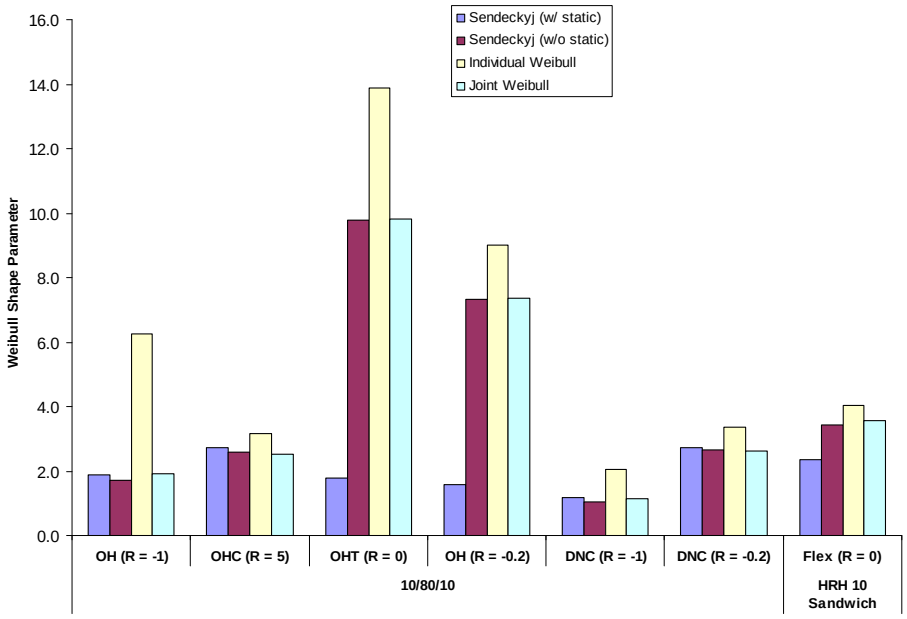

Figure 49. Fatigue-Life Shape Parameters of 7781-8HS From Different Analysis Methods

Table 32. Weibull Statistics for Combined Distribution of 7781-8HS

Analysis Method	Weibull Parameter	Fatigue Scatter Analysis Method			
		Sendeckyj (with static)	Sendeckyj (without static)	Individual Weibull	Joint Weibull
MLE	α	4.232	1.459	1.662	1.574
	β	2.237	4.542	6.726	5.748
	α_{Modal}	2.099	2.056	3.864	3.028
RRX	α	3.519	1.441	1.698	1.663
	β	2.251	4.482	6.614	5.622
	α_{Modal}	2.047	1.971	3.918	3.234
RRY	α	3.410	1.338	1.554	1.502
	β	2.262	4.605	6.801	5.809
	α_{Modal}	2.043	1.647	3.501	2.801

5.2.4 Adhesive Fatigue Data.

Fatigue scatter analysis of the FAA-D5656 material database [35], which contains ASTM D 5656 single-lap shear adhesive joints from four different adhesive systems, is included in this section. This database contains 390 adhesive specimens from 12 S/N curves, which represent three different test environments: CTD, RTA, and RTW. Each data set contains a minimum of three fatigue stress levels and at least nine data points in each stress level in addition to static-strength data. Fatigue-life scatter analysis data are shown in table 33. Figure 50 shows a comparison of fatigue-life scatter data obtained from different analysis techniques.

Table 33. Fatigue-Life Scatter Analysis for FAA-D5656

Specimen Configuration		Sendeckyj		Weibull	
Adhesive	Test Environment	$\hat{\alpha}_{Sendeckyj}$ (with static)	$\hat{\alpha}_{Sendeckyj}$ (without static)	$\hat{\alpha}_{IW}$	$\hat{\alpha}_{JW}$
Loctite	CTD	0.805	0.821	1.069	1.007
	RTA	0.662	1.624	1.226	1.077
	RTW	0.682	0.644	1.109	0.924
EA9696	CTD	0.847	4.119	2.372	2.294
	RTA	0.403	1.389	2.077	1.514
	RTW	0.379	2.189	1.110	1.047
PTM&W (0.06″)	CTD	0.870	1.376	1.541	1.254
	RTA	1.051	1.483	1.179	1.153
	RTW	0.681	1.169	1.417	1.005
PTM&W (0.16″)	CTD	0.363	0.669	1.165	0.908
	RTA	0.856	4.296	2.170	1.627
	RTW	0.671	1.618	1.061	0.958

Individual Weibull shape and scale parameters of PTM&W for six shape parameters shown in table 33 are 3.870 and 1.568, which result in a fatigue-life shape parameter of 1.451. Overall, the Sendeckyj analysis exhibits high scatter, especially for the case with static strength, compared to individual Weibull analysis. This is due to the scatter observed in adhesive fatigue data at each stress level.

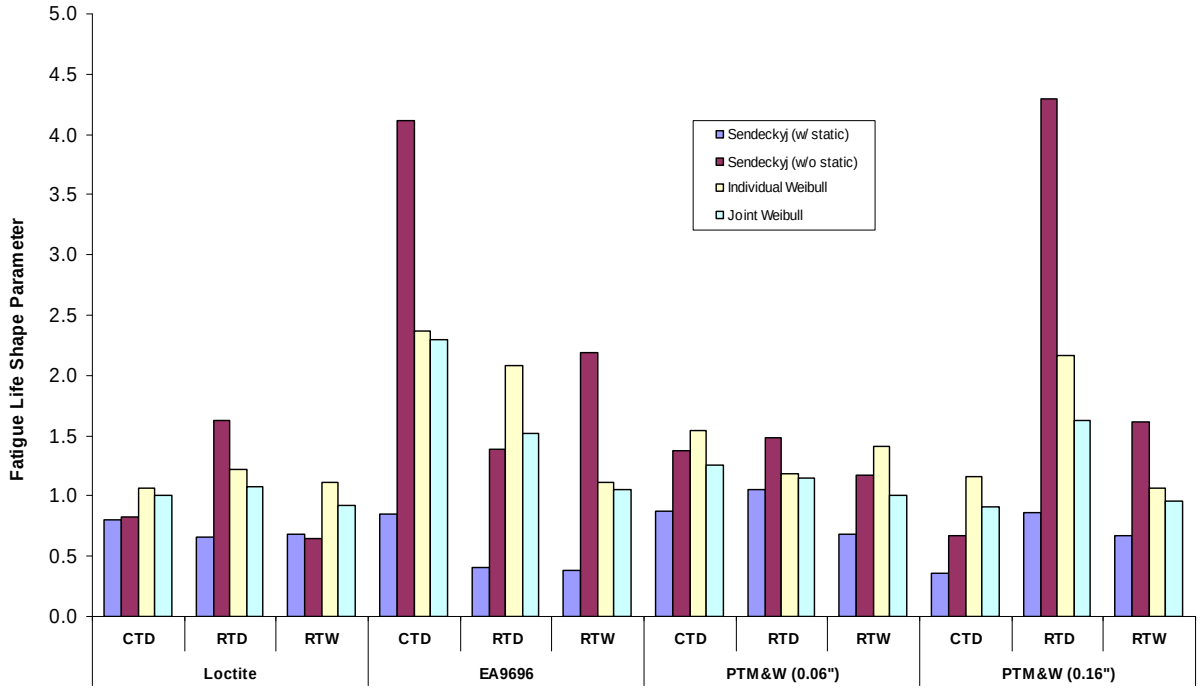

Figure 50. Fatigue-Life Shape Parameters of FAA-D5656 Data From Different Analysis Methods

Typically, the scatter in adhesive test data is significantly higher than that of composite test data. This is primarily due to the processing parameters and the multiple secondary loading modes that occur during testing of adhesive joints, i.e., peel stress at the ends of the overlap during single-lap shear tests. Postfatigue microscopic analysis of Loctite paste adhesive test specimens indicated that fractures initiated from the clusters of glass beads, which were mixed into the adhesive to control bondline thickness. Furthermore, the moisture-conditioned specimens indicated localized swelling around the glass beads. The random distribution of glass beads and the effects of the two above-mentioned phenomena resulted in large data scatter. The change in bondline thickness and the amount of adhesive that squeezes out at the ends of the overlap causes significant changes to the stress distribution of the adhesive layer, and consequently a large data scatter. For the adhesive fatigue-life data in the current analysis, scatter significantly increases with fatigue test times to failure, i.e., data from low stress levels indicated significant data scatter. Therefore, individual Weibull analysis is recommended for adhesive test data. Also, the modal shape parameters obtained for individual Weibull analysis data are consistent throughout RRX, RRY, and MLE (table 34).

Table 34. Weibull Statistics for Combined Distribution of FAA-D5656 Data

Analysis Method	Weibull Parameter	Fatigue Scatter Analysis Method			
		Sendeckyj (with static)	Sendeckyj (without static)	Individual Weibull	Joint Weibull
MLE	α	3.854	1.679	3.339	3.141
	β	0.764	2.016	1.626	1.371
	α_{Modal}	0.707	1.176	1.461	1.213
RRX	α	3.374	1.993	4.487	4.833
	β	0.765	1.944	1.572	1.320
	α_{Modal}	0.689	1.371	1.486	1.258
RRY	α	3.064	1.741	3.247	3.426
	β	0.777	2.020	1.644	1.381
	α_{Modal}	0.683	1.237	1.468	1.249

As shown in figure 50, the Sendeckyj model with static data indicate significant scatter in the adhesive data, whereas without static data, in some cases, scatter is higher than for individual Weibull analysis. When including static data for the Sendeckyj analysis, it is recommended that a minimum of six static data points be included. At this point, it is recommended that adhesive S/N curves be analyzed using individual Weibull analysis. Thus, these S/N curves must have a minimum of six data points in each stress level, and each S/N curve must have a minimum of three stress levels in addition to static data.

5.3 SUMMARY OF FATIGUE SCATTER ANALYSIS.

Overall, the individual Weibull analysis provided the highest fatigue-life shape parameter, while the Sendeckyj analysis provided the lowest (most conservative) fatigue-life shape parameter. For most cases, when the static data are included in the Sendeckyj analysis, the analysis resulted in significantly lower fatigue-life shape parameters than that without the static test data. For example, 7781-8HS OHT (R = 0) S/N data resulted in a fatigue-life shape parameter of 9.794 for Sendeckyj analysis without static data. When the static test data are included in the analysis, this value was reduced to 1.769. For most composite analysis cases, the Sendeckyj analysis without static test data and the joint Weibull analysis resulted in similar shape parameters.

Figure 51 shows a comparison of fatigue-life shape parameters calculated using the Sendeckyj model for three composite material systems and three adhesive systems discussed in this section. Sendeckyj analysis for each composite and adhesive S/N curve is conducted with and without static data. Then, shape parameters for adhesive S/N curves are combined with shape parameters for each composite system. Fatigue-life scatter with static and adhesive data indicate the highest scatter for all three composite materials. Removing the adhesive data had the greatest effect on 7781-8HS life scatter, while removing the adhesive and static data had the greatest effect on AS4-PW life scatter. For all three composites, removal of static and adhesive data resulted in

significantly less scattered life shape parameters. For both AS4-PW and T700-PW, the shape parameter distribution obtained without static and adhesive data indicated the least scatter.

For composite material systems included in this section, R = -1 stress ratio resulted in the most critical OH fatigue life. For T700-PW, this stress ratio resulted in the least scatter. Typically, load reversal (R <0) causes low fatigue life and less scatter in test data.

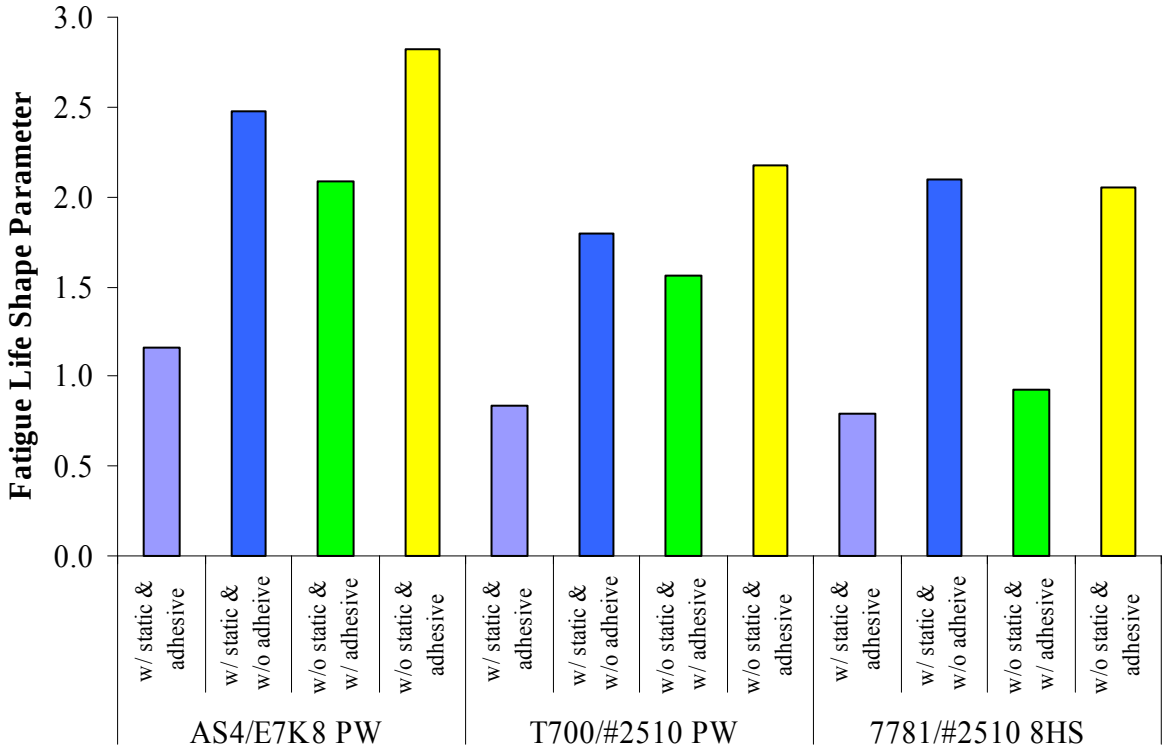

Figure 51. Comparison of Fatigue-Life Shape Parameter for FAA-LEF Database

To generate a life shape parameter that represents the general scatter of current typically used aircraft composite materials, the shape parameters representing all composite fatigue data sets included in this report were pooled. However, the authors recommend generating shape parameters based on the materials, processes, and design details related to the critical areas of a particular structure rather than using pooled data to ensure safety and reliability of fatigue life predictions based on scatter analysis. This exercise was done to establish generic scatter distribution of modern composite fatigue data and to compare that against the values proposed by Whitehead, et al. [2]. A summary of fatigue shape parameters obtained using different Weibull analysis methods and different fatigue analysis techniques is shown in table 35. The resulting MLSP (α_L) is 2.13 (designated in the table with a dotted line), which was obtained using Sendeckyj analysis (without static data in the S/N curves) for composite test data. It was determined as 2.98 and 2.61 for individual and joint Weibull analyses, respectively. For an α_L of 2.13, the life factor is 4.3. When the adhesive fatigue data are pooled with composite data, α_L was 1.60 using joint Weibull analysis, while it was 1.73 and 1.94 for Sendeckyj and individual Weibull analyses, respectively. For an α_L of 1.60, the life factor is 7.3.

Table 35. Weibull Statistics for Pooled Composite and Adhesive Data From Different Analytical Techniques

Analysis Data Set	Analysis Method	Weibull Parameter	Sendeckyj (with static)	Sendeckyj (without static)	Individual Weibull	Joint Weibull
Pooled composite fatigue data	MLE	α	3.342	1.826	1.826	1.853
		β	2.408	3.291	4.602	3.974
		α_{Modal}	**2.165**	**2.131**	**2.980**	**2.614**
	RRX	α	3.900	2.674	2.801	3.105
		β	2.371	3.150	4.362	3.752
		α_{Modal}	**2.198**	**2.644**	**3.725**	**3.310**
	RRY	α	3.656	2.320	2.285	2.432
		β	2.394	3.251	4.561	3.942
		α_{Modal}	**2.193**	**2.550**	**3.546**	**3.170**
Pooled composite and adhesive fatigue data	MLE	α	2.070	1.698	1.565	1.586
		β	1.968	2.917	3.726	3.229
		α_{Modal}	**1.430**	**1.729**	**1.943**	**1.723**
	RRX	α	2.000	2.206	2.130	2.167
		β	1.961	2.826	3.556	3.095
		α_{Modal}	**1.387**	**2.150**	**2.641**	**2.326**
	RRY	α	1.951	2.063	1.888	1.938
		β	1.975	2.876	3.679	3.190
		α_{Modal}	**1.366**	**2.086**	**2.466**	**2.194**

5.4 LOAD-ENHANCEMENT FACTOR.

In this section, the LEF is calculated using the static strength and fatigue life distributions derived from the data obtained in this study and historical data available at National Institute for Aviation Research (NIAR). Data for three different composite material systems in the FAA-LEF data set were combined with adhesive fatigue data in the FAA-D5656 material database to obtain life factors and LEFs. As discussed in section 3.2, the life factor, N_F, is a function of MLSP, or α_L, and is not influenced by the MSSP, or α_R. However, LEF is a function of both parameters. A combined load-life approach is also discussed.

Different combinations of MSSP and MLSP from sections 4.2 and 5.3, respectively, are combined to calculate the corresponding LEF curves. Table 36 shows the life factors for MLSP of composite data only and MLSP obtained by combining adhesive fatigue-life shape parameters from individual Weibull analysis for adhesives and Sendeckyj analysis for composites (denoted C and C+A, respectively, in table 36). MSSP for T700-PW also includes element test data from the FAA-EOD database. The influence of test duration on the B-basis LEF for these three materials is shown in figure 52 for one test article. This figure compares the LEF curves generated for the data in this report against the LEF curves generated by Whitehead, et al. [2], and Lameris [3] (referred to as NAVY and CASA, respectively). In addition, the strength and

MLSP obtained by pooling the data in this report (26.31 and 2.13, respectively) are used to generate the LEF curve (referred to as NIAR for comparison in figure 52). Due to the significant improvement in the MSSP used for the NIAR curve, the LEF requirements for lower test durations are significantly reduced compared to both NAVY and CASA data. However, for test durations of more than two lifetimes, CASA data resulted in lower LEF requirements than NIAR data due to the lower MLSP obtained for CASA data. Note that CASA data include only 48 fatigue data points and the method of obtaining the fatigue shape parameter (i.e., Weibull or Sendeckyj) is not specified. In contrast, NIAR data include over 800 composite fatigue data points. Furthermore, the NIAR fatigue shape parameter selected for this curve is the most conservative value (MLE and Sendeckyj in table 35) of the three fatigue analysis techniques discussed in this report, corresponding to the largest life scatter. Nevertheless, NIAR data show a significant reduction in LEF requirements compared to NAVY data, as shown in figure 52.

Table 36. Weibull Statistics for Combined Composites and Adhesives

Composite Material	α_L	N_F
AS4/E7K8 PW (C)	2.475	3.431
AS4/E7K8 PW (C+A)	1.880	5.267
T700/#2510 PW (C)	1.793	5.752
T700/#2510 PW (C+A)	1.576	7.516
7781/#2510 8HS (C)	2.099	4.364
7781/#2510 8HS (C+A)	1.660	6.715

Table 37 and figure 53 show a comparison of MLSP obtained for AS4-PW by using different analytical techniques, i.e., individual Weibull or Sendeckyj model, for composites and adhesives. AS4-PW data were analyzed with and without adhesive data (denoted C+A and C, respectively). Composite data were analyzed using Sendeckyj method, while adhesive data were analyzed using the individual Weibull method.

As observed in these examples, the LEF calculated as a function of test duration for these materials is significantly lower than for NAVY. In addition, application of the life factor, rather than LEF, for high loads in spectrum required fewer repetitions for improved MLSP than for NAVY. However, guidance for generating reliable shape parameters must be established to prevent unrealistic LEFs that compromise the structural integrity of composite aircraft. It is recommended that specimens or elements representative of features of a particular structure (i.e., materials, design details, failure modes, loading conditions, and environments) be included in the analysis rather than pooling various material databases. Also, it is noted that the primary goal in scatter analysis is not selecting shape parameters from the critical lay-up, R-ratio, environment, etc., (which may result in skewed data that will produce unconservative LEF), but rather selecting the design details representing the critical areas of the structure.

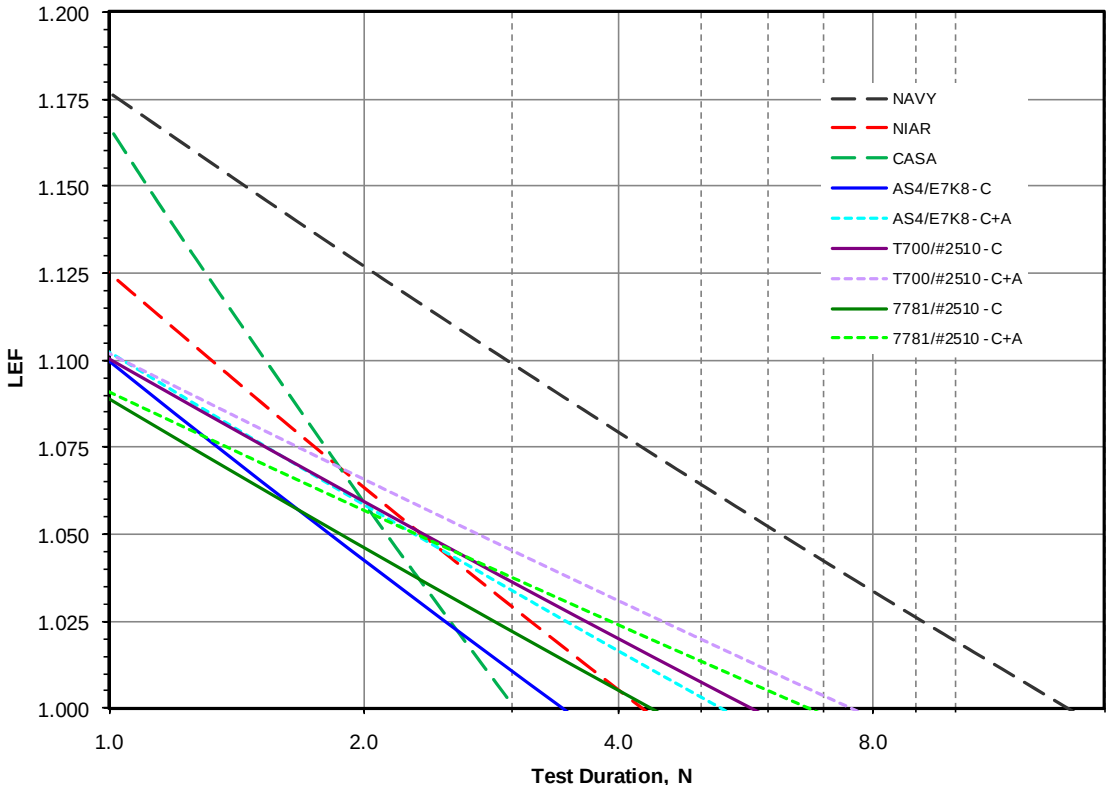

	NAVY	NIAR
Strength Shape Parameter	20.000	26.310
Life Shape Parameter	1.250	2.131
Life Factor	13.558	4.259

# of Lives (N)	LEF	
1.00	1.177	1.125
1.50	1.148	1.088
2.00	1.127	1.063
2.50	1.111	1.044
3.00	1.099	1.029
4.25	1.075	1.000
5.00	1.064	
8.00	1.034	
13.60	1.000	

Figure 52. Influence of Test Duration on B-Basis LEFs for Different Materials

Table 37. Weibull Statistics for AS4-PW Composites and Adhesives From Different Analytical Techniques

Analysis Method	α_L	N_F
Individual Weibull (C)	4.056	2.070
Individual Weibull (C+A)	2.082	4.418
Sendeckyj (C)	2.475	3.431
Sendeckyj (C+A)	1.021	26.296
Sendeckyj (C)+Individual Weibull (A)	1.880	5.267

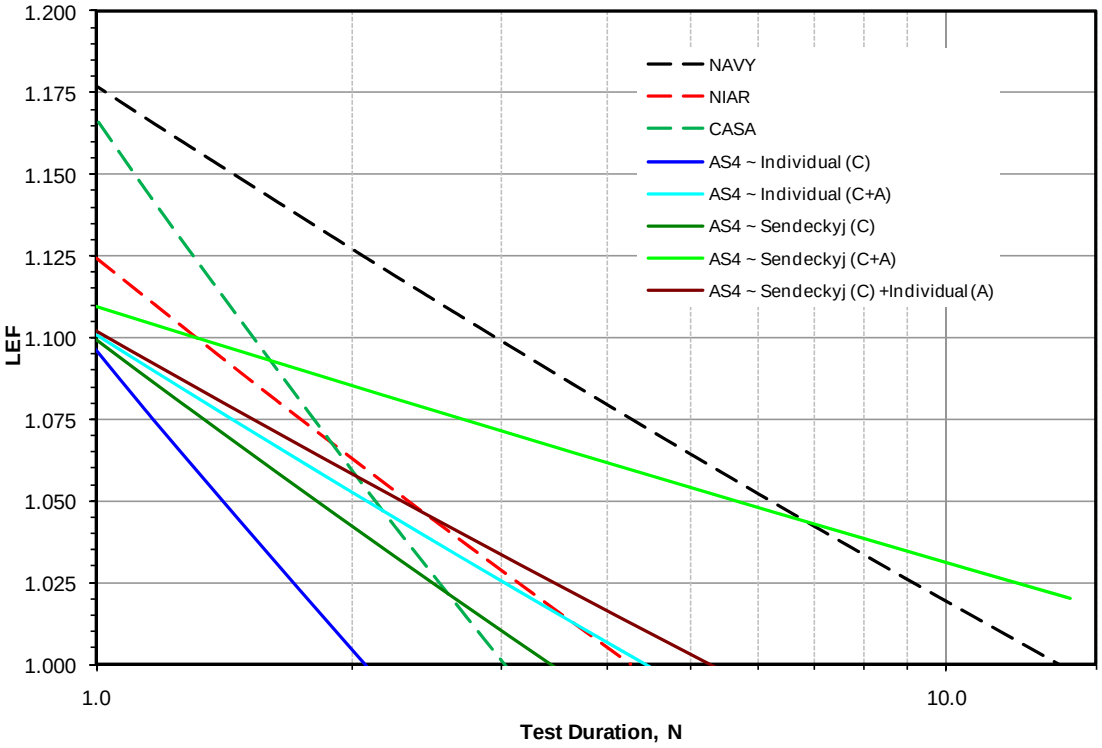

Figure 53. Influence of Test Duration on B-Basis LEFs of AS4-PW From Different Analytical Techniques

The primary objective of the analyses in sections 4 and 5 was to evaluate the parameters affecting MSSP (α_R) and MLSP (α_L) so that minimum requirements to generate safe and reliable, yet economical, LEFs and life factors (N_F) can be outlined along with a recommendation for benchmark test matrices. The secondary objective was to create a readily available shared database of static-strength and fatigue-life shape parameters for commonly used composite materials and structural details to support on-going and future certification programs, thereby reducing testing time and cost. Finally, well-documented procedures and a user-friendly computer code for generating statistically reliable life factor and LEFs were developed. Using equation 9, tables 5 and 6 include A- and B-basis LEFs, respectively, for different combinations of MSSPs and MLSPs for different test durations and numbers of test articles.

5.5 CASE STUDY—LIBERTY AEROSPACE XL2 FUSELAGE.

This section demonstrates an application of LEF on a composite fuselage of the Liberty Aerospace XL2 aircraft (figure 54) that was primarily fabricated using T700/#2510 PW (T700-PW) and Airex R82-80 foam core. To generate LEF for the fuselage material systems, several sandwich coupon configurations were tested.

Figure 54. Liberty Aerospace XL2 Aircraft

A reduced test matrix was developed, including compression- and shear-loaded sandwich coupons using an R82-80 core. Both notched and unnotched compression sandwich specimens were tested using windowed anti-buckling fixtures. One-, two-, and three-ply facesheet lay-ups and 3- and 5-mm-thick cores with and without core splices were included in the test matrix. Several ETD static-compression specimens were also included. The total Liberty database included 198 static data points and 82 fatigue data points. Each static data set had a minimum of six specimens (table 38).

Table 38. Weibull Analysis Results of Liberty Sandwich Static Test Data

Specimen Configuration	Loading Configuration	Core Size (mm)	Plies per Facesheet	Core Splice	Number of Specimens	Weibull Parameters	
						$\hat{\alpha}$	$\hat{\beta}$
RTA unnotched	Compression	3	1		6	17.234	2.606
	Compression	3	2		6	51.431	5.307
	Compression	3	3		6	35.754	7.011
RTA notched	Compression	3	1		6	22.962	2.133
	Compression	3	2		6	19.597	4.224
	Compression	3	3		6	105.229	5.438

Table 38. Weibull Analysis Results of Liberty Sandwich Static Test Data (Continued)

Specimen Configuration	Loading Configuration	Core Size (mm)	Plies per Facesheet	Core Splice	Number of Specimens	Weibull Parameters	
						$\hat{\alpha}$	$\hat{\beta}$
RTA shear	Shear	3	1		6	23.376	0.226
	Shear	3	2		6	30.213	0.245
	Shear	3	3		6	30.058	0.251
	Shear	5	1		6	14.520	0.196
	Shear	5	2		6	16.305	0.209
	Shear	5	3		6	53.031	0.190
ETD static	Compression	3	1		6	7.450	2.525
	Compression	3	2		6	12.065	5.046
	Compression	3	3		6	28.349	6.296
	Compression	3	1	Yes	6	14.895	2.543
	Compression	3	2	Yes	6	38.642	4.690
	Compression	3	3	Yes	6	17.858	6.327
	Compression	3	1		6	8.145	1.975
	Compression	3	2		6	29.879	3.736
	Compression	3	3		6	33.781	4.689
	Compression	3	1	Yes	6	9.153	2.802
	Compression	3	2	Yes	6	17.646	3.730
	Compression	3	3	Yes	6	31.001	5.414

However, fatigue data sets did not have the minimum recommended five specimens per stress level to generate accurate individual Weibull shape parameters. Therefore, MLSP was generated using the Sendeckyj method for fatigue data sets that had a minimum of three stress levels, in which at least two fatigue failures existed (table 39). MSSP was generated using several scenarios: (1) only Liberty database [46]; (2) Liberty (without adhesive data) and FAA-LVM databases; (3) Liberty (with adhesive data) and FAA-LVM databases; and (4) Liberty, FAA-LVM, and FAA-EOD databases.

Table 39. Sendeckyj Analysis Results of Liberty Sandwich Fatigue Test Data

Specimen Configuration	Loading Configuration	Core Size (mm)	Plies per Facesheet	Core Splice	Number of Specimens	Shape Parameter, $\hat{\alpha}$
Unnotched	Compression	3	3		10	1.346
	Compression	5	3	Yes	9	17.410
Notched	Compression	3	3		7	4.559
	Compression	5	3		7	3.972

Table 39. Sendeckyj Analysis Results of Liberty Sandwich Fatigue Test Data (Continued)

Specimen Configuration	Loading Configuration	Core Size (mm)	Plies per Facesheet	Core Splice	Number of Specimens	Shape Parameter, $\hat{\alpha}$
Shear	Shear	3	1		9	7.254
	Shear	3	2		8	4.965
	Shear	3	3		9	1.229
	Shear	5	1		7	4.016
	Shear	5	2		7	7.024
	Shear	5	3		9	0.804

Only 10/80/10 T700-PW (0/100/0 data was not available) and 50/40/10 T700-UT data from the FAA-LVM database were included in the fatigue analysis of the Liberty XL2 fuselage materials [46] because the Liberty XL2 fuselage was primarily fabricated using T700-PW with ±45° lay-up and highly orthotropic lay-ups of T700-UT around some of the highly loaded areas. This is an example of using a shared database for generating reliable LEFs with minimum test efforts, i.e., only testing the R82-80 core. B-basis LEFs are shown for all four analysis scenarios with respect to different test durations in table 40. These data are also illustrated in figure 55.

Table 40. Comparison of Weibull Statistics for Liberty XL2 Database

Test Duration (N)	NAVY	CASA	Analysis Scenario for Liberty XL2			
			1	2	3	4
1.00	1.177	1.167	1.166	1.141	1.148	1.157
1.10	1.170	1.151	1.158	1.131	1.138	1.146
1.25	1.161	1.131	1.147	1.118	1.124	1.132
1.50	1.148	1.103	1.133	1.100	1.106	1.112
1.75	1.137	1.079	1.121	1.085	1.090	1.095
2.00	1.127	1.059	1.110	1.073	1.076	1.081
3.00	1.099	1.001	1.079	1.035	1.037	1.039
4.00	1.079		1.057	1.009	1.009	1.010
MSSP (α_R)	20.000	19.630	20.886	23.526	22.419	21.199
MLSP (α_L)	1.250	2.740	1.469	2.082	2.082	2.082
Life Factor (N_F)	13.558	3.019	8.837	4.422	4.422	4.422

Since MLSP from the Liberty data (scenario 1) are lower than for the NAVY database, the life factor is reduced to 8.837 from 13.558. This is further reduced to 4.422 after adding the FAA-LVM data. For a given MLSP, the life factor is fixed since it does not depend on MSSP. Therefore, further improvements to MSSP results in a decrease in the slope of the curve, which pivots about N_F (LEF = 1), as shown in figure 55. Consequently, this lowers the LEF, especially

for smaller test durations. In scenario 3, MSSP is reduced when the Liberty adhesive data are included, indicating a small increase in scatter for the Weibull distribution of static scatter parameters. MSSP is further decreased in scenario 4, when element-level adhesive joint data from FAA-EOD are included. FAA-EOD element test specimens are bonded using EA9394. However, the Liberty XL2 is bonded using EPIBOND 1590. Therefore, scenario 3 is more applicable to this structure.

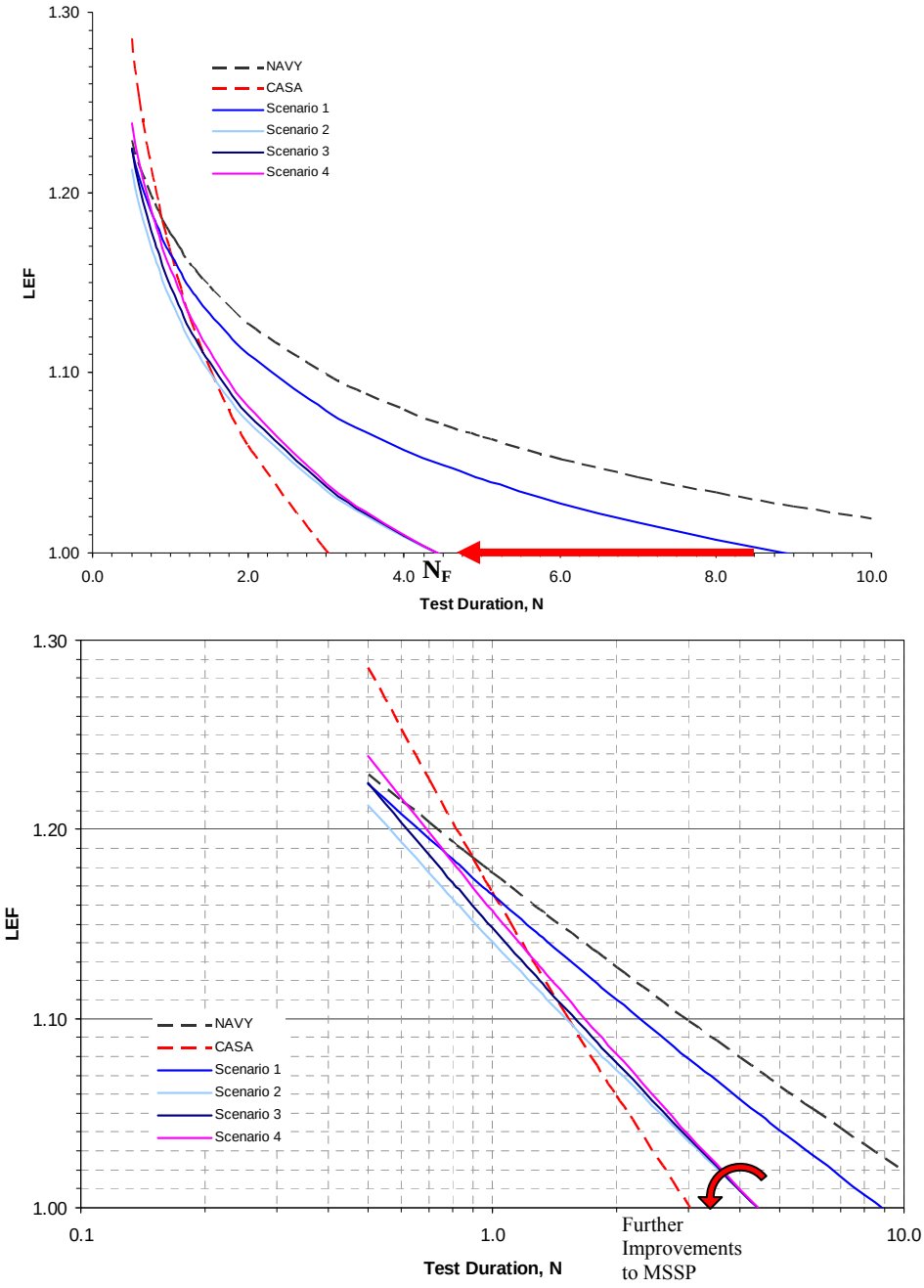

Figure 55. Influence of Test Duration on B-Basis LEFs for Liberty XL2

Although scenario 3 did not show significant improvements for LEF, the life factor was about 50 percent lower than for scenario 1. Also, B-basis LEFs for this scenario were considerably lower than for NAVY. The original fatigue tests of the Liberty XL2 fuselage were conducted using the NAVY life factor and an LEF of 1.15, which corresponds to a test duration of 1.5 DLT. The Liberty fuselage fatigue test was conducted for three test lives with NAVY LEF and included a damage tolerance phase. According to scenario 3, an LEF of 1.15 corresponds to a test duration of 1 DLT. Thus, the full-scale test with an LEF of 1.15 corresponds to a B-basis life factor of 1. The actual test was conducted with two DLTs more than what is required to achieve the same level of reliability demonstrated by the metal structure. This increases the confidence in DLT, i.e., number of hours corresponding to a test duration of 1 DLT.

During full-scale tests, certain spectrum load cycles above a percentage of the DLLs (high-load cycles) were multiplied by the NAVY life factor rather than applying LEF, as described in section 3.4. Due to the improvement in data scatter, the life factor was reduced to 4.422 from the value of 13.558 proposed for composites by Whitehead, et al. [2]. Therefore, the high-load cycles were repeated approximately three times more than the required number of repetitions to achieve the B-basis life factor. This further increased the level of confidence in DLT.

To compare the B-basis LEF requirements for different databases, the Liberty XL2 fuselage durability and damage tolerance (DaDT) test was compared against two scatter analysis material databases: (1) NAVY and (2) Liberty data (scenario 4 in figure 55). This approach evaluated the modified DLT in the event that a certification test duration or LEF was different from the minimum required to achieve B-basis reliability. Figure 56 shows the B-basis LEF requirements with respect to different test durations based on data from the above-mentioned two databases. Liberty LEF requirements reflect the material and process as well as test method improvements related to composites, which consequently reduced the data scatter compared to the test data used for the NAVY approach. Points C and Z correspond to the life factor for Liberty and NAVY databases, respectively. Points X and Y show the LEF required for 1.5- and 3-DLT test durations, respectively, according to the NAVY approach. For the same test durations, points A and B show the LEF requirements for the improved composite test data for Liberty XL2 fuselage materials.

A full-scale DaDT test of the 1653-pound Liberty XL2 fuselage was performed at NIAR for three lifetimes. Point T in figure 56 shows the LEF used during the DaDT full-scale test substantiation. The load spectra used for cyclic loading was developed using the exceedance curves from DOT/FAA/CT-91/20 [47] (maneuver and gusts) and AFS-120-73-2 [48] (taxi and landing). The test spectra were truncated below the 30-percent DLL to shorten the test without significant effects on the fatigue characteristics of the structure. No load in excess of DLL was applied during cyclic tests.

Since Liberty LEF testing was in progress at the time of full-scale test substantiation, an LEF of 1.15 corresponding to 1.5 lifetimes per the NAVY approach [2] was applied to loads below an 80-percent limit load, and an N_F of 28.5 (conservatively, this factor was selected during full-scale substantiation until the LEF data is available) was applied for loads above an 80-percent limit load, similar to the approach outlined in figure 19(b). This approach allowed for a lower LEF in

a trade-off for more life cycles, which would reduce the severity of the overload for high stress levels.

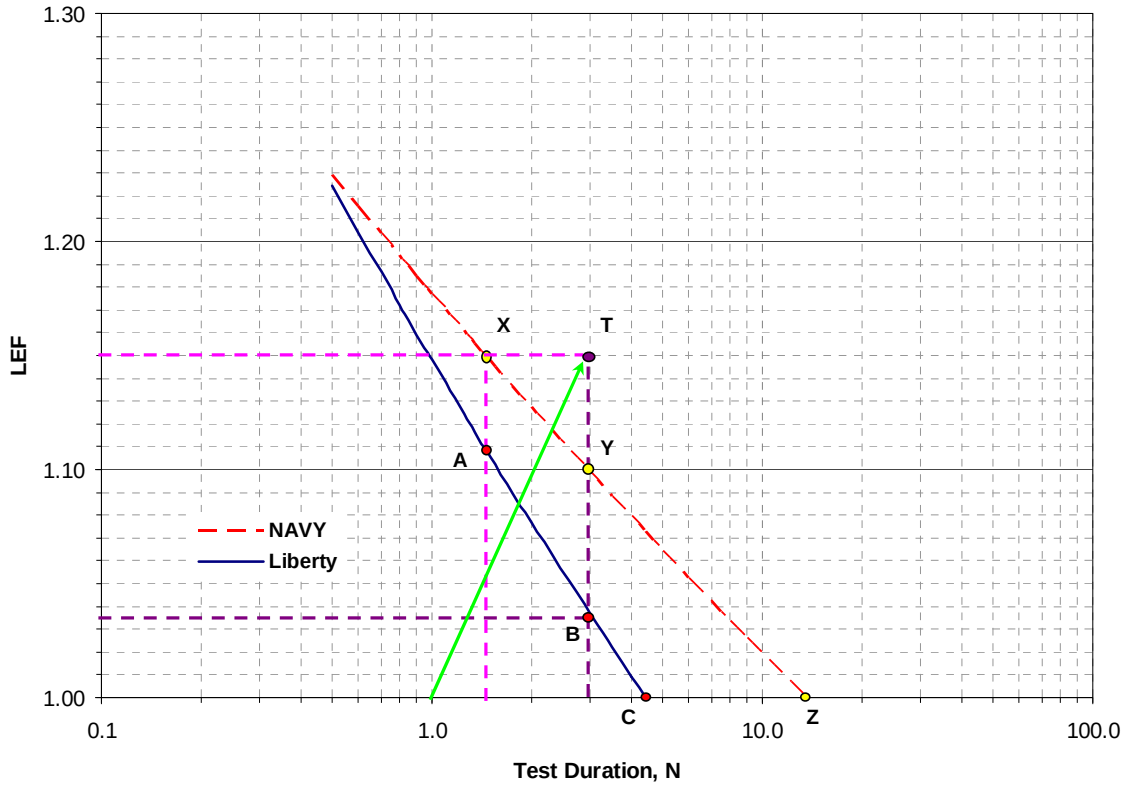

Figure 56. Comparison of Tested and Required LEFs for Liberty XL2

Based on the NAVY approach, B-basis reliability was obtained either by increasing the loads by an LEF of 1.15 for a test duration of 1.5 DLTs or by applying an N_F of 13.6. This is equivalent to an N_F of 2 DLTs, which is typically used to demonstrate B-basis reliability of metal structures. However, as shown in figure 56, the Liberty XL2 fatigue test article was tested for twice the required test duration (3-DLTs) with no indication of damage growth, demonstrating residual strength after repeated loading. Therefore, it is evident that the test article demonstrated B-basis reliability for twice the DLT of 5000 hours. Typically, this argument alone would not justify the new DLT, as the load segments above 80-percent DLL are multiplied by N_F instead. However, in this case, N_F should have been 13.6 or 4.422, based on the NAVY or Liberty approach, respectively. The applied N_F is more than twice that of the NAVY approach and six times that of the Liberty approach. Thus, the above-mentioned argument for a design lifetime of 10,000 hours is justified. An N_F of 28.5 corresponds to an MLSP, or α_L, of 1.00 (figure 14 or solving equation 8 for α_L), which corresponds to materials that exhibit higher scatter in fatigue life data than the data set in the NAVY approach.

Alternately, considering only the NAVY approach and based on the difference between applied and required LEFs for B-basis reliability, it can be shown that this structure is capable of carrying 5 percent more load than the tested load spectrum for substantiation of a 5000-hour DLT. Based on the test data applicable to Liberty XL2 fuselage materials and design details, an

LEF of 1.035 for three lifetimes (table 40), or an N_F of 4.422, was sufficient to demonstrate B-basis reliability for a 5000-hour DLT. Therefore, considering the improved LEF curve and based on the difference between applied and required LEFs for B-basis reliability, it can be shown that a 1653-pound fuselage structure is capable of carrying 11.5 percent more loads than the designed load spectrum for a DLT of 5000 hours. This additional information can be used to support design changes that result in higher load requirements, given that the load spectra, failure modes, and critical locations of the structure are not changed.

This case study addresses concerns related to the application of LEF and N_F during full-scale test substantiation. Once the LEF curve is generated, as shown in figure 56, any combination of LEF and test duration, N, provides the same level of reliability that is required to be demonstrated by metal structures, N = 2-DLT. Thus, the test duration and life factor are no longer required to be multiplied by 2 to achieve B-basis reliability for the designed lifetime.

5.6 CASE STUDY—SCATTER ANALYSIS OF BONDED JOINTS.

To investigate the scatter in adhesive data with respect to composite data, a scatter analysis was conducted on adhesive data generated on the composite-titanium bonded joint shown in figure 57. Berens and West [49] conducted static tests in different test temperatures and loading rates, while conducting fatigue tests in two different temperatures and multiple stress levels. The Weibull analysis for static test data and fatigue test data are shown in tables 41 and 42, respectively. This data set is referred to as STP580.

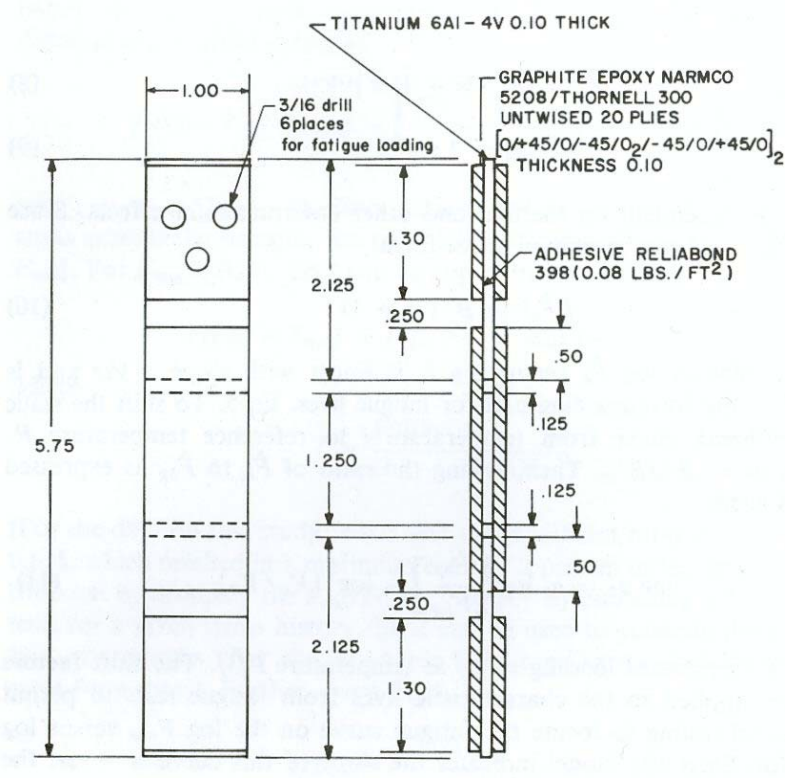

Figure 57. Composite-Titanium Bonded Joint Test Specimen [49]

Table 41. Weibull Parameter Estimates for Static Tests [49]

Test Temperature (°F)	Loading Rate (lb/min)	Number of Specimens	Scale Parameter, $\hat{\beta}$ (psi)	Shape Parameter, $\hat{\alpha}$
-40	120	10	5165	8.01
	1200	10	5756	11.37
	12000	10	5638	13.87
73	120	10	5057	12.32
	1200	10	4955	8.44
	12000	10	5145	14.41
150	120	10	4449	11.37
	1200	10	4510	8.88
	12000	10	4624	14.26
200	1200	10	3949	12.98
250	120	10	2840	22.06
	1200	10	3143	13.68
	12000	10	3486	16.01
300	120	10	1693	10.95
	1200	10	2148	9.08
	12000	10	2879	16.51

Table 42. Weibull Parameter Estimates for Fatigue Tests [49]

Test Temperature (°F)	Maximum Load (lb)	Number of Specimens	Scale Parameter, $\hat{\beta}$ (Cycles)	Shape Parameter, $\hat{\alpha}$
73	3100	10	53	2.62
	2900	10	140	2.22
	2700	10	124	1.99
	2500	9	1020	1.43
	2350	6	777	0.92
	2150	8	485	1.56
	2000	9	2870	0.69
200	2000	15	367	1.34

Shape parameters corresponding to different static data sets in table 41 were pooled and the shape and scale parameters that correspond to their probability density function were calculated as 3.733 and 14.088, respectively. Then, the MSSP for STP580 data was calculated as 12.959.

Since there was not enough fatigue data, the shape parameters in table 42 were considered as separate fatigue data sets and the shape and scale parameters corresponding to their probability density function were calculated as 2.898 and 1.796, respectively. Then, the MLSP for STP580 data was calculated as 1.552. Note that, typically, shape parameters obtained for several S/N curves are analyzed to obtain MLSP, as shown in the examples in this section. In the absence of multiple S/N curves, the distribution of Weibull shape parameters obtained for multiple stress levels can be used to generate MLSP as long as there are data from more than six stress levels and each stress level has more than six fatigue (failure) data points. This method is introduced through this case study and referred to as the modified individual Weibull analysis. Unlike the individual Weibull method that calculates the arithmetic mean of shape parameters obtained for each stress level, the modified individual Weibull method considers the Weibull distribution of shape parameters in each stress level to calculate the MLSP that represents the data scatter of the S/N curve. For the 73°F data in table 42, the MLSP was calculated as 1.578 using shape and scale parameters corresponding to the modified individual Weibull method (2.836 and 1.839, respectively). The individual Weibull analysis for this data set resulted in a shape parameter of 1.633. Therefore, the modified individual Weibull method is considered more conservative than the individual Weibull method and is recommended for adhesive data that satisfy the above-mentioned requirements.

To compare the STP580 fatigue scatter analysis data with some newer adhesive joint data, the shape parameters corresponding to adhesive joint data were extracted from the FAA-LEF and FAA-D5656 databases. The strength shape parameters of SLS data in the FAA-LEF database (tables 8 and 11) were used for calculating the MSSP, while the FAA-D5656 data set was used for calculating the MLSP. The scatter analysis of bonded joint static data in the FAA-LEF database resulted in shape and scale parameters of 2.181 and 28.262, respectively. The MSSP corresponding to these parameters was calculated as 21.334. The MLSP corresponding to newer forms of bonded joints was selected as 1.461 from the individual Weibull analysis data shown in table 34 using the MLE approach. These modal strength and life shape parameters are tabulated in table 43 along with the NAVY and NIAR data (figure 52). Then, the LEFs obtained from STP580 are compared with the LEFs obtained from the NAVY, NIAR, and FAA-LEF/FAA-D5656 adhesive data sets (figure 58). With the limited amount of bonded joint data included in these analyses, especially in STP580, it is evident that the fatigue life data scatter in bonded joints is higher than the newer composite data. Note that except for NIAR data, the rest of the fatigue scatter analyses were conducted using individual Weibull. The NIAR fatigue data shown here was analyzed using the Sendeckyj method, which is significantly more conservative than the individual Weibull method.

Table 43. Summary of Strength and Life Shape Parameters of Composite and Adhesive Data

	NAVY	NIAR	STP580	FAA-LEF (Adhesive) and FAA-D5656
MSSP	20.000	26.310	12.959	21.334
MLSP	1.250	2.131	1.552	1.461

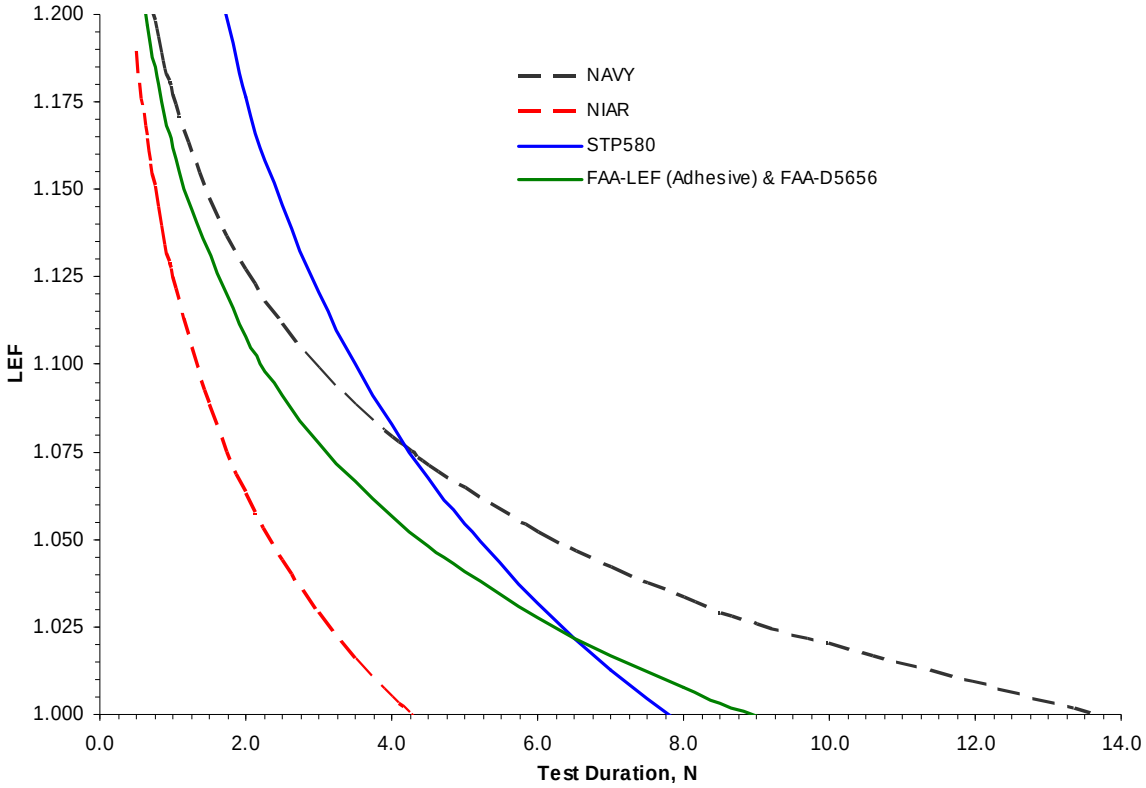

Figure 58. Comparison of LEFs Generated Using Composite and Adhesive Test Data

Contrary to the observation in fatigue data scatter, table 43 shows a significant improvement in the static data scatter in newer bonded joints compared to STP580 data, which is possibly due to improvements in adhesives, processes, and test methods. Thus, the reliability of bonded joint test data is still a concern for durability and damage tolerance test substantiation and must be included in the development of LEFs, if bonded joints are present in a structure. Furthermore, the use of individual Weibull analysis of bonded joint fatigue data is recommended for preventing overly conservative LEFs as significant differences are observed on the shape parameters obtained at different stress levels (table 42). An LEF curve based on newer bonded joint test data indicates that the NAVY values are conservative.

6. CONCLUSIONS AND RECOMMENDATIONS.

The procedure for generating load enhancement factors (LEF) based on the most critical design details of a composite structure at the coupon level was developed. The approach for obtaining the modal static-strength shape parameter (MSSP) and modal fatigue-life shape parameter (MLSP) to calculate the LEFs for different test durations was investigated in detail using static and fatigue test data for several different composite material systems. It was shown that the scatter in notched (damaged) composite test data was significantly lower than in unnotched composite. Such improvements in fatigue-life shape parameter can significantly reduce the life factor. However, the life factor becomes insensitive to small changes in the life shape parameter beyond a value of 4, which is considered to be the life shape parameter for metal. The composite MLSP of 1.25, which was used for the U.S. Navy F/A-18 certification (or NAVY) approach, lies within the highly sensitive region of the life factor versus shape parameter curve; thus, even a

small improvement resulted in a dramatic reduction in life factor, which reflects the required number of test durations to achieve a certain level of reliability in the design lifetime. The analysis in this report forms the supporting data for the load-life damage hybrid approach that can be applied to a full-scale durability test article during the certification process.

There are several approaches for the scatter analysis of fatigue data, including the individual Weibull, joint Weibull, and Sendeckyj wearout models. When analyzing small fatigue data sets, the latter two methods can be used to pool data across fatigue stress levels. Furthermore, Sendeckyj analysis allows the user to include the static and residual strength of run-out specimens. In addition to a probabilistic description of the data scatter, the Sendeckyj wearout model provides a deterministic equation to define the shape of the stress to number of cycles (S/N) curve and an expression for the monotonically decreasing residual strength as a function of the number of cycles.

Compared to metals, composite materials are known for higher scatter in both static and fatigue test data due to their heterogeneous nature, higher sensitivity to batch variability, environment, and complex failure modes. Over the years, improvements in test methods, materials, and process techniques have resulted in a significant reduction in data scatter. A detailed scatter analysis conducted on several material test databases (from past and current Federal Aviation Administration-funded research programs) representing multiple batches, loading modes, environments, and laminate stacking sequences for several commonly used composite material systems has shown that both static-strength and fatigue-life scatter have been reduced significantly. These improvements have a direct impact on the probabilistic or reliability-based analysis techniques for predicting the life of a composite structure, such as life factor and LEF analysis.

It is recommended that specimens or elements representative of features of a particular structure (i.e., materials, design details, failure modes, loading conditions, and environments) be included in the analysis rather than pooling various material databases. Also, it is noted that the primary goal in scatter analysis is not to select shape parameters from the critical lay-up, R-ratio, environment, etc. (which may result in skewed data that will produce an unconservative LEF), but rather to select the design details representing the critical areas of the structure. It is essential to note that all critical design details and/or loading modes, i.e., open-hole fatigue with a stress ratio of -1 for carbon composites, may result in low fatigue life due to notch effects and severe load reversal. Such data often tend to produce low data scatter. Therefore, the details with poor fatigue characteristics or fatigue critical designs may not always produce large data scatter and may produce unconservative LEFs. When designing test matrices for generating fatigue shape parameters, it is essential to investigate the design details/conditions that will produce the most data scatter, which will consequently affect the reliability of test data in higher levels of building blocks of testing.

It is important that the test matrix include sufficient information to translate the statistical significance of such phenomenon in a meaningful manner into a full-scale test substantiation. Such test matrices can be significantly reduced by focusing on critical aspects of the structure to address the minimum requirements. As demonstrated in the case study of the Liberty XL2 fuselage, the use of shared databases can significantly reduce the amount of additional tests and

time required for a certain application, but care must be taken to make certain that the shared data are equivalent to what is used for that application. Adhesive joints, if applicable, may require the use of individual Weibull analysis rather than pooling techniques such as the Sendeckyj analysis method, as adhesive joints tend to produce large scatter, mainly due to imperfections during bonding and high sensitivity to load eccentricity (especially in asymmetric joints). In the absence of multiple S/N curves, the distribution of Weibull shape parameters obtained for multiple stress levels can be used to generate MLSP as long as there are data from more than six stress levels and each stress level has more than six fatigue (failure) data points. This method is introduced through the case study of bonded joint data and referred to as the modified individual Weibull analysis. Unlike the individual Weibull method that calculates the arithmetic mean of shape parameters obtained for each stress level, the modified individual Weibull method considers the Weibull distribution of shape parameters (indicator of data scatter) in each stress level to calculate shape parameter that represents the data scatter of the S/N curve. The modified individual Weibull method is considered more conservative than the individual Weibull method and recommended for adhesive data that satisfy the above-mentioned requirements.

Although the shape parameters can vary within a large spectrum of values, care must be taken to address unrealistic values individually to produce safe and reliable scatter analysis. For example, the Sendeckyj model provides a way to graphically inspect the data fit, as illustrated in appendix A, to evaluate the quality of the fitting parameters, which are used to generate the S/N curve fit and the scatter analysis. For Weibull analysis, the maximum-likelihood estimation (MLE) can be used to generate shape parameters when there are more than 18 data points, while regression in the number of cycles is recommended for small data sets. For the MLSP calculations of composite data in this report, both techniques produced similar values, while for adhesives, regression in the number of cycles produced higher shape parameters than from the MLE.

7. REFERENCES.

1. Aniversario, R.B., Harvey, S.T., McCarty, J.E., Parson, J.T., Peterson, D.C., Pritchett, L.D., Wilson, D.R., and Wogulis, E.R., "Full-Scale Testing, Production and Cost Analysis Data for the Advanced Composite Stabilizer for Boeing 737 Aircraft," Vol. 2, NASA CR-166012, December 1982.

2. Whitehead, R.S., Kan, H.P., Cordero, R., and Saether, E.S., "Certification Testing Methodology for Composite Structures," Report No. NADC-87042-60, Volumes I and II, October 1986.

3. Lameris, J., "The Use of Load Enhancement Factors in the Certification of Composite Aircraft Structures," NLR Report: NLR TP 90068 U, February 1990.

4. Seneviratne, W.P., "Fatigue-Life Determination of Damage-Tolerant Composite Airframe," Dissertation, Wichita State University, December 2008.

5. Sanger, K.B., "Certification Testing Methodology for Composite Structures," Report No. NADC-86132-60, January 1986.

6. Deo, R., Starnes, Jr., J.H., and Holzwarth, R., "Low-Cost Composite Materials and Structures for Aircraft Applications," *NATO Applied Vehicle Technology Panel (AVT) Specialists' Meeting*, RTO-MP-069(II), Leon, Norway, May 2001.

7. Kan, H.P. and Whitehead, R.S., "Damage Tolerance Certification Methodology for Composite Structures," *Proceedings of Eighth DoD/NASA/FAA Conference on Fibrous Composites in Structural Design,* NASA CP-3087, Part 2, Norfolk, Virginia, November 1989, pp. 479-498.

8. Shah, C.H., Kan, H.P., and Mahler, M., "Certification Methodology for Stiffener Termination," FAA report DOT/FAA/AR-95/10, April 1996.

9. Kan, H.P. and Dyer, T.A., "Structural Integrity Evaluation of the Lear Fan 2100 Aircraft," FAA report DOT/FAA/AR-95/13, May 1996.

10. McCarty, J.E., Johnson, R.W., and Wilson, D.R., "737 Graphite-Epoxy Horizontal Stabilizer Certification," *Proceedings of the 23rd AIAA/ASME/ASCE/AHS Structures, Structural Dynamics and Materials Conference*, May 1982, pp. 307-322.

11. Gogkol, O., "A310-300 CRFP Fin – Damage Tolerance Demonstration," *Proceedings of the 7th International Conference of SAMPE,* European Chapter, Munich, June 1986.

12. Brandecker, B. and Hilgert, R., "A320 Full Scale Structural Testing for Fatigue and Damage Tolerance Certification of Metallic and Composite Structure," *Proceedings of the 16th Congress of the International Council of the Aeronautical Sciences,* ICAS-88-5.8.1, Jerusalem, Israel, 1988.

13. Fawcett, A., Trostle, J., and Ward, S., "777 Empennage Certification Approach," *Proceedings of the 11th International Conference on Composite Materials,* Australia, July 1997.

14. Vosteen, L.F. and Hadcock, R.N., "Composite Chronicles: A Study of the Lessons Learned in the Development, Production, and Service of Composite Structures," NASA CR-4620, November 1994.

15. Wong, R. and Abbott, R., "Durability and Damage Tolerance of Graphite/Epoxy Honeycomb Structures," *Proceedings of the 34th International Symposium,* Anaheim, California, 1990.

16. Kan, H.P. and Kane, D.M., "Probabilistic Certification of Integrally Bonded Composite Structures—an Assessment," *Proceedings of the 43rd AIAA/ASME/ASCE/AHS/ASC Structures, Structural Dynamics and Materials*, Denver, Colorado, April 2002.

17. Sumich, M. and Kedward, K.T., "Development of a Fatigue-Life Methodology for Composite Structures Subjected to Out-of-Plane Load Components," NASA TM-102885, February 1991.

18. Halpin, J., Jerina, K., and Johnson, T., "Characterization of Composites for the Purpose of Reliability Evaluation," *Analysis of Test Methods for High Modulus Fibers and Composites, ASTM STP 521,* American Society for Testing Materials, 1973, pp. 5-64.

19. Sendeckyj, G.P., "Fitting Models to Composite Materials Fatigue Data," *Test Methods and Design Allowables for Fibrous Composites, ASTM STP 734*, Chamis, C.C., ed., American Society for Testing and Materials, 1981, pp. 245-260.

20. Sendeckyj, G.P., "Life Prediction for Resin Matrix Composite Materials," *Fatigue of Composite Materials*, Reifsnider, K.L., ed., Elsevier, Amsterdam, 1990.

21. O'Brien, T.K. and Reifsnider, K.L., "Fatigue Damage Evaluation Through Stiffness Measurements in Boron-Epoxy Laminates," *Journal of Composite Materials,* No. 15, 1981, pp. 55-70.

22. Hahn, H.T. and Kim, R.Y., "Fatigue Behavior of Composite Laminates," *Journal of Composite Materials,* Vol. 10, No. 2, 1976, pp. 156-180.

23. Hwang, W. and Han, K.S., "Cumulative Damage Model and Multi-Stress Fatigue Life Prediction," *Journal of Composite Materials,* Vol. 20, No. 2, 1986, pp. 125-153.

24. Hwang, W. and Han, K.S., "Fatigue of Composites—Fatigue Modulus Concept and Life Prediction," *Journal of Composite Materials,* Vol. 20, No. 2, 1986, pp. 154-165.

25. Mahfuz, H., Zaman, K., Haque, A., Foy, C., Mohamed, H., and Jeelani, S., "Fatigue Life Prediction of Thick-Section S2-Glass/Vinyl-Ester Composites Under Flexural Loading," *Journal of Engineering Materials and Technology,* Vol. 122, No. 4, October 2000, pp. 402-408

26. Halpin, J.C., Jerina, K.L., and Johnson, T.A., "Characterization of Composites for the Purpose of Reliability Evaluation," AFML-TR-77-289, Wright-Patterson Air Force Base, Ohio, 1972.

27. Jeans, L.L., Grimes, G.C., and Kan, H.P., "Fatigue Spectrum Sensitivity Study for Advanced Composite Materials," U.S. Air Force Flight Dynamic Laboratory, Technical Report AFWAL-TR-80-3130, Volumes I, II, and III, 1980.

28. Rosenfeld, M.S. and Huang, S.L., "Fatigue Characteristics of Graphite/Epoxy Laminates Under Compression Loading," *Journal of Aircraft,* Vol. 15, No. 5, 1978, pp. 264-268.

29. Agarwal, B.D. and James, W.D., "Prediction of Low-Cycle Fatigue Behavior of GFRP: An Experimental Approach," *Journal of Materials Science,* Vol. 10, No. 2, 1975, pp. 193-199.

30. Yang, J.N. and Du, S., "An Exploratory Study Into the Fatigue of Composites Under Spectrum Loading," *Journal of Composite Materials,* Vol. 17, No. 6, 1983, pp. 511-526.

31. Kassapoglou, C., "Fatigue Life Prediction of Composite Structures Under Constant Amplitude Loading," *Journal of Composite Materials,* Vol. 41, No. 22, 2007.

32. Tomblin, J.S. and Seneviratne, W.P., "FAA Research on Large-Scale Test Substantiation," FAA Damage Tolerance and Maintenance Workshop, Rosemont, Illinois, July, 2006.

33. Tomblin, J.S. and Seneviratne, W.P., "Laminate Statistical Allowable Generation for Fiber-Reinforced Composite Materials: Lamina Variability Method," FAA report DOT/FAA/AR-06/53, January 2009.

34. Shyprykevich, P., Seneviratne, W.P., and Tomblin, J.S., "Lamina Variability Method for Determining Laminate Basis Values," *22nd Annual Technical Conference of the American Society for Composites (ASC)*, Seattle, Washington, September 2007.

35. Tomblin, J.S., Seneviratne, W.P., Escobar, P., and Yap, Y., "Fatigue and Stress Relaxation of Adhesives in Bonded Joints," FAA report DOT/FAA/AR-03/56, Ocrtober 2003.

36. Tomblin, J.S., Seneviratne, W.P., and Pillai, G.R., "Effects of Disbonds, Lightning Strikes, and Low-Velocity Impact Damage on Adhesively Bonded Composite Joints," FAA report DOT/FAA/AR-09/4, December 2009.

37. *Composite Material Handbook (CMH-17), Volume 2: Polymer Matrix Composites Material Properties*, Chapter 4—Carbon Fiber Properties, Material Sciences Corp., in cooperation with ASTM, 1999.

38. Tomblin, J., Harter, P., Seneviratne, W., and Yang, C., "Characterization of Bondline Thickness Effects in Adhesive Joints," *ASTM Journal of Testing and Evaluation, JCTRER,* Vol. 24, No. 2, 2002, pp. 332-344.

39. Tomblin, J.S., Seneviratne, W.P., Kim, H., and Lee, J., "Box Beam Lap Shear Torsion Testing for Evaluating Structural Performance of Adhesive Bonded Joints," *Joining and Repair of Composites Structures, ASTM STP 1455,* Kedward, K.T. and Kim, H., eds., ASTM International, 2004, pp. 42-54.

40. ARAMIS, v. 5.3.0 User Manual, GOM mbH.

41. Tomblin, J.S., Seneviratne, W.P., and Borgman, M.D., "Electronic Speckle Pattern Interferometry for Investigating Defect Propagation of Honeycomb Sandwich Specimens," *SAMPE Technical Conference*, Baltimore, Maryland, November 2001.

42. *Life Data Analysis Reference*, ReliaSoft Corporation, Tucson, Arizona.

43. Badaliance, R. and Dill, H.D., "Compression Fatigue Life Prediction Methodology for Composite Structures," NADC-83060-60, Volumes I and II, September 1982.

44. Rust, S.W., Todt, F.R., Harris, B., Neal, D., and Vangel, M., "Statistical Methods for Calculating Material Allowables for MIL-HDBK-17," *Test Methods for Design Allowables for Fibrous Composites, ASTM STP 1003,* Chamis, C.C. ed., ASTM, Philadelphia, Pennsylvania, 1989, pp. 136-149.

45. Whitehead, R.S. and Schwarz, M.G., "The Role of Fatigue Scatter in the Certification of Composite Structures," ASTM Symposium on the Long-Term Behavior of Composites, Williamsburg, Virginia, March 1982.

46. Seneviratne, W.P., "Fatigue Analysis of Liberty XL2 Fuselage Materials," National Institute for Aviation Research, STR-RP-2008-005, September 2008.

47. Gabriel, E.A., DeFiore, T., Locke, J.E., and Smith, H.W., "General Aviation Aircraft—Normal Acceleration Data Analysis and Collection Project," FAA report DOT/FAA/CT-91/20, February 1993.

48. "Fatigue Evaluation of Wing and Associated Structure of Small Airplanes," FAA report AFS-120-73-2, May 1973.

49. Berens, A.P. and West, B.S., "Evaluation of an Accelerated Characterization Technique for Reliability Assessment of Adhesive Joints," *Composite Reliability, ASTM STP 580,* ASTM, Philadelphia, Pennsylvania, 1975, pp. 90-101.

APPENDIX A—FATIGUE TEST RESULTS OF FEDERAL AVIATION ADMINISTRATION LOAD-ENHANCEMENT FACTOR DATABASE

This appendix contains the stress to number of cycles (S/N) curves that were used for the fatigue life scatter analysis of the Federal Aviation Administration load-enhancement factor (FAA-LEF) database. Sendeckyj analysis [A-1] was conducted on the S/N data, and the fitting curves are displayed here for a graphical confirmation that the analysis represents a reasonable trend. S/N curves based on the Sendeckyj analysis are compared with the life predictions based on the Kassapoglou method [A-2], which only uses static-strength data to predict fatigue life. In addition, for several selected fatigue specimens, the compliance change and the damage growth are compared.

A.1 THE S/N DATA FOR AS4/E7K8 PLAIN-WEAVE FABRIC.

This section contains the S/N data for the AS4/E7K8 plain-weave fabric tests included in the FAA-LEF database. Tables A-1 through A-6 include the individual data points, and figures A-1 through A-14 show the S/N curves that were used for generating LEFs for AS4-PW. Figure A-15 shows the Goodman diagram for AS4-PW open-hole (OH) test data. In these tables, n is the number of cycles survived and n = 1 indicates static failure. Also, σ_A and σ_R correspond to the fatigue stress level (or static failure stress level) and the residual strength after surviving the corresponding number of cycles, respectively.

Table A-1. S/N Data for AS4-PW 10/80/10 OH Tests (FAA-LEF)

OH Compression/Tension (R = -1)			OH Compression (R = 5)			OH Tension (R = 0)			OH Tension (R = -0.2)		
σ_A	N	σ_R	σ_A	N	σ_R	σ_A	N	σ_R	σ_A	N	σ_R
41228	1		41228	1		43792	1		43792	1	
39404	1		39404	1		44405	1		44405	1	
40497	1		40497	1		43580	1		43580	1	
39811	1		39811	1		43112	1		43112	1	
43154	1		43154	1		42126	1		42126	1	
38740	1		38740	1		43717	1		43717	1	
30354	301		30354	2645		34764	20505		32591	18137	
26307	2195		30354	15660		34764	15422		32591	18575	
26307	1407		30354	11740		34764	10607		32591	21301	
26307	1412		30354	9151		34764	11684		32591	22457	
26307	1751		30354	10990		34764	6077		32591	34293	
26307	1996		30354	8239		34764	11195		32591	17588	
26307	1442		30354	11057		32591	38373		28246	153000	
26307	1927		28330	69069		32591	55456		28246	119454	
26307	4746		28330	44082		32591	46146		28246	31998	
20236	36171		28330	98781		32591	71250		28246	151318	
20236	29470		28330	90522		32591	57471		28246	142394	
20236	31608		28330	114108		32591	54131		28246	178984	
20236	32681		28330	52521		28246	474638		26073	226885	
20236	30972		28330	50311		28246	377554		26073	390390	
20236	26187		28330	70955		28246	368844		26073	451383	
20236	30657		26307	188105		28246	314495		26073	270902	
20236	75965		25497	229685		28246	365748		26073	425390	
16189	549419		25497	445665		28246	389959		26073	281893	
16189	652440		25497	348791		21728	1000000	41546	26073	332591	
16189	545138		25497	443210					23900	1000000	30517
16189	715247		25497	726570					23900	1000000	29613
16189	519140		25497	574103					23900	1000000	26546
16189	503585		24283	1000000	36385						
16189	881812		24283	1000000	34324						
16189	771513										

Table A-2. S/N Data for AS4-PW 10/80/10 Compression After Impact and Double-Notched Compression Tests (FAA-LEF)

Compression After Impact (R = 5) [20 ply] - Barely Visible Impact Damage			Compression After Impact (R = 5) [40 ply] - Visible Impact Damage			Double-Notched Compression (R = -1)			Double-Notched Compression (R = -0.2)		
σ_A	n	σ_R	σ_A	n	σ_R	σ_A	n	σ_R	σ_A	n	σ_R
34974	1		28945	1		4236	1		4236	1	
35928	1		31307	1		3804	1		3804	1	
32913	1		30476	1		3836	1		3836	1	
27684	9071		30525	1		3948	1		3948	1	
27684	5856		29743	1		4037	1		4037	1	
27684	8980		30585	1		4068	1		4068	1	
27684	16161		22698	9471		1595	7231		1994	25321	
27684	10644		22698	15663		1595	7524		1994	28298	
27684	9777		22698	7994		1595	6586		1795	27417	
25954	34539		22698	21448		1595	8621		1795	17379	
25954	66766		22698	6833		1595	8212		1795	10624	
25954	42237		22698	8538		1595	7256		1795	28230	
25954	17223		21184	29471		1595	7150		1795	54216	
25954	43665		21184	47593		1196	25573		1795	27694	
25954	46917		21184	28418		1196	35487		1795	16090	
24224	99627		21184	63444		1196	34290		1595	72855	
22493	454828		21184	46077		1196	47904		1595	99058	
22493	740070		19671	601081		1196	48215		1595	50752	
22493	650366		19671	203021		1196	59366		1595	39812	
22493	468695		19671	145252		997	262210		1595	40000	
22493	450007		19671	538785		997	361803		1595	34484	
22493	709191		19671	374069		997	271419		1595	170739	
20763	1000000	35656				997	307399		1396	393302	
						997	194263		1396	238336	
						997	104738		1396	265252	
						678	1000000	3591	1396	170266	
									1396	221148	
									1396	121619	
									1196	711710	
									1196	1000000	3381
									1196	1000000	3540

Table A-3. S/N Data for AS4-PW 0/100/0 Compression After Impact and Double-Notched Compression Tests (FAA-LEF)

OH Tension (R = -1)			Tension After Impact (R = 0) - Barely Visible Impact Damage			Tension After Impact (R = 0) - Visible Impact Damage		
σ_A	n	σ_R	σ_A	n	σ_R	σ_A	n	σ_R
21231	1		17631	1		15690	1	
21970	1		17409	1		15744	1	
22082	1		17550	1		14612	1	
21821	1		18326	1		14150	1	
22254	1		18078	1		15333	1	
21890	1					15180	1	
13125	1211		14239	137		10583	464	
10937	6730		9789	500		9071	860	
10937	13547		9789	392		9071	808	
10937	7729		8899	3001		9071	976	
10937	7957		8899	2709		9071	1933	
10937	7893		8899	695		9071	667	
10937	6812		8899	675		9071	768	
8750	57561		8899	717		8315	1226	
8750	83056		8899	621		8315	5471	
8750	47243		8899	745		7559	4243	
8750	65033		8009	7164		7559	15903	
8750	121089		8009	9277		7559	5396	
8750	66003		8009	2982		7559	7275	
7656	210460		8009	7037		7559	7844	
7656	191852		8009	7196		7559	29967	
7656	194105		8009	5607		6803	66940	
7656	216642		7120	249488		6803	38624	
7656	216727		7120	448722		6803	70854	
7656	254909		7120	79665		6803	142973	
6562	990178		7120	138485		6803	107914	
			7120	173554		6803	25250	
			7120	153293		6501	556214	
			6764	807275		6501	1000020	
			6764	840693		6047	698405	
			6230	1000027	12663	6047	1000011	13543
						6047	1000022	14565

Table A-4. S/N Data for AS4-PW 25/50/25 OH Tension and Compression After Impact Tests (FAA-LEF)

OH Tension (R = -1)		Compression After Impact (R = 5) - Barely Visible Impact Damage		Compression After Impact (R = 5) - Visible Impact Damage		Compression After Impact (R = 5) - Large Impact Damage	
σ_A	n	σ_A	n	σ_A	n	σ_A	n
44593	1	37188	1	29149	1	25147	1
46643	1	34745	1	31335	1	25601	1
43391	1	35658	1	29443	1	24627	1
44080	1	36526	1	29282	1	25370	1
45918	1	36364	1	29950	1	25228	1
47623	1	35669	1	28866	1	26695	1
27225	14982	28820	12243	22374	37690	19083	42897
27225	11988	28820	14342	22374	24001	19083	38476
27225	15400	28820	9651	22374	55768	19083	18155
27225	7335	28820	8152	22374	28958	19083	13719
27225	8149	28820	15155	22374	11897	19083	32463
27225	16101	28820	26005	22374	16335	19083	17564
22687	129345	27019	92926	20882	127451	16539	201380
22687	105310	27019	31634	20882	94625	16539	214807
22687	142170	27019	104891	20882	128689	16539	374375
22687	103758	27019	152023	20882	59749	16539	278234
22687	117594	27019	47635	20882	143030	16539	165086
22687	117183	27019	31642	20882	180742	16539	193821
20419	446962	25217	678421	19391	626039	15267	2233805
20419	524270	25217	596825	19391	397153	15267	1352887
20419	604378	25217	323026	19391	270784	15267	1618147
20419	498321	25217	252255	19391	638545	15267	1236307
20419	949760	25217	575983	19391	222775	15267	928401
20419	916940	25217	252433	19391	595875	15267	1228113

Table A-5. S/N Data for AS4-PW 40/20/40 Compression After Impact Tests (FAA-LEF)

Compression After Impact (R = 5) - Visible Impact Damage		
σ_A	n	σ_R
30623	1	
31444	1	
33538	1	
31473	1	
32526	1	
31465	1	
25476	11230	
25476	21414	
25476	10473	
25476	9354	
25476	10449	
23884	37414	
23884	27422	
23884	31761	
23884	40216	
23884	59635	
23884	45263	
20699	538811	
20699	800295	
20699	849092	
20699	774653	
20699	860179	
20699	726956	
20699	1000030	31056
20699	1000032	31272
20699	1000051	30183

Table A-6. S/N Data for AS4-PW Sandwich Tests (FAA-LEF)

Flexure (R = 0)		
σ_A	n	σ_R
143.828	1	
145.592	1	
146.042	1	
146.530	1	
147.151	1	
139.028	1	
87.000	26661	
87.000	26077	
87.000	23272	
87.000	20000	
87.000	22000	
87.000	18898	
87.000	19928	
72.500	48648	
72.500	170000	
72.500	60000	
72.500	80000	
72.500	145000	
72.500	190000	
72.500	235000	
65.250	150000	
58.000	470000	
58.000	580000	
58.000	340000	
58.000	500000	
58.000	250000	
58.000	420000	
58.000	1000000	145.545

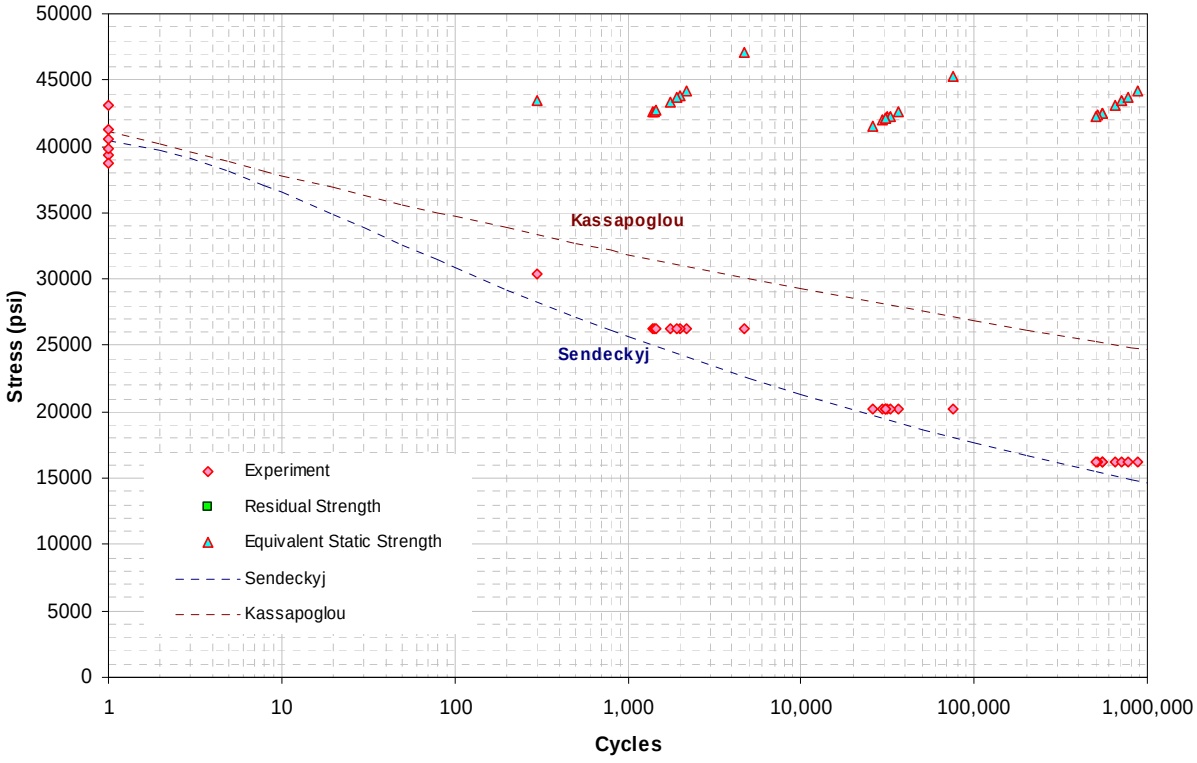

Figure A-1. AS4/E7K8 PW—10/80/10, OH, R = -1

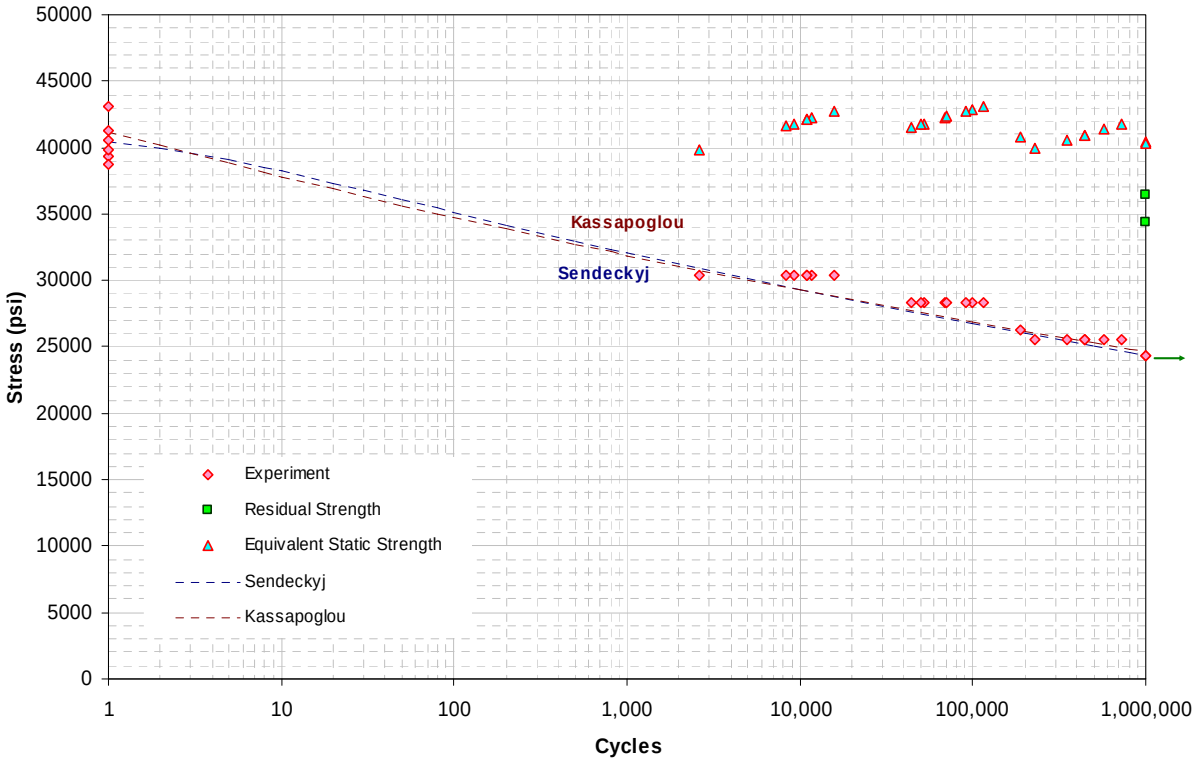

Figure A-2. AS4/E7K8 PW—10/80/10, OH, R = 5

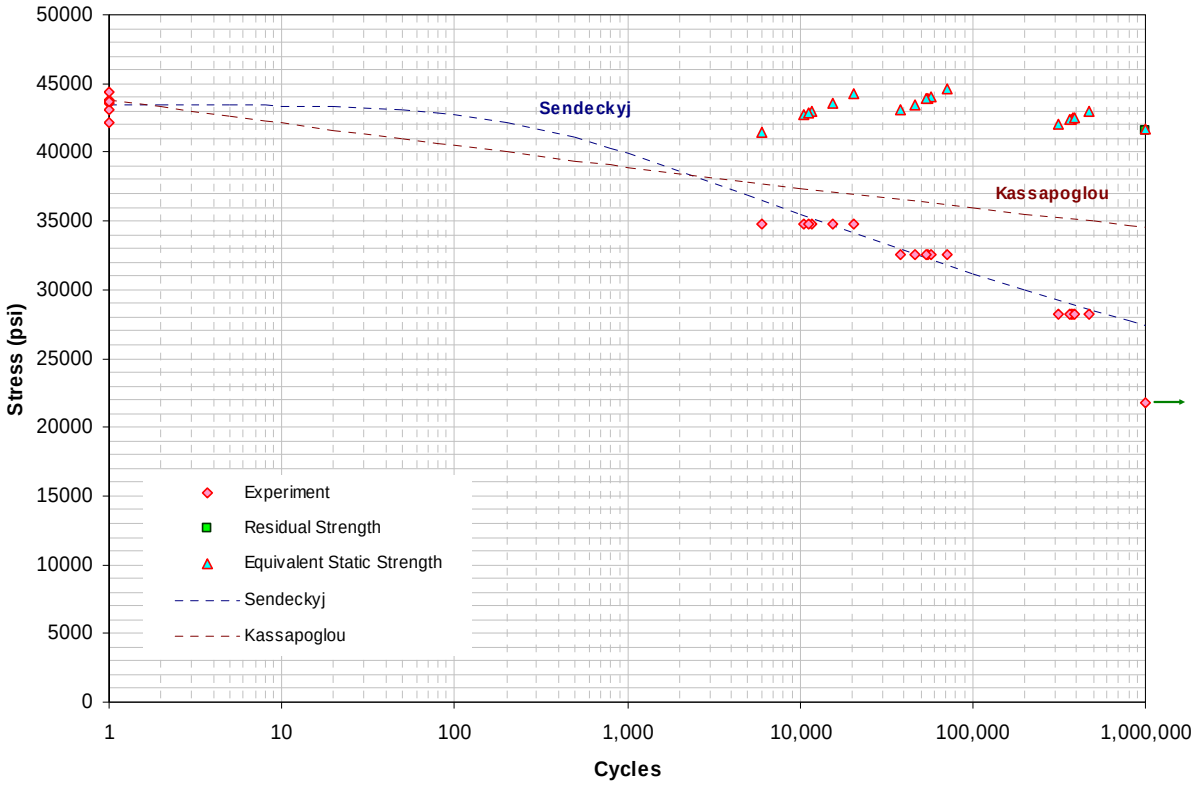

Figure A-3. AS4/E7K8 PW—10/80/10, OH, R = 0

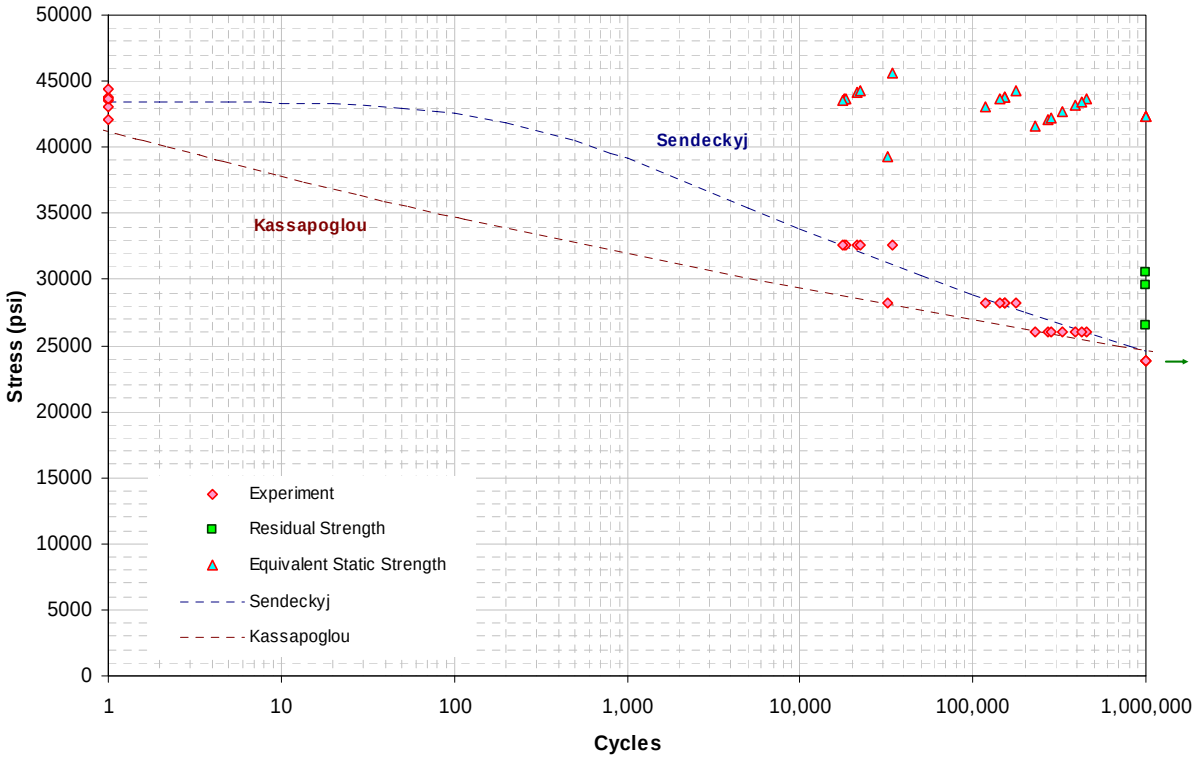

Figure A-4. AS4/E7K8 PW—10/80/10, OH, R = -0.2

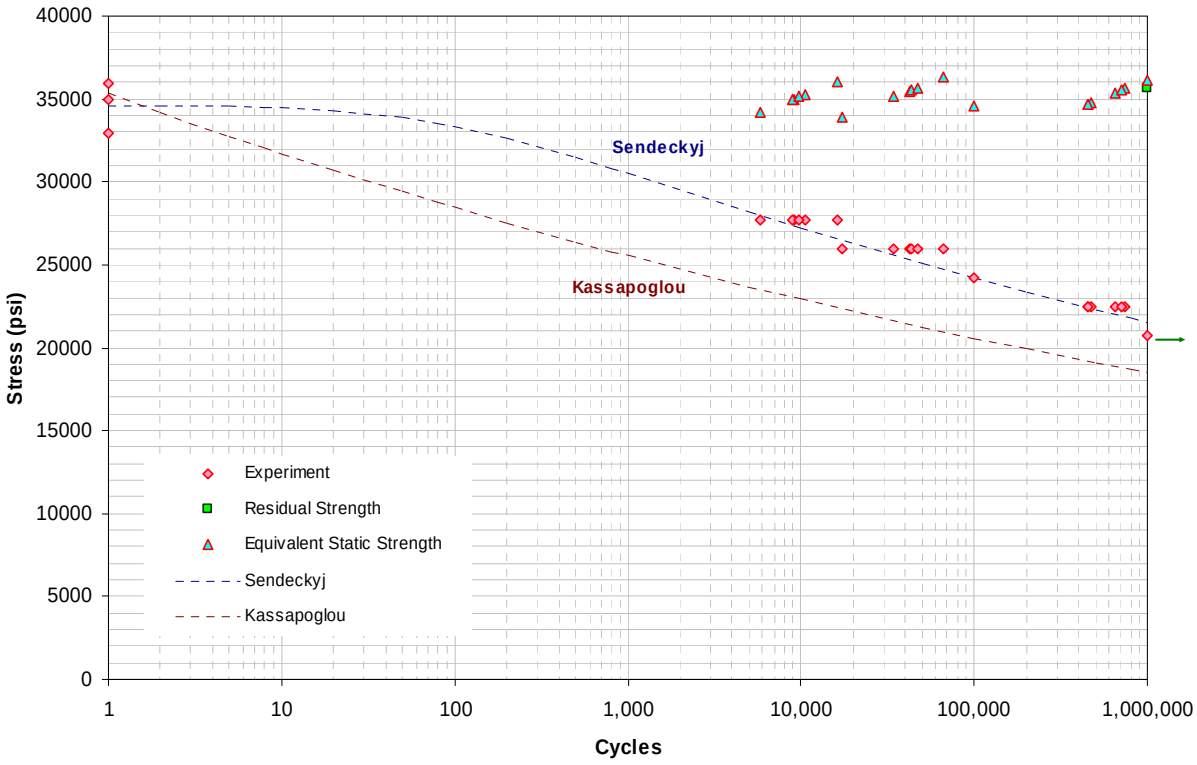

Figure A-5. AS4/E7K8 PW—10/80/10, CAI (20 ply)—BVID, R = 5

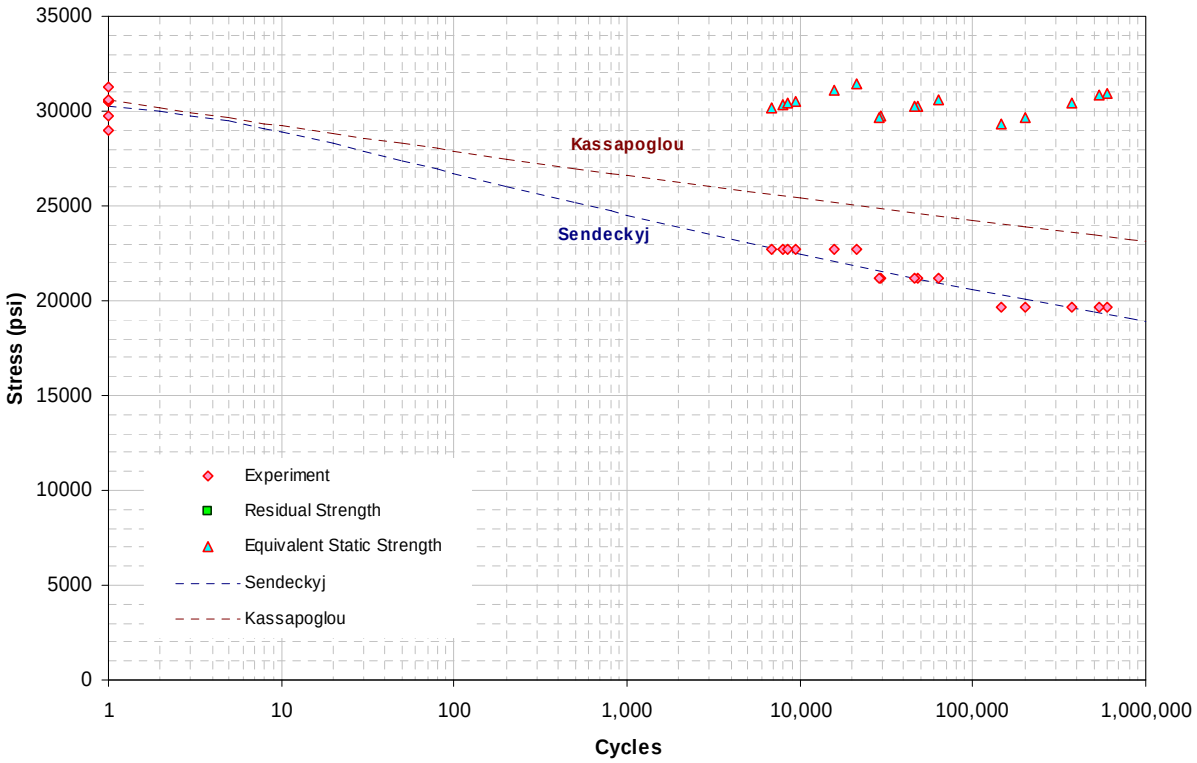

Figure A-6. AS4/E7K8 PW—10/80/10, CAI (40 ply)—BVID, R = 5

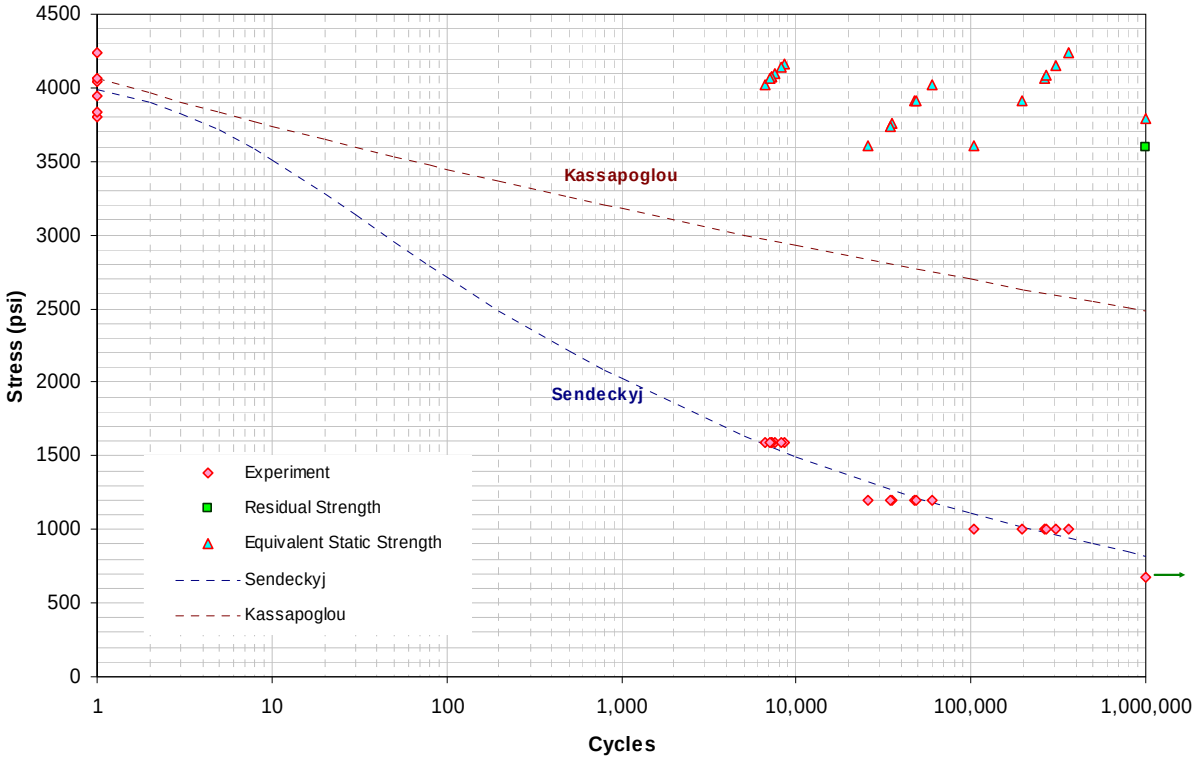

Figure A-7. AS4/E7K8 PW—10/80/10, DNC, R = -1

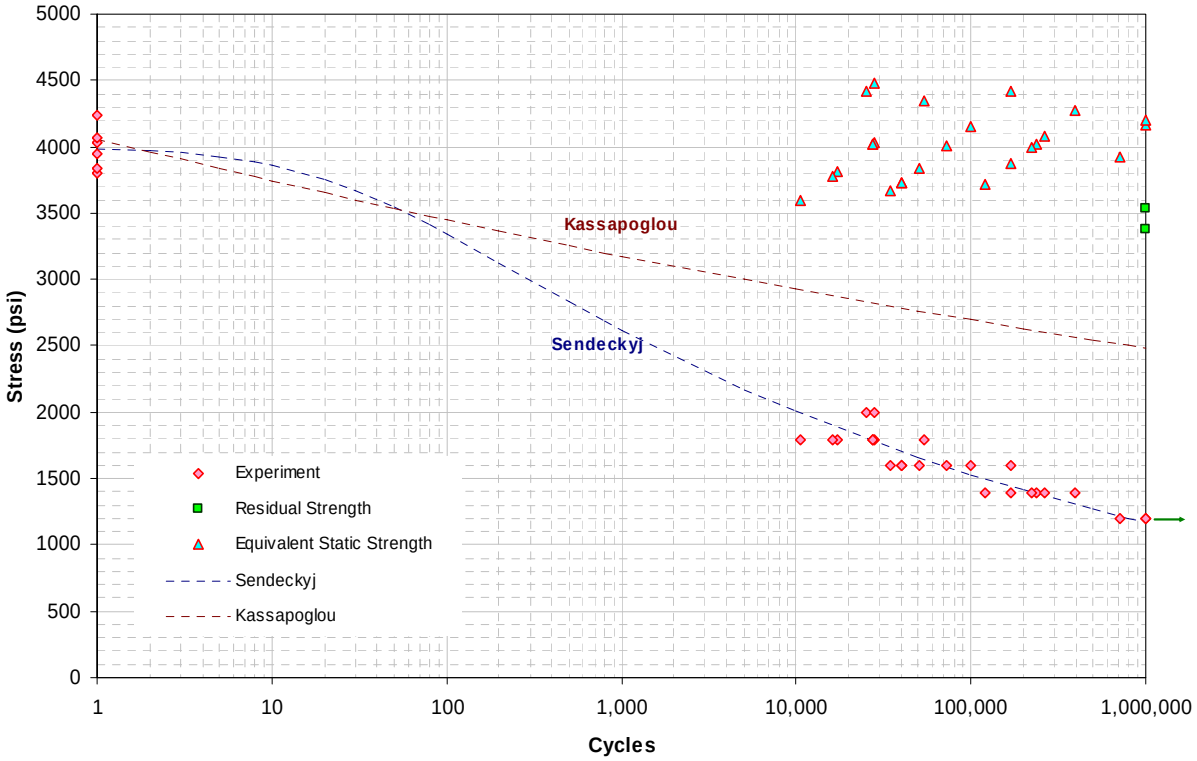

Figure A-8. AS4/E7K8 PW—10/80/10, DNC, R = -0.2

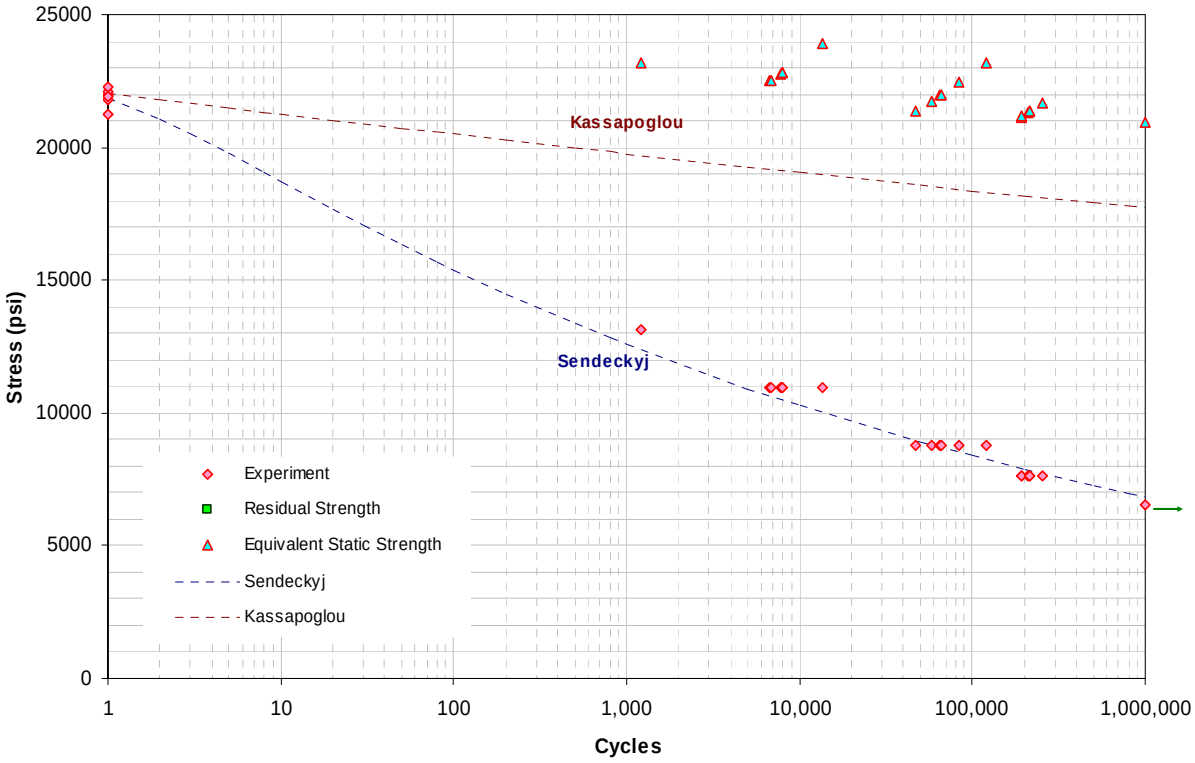

Figure A-9. AS4/E7K8 PW—0/100/0, OH, R = -1

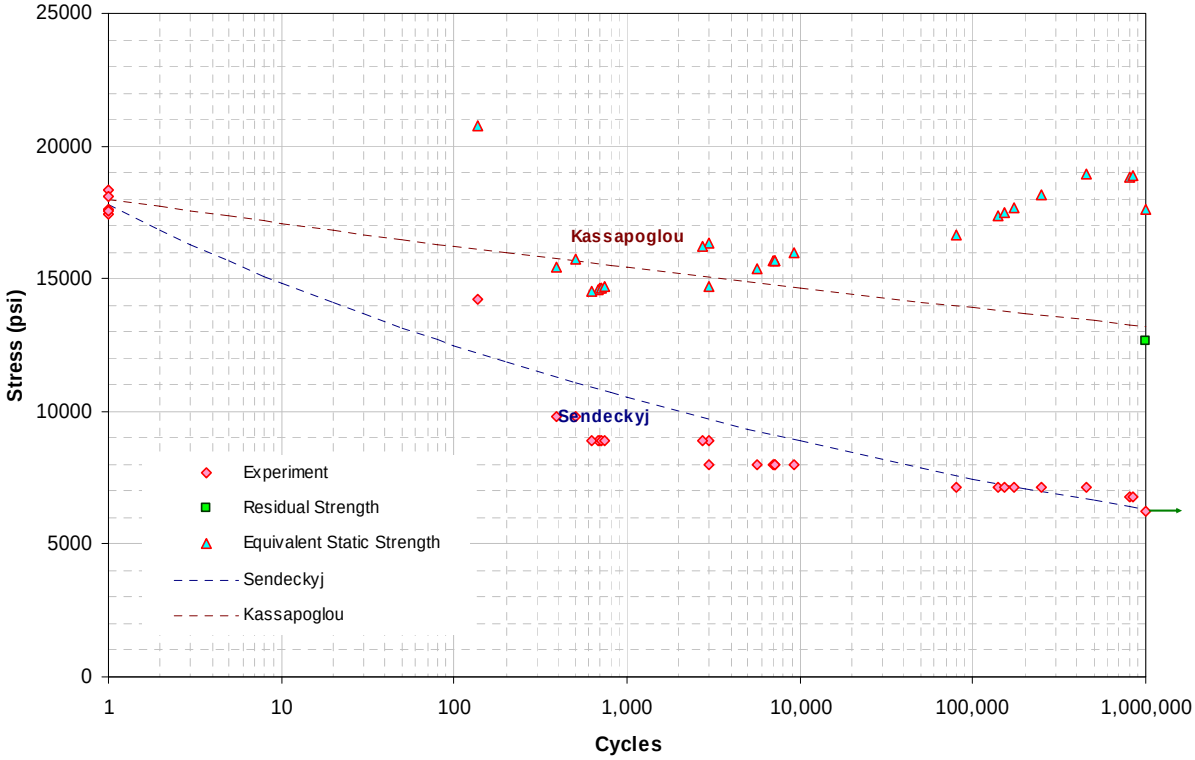

Figure A-10. AS4/E7K8 PW—0/100/0, TAI—BVID, R = 0

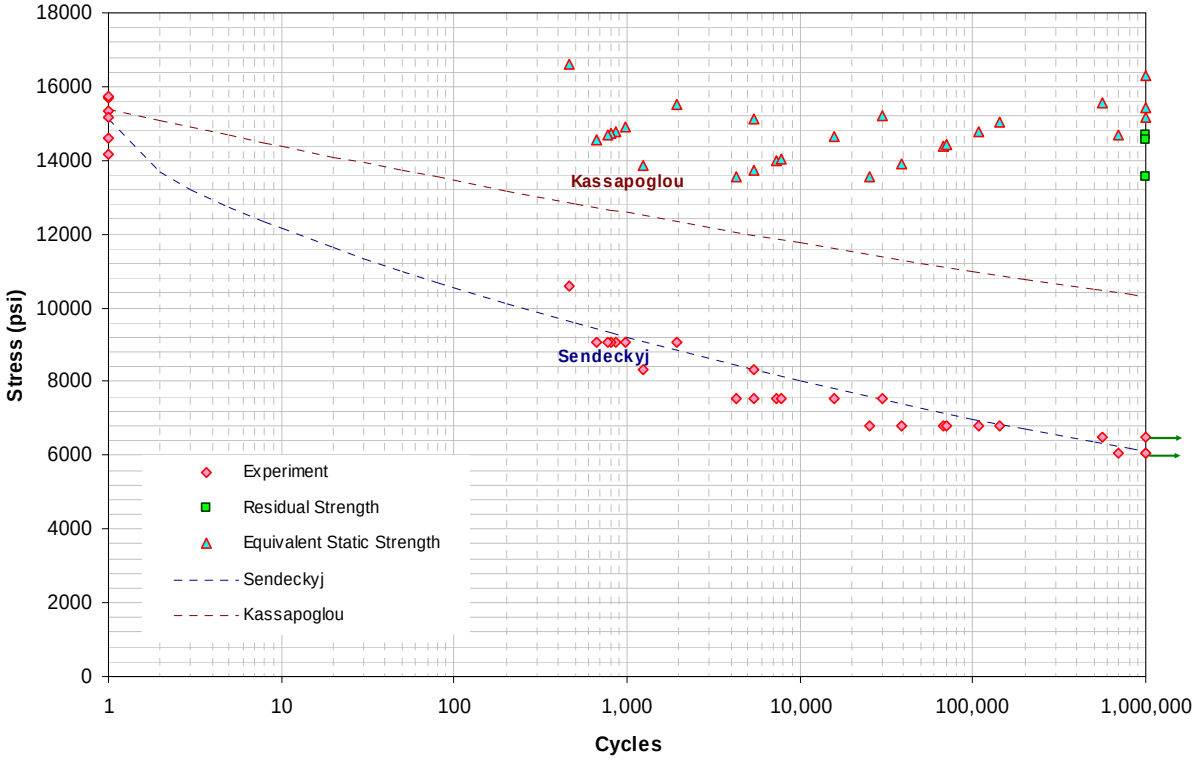

Figure A-11. AS4/E7K8 PW—0/100/0, TAI—VID, R = 0

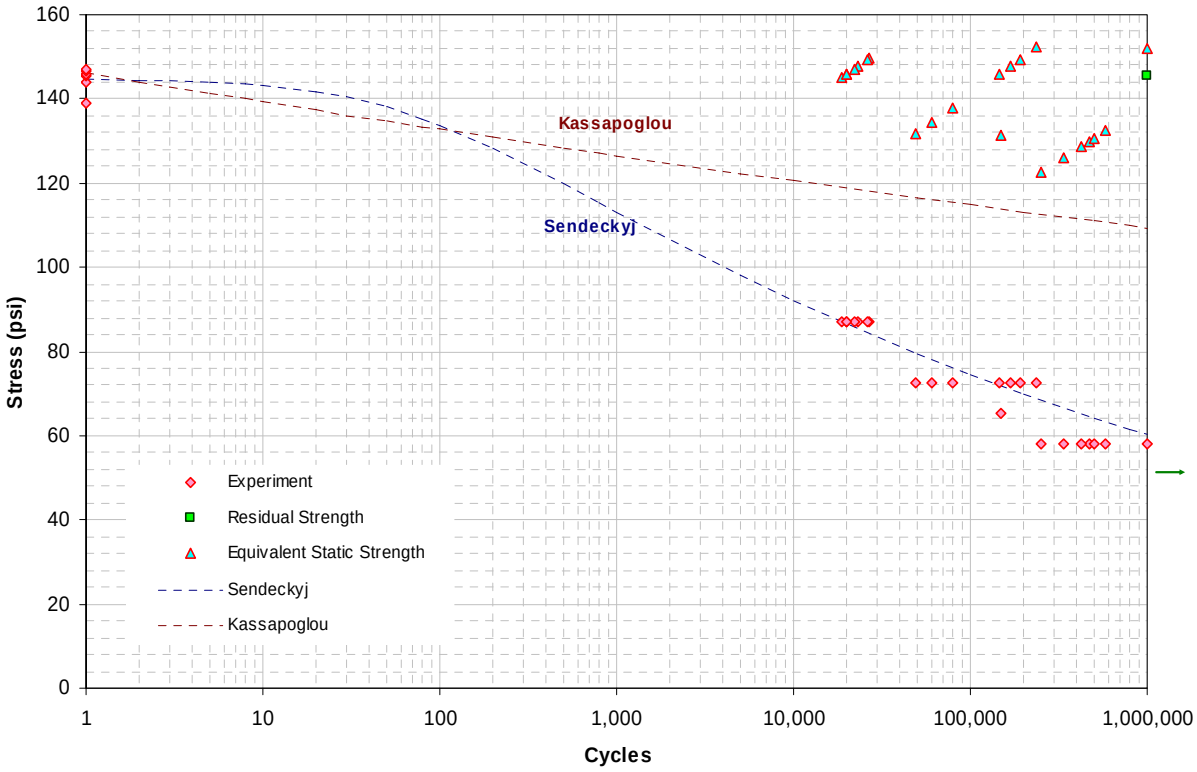

Figure A-12. AS4/E7K8 PW—HRH 10, Flexture, R = 0

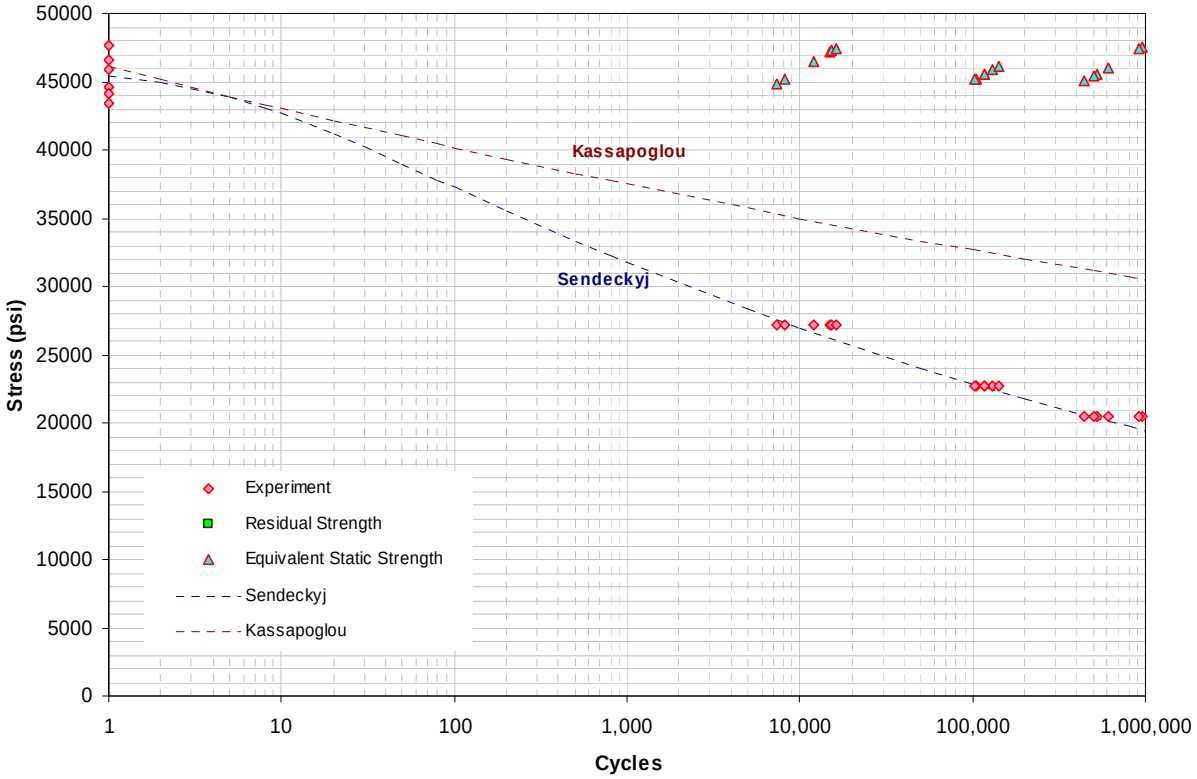

Figure A-13. AS4/E7K8 PW—25/50/25, OH, R = -1

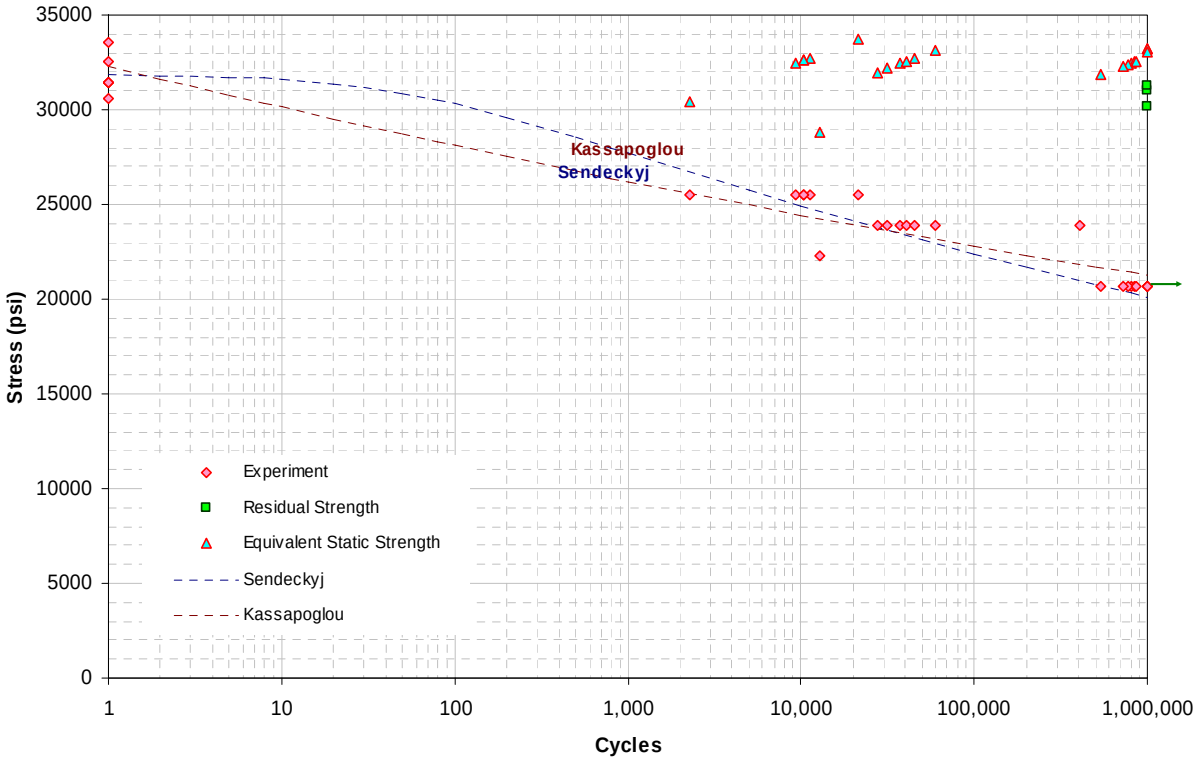

Figure A-14. AS4/E7K8 PW—40/20/40, CAI—VID, R = 5

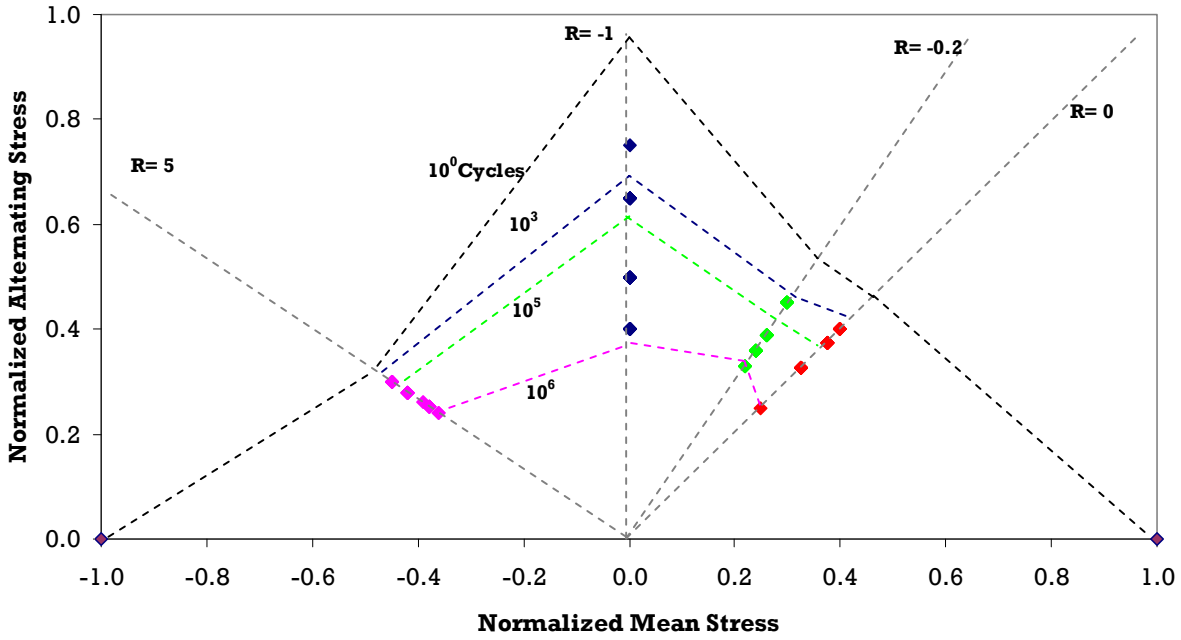

Figure A-15. Goodman Diagram Based on AS4/E7K8 PW OH Test Data

A.2 PROGRESSIVE DAMAGE FAILURE AND COMPLIANCE CHANGE.

The damage progression of several selected fatigue specimens was monitored by through-transmission ultrasonic (TTU) C-scanning. The damage growth was then compared with the compliance change of those specimens during fatigue tests. Compliance was measured by the following:

- Stopping the fatigue test and periodically conducting a quasi-static test (static)
- Collecting load-displacement data during fatigue at several fatigue intervals (dynamic)
- Using extensometer data (ext.)
- Using a laser extensometer (laser)

These data are shown in figures A-16 though A-22 for several open-hole compression (OHC) and flexure specimens.

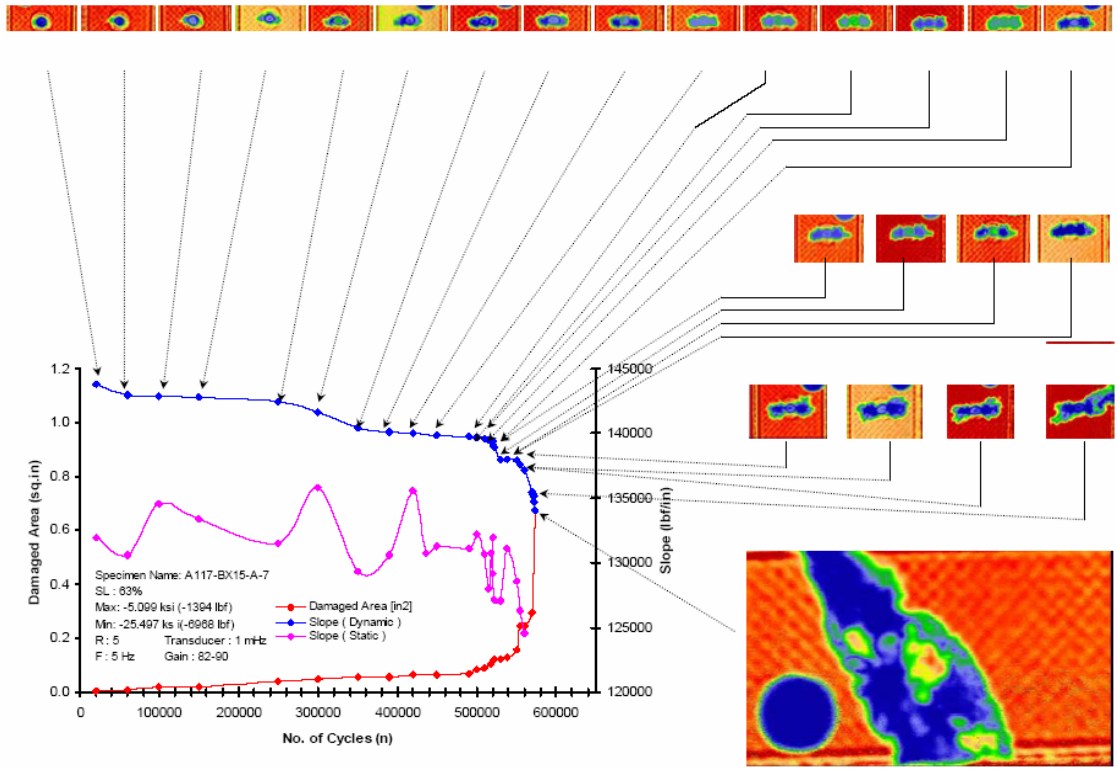

Figure A-16. AS4/E7K8 PW—10/80/10, OHC, R = 5, Stress Level = 63% of Static

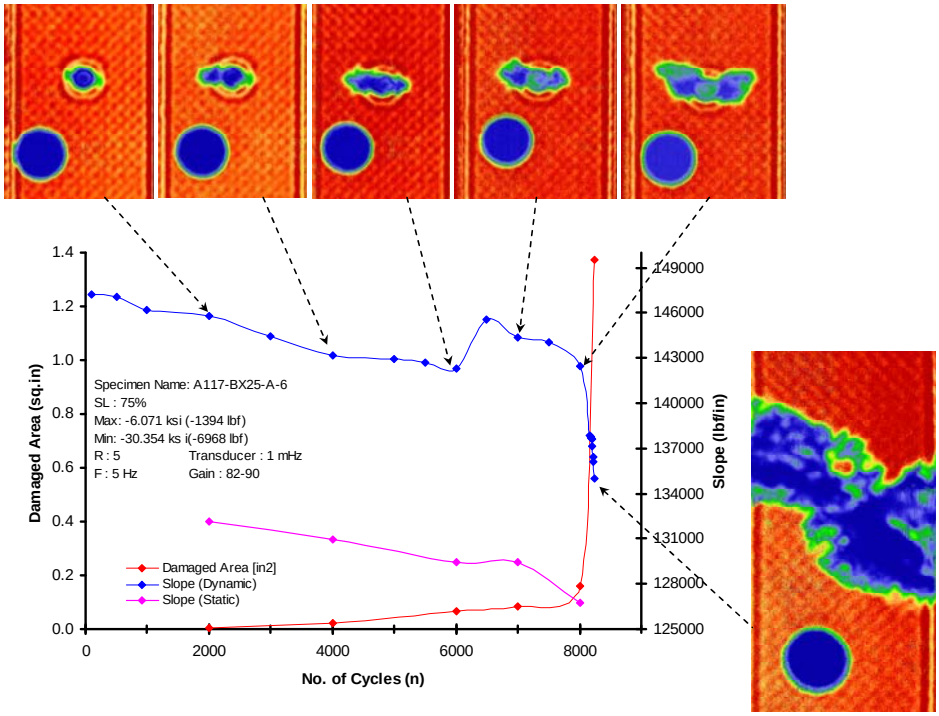

Figure A-17. AS4/E7K8 PW 01—10/80/10, OHC, R = 5, Stress Level = 75% of Static (Specimen A)

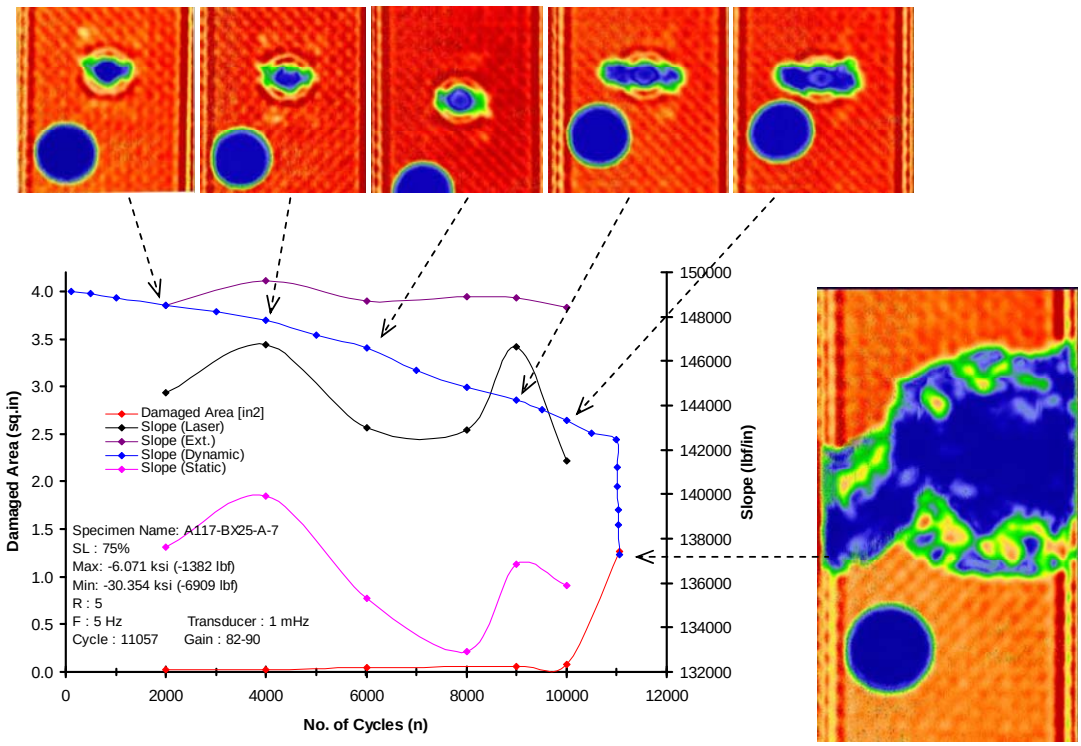

Figure A-18. AS4/E7K8 PW—10/80/10, OHC, R = 5, Stress Level = 75% of Static (Specimen B)

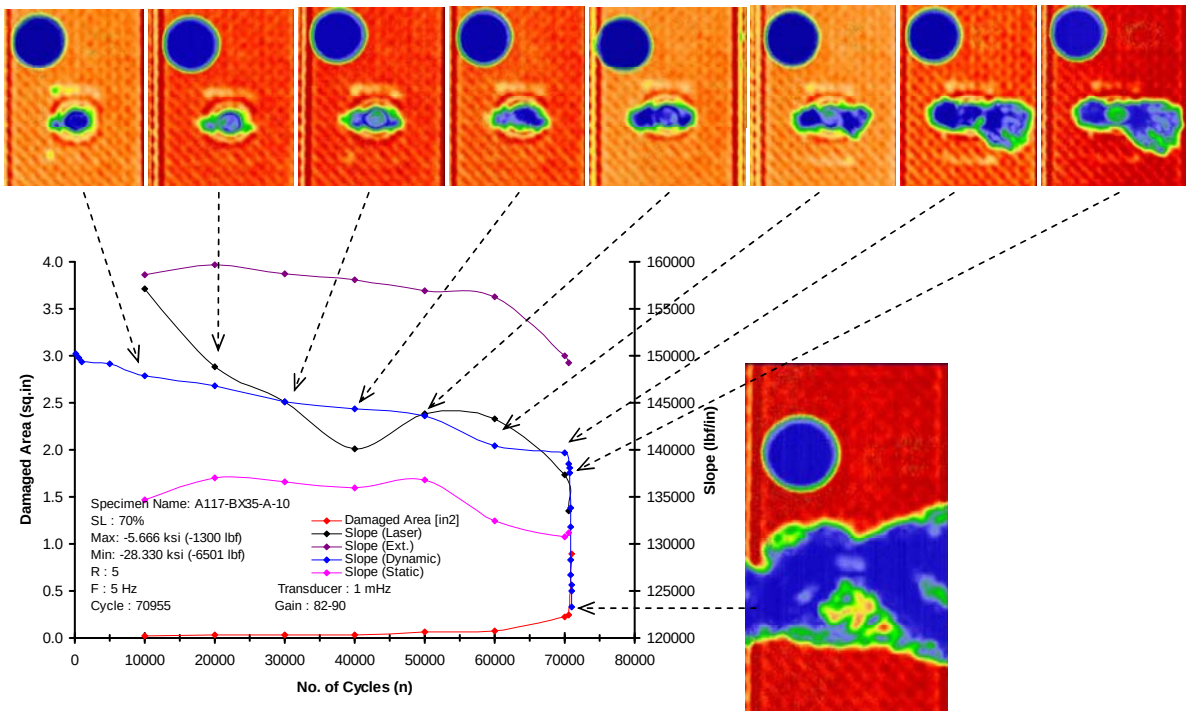

Figure A-19. AS4/E7K8 PW—10/80/10, OHC, R = 5, Stress Level = 70% of Static (Specimen A)

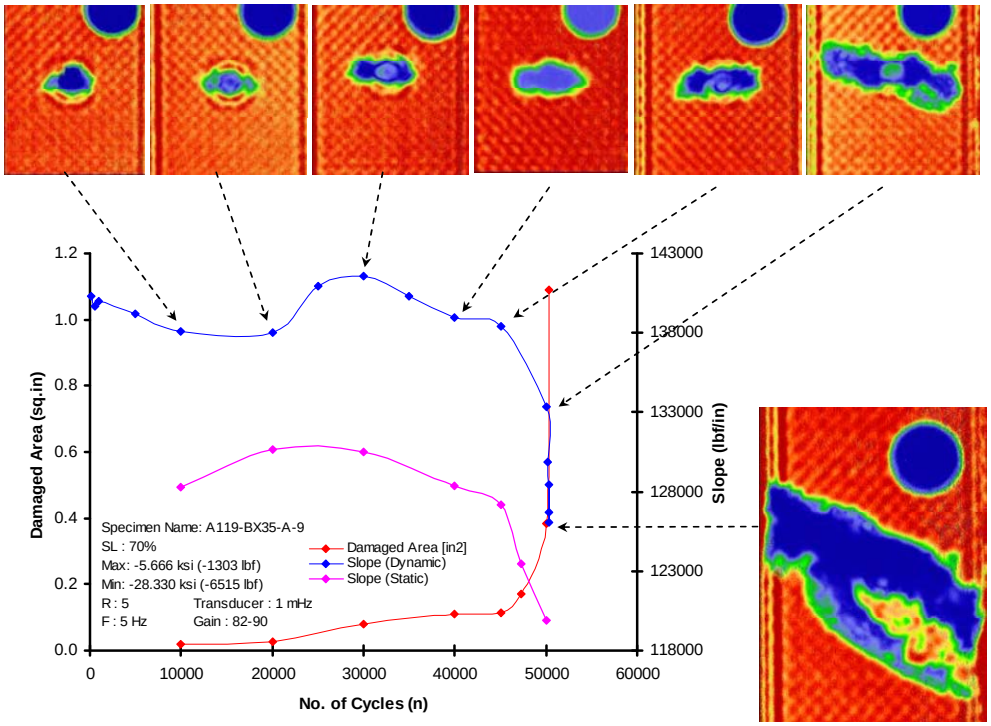

Figure A-20. AS4/E7K8 PW—10/80/10, OHC, R = 5, Stress Level = 70% of Static (Specimen B)

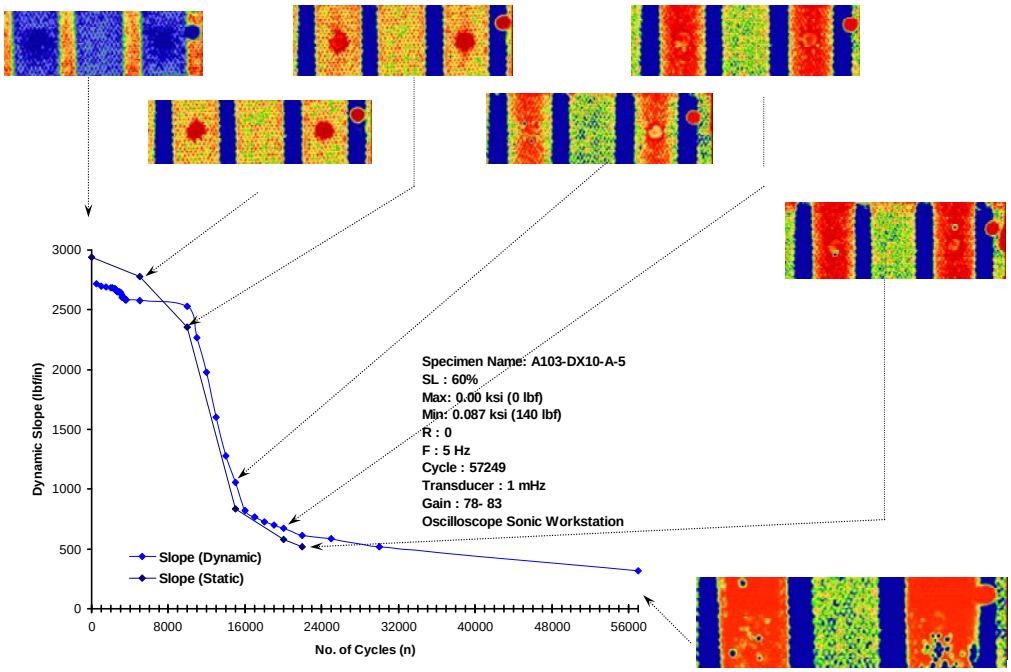

Figure A-21. AS4/E7K8 PW and HRH10—Sandwich, Flexure, R = 0, Stress Level = 60% of Static

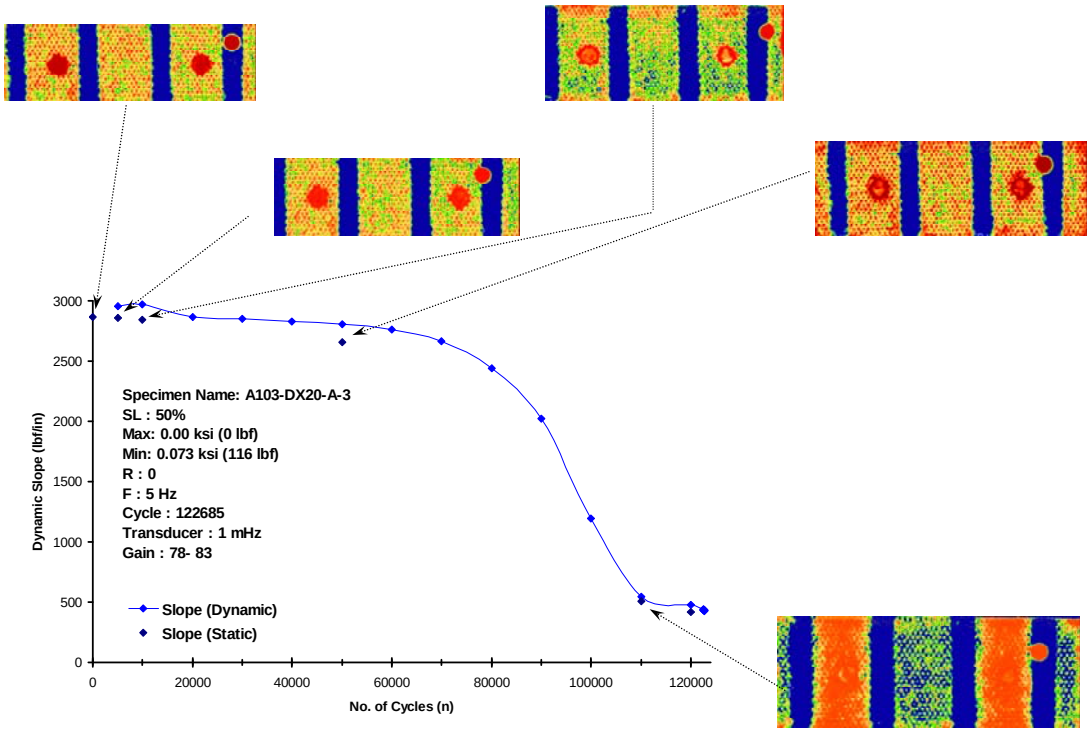

Figure A-22. AS4/E7K8 PW and HRH10—Sandwich, Flexure, R = 0, Stress Level = 50% of Static

Figures A-21 and A-22 show that the sandwich specimens carried the fatigue loads after significant damage propagation because the sandwich facesheets carried most of the loads in in-plane tension after the core shear capabilities were diminished. A 10-percent decrease in compliance was considered as fatigue failure.

The compliance changes and the corresponding C-scan damage area for the three stress levels, i.e., 75, 70, and 63 percent of OHC static strength, of several selected fatigue specimens with a stress ratio of 5 are superimposed for comparison in figure A-23.

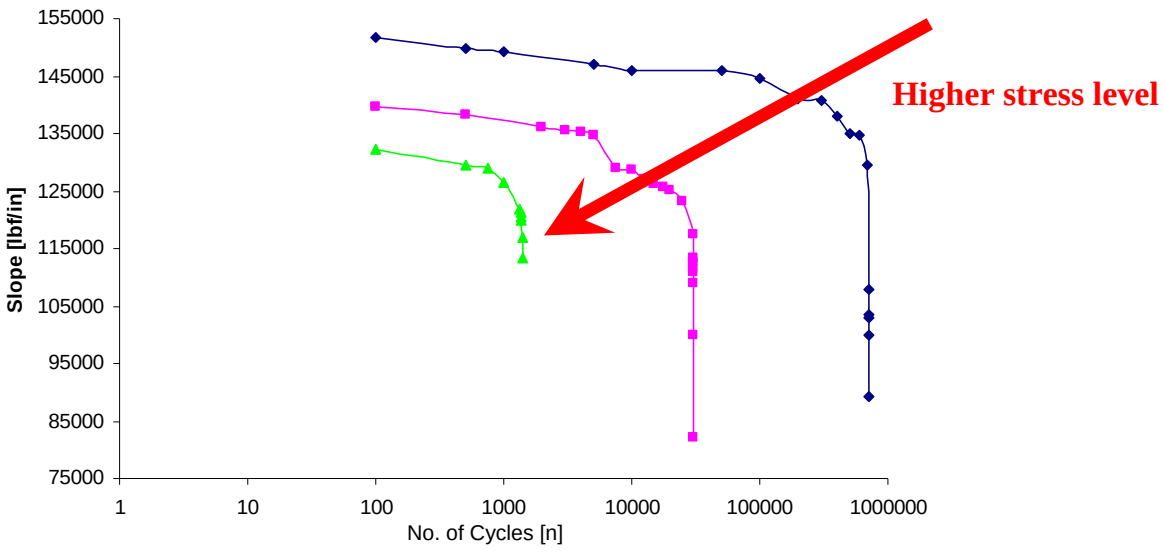

(a) Compliance Change

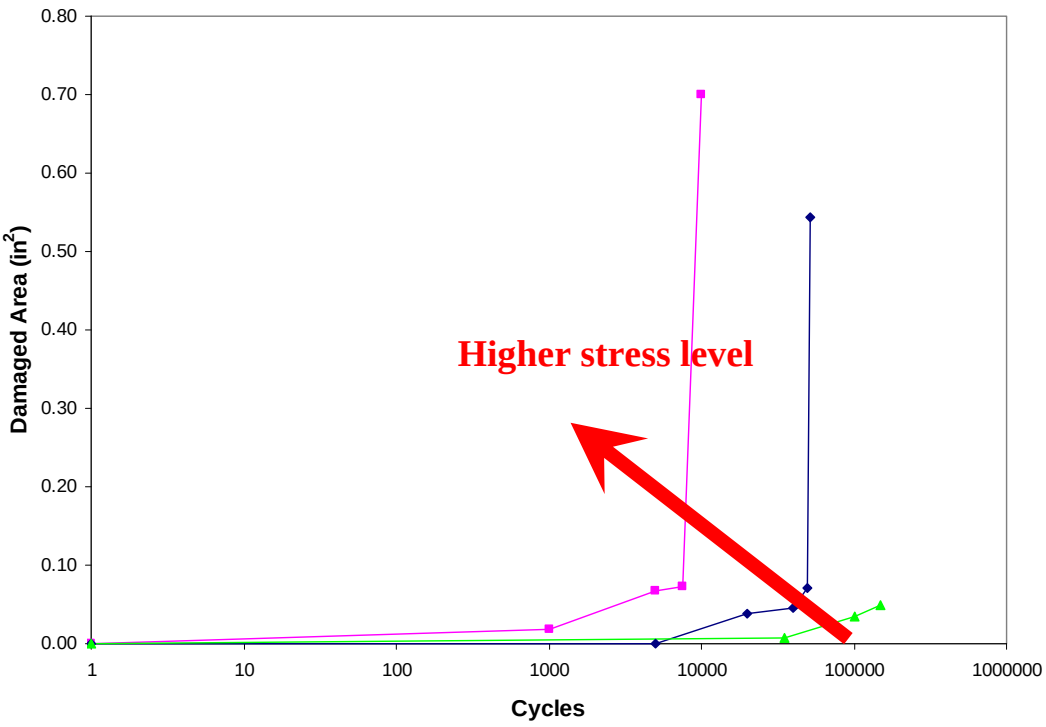

(b) Damage Growth

Figure A-23. General Trends of Compliance Change and Damage Growth for AS4-PW OH Fatigue Specimens

A.3 S/N Data for T700/#2510 Plain-Weave Fabric.

This section contains the S/N data for the T700/#2510 plain-weave fabric (T700-PW) tests included in the FAA-LEF database. Tables A-7 and A-8 include the individual data points, and figures A-24 through A-27 show the S/N curves that were used for generating LEFs for T700-PW. In these tables, n is the number of cycles survived and n = 1 indicates static failure. Also, σ_A and σ_R correspond to the fatigue stress level (or static failure stress level) and the residual strength after surviving the corresponding number of cycles, respectively.

Table A-7. S/N Data for T700-PW OH Tests (FAA-LEF)

OHC/T (R = -1)			OHC (R = 5)			OHT (R = 0)			OHT (R = -0.2)		
σ_A	n	σ_R	σ_A	n	σ_R	σ_A	n	σ_R	σ_A	n	σ_R
33650	1		33650	1		41414	1		41414	1	
34576	1		34576	1		43186	1		43186	1	
35063	1		35063	1		41602	1		41602	1	
36487	1		36487	1		40934	1		40934	1	
35204	1		35204	1		42189	1		42189	1	
34936	1		34936	1		40789	1		40789	1	
24490	2532		31487	2185		35433	2338		33349	8451	
24490	2701		31487	1889		35433	780		33349	7003	
24490	3810		31487	1426		35433	500		33349	8196	
24490	3644		31487	4263		35433	331		33349	7766	
24490	5948		31487	2152		35433	1521		33349	11553	
24490	6102		31487	2466		34599	1879		33349	17718	
20992	47865		29738	27956		34599	3919		31264	36959	
20992	32017		29738	15207		34599	6211		31264	28014	
20992	34468		27989	89462		34599	12937		31264	43575	
20992	54001		27989	27907		34599	17960		31264	69444	
20992	32295		27989	38103		33349	21575		31264	71510	
20992	38393		27989	101532		33349	8256		31264	34351	
19242	231143		27989	16926		33349	17272		29180	157157	
19242	251069		27989	72487		33349	13863		29180	270388	
19242	245405		26239	455423		33349	18214		29180	524950	
19242	112840		26239	853210		33349	22073		29180	359994	
19242	116223		26239	427342		31264	169971		29180	381294	
19242	146589		26239	351708		31264	128793		29180	527262	
17493	1056026	29027	26239	218416		31264	188066		29180	1000183	29513
17493	1046017	29668	26239	614718		31264	65969				
17493	1000019	27191	26239	1000014	34559	31264	159350				
			24490	1032657	35164	31264	82926				
						30014	240064				
						29180	1089903				
						29180	1000000	35566			

Table A-8. S/N Data for T700-PW DNC and Sandwich Tests (FAA-LEF)

DNC (R = -1)			DNC (R = -0.2)			Flexure (R = 0)		
σ_A	n	σ_R	σ_A	n	σ_R	σ_A	n	σ_R
2878	1		2878	1		131	1	
3244	1		3244	1		137	1	
2786	1		2786	1		139	1	
3245	1		3245	1		138	1	
3009	1		3009	1		138	1	
2878	1		2878	1		141	1	
1503	5331		1804	6616		82	11500	
1503	7402		1804	5045		82	5100	
1503	7835		1804	7781		82	5500	
1503	1512		1804	4842		82	21000	
1503	1661		1804	1757		82	22500	
1503	11515		1804	6017		82	6750	
1353	10811		1503	26712		82	24673	
1203	51912		1503	40696		82	34800	
1203	54388		1503	55920		82	24006	
1203	44383		1503	38398		69	44036	
1203	53626		1503	209297		69	60000	
1203	174360		1503	40675		69	114000	
1203	51686		1503	76358		69	78025	
1203	43064		1353	403412		69	140000	
1052	293357		1353	361713		69	123500	
1052	243965		1353	226962		62	310133	
1052	94645		1353	115567		62	110000	
1052	207966		1353	150687		62	370000	
1052	46212		1353	347703		62	340000	
1052	291053		1203	473922		62	375000	
1052	74427		1203	981488		62	492500	
1052	32596		1203	1000023		62	364181	
1052	132350							
1052	144424							
902	1000029	2190						

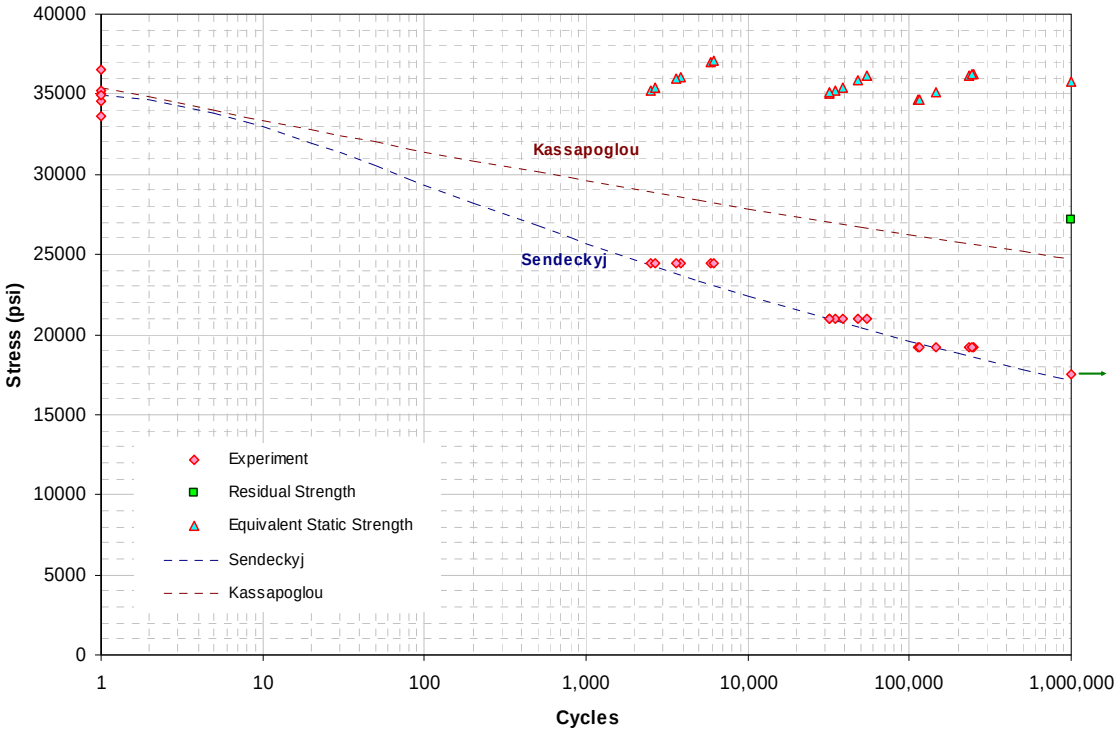

Figure A-24. T700-PW—10/80/10, OH, R = -1

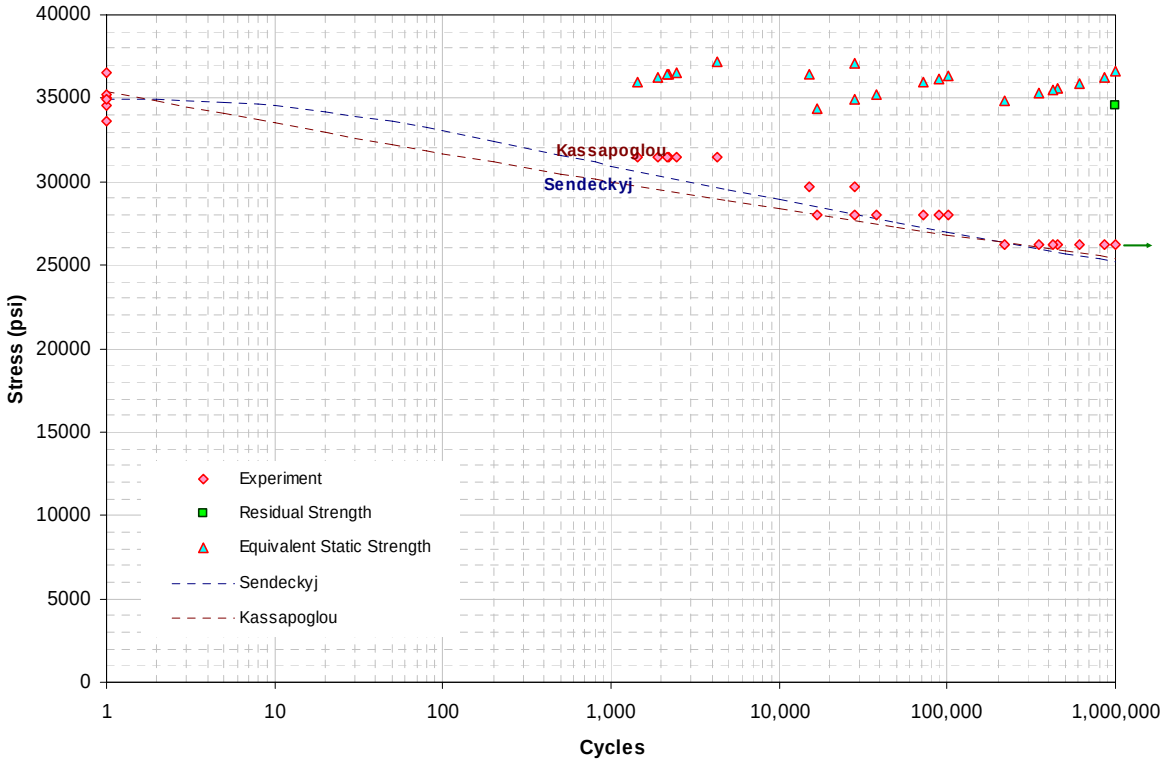

Figure A-25. T700-PW—10/80/10, OH, R = 5

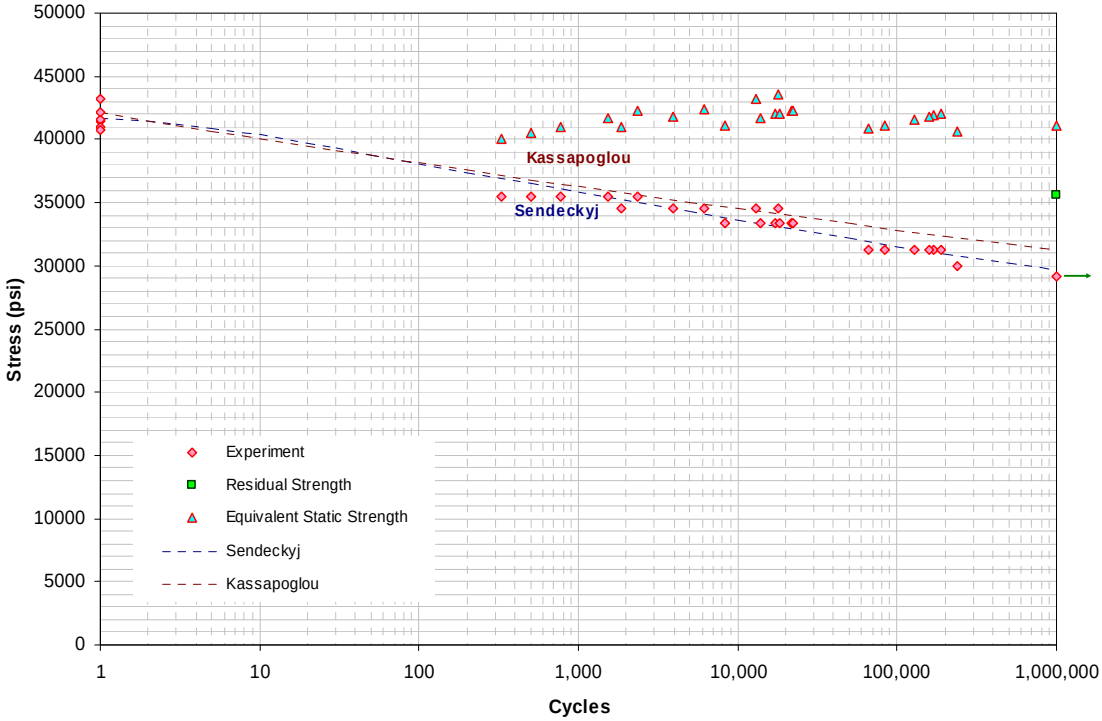

Figure A-26. T700-PW—10/80/10, OH, R = 0

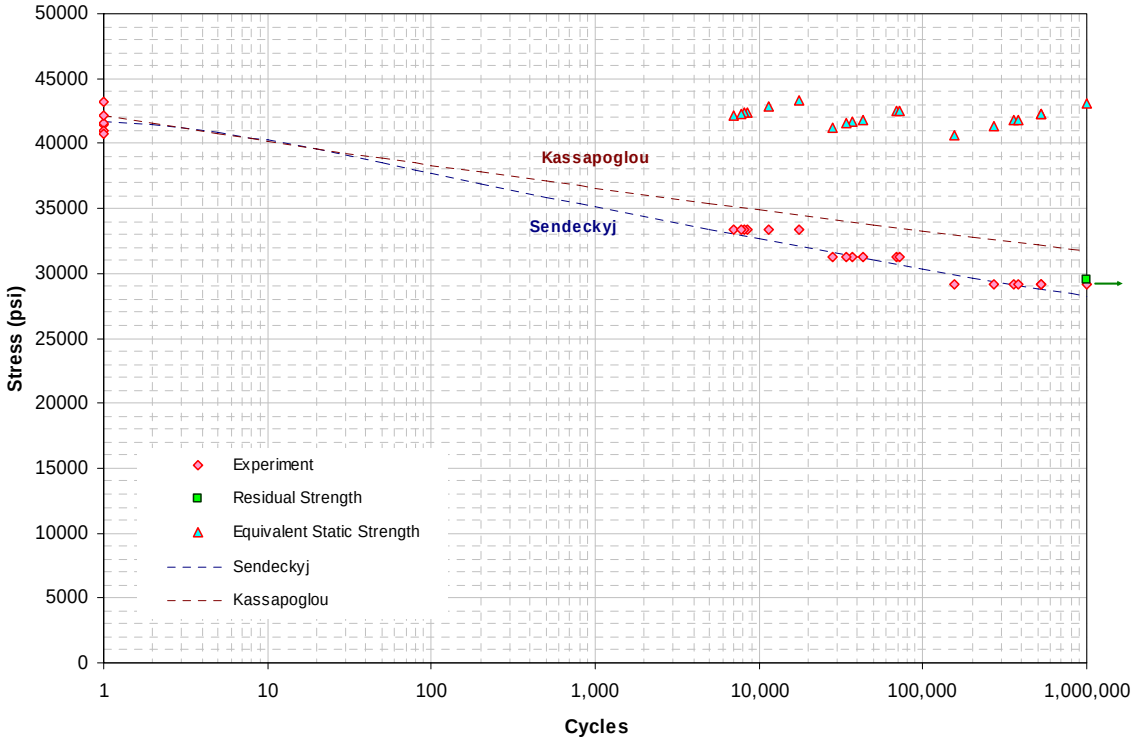

Figure A-27. T700-PW—10/80/10, OH, R = -0.2

A.4 S/N DATA FOR 7781/#2510 8-HARNESS SATIN-WEAVE FABRIC.

This section contains the S/N data for the 7781/#2510 8-harness satin-weave fabric (7781-8HS) tests included in the FAA-LEF database. Tables A-9 and A-10 include the individual data points, and figures A-28 through A-31 show the S/N curves that were used for generating LEFs for 7781-8HS. In these tables, n is the number of cycles survived and n = 1 indicates static failure. Also, σ_A and σ_R correspond to the fatigue stress level (or static failure stress level) and the residual strength after surviving the corresponding number of cycles, respectively.

Table A-9. S/N Data for 7781-8HS OH Tests (FAA-LEF)

OHC/T (R = -1)			OHC (R = 5)			OHT (R = 0)			OHT (R = -0.2)		
σ_A	n	σ_R	σ_A	n	σ_R	σ_A	n	σ_R	σ_A	n	σ_R
33130	1		33130	1		27267	1		27267	1	
33141	1		33141	1		27150	1		27150	1	
33506	1		33506	1		26895	1		26895	1	
33514	1		33514	1		26613	1		26613	1	
33407	1		33407	1		26294	1		26294	1	
32666	1		32666	1		26632	1		26632	1	
23256	260		26582	2813		16085	4879		16085	4159	
16621	756		26582	2254		16085	4689		16085	3290	
13297	7502		26582	1587		16085	5153		16085	4340	
13292	4575		26582	1716		16085	4695		16085	4006	
13292	5335		26582	1673		16085	4478		16085	3901	
10723	32634		26582	1949		16085	5230		16085	5410	
10723	32224		24921	9408		13404	31239		13404	19991	
10723	33829		24921	29368		13404	29110		13404	26597	
10723	40038		24921	16482		13404	24024		13404	25380	
10723	30692		24921	27249		13404	23870		13404	24603	
10723	38903		24921	8833		13404	25278		13404	24317	
10723	40451		24921	13012		13404	29622		13404	22742	
10013	74386		24921	23041		10723	377715		10723	87248	
9973	81665		24921	7358		10723	352927		10723	193468	
9973	70390		24921	8213		10723	272790		10723	227929	
9973	362895		23259	216131		10723	353214		10723	193446	
9959	111843		23259	274091		10723	325874		10723	177910	
9383	123527		23259	595433		10723	288778		10723	193217	
9383	145031		23259	189941							
9383	134683		23259	347856							
9383	165288		23259	362656							
9383	179403		22595	1106426	29906						
9383	193388		21598	1000000	31661						
8043	593003		19936	1000100	30532						

Table A-9. S/N Data for 7781-8HS OH Tests (FAA-LEF) (Continued)

OHC/T (R = -1)			OHC (R = 5)			OHT (R = 0)			OHT (R = -0.2)		
σ_A	n	σ_R	σ_A	n	σ_R	σ_A	n	σ_R	σ_A	n	σ_R
8043	1000032										
8043	883245										
8043	942271										
8043	769637										
8043	778751										
8043	1144259	25937									

Table A-10. S/N Data for 7781-8HS DNC and Sandwich Tests (FAA-LEF)

DNC (R = -1)			DNC (R = -0.2)			Flexure (R = 0)		
σ_A	n	σ_R	σ_A	n	σ_R	σ_A	n	σ_R
3630	1		3630	1		140.342	1	
3625	1		3625	1		141.508	1	
3429	1		3429	1		141.772	1	
3195	1		3195	1		143.715	1	
3614	1		3614	1		139.256	1	
3468	1		3468	1		139.038	1	
1747	3121		2446	1692		83	28924	
1747	5270		2096	9267		83	42000	
1747	2028		2096	12301		83	39000	
1747	6133		2096	18245		83	50000	
1747	2759		2096	5612		83	36500	
1747	3916		2096	15366		83	64000	
1572	4004		2096	11326		70	265000	
1572	10732		1747	65045		70	216004	
1572	6779		1747	45870		70	205000	
1397	28078		1747	99557		70	230000	
1397	18684		1747	85112		70	167500	
1397	5724		1747	105136		70	262000	
1397	2138		1747	83695		70	70000	
1397	6291		1572	320302		63	410000	
1397	23500		1572	37069		63	270000	
1223	451048		1572	455873		63	190000	
1223	47332		1572	237356		60	325000	
1223	31537		1572	281584		60	490000	
1048	146896		1572	107805		60	625000	
1048	206313		1572	168387		60	1000042	
1048	379484		1397	1000088	2745	60	1000042	
1048	157833					60	790000	
1048	197364					60	1000042	

Table A-10. S/N Data for 7781-8HS DNC and Sandwich Tests (FAA-LEF) (Continued)

DNC (R = -1)			DNC (R = -0.2)			Flexure (R = 0)		
σ_A	n	σ_R	σ_A	n	σ_R	σ_A	n	σ_R
1048	57311					60	1000042	
						60	1000042	
						60	1000042	
						56	940000	

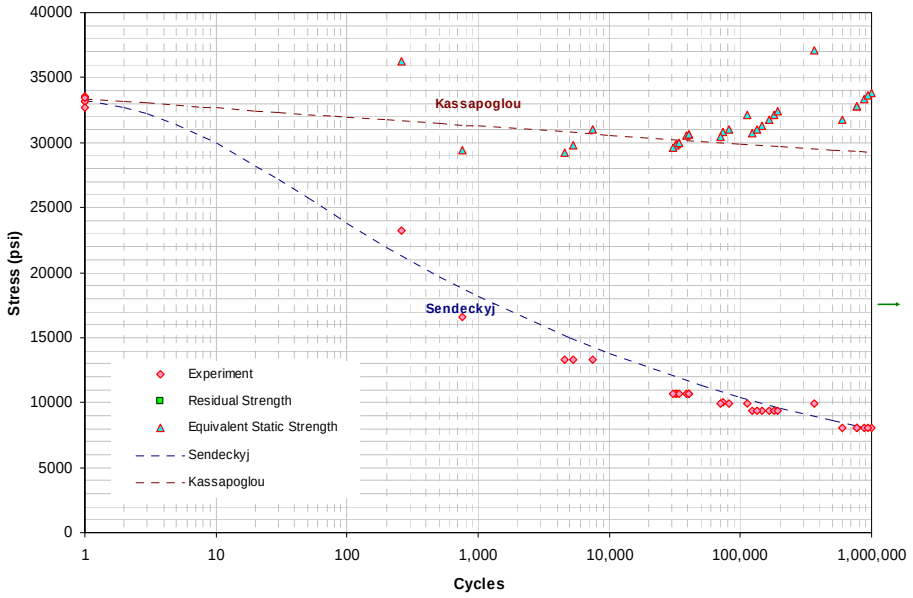

Figure A-28. 7781-8HS—10/80/10, OH, R = -1

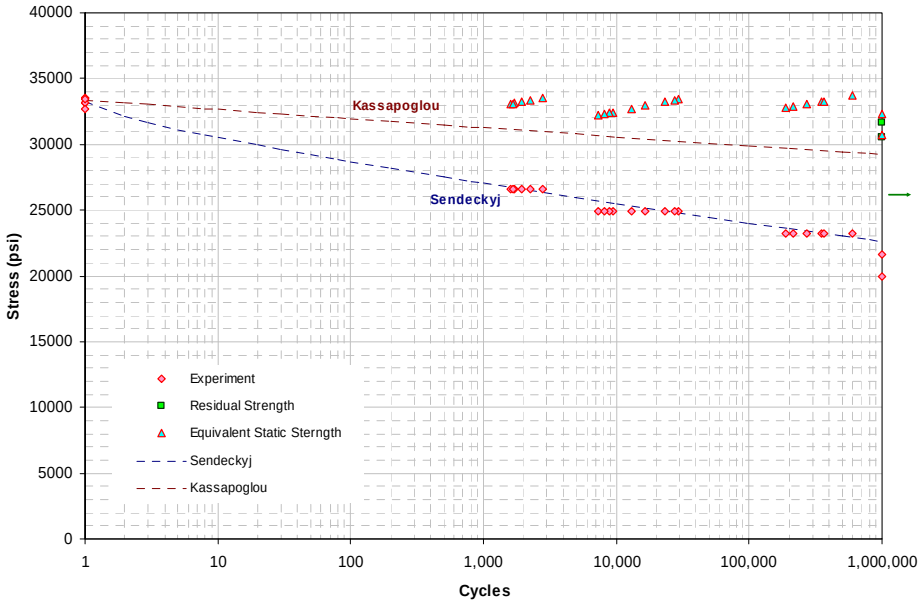

Figure A-29. 7781-8HS—10/80/10, OH, R = 5

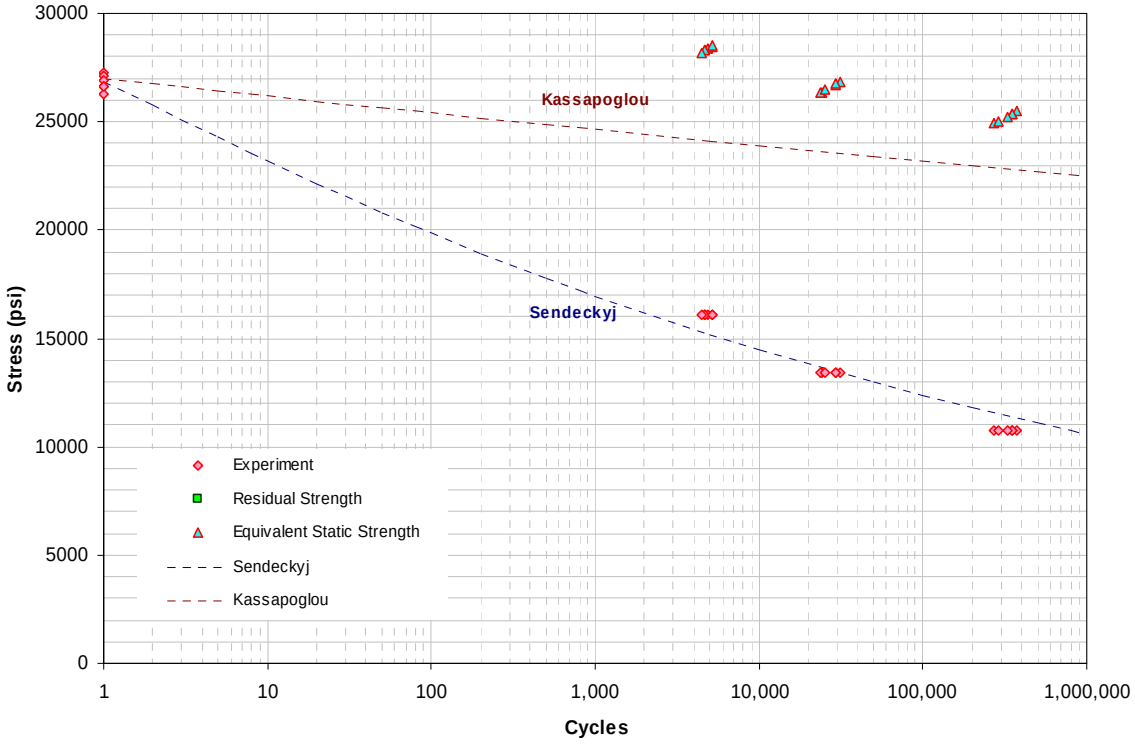

Figure A-30. 7781-8HS—10/80/10, OH, R = 0

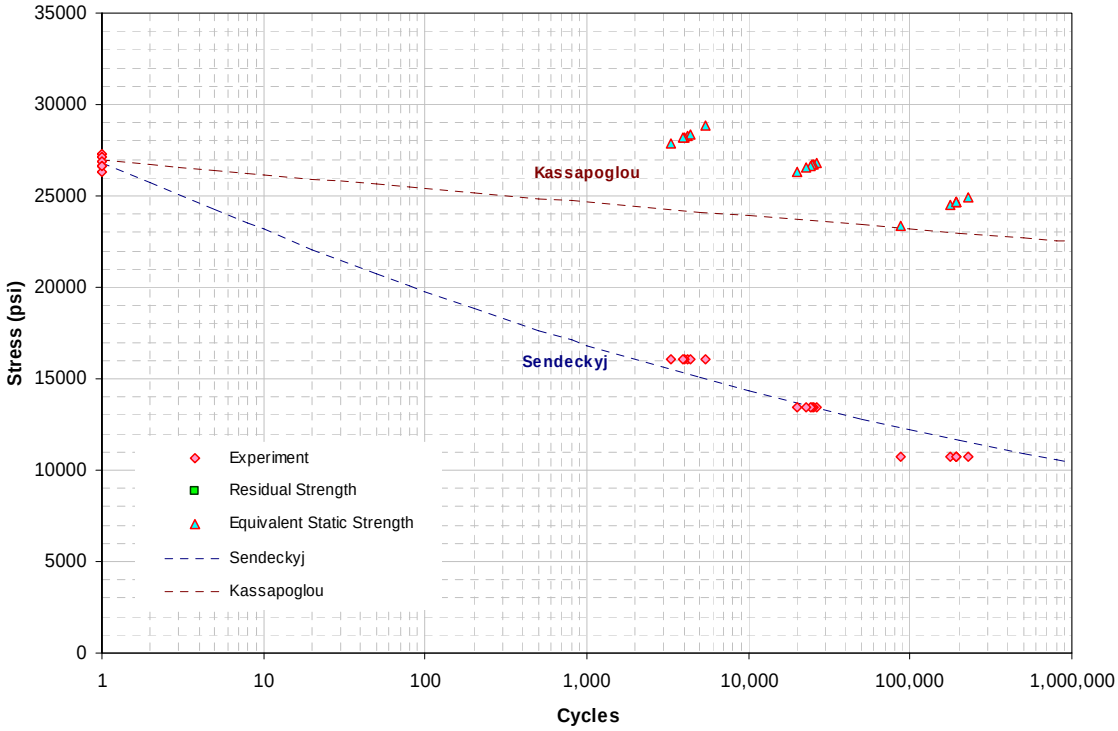

Figure A-31. 7781-8HS—10/80/10, OH, R = -0.2

A.5 REFERENCES.

A-1. Sendeckyj, G.P., "Fitting Models to Composite Materials Fatigue Data," *Test Methods and Design Allowables for Fibrous Composites, ASTM STP 734*, Chamis, C.C., ed., ASTM, 1981, pp. 245-260.

A-2. Kassapoglou, C., "Fatigue Life Prediction of Composite Structures Under Constant Amplitude Loading," *Journal of Composite Materials,* Vol. 41, No. 22, 2007.

APPENDIX B—SCATTER ANALYSIS RESULTS FOR FEDERAL AVIATION ADMINISTRATION LOAD-ENHANCEMENT FACTOR DATABASE

This appendix contains the static data scatter analysis results of Federal Aviation Administration lamina variability method (FAA-LVM) database. This analysis includes data for T700/#2510 unidirectional tape (T700-UT), AS4C/MTM45 unidirectional tape (AS4C-UT), AS4C/MTM45 5-harness satin-weave fabric (AS4C-5HS), T700/E765 unidirectional tape (E765-UT), and T300/E765 plain-weave fabric material systems. The scatter analysis of T700/#2510 plain-weave fabric (T700-PW) data belonging to the FAA-LVM database is included in section 4.1.2 of the main document.

B.1 STATIC SCATTER ANALYSIS OF T700-UT.

This section contains the shape parameters of 853 T700-UT specimens from 47 data sets obtained from the FAA-LVM database. Tables B-1, B-2, and B-3 contain shape parameters corresponding to static-strength distributions of individual test methods and environmental conditions of hard (50/40/10), quasi-isotropic (25/50/25), and soft (10/80/10) laminates, respectively. The scatter analysis in section 4.1.4 of the main document was conducted by analyzing the shape parameters in these three tables.

Table B-1. Weibull Parameters for Static-Strength Distributions of 50/40/10 T700-UT (FAA-LVM)

Test Description	Test Environment	Shape Parameter, $\hat{\alpha}$	Number of Specimens
Single-shear bearing tension	RTA	52.085	19
Double-shear bearing tension	RTA	40.405	20
Bearing-bypass 50% compression	RTA	38.043	15
Bearing-bypass 50% tension [t/D = 0.320]	RTA	41.398	18
Bearing-bypass 50% tension [t/D = 0.384]	RTA	44.098	18
Bearing-bypass 50% tension [t/D = 0.640]	RTA	42.257	17
Bearing-bypass 50% tension [t/D = 0.480]	RTA	59.840	15
Unnotched tension	RTA	20.702	19
Unnotched compression	RTA	33.121	19
Open-hole compression	RTA	22.705	21
Filled-hole tension	CTD	36.224	18
Filled-hole tension	RTA	17.585	18
Filled-hole tension	ETW	20.516	19
V-notched rail shear	RTA	22.705	18
Open-hole tension [w/D = 3]	RTA	22.553	18
Open-hole tension [w/D = 4]	RTA	20.420	18
Open-hole tension [w/D = 8]	RTA	32.794	19

CTD = Cold temperature dry
ETW = Elevated temperature wet
w/D = Width to diameter
RTA = Room temperature ambient
t/D = Thickness to diameter

Table B-2. Weibull Parameters for Static-Strength Distributions of 25/50/25 T700-UT (FAA-LVM)

Test Description	Test Environment	Shape Parameter, $\hat{\alpha}$	Number of Specimens
Double-shear bearing tension	CTD	31.499	22
Double-shear bearing tension	RTA	10.310	19
Double-shear bearing tension	ETW	41.221	18
Single-shear bearing tension	CTD	37.563	18
Single-shear bearing tension	RTA	14.452	18
Single-shear bearing tension	ETW	18.924	18
Bearing-bypass 50% tension	RTA	74.669	15
Bearing-bypass 50% compression	RTA	57.956	15
Open-hole tension [w/D = 6]	CTD	37.058	18
Open-hole tension [w/D = 6]	RTA	25.000	18
Open-hole tension [w/D = 6]	ETW	27.714	21
Unnotched tension	CTD	45.075	18
Unnotched tension	RTA	39.641	18
Unnotched tension	ETW	32.490	18
Unnotched compression	CTD	23.026	18
Unnotched compression	RTA	22.034	18
Unnotched compression	ETW	34.869	18
Open-hole compression	CTD	37.455	21
Open-hole compression	RTA	27.930	18
Open-hole compression	ETW	22.122	22
V-notched rail shear	RTA	9.054	18

Table B-3. Weibull Parameters for Static-Strength Distributions of 10/80/10 T700-UT (FAA-LVM)

Test Description	Test Environment	Shape Parameter, $\hat{\alpha}$	Number of Specimens
Bearing-bypass 50% tension	RTA	64.772	15
Bearing-bypass 50% compression	RTA	49.444	15
Open-hole tension [w/D = 6]	RTA	67.241	18
Unnotched tension	RTA	20.186	18
Unnotched compression	RTA	26.157	18
Open-hole compression	RTA	41.378	18
V-notched rail shear	CTD	7.262	18
V-notched rail shear	RTA	19.659	19
V-notched rail shear	ETW	10.595	18

B.2 STATIC SCATTER ANALYSIS OF AS4C/MTM45 UNIDIRECTIONAL TAPE.

This section contains the shape parameters of 1151 AS4C-UT specimens from 86 data sets obtained from the FAA-LVM database. Tables B-4 through B-6 contain shape parameters corresponding to static-strength distributions of individual test methods and environmental conditions of hard (50/40/10), quasi-isotropic (25/50/25), and soft (10/80/10) laminates, respectively. In addition, shape parameters corresponding to AS4C-UT lamina data are included in table B-7. The scatter analysis in section 4.1.5 of the main document was conducted by analyzing the shape parameters in these three tables.

Table B-4. Weibull Parameters for Static-Strength Distributions of 50/40/10 AS4C-UT (FAA-LVM)

Test Description	Test Environment	Shape Parameter, $\hat{\alpha}$	Number of Specimens
Unnotched tension	CTD	36.6884	7
Unnotched tension	RTD	39.6101	6
Unnotched tension	ETW2	105.7766	6
Open-hole tension	CTD	8.2884	18
Open-hole tension	RTD	46.3690	6
Open-hole tension	ETW2	60.1876	6
Filled-hole tension	CTD	18.7167	6
Filled-hole tension	RTD	18.1374	6
Unnotched compression	RTD	46.4812	6
Unnotched compression	ETW	39.6044	7
Open-hole compression	RTD	51.4916	6
Open-hole compression	ETW2	28.7315	19
Filled-hole compression	RTD	7.6270	7
Filled-hole compression	ETW2	13.1700	21
Double-shear bearing	RTD	52.4169	6
Double-shear bearing	ETW2	30.4239	20

CTD = Cold temperature dry
RTD = Room temperature dry
ETW2 = Elevated temperature 220°F, wet

Table B-5. Weibull Parameters for Static-Strength Distributions of 25/50/25 AS4C-UT (FAA-LVM)

Test Description	Test Environment	Shape Parameter, $\hat{\alpha}$	Number of Specimens
Unnotched tension	CTD	36.9107	18
Unnotched tension	RTD	36.7091	18
Unnotched tension	ETW2	73.1509	6
Open-hole tension	CTD	27.1127	15
Open-hole tension	RTD	35.9034	16
Open-hole tension	ETW	45.0771	5
Open-hole tension	ETW2	29.5619	18
Filled-hole tension	CTD	30.4239	18
Filled-hole tension	RTD	32.5909	6
Unnotched compression	RTD	35.8363	19
Unnotched compression	ETW	45.5883	7
Unnotched compression	ETW2	25.0000	18
Open-hole compression	RTD	24.9999	14
Open-hole compression	ETW	23.6168	6
Open-hole compression	ETW2	28.0623	17
Filled-hole compression	RTD	24.9999	6
Filled-hole compression	ETW2	21.4617	7
Double-shear bearing	RTD	21.0857	18
Double-shear bearing	ETW2	22.9000	18
Compression after impact	RTD	16.0114	6

CTD = Cold temperature dry
RTD = Room temperature dry
ETW2 = Elevated temperature 220°F, wet

Table B-6. Weibull Parameters for Static-Strength Distributions of 10/80/10 AS4C-UT (FAA-LVM)

Test Description	Test Environment	Shape Parameter, $\hat{\alpha}$	Number of Specimens
Unnotched tension	CTD	35.1583	6
Unnotched tension	RTD	31.4154	6
Unnotched tension	ETW2	47.2541	6
Open-hole tension	CTD	48.8726	17
Open-hole tension	RTD	47.2759	5

Table B-6. Weibull Parameters for Static-Strength Distributions of 10/80/10 AS4C-UT (FAA-LVM) (Continued)

Test Description	Test Environment	Shape Parameter, $\hat{\alpha}$	Number of Specimens
Open-hole tension	ETW2	38.5491	6
Filled-hole tension	CTD	60.3965	6
Filled-hole tension	RTD	40.4534	6
Filled-hole tension	ETW2	38.2105	7
Unnotched compression	RTD	33.1313	6
Unnotched compression	ETW2	47.7841	6
Open-hole compression	RTD	33.2611	5
Open-hole compression	ETW2	27.2031	18
Filled-hole compression	RTD	38.5239	5
Filled-hole compression	ETW2	27.6622	21
Double-shear bearing	RTD	31.2818	6
Double-shear bearing	ETW2	18.3542	12
Short-beam shear	RTD	22.0431	18
Short-beam shear	ETW	23.9989	6
Short-beam shear	ETW2	27.0304	18

CTD = Cold temperature dry
RTD = Room temperature dry
ETW2 = Elevated temperature 220°F, wet

Table B-7. Weibull Parameters for Static-Strength Distributions of AS4C-UT Lamina Data (FAA-LVM)

Lay-Up	Test Description	Test Environment	Shape Parameter, $\hat{\alpha}$	Number of Specimens
100/0/0	Longitudinal tension	CTD	13.8596	20
	Longitudinal tension	RTD	15.0419	18
	Longitudinal tension	ETW	16.9554	12
	Longitudinal tension	ETW2	18.9761	12
0/0/100	Transverse tension	CTD	13.2656	20
	Transverse tension	RTD	13.7326	20
	Transverse tension	ETW	12.5037	23
	Transverse tension	ETW2	16.5834	21

Table B-7. Weibull Parameters for Static-Strength Distributions of AS4C-UT Lamina Data (FAA-LVM) (Continued)

Lay-Up	Test Description	Test Environment	Shape Parameter, $\hat{\alpha}$	Number of Specimens
0/0/100	Transverse compression	CTD	22.5142	19
	Transverse compression	RTD	32.6974	18
	Transverse compression	ETW	31.1187	18
	Transverse compression	ETW2	23.3048	19
0/100/0	In-plane shear	CTD	30.8707	18
	In-plane shear	RTD	43.3159	18
	In-plane shear	ETW	37.3768	17
	In-plane shear	ETW2	31.4522	19
100/0/0	Short-beam shear	CTD	30.0698	20
	Short-beam shear	RTD	32.5469	20
	Short-beam shear	ETD	26.2652	20
	Short-beam shear	ETW	36.3365	21
	Short-beam shear	ETW2	19.1586	18
50/0/50	Unnotched tension	CTD	18.9930	18
	Unnotched tension	RTD	19.3424	18
	Unnotched tension	ETW	16.0501	18
	Unnotched tension	ETW2	17.8260	17
50/0/50	Unnotched compression	CTD	14.1693	22
	Unnotched compression	RTD	28.1360	18
	Unnotched compression	ETD	20.7004	18
	Unnotched compression	ETW	20.0349	18
	Unnotched compression	ETW2	12.5308	18

CTD = Cold temperature dry
RTD = Room temperature dry
ETW2 = Elevated temperature 220°F, wet

B.3 STATIC SCATTER ANALYSIS OF AS4C/MTM45 5-HARNESS SATIN-WEAVE FABRIC.

This section contains the shape parameters of 1083 AS4C-5HS specimens from 78 data sets obtained from the FAA-LVM database. Tables B-8 through B-10 contain shape parameters corresponding to static-strength distributions of individual test methods and environmental conditions of hard (40/20/40), quasi-isotropic (25/50/25), and soft (10/80/10) laminates, respectively. In addition, shape parameters corresponding to AS4C-5HS lamina data are included in table B-11. The scatter analysis in section 4.1.6 of the main document was conducted by analyzing the shape parameters in these three tables.

Table B-8. Weibull Parameters for Static-Strength Distributions of 40/20/40 AS4C-5HS (FAA-LVM)

Test Description	Test Environment	Shape Parameter, $\hat{\alpha}$	Number of Specimens
Unnotched tension	CTD	50.3322	6
Unnotched compression	RTD	13.4587	6
Unnotched compression	ETW2	23.7333	6
Open-hole tension	CTD	25.5530	21
Open-hole tension	RTD	33.2549	7
Open-hole tension	ETW2	28.5810	6
Filled-hole tension	CTD	20.9094	6
Filled-hole tension	RTD	29.0854	6
Open-hole compression	RTD	32.2012	6
Open-hole compression	ETW2	27.0483	18
Filled-hole compression	RTD	14.1911	6
Filled-hole compression	ETW2	19.3906	20
Double-shear bearing	RTD	34.7686	6
Double-shear bearing	ETW2	15.5135	24

CTD = Cold temperature dry
RTD = Room temperature dry
ETW2 = Elevated temperature 220°F, wet

Table B-9. Weibull Parameters for Static-Strength Distributions of 25/50/25 AS4C-5HS (FAA-LVM)

Test Description	Test Environment	Shape Parameter, $\hat{\alpha}$	Number of Specimens
Unnotched tension	CTD	62.6999	23
Unnotched tension	RTD	34.3319	18
Unnotched tension	ETW2	44.9484	6
Unnotched compression	RTD	20.4637	18
Unnotched compression	ETW	19.1119	6
Unnotched compression	ETW2	19.6297	18
Open-hole tension	RTD	40.4981	18
Open-hole tension	CTD	24.3826	18
Open-hole tension	ETW	86.9983	6
Open-hole tension	ETW2	28.7676	18
Filled-hole tension	RTD	41.9103	6
Filled-hole tension	CTD	34.6634	18

Table B-9. Weibull Parameters for Static-Strength Distributions of 25/50/25 AS4C-5HS (FAA-LVM) (Continued)

Test Description	Test Environment	Shape Parameter, $\hat{\alpha}$	Number of Specimens
Open-hole compression	RTD	29.5250	18
Open-hole compression	ETW	15.5124	6
Open-hole compression	ETW2	24.5294	18
Filled-hole compression	RTD	27.7953	6
Filled-hole compression	ETW2	31.8401	18
Double-shear bearing	RTD	13.9867	18
Double-shear bearing	ETW2	13.6569	23
Short-beam shear	RTD	35.7819	18
Short-beam shear	ETW	61.9031	6
Short-beam shear	ETW2	57.5735	18

CTD = Cold temperature dry RTD = Room temperature dry ETW2 = Elevated temperature 220°F, wet

Table B-10. Weibull Parameters for Static-Strength Distributions of 10/80/10 AS4C-5HS (FAA-LVM)

Test Description	Test Environment	Shape Parameter, $\hat{\alpha}$	Number of Specimens
Unnotched tension	CTD	36.4157	6
Unnotched tension	RTD	74.8199	6
Unnotched tension	ETW2	26.8754	6
Unnotched compression	RTD	23.2597	6
Unnotched compression	ETW2	32.6546	6
Open-hole tension	CTD	41.9517	18
Open-hole tension	RTD	53.7592	9
Open-hole tension	ETW2	40.8813	6
Filled-hole tension	RTD	53.8676	6
Filled-hole tension	CTD	64.3808	6
Filled-hole tension	ETW2	43.5941	6
Open-hole compression	RTD	32.1458	6
Open-hole compression	ETW2	40.5532	18
Filled-hole compression	RTD	64.9168	6
Filled-hole compression	ETW2	41.6289	18
Double-shear bearing	RTD	21.9478	6
Double-shear bearing	ETW2	14.6494	24

CTD = Cold temperature dry RTD = Room temperature dry ETW2 = Elevated temperature 220°F, wet

Table B-11. Weibull Parameters for Static-Strength Distributions of 50/0/50 AS4C-5HS (FAA-LVM)

Test Description	Test Environment	Shape Parameter, $\hat{\alpha}$	Number of Specimens
Warp tension	CTD	41.7447	19
Warp tension	RTA	31.7590	22
Warp tension	ETW	34.1953	20
Warp tension	ETW2	25.6064	22
Filled tension	CTD	27.5161	18
Filled tension	RTA	31.6162	18
Filled tension	ETW	36.2862	21
Filled tension	ETW2	25.4495	19
Warp compression	CTD	11.9994	18
Warp compression	RTA	16.1442	19
Warp compression	ETW	12.2082	18
Warp compression	ETW2	9.7697	18
Filled compression	CTD	17.3767	18
Filled compression	RTA	18.1475	18
Filled compression	ETD	13.3973	18
Filled compression	ETW	15.3266	18
Filled compression	ETW2	18.4131	18
In-plane Shear	CTD	14.1296	16
In-plane Shear	RTA	14.7233	16
In-plane Shear	ETW	61.6350	16
In-plane Shear	ETW2	13.9587	16
Short-beam shear	CTD	24.7163	19
Short-beam shear	RTA	36.7471	17
Short-beam shear	ETW	26.2523	18
Short-beam shear	ETW2	28.0774	18

RTA = Room temperature ambient
RTD = Room temperature dry
CTD = Cold temperature dry
ETW2 = Elevated temperature 220°F, wet

B.4 STATIC SCATTER ANALYSIS OF T700/E765 UNIDIRECTIONAL TAPE.

This section contains the shape parameters of 834 E765-UT specimens from 47 data sets obtained from the FAA-LVM database. Tables B-12 through B-14 contain shape parameters corresponding to static-strength distributions of individual test methods and environmental conditions of hard (50/40/10), quasi-isotropic (25/50/25), and soft (10/80/10) laminates, respectively. The scatter analysis in section 4.1.7 of the main document was conducted by analyzing the shape parameters in these three tables.

Table B-12. Weibull Parameters for Static-Strength Distributions of 50/40/10 E765-UT (FAA-LVM)

Test Description	Test Environment	Shape Parameter, $\hat{\alpha}$	Number of Specimens
Single-shear bearing tension	RTA	30.814	18
Double-shear bearing tension	RTA	17.957	21
Bearing-bypass 50% compression	RTA	28.550	13
Bearing-bypass 50% tension [t/D = 0.320]	RTA	30.861	17
Bearing-bypass 50% tension [t/D = 0.384]	RTA	46.294	18
Bearing-bypass 50% tension [t/D = 0.640]	RTA	24.909	18
Bearing-bypass 50% tension [t/D = 0.480]	RTA	26.362	15
Unnotched tension	RTA	7.347	20
Unnotched compression	RTA	8.897	18
Open-hole compression	RTA	21.189	20
Filled-hole tension	CTD	31.088	18
Filled-hole tension	RTA	33.685	18
Filled-hole tension	ETW	18.421	18
V-notched rail shear	RTA	19.226	18
Open-hole tension [w/D = 3]	RTA	35.484	18
Open-hole tension [w/D = 4]	RTA	77.305	16
Open-hole tension [w/D = 8]	RTA	27.486	18

RTA = Room temperature ambient
CTD = Cold temperature dry
ETW = Elevated temperature wet

Table B-13. Weibull Parameters for Static-Strength Distributions of 25/50/25 E765-UT (FAA-LVM)

Test Description	Test Environment	Shape Parameter, $\hat{\alpha}$	Number of Specimens
Double-shear bearing tension	CTD	13.077	19
Double-shear bearing tension	RTA	28.116	18
Double-shear bearing tension	ETW	8.356	21
Single-shear bearing tension	CTD	17.509	18

Table B-13. Weibull Parameters for Static-Strength Distributions of 25/50/25 E765-UT (FAA-LVM) (Continued)

Test Description	Test Environment	Shape Parameter, $\hat{\alpha}$	Number of Specimens
Single-shear bearing tension	RTA	26.754	18
Single-shear bearing tension	ETW	31.724	20
Bearing-bypass 50% tension	RTA	40.112	16
Bearing-bypass 50% compression	RTA	30.226	15
Open-hole tension [w/D = 6]	CTD	37.529	18
Open-hole tension [w/D = 6]	RTA	50.949	18
Open-hole tension [w/D = 6]	ETW	48.482	18
Unnotched tension	CTD	14.611	19
Unnotched tension	RTA	25.580	14
Unnotched tension	ETW	24.874	18
Unnotched compression	CTD	18.276	18
Unnotched compression	RTA	28.061	17
Unnotched compression	ETW	10.442	18
Open-hole compression	CTD	18.715	19
Open-hole compression	RTA	50.933	18
Open-hole compression	ETW	13.645	20
V-notched rail shear	RTA	10.840	18

RTA = Room temperature ambient CTD = Cold temperature dry ETW = Elevated temperature wet

Table B-14. Weibull Parameters for Static-Strength Distributions of 10/80/10 E765-UT (FAA-LVM)

Test Description	Test Environment	Shape Parameter, $\hat{\alpha}$	Number of Specimens
Bearing-bypass 50% tension	RTA	38.362	15
Bearing-bypass 50% compression	RTA	39.852	14
Open-hole tension [w/D = 6]	RTA	32.358	18
Unnotched tension	RTA	40.424	15
Unnotched compression	RTA	27.476	18
Open hole compression	RTA	28.881	20
V-notched rail shear	CTD	6.335	18
V-notched rail shear	RTA	16.180	18
V-notched rail shear	ETW	11.573	18

RTA = Room temperature ambient CTD = Cold temperature dry ETW = Elevated temperature wet

B.5 STATIC SCATTER ANALYSIS OF T300/E765 3K PLAIN-WEAVE FABRIC.

This section contains the shape parameters of 722 E765-PW specimens from 48 data sets obtained from the FAA-LVM database. Tables B-15 through B-17 contain shape parameters corresponding to static-strength distributions of individual test methods and environmental conditions of hard (40/20/40), quasi-isotropic (25/50/25), and soft (10/80/10) laminates, respectively. The scatter analysis in section 4.1.8 of the main document was conducted by analyzing the shape parameters in these three tables.

Table B-15. Weibull Parameters for Static-Strength Distributions of (40/20/40 E765-PW (FAA-LVM)

Test Description	Test Environment	Shape Parameter, $\hat{\alpha}$	Number of Specimens
Single-shear bearing tension	RTA	14.391	15
Double-shear bearing tension	RTA	39.826	13
Bearing-bypass 50% compression	RTA	34.680	9
Bearing-bypass 50% tension [t/D = 0.320]	RTA	49.915	12
Bearing-bypass 50% tension [t/D = 0.384]	RTA	43.274	12
Bearing-bypass 50% tension [t/D = 0.640]	RTA	2.986	6
Bearing-bypass 50% tension [t/D = 0.480]	RTA	27.165	12
Unnotched tension	RTA	27.277	13
Unnotched compression	RTA	23.693	13
Open-hole compression	RTA	31.510	12
Filled-hole tension	CTD	20.391	12
Filled-hole tension	RTA	45.561	12
Filled-hole tension	ETW	35.757	12
V-notched rail shear	RTA	65.531	12
Open-hole tension [w/D = 3]	RTA	34.781	12
Open-hole tension [w/D = 4]	RTA	51.052	13
Open-hole tension [w/D = 6]	RTA	29.581	12
Open-hole tension [w/D = 8]	RTA	32.084	12

RTA = Room temperature ambient
CTD = Cold temperature dry
ETW = Elevated temperature wet

Table B-16. Weibull Parameters for Static-Strength distributions of 25/50/25 E765-PW (FAA-LVM)

Test Description	Test Environment	Shape Parameter, $\hat{\alpha}$	Number of Specimens
Double-shear bearing tension	CTD	19.297	20
Double-shear bearing tension	RTA	38.719	20
Double-shear bearing tension	ETW	28.345	19
Single-shear bearing tension	CTD	12.403	18
Single-shear bearing tension	RTA	22.420	18
Single-shear bearing tension	ETW	19.406	18
Bearing-bypass 50% tension	RTA	40.069	10
Bearing-bypass 50% compression	RTA	34.458	8
Open-hole tension [w/D = 6]	CTD	19.337	18
Open-hole tension [w/D = 6]	RTA	18.427	18
Open-hole tension [w/D = 6]	ETW	23.693	18
Unnotched tension	CTD	43.886	18
Unnotched tension	RTA	43.824	18
Unnotched tension	ETW	42.304	21
Unnotched compression	CTD	26.180	18
Unnotched compression	RTA	33.422	15
Unnotched compression	ETW	20.017	18
Open-hole compression	CTD	19.446	19
Open-hole compression	RTA	25.503	18
Open-hole compression	ETW	12.103	19
V-notched rail shear	RTA	20.670	18

RTA = Room temperature ambient CTD = Cold temperature dry ETW = Elevated temperature wet

Table B-17. Weibull Parameters for Static-Strength Distributions of (10/80/10 E765-PW (FAA-LVM)

Test Description	Test Environment	Shape Parameter, $\hat{\alpha}$	Number of Specimens
Bearing-bypass 50% tension	RTA	8.873	10
Bearing-bypass 50% compression	RTA	25.206	13
Open-Hole tension [w/D = 6]	RTA	28.001	18
Unnotched tension	RTA	44.073	18
Unnotched compression	RTA	41.200	18
Open-hole compression	RTA	39.190	18
V-notched rail shear	CTD	12.622	12
V-notched rail shear	RTA	7.238	19
V-notched rail shear	ETW	14.961	15

RTA = Room temperature ambient CTD = Cold temperature dry ETW = Elevated temperature wet

APPENDIX C—SCATTER ANALYSIS FOR LIFE AND LOAD-ENHANCEMENT FACTORS

Figure C-1 illustrates the procedure for analyzing stress to number of cycle (S/N) data using individual Weibull, joint Weibull, and Sendeckyj analysis for generating the fatigue-life shape parameter for a particular test configuration ($\hat{\alpha}_{IW}$, $\hat{\alpha}_{JW}$, and $\hat{\alpha}_{Sendeckyj}$, respectively). The details for each method are discussed in section 3.1 of the main document. As shown in this figure, the static data, if applicable, are analyzed using individual Weibull for generating the static-strength shape parameter ($\hat{\alpha}_{SS}$) for the same test configuration.

ThV-notched rail sheare procedure for generating the static-strength (α_R) and fatigue-life (α_L) shape parameters for calculating the life factor and load-enhancement factors for a particular structure is illustrated in figure C-2. This process requires analysis of static/residual strength data and fatigue (S/N) data for multiple test configurations that represent critical design details of the structure. The fatigue-life shape parameter ($\hat{\alpha}_{FL}$) for each design detail or test configuration can be obtained using one of the three methods ($\hat{\alpha}_{IW}$, $\hat{\alpha}_{JW}$, or $\hat{\alpha}_{Sendeckyj}$) shown in figure C-1. The details for calculating life factor, load factor, and load-enhancement factors are included in sections 3.2 through 3.4 of the main document.

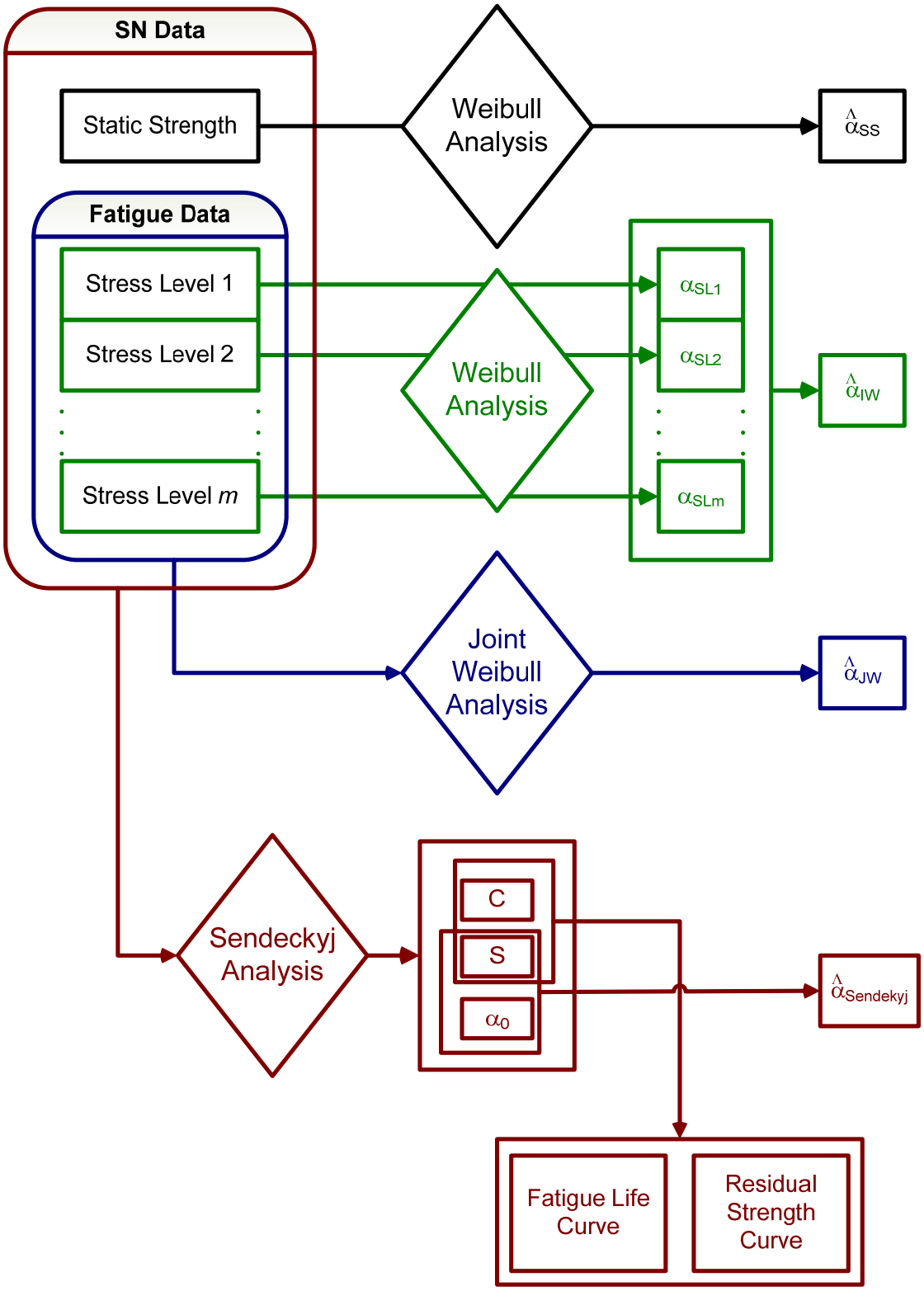

Figure C-1. Process for Obtaining the Fatigue-Life Shape Parameters for an Individual Test Configuration

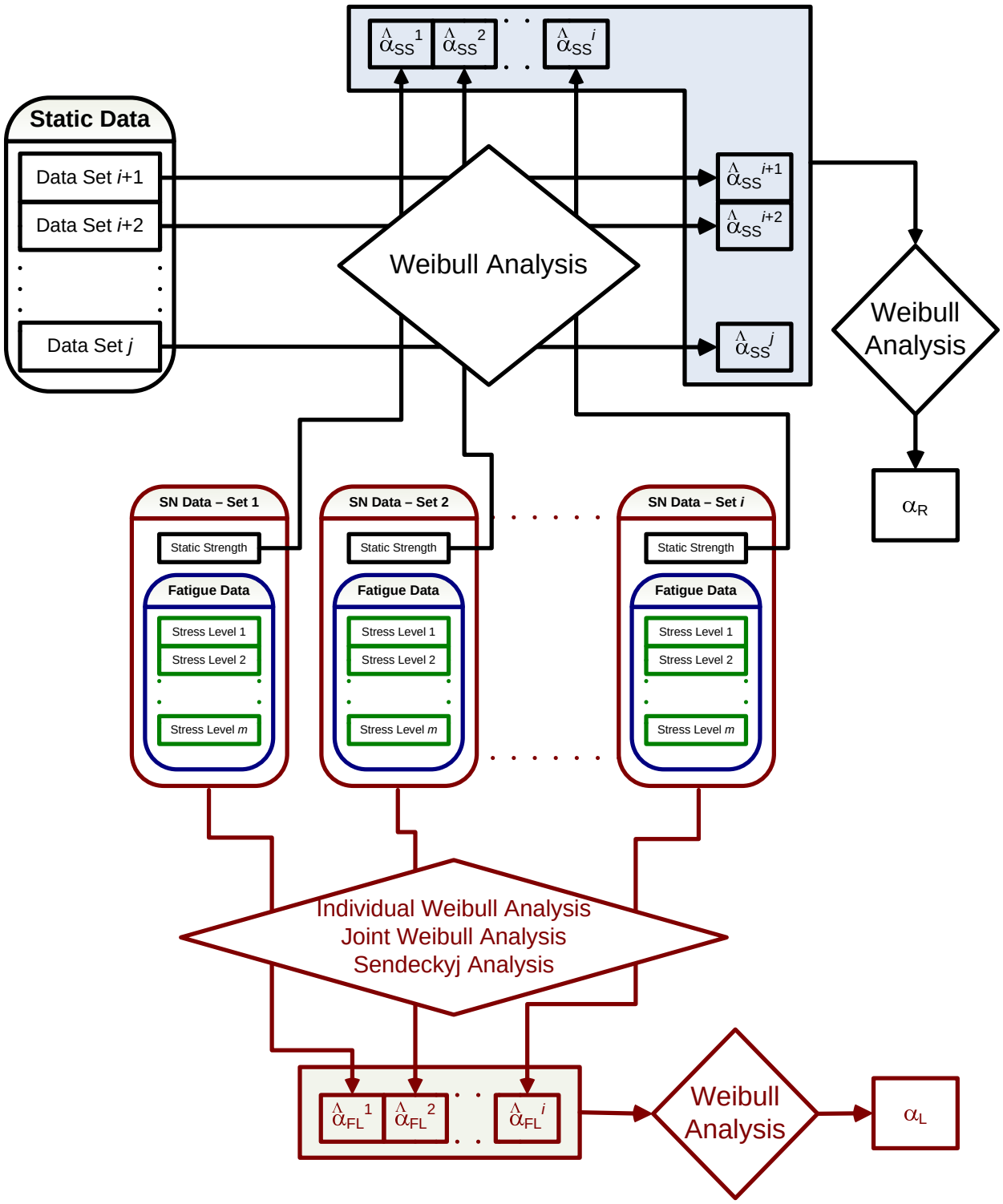

Figure C-2. Process for Generating the Static-Strength and Fatigue-Life Shape Parameters for Calculating the Life Factor and Load-Enhancement Factors for a Particular Structure